UNIVERSITÉ DE STRASBOURG

ÉCOLE DOCTORALE DES SCIENCES CHIMIQUES

THÈSE présentée par :

Cinzia SPINATO

soutenue le : **28 Septembre 2015**

pour obtenir le grade de : **Docteur de l'université de Strasbourg**

Discipline : Chimie

Development of chemical strategies to prepare multifunctional carbon nanotubes for anticancer therapy

THÈSE dirigée par :

M. BIANCO Alberto	Directeur de Recherche, CNRS

RAPPORTEURS :

M. MENNA Enzo	Professeur, Università degli Studi di Padova
M. DORIS Eric	Directeur de Recherche, CEA

EXAMINATEUR :

Mme BÉGIN-COLIN Sylvie	Professeur, Université de Strasbourg

"We must not forget that when radium was discovered, no one knew that it would prove useful in hospitals. The work was one of pure science. And this is a proof that scientific work must not be considered from the point of view of the direct usefulness of it. It must be done for itself, for the beauty of science, and then there is always the chance that a scientific discovery may become like the radium a benefit for mankind."

Marie Curie (1867 -1934) – Lecture at Vassar College, 1921

ACKNOWLEDGEMENTS

First of all, I would like to thank my supervisor, Dr. Alberto Bianco, for giving me the possibility to carry out my PhD under his supervision. It was a very pleasant and enriching experience to work in his group, in such an international and dynamic environment. I am especially deeply grateful for having had the chance to be involved in the Marie Curie network and to travel and carry out internships in other labs. Thanks for being a very present and interactive supervisor and for having firmly supported me in a few situations.

My second thanking - and it's an enormous one - goes to Dr. Cécilia Menard-Moyon, who has been (although not officially) my co-supervisor and who has (almost literally) followed me during these three years in the lab. Thank you for the many advises, scientific inputs and discussions, for your promptness and attention to details. Your extremely gentle attitude and enthusiasm toward science (and CNMs) definitely rendered lab work more endurable and enjoyable, and it was a real pleasure to share with you also many moments outside the lab.

I am very grateful to Prof. Sylvie Bégin-Colin, Prof. Enzo Menna and Dr. Eric Doris for accepting to be members of my defense commission and reading this manuscript.

I wish to thank Prof. Sylviane Muller for accepting me within the UPR 3572, which is a very inter-disciplinary department and allowed me to get a tiny understanding of the biologists world.

The completion of this research work would not have been possible without the contribution of many collaborators, and I would like to express my gratitude to them starting from Prof. Kostas Kostarelos and his co-workers in Manchester, for the biological assays performed on the aminated MWCNTs and the VHH conjugates. Thanks to the group of Dr. Gerard Tobias in Barcelona, especially to Magda and Markus, for providing all samples of pristine CNTs for the Raddel, and for fruitful discussions. Thanks to Dr. Belen Ballesteros and Elzbieta Pach in Barcelona, for all the time spent trying to get nice high-resolution images of my samples.

I would like to thank all the Raddel partners that hosted me during my internships and allowed me to have a great experience (not only scientifically), namely Dr. Gerard Tobias in Barcelona, Prof. Maurizio Prato and Prof. Tatiana Da Ros in Trieste, and Prof. Khuloud Al-Jamal in London. And a really special thanks goes to all the Raddel fellows who provided me with samples, or analyzed mine, or simply contributed to the scientific email exchanges. I must thank a lot our project manager, Dr. Jorge Perez, for the impeccable organization in all occasions, for assistance along the Marie Curie ITN and for his very friendly attitude, though always very professional.

I am mostly grateful to Aritz, my Raddel partner and 'personal biologist', for performing all the biological assays and re-explaining them to me a dozen times, for the traveling and lunch company. Thank you for your help during my BCA crazy experiment and for re-drawing the figures for me!

I would like to thank the people that helped me with (or entirely performed) some of the experiments here presented: Olivier Chaloin for the SPR analysis, Isabella for the XPS, Jean-Daniel, with the immunostaining and Julie Russier with gel electrophoresis.

Some of my samples have also been analyzed in the analytical platforms (HR-MS, EA, XPS, NMR, ICP-MS) of the University of Strasbourg and I wish to thank all the technicians that performed them.

And finally I would like to thank Dr. Jésus Raya for all the MAS NMR experiments (which I did not report here) and for all the precious explanations about this technique.

Now, the less official and more enjoyable part.

An immense thanks to my Italian colleagues, with whom I shared most of my time inside and outside the lab! Gloria, grazie, per le interminabili chiacchierate in ufficio, su skype, in sella all'incrocio, per condividere il mio umorismo, per i gossip, perché il tuo non saper dire di no mi è valso della buona compagnia in innumerevoli occasioni! Laura, per l'immancabile buon umore e gli immancabili 'pacchi', la semplicità, gli aneddoti su M, per avermi quasi fatto perdere un timpano e per non aver smesso di parlare un minuto nemmeno dopo 6 ore di macchina. Isabella, la mia ex-compagna di cappa, per la loquacità inziale e la silenziosità finale, e per aver rotto più cose di me. Grazie Alessia per il grande aiuto in lab, i suggerimenti sui nanotubi e non solo. Non mi dimenticherò dello sfortunato bagno di potassa, né delle nostre prelibate cene a frico e prosecco.

And thanks to the other lab mates: Maxime for help in the lab and for the chemical riddles, Julie and Aritz for answering all my naïve biological questions, Dinesh for delicious Indian food and lab help, Raji for psychological assistance for the Thesis and postdoc hunt, Quyen for helping with the western blot and for excessive cheerfulness. Thanks to the crazy japanese girl, piccola Eri, for plenty of hilarious moments and for teaching us how to prepare maki! and thanks to Adriano, Eijiro and Ilaria, and thanks to Suresh for not using the fumehood and leaving me alone in a 3-person one! Thanks to all those that 'self-offered' to proof-read this Thesis, or parts of it, especially Raji, Gloria and Aritz.

I want to warmly thank all the Raddel fellows: it was really amazing to share this project with you all, you were such great companions in this MC network and made it possible for every meeting to be a wonderful scientific, travelling and, most of all, social experience! Thank you Agne, Rebecca, Ela and for your friendship and for taking care of my social life during secondments, and thanks to all the others: Ana, Maxime, Magda & Markus, Anne, Sonia, Reida, Jose, Adem, Robert.

After these three years in Strasbourg I cannot forget: Valentina and Laurence (i miei amici MarieCoolati) for extensive climbing enthusiasm and after-climbing beers; Nadia for sharing these three months of Thesis writing and all the tips related to the submission bureaucracy; Remì, for anticipating it is possible to write a Thesis and be 'relaxed'; it would be too long to duly thanks all the other important people, but thanks to: the Italians from DeCola's group, Melanie, Ingrid, Diane, Vijay (hope you will party for me up there), Olga and all the UPR people, especially those that I bothered with (many) scientific questions.

Thanks to my Freiburg-friends for the support in the initial period of this PhD, it was fundamental: grazie Ste, Checco, Tj, Vincenzo.

I cannot forget to fondly thank my chemical Fathers, Fabrizio and 8, for the endless support and Love they have given me before, during (and most probably after) these three years.

Grazie Mamma e Papà, ancora una volta, per l'affetto e il supporto incondizionato, per continuare ad appoggiare le mie scelte (e per essere venuti per tutti i miei tre –a breve quattro- traslochi!). Vi voglio bene!

All this won't have been possible without: the Marie-Curie funding (thanks --d!), the language exchange meetings, the Tatra-team friends (Irene, Vanessa, Mats, Gloria, the Juliens), le scorte di biscotti Mulino Bianco, le Chariot e i mojitos dell'amico mio.

Thank you all! Merci! Grazie!

Cinzia

ABSTRACT

Doctoral Thesis

by Cinzia Spinato

In the last decades, the application of carbon nanotubes (CNTs) in the biomedical field has been widely explored thanks to their physico-chemical properties and their biocompatibility. By the external and/or internal functionalization of CNTs it is possible to prepare novel conjugates and biomolecular hybrids tailoring different properties and applications. The external decoration of this material by preliminary chemical functionalization is essential to render them biocompatible, water-dispersible and to allow further conjugation of biomolecules. In this research work, we have investigated the covalent derivatization of CNTs by different chemical strategies to achieve a suitable carrier for anticancer therapy. In one project, we have explored the possibility to convert the carboxylic groups of oxidized CNTs into amino groups, and the ability of these conjugates to complex genetic material, for gene delivery. In another project, CNTs have been functionalized with different linkers bearing or not a cleavable disulfide bond, and further conjugated to a therapeutic nanobody (a fragment of antibody), to achieve a controlled intracellular drug release. Ultimately, focusing on the targeted delivery of radiotherapy, we have investigated the reactivity of CNTs filled with radioactivable material (*e.g.* $SmCl_3$, $LuCl_3$) toward [2+1] cycloaddition reactions (namely Bingel and nitrene reactions). We have developed an optimized synthetic approach for the covalent functionalization of close-ended filled CNTs by nitrene reaction, and the conjugation of a targeting antibody, for the delivery of these nanocarriers to specific organs. By exploiting several characterization techniques (*e.g.* thermogravimetric analysis, gel electrophoresis, immunostaining) we have proved that the antibody is covalently grafted to the CNT-carrier and it still possesses its targeting ability. Further investigations on the biological profile of these conjugates (cytotoxicity, targeting, uptake, biodistribution) have been carried out in our laboratories and in collaboration with our partners.

INDEX

Acronyms and Abbreviations

aq.	aqueous
a. u.	arbitrary unit
AuNP	gold nanoparticle
t-BuOH	*tert*-butyl alcohol
Boc_2O	di-*tert*-butyl dicarbonate
Bq	Becquerel
BSA	bovine serum albumin
BuOH	buthanol
CCVD	catalytic carbon vapor deposition
CHO	Chinese Hamster Ovary
Cy	cyclohexane
CNT	carbon nanotube
CT	computed tomography
CVD	chemical vapor deposition
DCC	*N,N'*-dicyclohexylcarbodiimide
DCM	dichloromethane
DBU	1,8-diazabicyclo[5.4.0]undec-7-ene
ddH_2O	distilled deionized water
DEAD	diethyl azodicarboxylate
DIEA	*N,N*-diisopropylethylamine
DMAP	4-dimethylaminopyridine
DMF	*N,N*-dimethylformamide
DMSO	dimethyl sulfoxide
DOTA	1,4,7,10-tetraazacyclododecane-1,4,7,10-tetraacetic acid
DOX	doxorubicin
EDC	1-ethyl-3-(3-dimethylaminopropyl)carbodiimide
EDX	energy dispersive X-ray spectroscopy
EDTA	ethylenediaminetetraacetic acid
EELS	electron energy loss spectroscopy
EGFR	epidermal growth factor receptor
EPR	enhanced permeability and retention

ESI	electrospray ionization mass spectrometer
Et_3N	ethyl amine
Et_2O	diethyl ether
EtOAc	ethyl acetate
EtOH	ethanol
FC	flash chromatography
f-CNTs	functionalized carbon nanotubes
FITC	fluorescein isothiocyanate
FT-IR	Fourier transform infrared spectroscopy
GE	gel electrophoresis
GSH	glutathione
HEPES	4-(2-hydroxyethyl)-1-piperazineethanesulfonic acid
HOBt	*N*-Hydroxybenzotriazole
HR-MS	high resolution mass spectrometry
HRTEM	high resolution transmission electron microscopy
IgG	immunoglobulin
i.v.	intravenous
K.T.	Kaiser test
mAb	monoclonal antibody
MeCN	acetonitrile
MeOH	methanol
MES	2-(*N*-morpholino)ethanesulfonic acid
MRI	magnetic resonance imaging
Ms	methane sulphonyl ($-SO_2CH_3$)
MS	mass spectrometry
MW	microwave
MWCO	molecular weight cut-off
MWCNTs	multi-walled carbon nanotubes
NHS	*N*-hydroxy succinimide
nil	negligible
NIR	near infrared
NMP	*N*-methyl pyrrolidone
NMR	nuclear magnetic resonance
ODCB	*ortho*-dichlorobenzene

ox	oxidized
p	pristine
PEG	polyethylene glycol
PEG_4-SPDP	2-pyridylthiol-tetraoxatetradecane-*N*-hydroxysuccinimide
PET	positron emission tomography
PL-PEG	phospholipidic polyethylene glycol
$Pd(PPh_3)_4$	tetrakis(triphenylphosphine)palladium (0)
Pht	phthalimide
PTFE	polytetrafluoroethylene
Py	pyridine
PBS	phosphate buffered saline
PSA	prostate stem cell antigen
PTT	photothermal therapy
RADDEL	radioactivity delivery
RES	reticuloendothelial system
RGD	arginine-glycine-aspartic acid
r.t.	room temperature
siRNA	small interfering RNA
SPECT	single-photon emission computed tomography
SPECT/CT	single-photon emission computed tomography/computed tomography
SPION	superparamagnetic iron oxide nanoparticle
SPR	surface plasmon resonance
STEM	scanning transmission electron microscope
SWCNTs	single-walled carbon nanotubes
TEG	triethylene glycol
TEM	transmission electron microscopy
TFA	trifluoroacetic acid
TGA	thermogravimetric analysis
THF	tetrahydrofuran
TSTU	*N*,*N*,*N*′,*N*′-tetramethyl-*O*-(*N*-succinimidyl)uronium tetrafluoroborate
VHH	variable domain of heavy chain antibodies
UV-Vis	ultraviolet-visible spectroscopy
XPS	X-ray photoelectron spectroscopy

RESUMÉ DE THÈSE

I. INTRODUCTION

Les nanotubes de carbone (CNTs) sont une nouvelle forme allotropique du carbone telle que le graphite, le diamant et les fullerènes. Ils ont été découverts dans les années 1950/1960,[1,2] mais décrits pour la première fois à l'échelle atomique en 1991 par le chercheur japonais S. Iijima.[3] Au niveau structurel, les CNTs peuvent être représentés comme un ou plusieurs feuillets de graphène enroulés pour former un cylindre fermé ou ouvert aux extrémités. Selon qu'ils soient arrangés en un seul cylindre de graphène ou plusieurs cylindres concentriques, ils dont définis comme nanotubes à paroi simple (SWCNTs pour *Single-Walled Carbon Nanotubes*) ou à parois multiples (MWCNTs pour *Multi-Walled Carbon Nanotubes*) (Figure I.I). Les SWCNTs ont un diamètre qui varie de 0,7 à 3 nm et une longueur comprise entre quelques centaines de nanomètres et plusieurs micromètres, alors que les MWCNTs ont un diamètre qui peut atteindre 100 nm et une longueur qui peut varier jusqu'à quelque dizaines de micromètres.

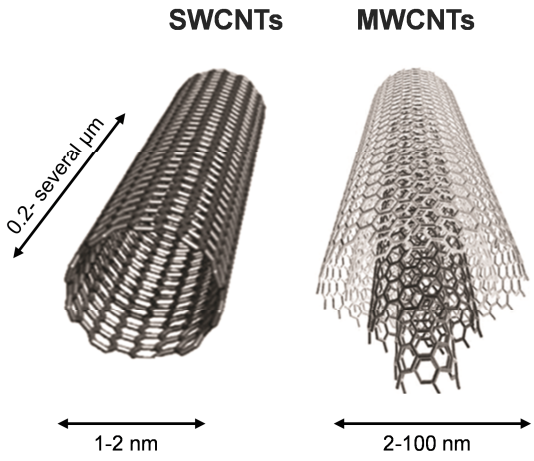

Figure I.I Représentation de nanotubes de carbone à simple paroi et à parois multiples.

La combinaison des propriétés mécaniques, thermiques et électroniques des nanotubes de carbone a permis leur exploitation dans les domaines de la science des matériaux et des nanotechnologies. En 2004, il a été découvert que les CNTs ont la capacité de traverser la membrane cellulaire par un mécanisme énergétiquement indépendant appelé "nanoaiguille".[4] Depuis cette découverte, la possibilité d'utiliser les CNTs comme véhicules pour le transport de médicaments a attiré un grand intérêt dans le domaine de la nanomédecine.[5–7] Il a été démontré que ces matériaux ont la capacité de former des complexes avec du matériel génétique comme l'ADN plasmidique ou les petits ARN interférents et de transfecter des cellules *in vitro*[8] et *in vivo*.[9] Des applications des nanotubes comme substrats pour le développement des cellules neuronales[10] ou comme biosenseurs[11] ont aussi été déjà largement exploitées. Le plus grand problème dans la manipulation des nanotubes, en particulier pour des applications biomédicales, est leur faible solubilité dans les

milieux aqueux. Cet obstacle peut être contourné par la fonctionnalisation de leur surface. Les approches de fonctionnalisation des CNTs à la surface peuvent être classées selon deux catégories:[12]

- fonctionnalisation covalente avec différentes molécules organiques par des réactions sur la surface ou sur les extrémités des nanotubes (*e.g.* cycloadditions ou amidation)

- fonctionnalisation non-covalente de la surface des nanotubes *via* des interactions faibles (*i.e.* forces de van der Waals, interactions hydrophobes, π-stacking).

Une troisième méthode de fonctionnalisation des nanotubes consiste en le remplissage de leur cavité avec des molécules comme des métaux, sels, médicaments *etc.*, aussi nommée fonctionnalisation endohédrale.

Récemment, la multifonctionnalisation des nanotubes de carbone s'est avérée être une approche prometteuse pour lier des molécules avec des caractéristiques spécifiques. Par exemple, la conjugaison d'une molécule médicament et d'un agent de ciblage permet la délivrance du médicament seulement dans les cellules ou l'organe désiré, en empêchant d'éventuels effets indésirables *in vivo* dus à la présence du médicament dans les organes sains. Dans ce contexte, au cours de mes travaux de Thèse, j'ai focalisé mes recherches sur l'étude de la modification des nanotubes par voie covalente pour leur utilisation comme vecteurs de biomolécules. Pendant ma Thèse, j'ai travaillé sur trois projets: l'application de différentes approches pour la conversion des groupes acides carboxyliques de MWCNTs oxydés en amines, dans le but de préparer des conjugués capables de complexer du siRNA (petits ARN interférents). Dans un second projet, j'ai développé des conjugués à base de nanotubes de carbone couplés avec un fragment d'anticorps thérapeutique *via* une liaison clivable afin d'en étudier le potentiel antitumoral. Le dernier projet a été mené en collaboration avec plusieurs partenaires au sein d'un réseau Européen. Il concerne la fonctionnalisation de CNTs remplis avec des molécules radioactivables et fonctionnalisés en surface avec un anticorps de ciblage tumoral. Le but est d'utiliser les nanotubes comme vecteurs pour la délivrance de radioactivité à l'intérieur des cellules tumorales ciblées par l'anticorps. Dans les paragraphes suivants, les résultats de ces trois projets sont détaillés

II. Strategies Chimiques d'Amination de MWCNTs Oxydes pour la Complexation et la Vectorisation de siRNA

Plusieurs études ont démontré des résultats prometteurs en exploitant des CNTs fonctionnalisés pour la vectorisation de matériel génétique *in vitro* and *in vivo*.[9,13] Le but de ce projet était de comprendre plus en détail la relation entre la stratégie de fonctionnalisation de la surface des nanotubes et leur capacité à complexer des siRNA. Dans des études précédentes réalisées au laboratoire, il avait été observé que le type de fonctionnalisation chimique utilisée pour la modification de la surface de MWCNTs oxydés (oxMWCNTs) a une influence sur l'internalisation des CNTs dans les cellules, ainsi que sur leur capacité à libérer le siRNA.[4,14,15] Dans ces études, les CNTs fonctionnalisés avec des fonctions amines *via* un bras espaceur avaient été obtenus par une réaction de cycloaddition 1,3-dipolaire. Dans mon projet de Thèse, je me suis concentrée sur la conversion des groupes carboxyliques présents à la surface des oxMWCNTs en fonctions amines. J'ai essayé plusieurs stratégies synthétiques permettant une transformation directe des groupements carboxyliques des CNTs en amines.

Afin d'envisager des applications dans le domaine biomédical, il est nécessaire de fonctionnaliser la surface des CNTs pour les rendre solubles dans les milieux aqueux, biocompatibles et moins toxiques.[16,17] La première étape de la synthèse des conjugués repose sur l'oxydation des nanotubes en milieu acide sous l'effet des ultrasons. Ce procédé a pour conséquence de raccourcir les nanotubes (de plusieurs microns jusqu'à quelques centaines de nanomètres) et d'introduire des groupes carboxyliques sur les pointes des nanotubes et au niveau des défauts structurels de la paroi qui sont plus sensibles au traitement oxydant. Pour obtenir la conversion des groupes COOH en amines, j'ai étudié et mis en place six stratégies différentes (Schéma II.1), en combinant plusieurs étapes synthétiques ou en suivant des procédures déjà décrites dans la littérature :

I. Réarrangement de Hofmann

II. Réarrangement de Curtius

III. *Via* une réaction de cyanation

IV. Réaction de Hunsdiecker

V. *Via* l'introduction d'un groupement phtalimide

VI. *Via* une réaction de mésylation

Les trois premières approches commencent par l'activation des groupes carboxyliques en chlorures d'acide, suivie de leur dérivatisation et conduisent aux fonctions amines soit *via* un réarrangement (I et II), soit *via* un intermédiaire cyanide. La quatrième stratégie repose sur une réaction de halodécarboxylation (réaction de Hunsdiecker) suivie par la substitution de l'halogène. Dans les deux dernières procédures, la réduction des fonctions carboxyliques est suivie d'une réaction d'amination *via* l'introduction d'un groupement phtalimide (V), ou par dérivatisation séquentielle (VI). La description des six stratégies ne sera pas détaillée dans ce résumé, toutefois le panorama de toutes les voies synthétiques est présenté dans le schéma ci-dessous.

Les différents conjugués ont été caractérisés par différentes techniques complémentaires afin d'étudier les propriétés de surface des nanotubes. En particulier, la morphologie des nanotubes a été observée par microscopie à transmission électronique (MET). Leur structure après fonctionnalisation n'a pas subi de changements par rapport à celles des nanotubes oxydés. La spectroscopie infrarouge à transformée de Fourier et la spectroscopie photoélectronique par rayons X ont confirmé la présence de fonctions amines et ont permis de déterminer le taux d'azote. Par contre, parmi les conjugués, deux ont démontré une très faible dispersabilité dans l'eau. Cette caractéristique est évidement incompatible avec leur application comme vecteur de biomolécules, ces deux échantillons n'ont donc pas utilisés par la suite. Certains échantillons ont été évalués pour leur capacité à complexer efficacement du siRNA et à le transférer dans les cellules. Les études biologiques ont été effectuées en collaboration avec le groupe du Prof. K. Kostarelos à Manchester (Royaume Uni). Nous avons pu démontrer que parmi les échantillons testés, deux présentent une très bonne capacité de complexation du siRNA et sont capables de le transfecter dans une lignée de cellules tumorales (A549) sans générer d'effets toxiques.

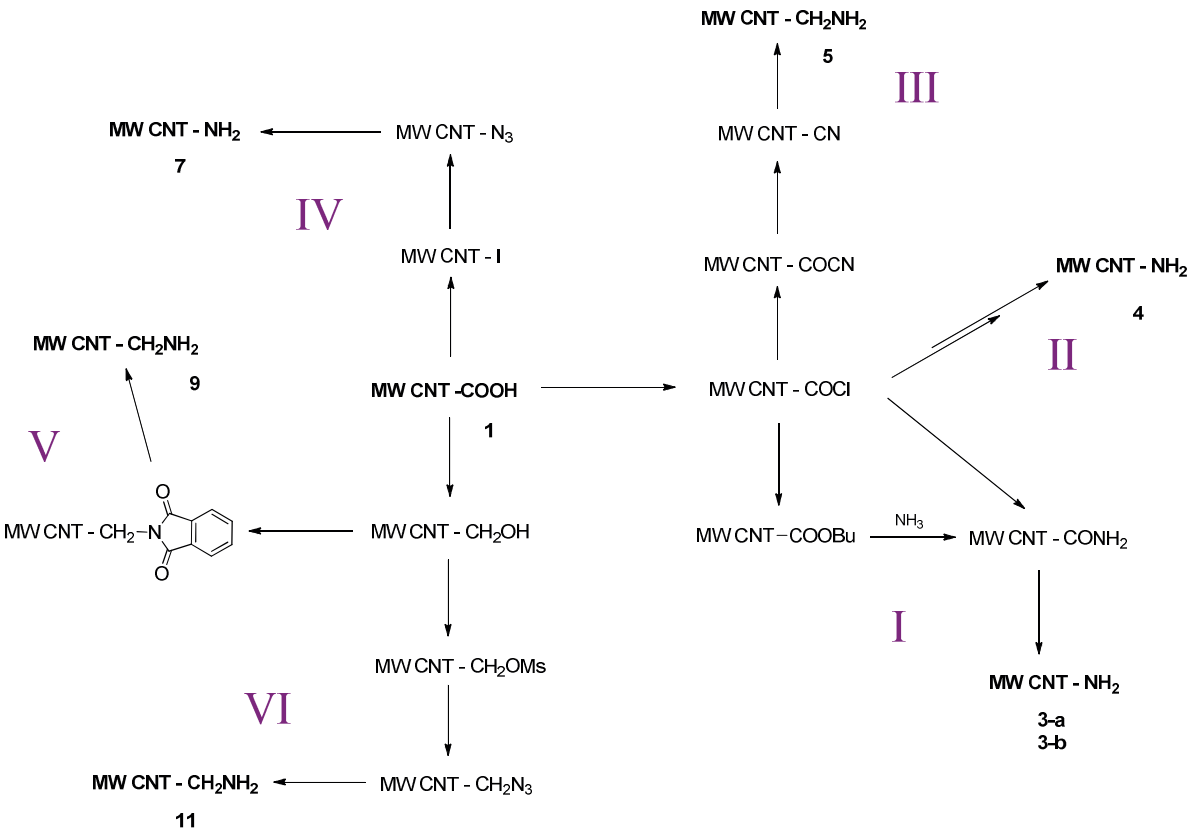

Schéma II.1 Stratégies synthétiques pour la conversion de fonctions COOH en NH_2.

III. Fonctionnalisation de MWCNTs via un Pont Disulfure Clivable pour la Vectorisation d'un Fragment d'Anticorps Therapeutique

Dans ce deuxième projet, j'ai préparé des conjugués de nanotubes avec un fragment d'anticorps ayant des propriétés thérapeutiques et de ciblage de cellules tumorales. Les VHH (high-affinity single variable domain of heavy-chain antibodies) sont constitués du domaine variable des anticorps à chaîne lourde et ils sont considérés comme les plus petits fragments d'anticorps qui conservent la spécificité pour l'antigène.[18] Ils ont attiré beaucoup d'intérêt dans le domaine de la nanomédicine grâce à leurs avantages par rapport aux anticorps, comme par exemple une grande affinité pour leur cible, une faible toxicité et une facilité de production. La société UCB (Royaume Uni), partenaire dans le cadre d'un projet Européen, a préparé un VHH thérapeutique capable de cibler sélectivement la β-caténine, une protéine dont la surexpression est associée à plusieurs cancers. Il nous a semblé intéressant de combiner le potentiel de ce VHH thérapeutique avec la capacité des nanotubes de pénétrer les membranes cellulaires et de vectoriser des molécules à l'intérieur des cellules. Afin de contrôler le relargage du VHH une fois le conjugué internalisé dans les cellules, j'ai introduit un pont disulfure entre les CNTs et le VHH. La liaison S-S est rapidement clivée par des agents réducteurs intracellulaires comme la glutathione (GSH).

A partir de MWCNTs oxydés, j'ai synthétisé un nouveau conjugué (CNT-SS-mal-VHH) constitué de : 1) un bras espaceur à base de triéthylène glycol (TEG) (pour augmenter la solubilité dans l'eau et la biocompatibilité), 2) un lien contenant la liaison S-S et 3) une fonction maléimide

terminale. Ensuite, j'ai attaché le VHH aux CNTs *via* le maléimide qui est une fonction sélective vis-à-vis des thiols tels que ceux qui sont présents dans les protéines (Schéma III.1). Les oxMWCNTs ont été d'abord dérivatisés par amidation avec une chaîne TEG terminée par une fonction amine, obtenant ainsi le dérivé **4**. Le composé **13** a été synthétisé en plusieurs étapes à partir de la cystamine.

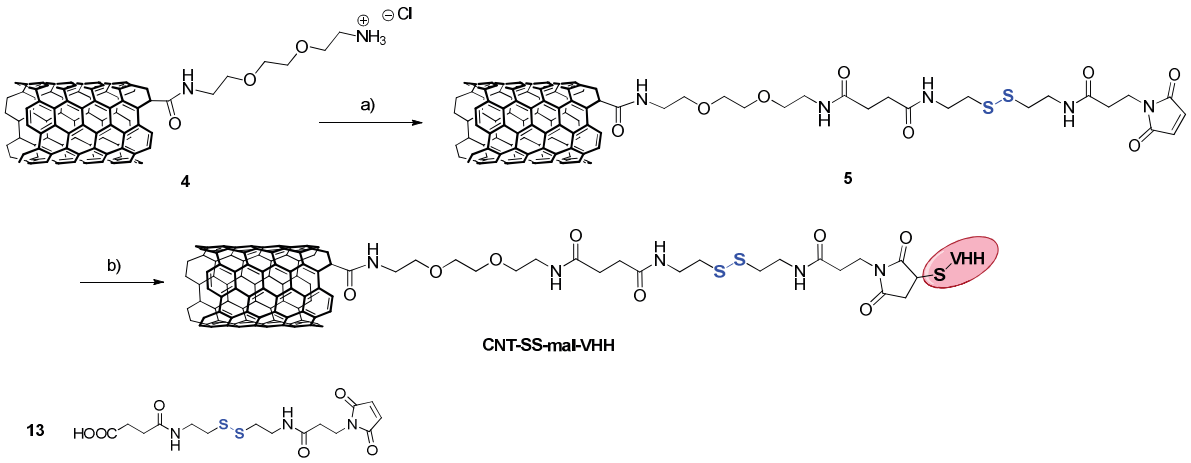

Schéma III.1 Synthèse du conjugué CNT-SS-mal-VHH: a) **13**, DIEA, HOBt, EDC, DMF, t.a., 56 h; b) VHH, EDTA/PBS pH 6.4, t.a., 6 h.

J'ai ensuite synthétisé un deuxième conjugué constitué d'aucun bras espaceur entre le VHH et le site de clivage. Le conjugué **4** a été dérivatisé avec du PEG_4-SPDP, qui est une molécule hétérobifonctionnelle permettant la conjugaison de protéines et qui contient une liaison disulfure clivable ainsi qu'une chaîne de polyéthylène glycol (PEG) à quatre unités oxoéthylènes. La liaison du VHH aux CNTs se fait par échange thiol-disulfure entre un thiol du VHH et la fonction pyridylthiol présentes sur les CNTs fonctionnalisés, conduisant ainsi au conjugué CNT-SS-VHH (Schéma III.2). Enfin, le dernier conjugué (CNT-VHH) ne contenant aucune liaison clivable a été synthétisé à partir des nanotubes fonctionnalisés avec les groupements ammonium **4**.

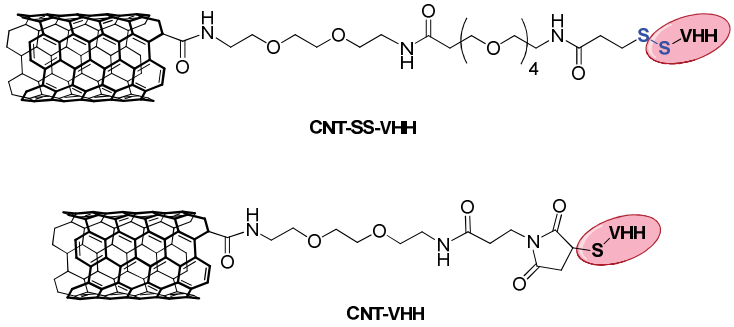

Schéma III.2 Représentation du conjugué avec une liaison disulfure entre les nanotubes et le VHH (CNT-SS-VHH) et du conjugué sans liaison disulfure.

Tous les conjugués ont été caractérisés par différentes méthodes analytiques et la présence du VHH dans les conjugués finaux a été déterminée en utilisant trois techniques: l'analyse thermogravimétrique (ATG), le gel d'électrophorèse et la résonance plasmonique de surface. Par ATG, nous avons pu estimer la quantité de VHH conjuguée aux tubes. Cette technique est basée sur la décomposition thermique des groupes fonctionnels ancrés à la surface des tubes. Le gel d'électrophorèse a permis d'évaluer la nature de la liaison entre les tubes et le VHH (covalente ou non), et de déterminer si celui-ci était toujours intact. L'activité biologique du VHH a été évaluée par résonance plasmonique de surface. Cette technique a permis de montrer que la reconnaissance de

l'antigène par l'anticorps n'a pas été affectée par la conjugaison aux nanotubes. En collaboration avec l'équipe du Prof. K. Kostarelos, des études *in vitro* et *in vivo* ont été effectuées dans le but d'évaluer la capacité des conjugués à exercer leur effet antitumoral dans les cellules et dans des souris. Des études de viabilité cellulaire ont été réalisées sur des cellules du cancer colorectal qui surexpriment la β-catenine. Les trois conjugués sont capables d'induire un effet toxique sur les cellules après 48 heures, bloquant ainsi le chemin de survie des cellules (Figure III.I). Ces résultats suggèrent que le VHH lié aux nanotubes a préservé son effet thérapeutique.

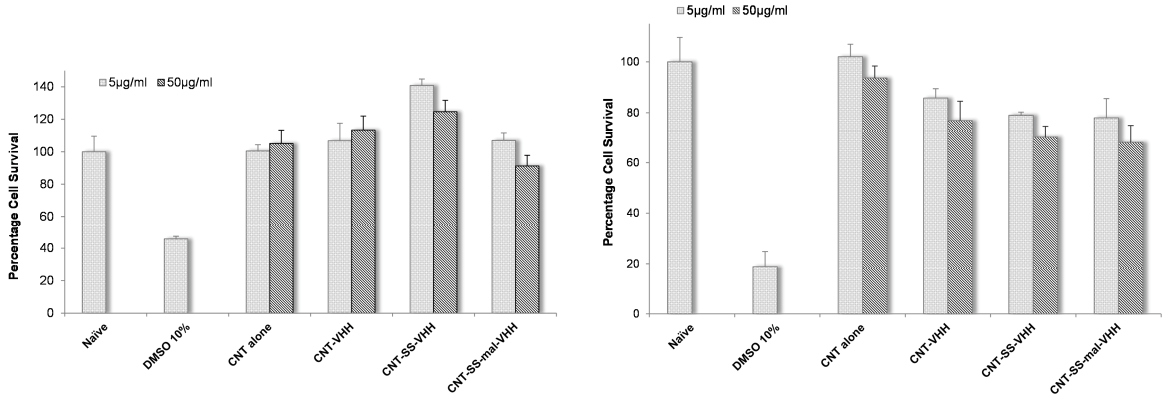

Figure III.I Viabilité cellulaire des cellules du cancer colorectal (HCT116) après (A) 24 h et (B) 48 h d'incubation avec les conjugués suivants : CNT, CNT-VHH, CNT-SS-VHH et CNT-SS-mal-VHH à 5 and 50 µg/ml. DMSO (10%) est utilisé comme contrôle positif.

Les conjugués se sont avérés efficaces pour traiter la tumeur dans la souris. En effet, après injection des CNT-VHH dans des souris inoculées avec le carcinome HCT116, la taille de la tumeur a diminué sensiblement et la survie des souris a été rallongée. Nous n'avons cependant pas observé de différence substantielle entre les conjugués avec la liaison clivable et celui sans liaison S-S. Les résultats sont très encourageants et suggèrent que ces nouveaux conjugués peuvent représenter un outil prometteur pour la délivrance de fragments d'anticorps thérapeutiques.

IV. FONCTIONNALISATION DE CNTS POUR LA VECTORISATION CIBLEE DE RADIOACTIVITE

Ce projet de recherche fait partie du réseau Marie Curie RADDEL (*DELivery of RADioactivity)* qui vise à la mise au point d'un système pour la délivrance ciblée de radioactivité. Le but général est le développement de nanocapsules de carbone remplies avec des isotopes radioactifs, fermées aux extrémités et décorées en surface avec un agent de ciblage et des groupements fonctionnels permettant d'augmenter la biocompatibilité de la nanocapsule.[19] Les radioisotopes choisis pour ce projet sont le chlorure de samarium ($SmCl_3$) et de lutétium ($LuCl_3$), ainsi que l'iodure de sodium. Le remplissage des nanotubes (SWCNTs et MWCNTs) par les radioisotopes a été effectué par l'équipe du Dr. G. Tobias à Barcelone (Espagne). Au sein de ce réseau, notre groupe s'est focalisé sur le développement de méthodes pour la fonctionnalisation covalente de différents types de CNTs remplis, en particulier des réactions de cycloaddition [2+1] (réaction de Bingel et cycloaddition de nitrènes) qui conduisent à la formation de cycles à 3 chaînons sur la surface des CNTs (Schèma IV.1).[20] Dans les deux cas, j'ai utilisé des précurseurs organiques constitués par une chaîne TEG pour augmenter la dispersabilité des tubes dans l'eau, et terminés par une fonction amine protégée

par un phtalimide. Ainsi, après clivage du groupement protecteur par traitement avec de l'hydrazine, les fonctions amines ont été quantifiées par le test de Kaiser test et dérivatisées avec des molécules d'intérêt.

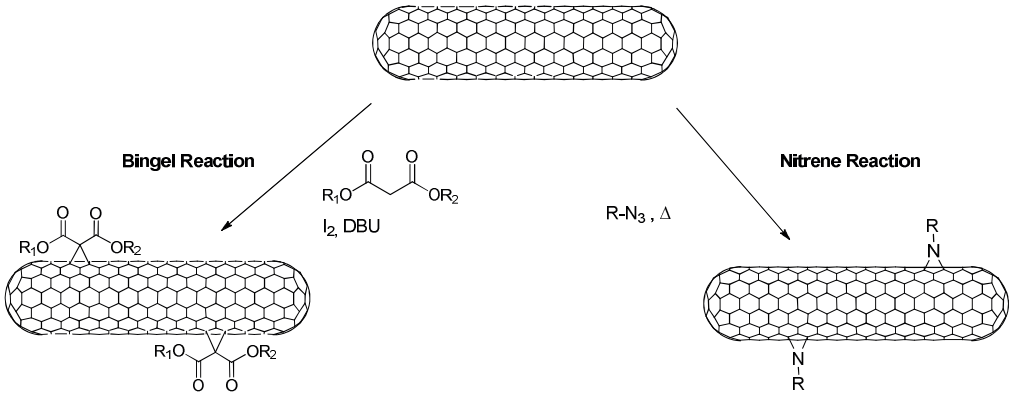

Schéma IV.1 Fonctionnalisation des nanotubes de carbone par réaction de Bingel et cycloaddition de nitrènes.

La réaction de Bingel implique des malonates et conduit à la formation de cyclopropanes à la surface des CNTs.[21,22] J'ai testé la réaction de Bingel sur des CNTs vides et remplis en utilisant différents types de précurseurs malonates dérivatisés avec des chaînes TEG et portant une fonction amine terminale. Plusieurs conditions de réaction ont été essayées en modifiant la température, le temps ou le solvant de réaction, ou en utilisant des micro-ondes. Toutefois, je n'ai pas réussi à obtenir des valeurs de fonctionnalisation satisfaisantes.

Par contre, la fonctionnalisation des CNTs remplis par cycloaddition de nitrènes a conduit à des taux de fonctionnalisation satisfaisants. Cette réaction s'effectue en présence d'un azoture portant une chaîne TEG et induit la formation de cycles aziridines sur la paroi des nanotubes.[23,24] En plus du test de Kaiser et de l'ATG, les CNTs fonctionnalisés ont été caractérisés par MET à haute résolution après dérivatisation des fonctions amines avec un groupement fonctionnel iodé. Nous avons ensuite optimisé un certain nombre de paramètres (*e.g.* température, solvant, temps de réaction, micro-ondes) afin de trouver les meilleures conditions de réaction donnant les plus hauts degrés de fonctionnalisation dans le temps le plus court. J'ai ensuite dérivatisé les CNTs portant les fonctions amines terminales avec un groupement maléimide pour pouvoir conjuguer un anticorps spécifique afin de cibler des cellules tumorales (Figure IV.I). Cette stratégie n'a cependant pas permis d'atteindre des taux de fonctionnalisation satisfaisants.

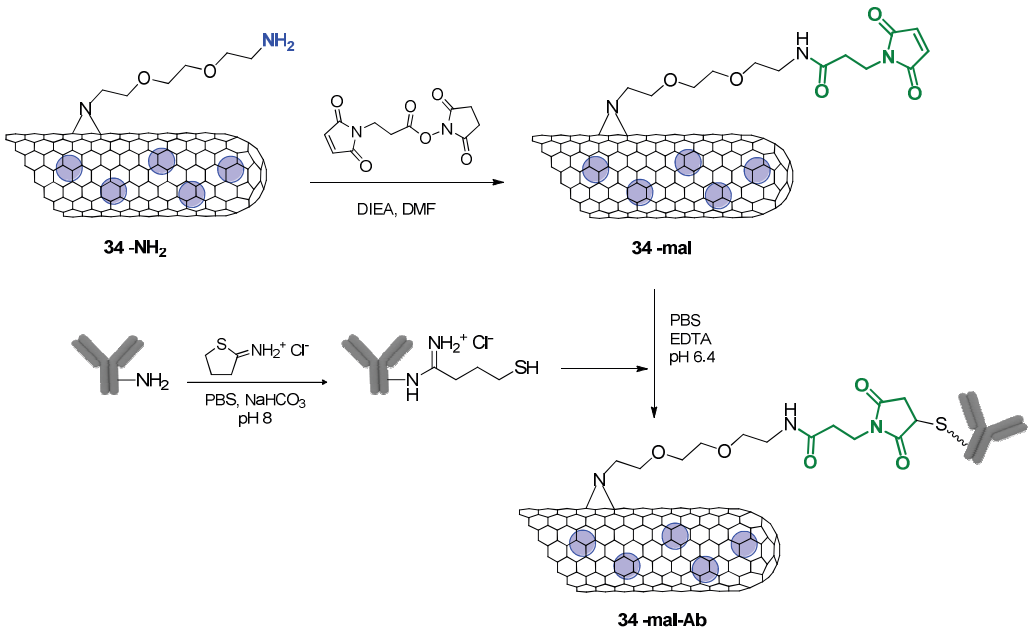

Figure IV.I Dérivatisation de CNTs remplis et fonctionnalisés par cycloaddition de nitrènes, avec une maléimide, suivi par la conjugaison de l'anticorps.

Nous avons utilisé une stratégie alternative en attachant l'anticorps directement aux nanotubes par une réaction d'amidation entre les amines présentes sur les CNTs et les groupes carboxyliques de l'anticorps (Figure IV.II).

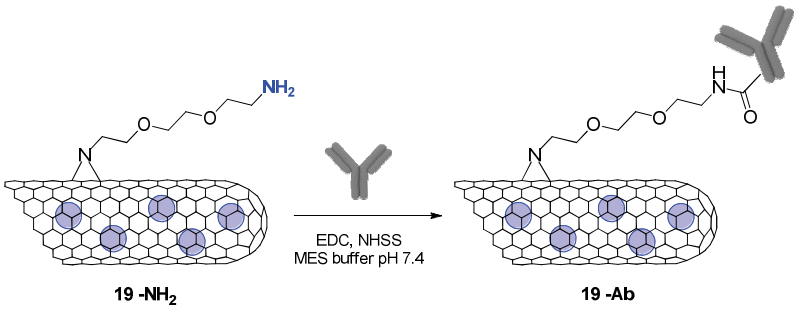

Figure IV.II Conjugaison de l'anticorps aux CNTs remplis et fonctionnalisés par cycloaddition de nitrènes.

En plus de l'ATG et du gel d'électrophorèse, la présence de l'anticorps dans les conjugués a été déterminée par MET *via* une expérience d'immunomarquage en utilisant un antigène complémentaire marqué avec des billes d'or. Celles-ci sont bien visibles à la surface des nanotubes, confirmant la présence de l'anticorps, alors que pour les réactions de contrôle (mélange non-covalent de CNTs et d'anticorps) il n'y a presque pas de billes visibles (Figure IV.III).

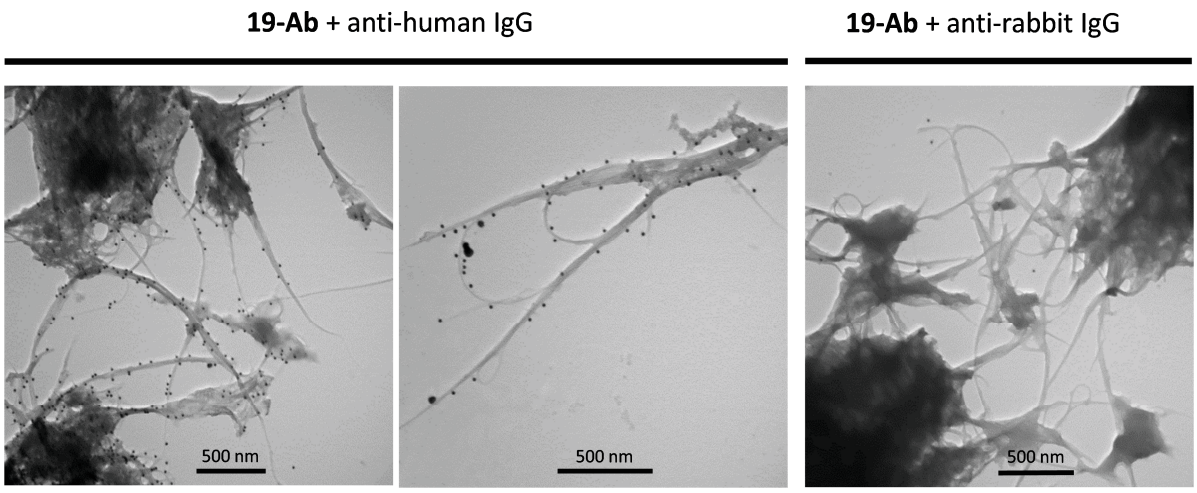

Figure IV.III Images MET du conjugué covalent (**19-Ab**) et du conjugué obtenu par la réaction contrôle (**19/Ab**) après marquage avec un anticorps secondaire anti-humain relié à des billes d'or (anti-human IgG).

Les conjugués CNTs-anticorps ont ensuite été testés *in vitro* et *in vivo* afin d'en étudier le profil toxicologique et les propriétés biologiques. Les essais *in vitro* sur des macrophages murins RAW264.7 (Figure IV.IV) et des cellules humaines primaires du sang (PBMC) ont montré une bonne viabilité cellulaire.

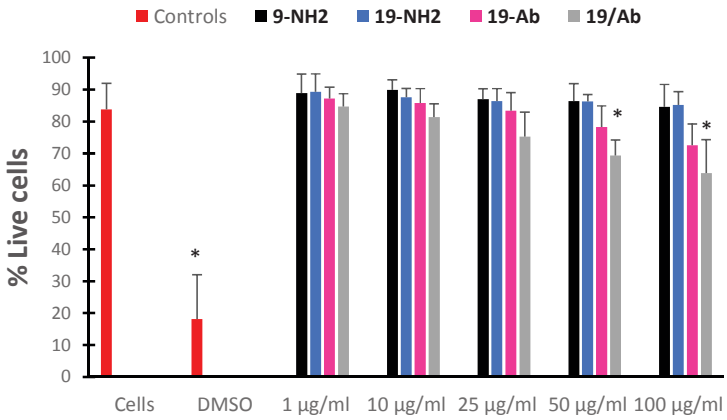

Figure IV.IV Viabilité cellulaire de macrophages RAW264.7 après 24 heures d'incubation avec **9-NH_2** (précurseur aminé des nanotubes vides), **19-NH_2** (précurseur aminé des nanotubes remplis), **19-Ab** (conjugué covalent) et **19/Ab** (conjugué contrôle) à différentes concentrations (1, 10, 25, 50 et 100 µg/ml). Les barres rouges représentent le contrôle positif (cellules non traitées) et négatif (DMSO 20%).

De plus, aucune toxicité apparente, ni de réponse pro-inflammatoire n'ont été observées dans les études *in vivo*, soulignant une bonne biocompatibilité des conjugués. D'autres études biologiques sur la capacité des conjugués à cibler efficacement les cellules tumorales ont été effectuées dans notre laboratoire et en collaboration avec l'équipe du Prof. K. Al-Jamal (Londres). Deux lignées cellulaires tumorales ont été incubées avec les conjugués de CNT-anticorps : une lignée qui surexprime le facteur EGFR (cellules U87) et l'autre qui ne l'exprime pas (cellules CHO). Nous avons observé que les CNT-anticorps reconnaissent bien leur cible et qu'ils sont internalisés par les cellules U87, alors qu'il n'y a pas d'interaction avec les cellules CHO (Figure IV.V). De plus, le conjugué précurseur (**19-NH_2**) qui n'a pas d'anticorps n'est internalisé par aucune des deux lignées cellulaires, suggérant qu'il n'y a pas d'interactions non-spécifiques entre les nanotubes et les cellules. Nous avons tout de

même remarqué qu'il n'y a pas de différences substantielles entre le conjugué covalent et le conjugué contrôle.

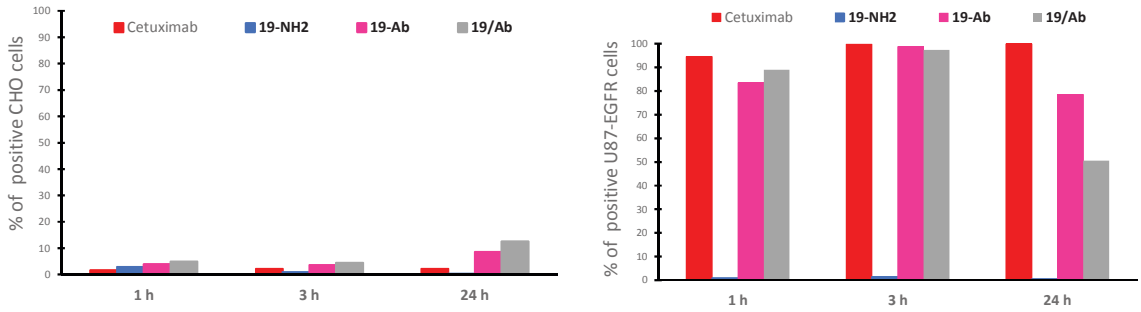

Figure IV.V Barres représentant le pourcentage de cellules positives à la cyanine 3 dans la lignée cellulaire CHO (à gauche) et U87 (à droite) après incubation pendant 1, 3 ou 24 heures avec les conjugués **19-NH_2**, **19-Ab** et **19/Ab** à 10 µg/ml.

Des études d'internalisation et de ciblage ont été effectuées avec les nanotubes conjugués avec un anticorps marqué avec une sonde fluorescente (cyanine 5). Les résultats ont également montré que la capacité de ciblage de l'anticorps est préservée après sa conjugaison avec les nanotubes.

La fonctionnalisation des nanotubes après radioactivation des isotopes, ainsi que les tests biologiques sur un modèle de souris tumorale ont été effectués très récemment. L'analyse des données est en cours d'évaluation.

Nous pouvons tout de même conclure que cette stratégie de fonctionnalisation des nanotubes remplis basée sur la réaction de nitrènes suivie par la conjugaison direct de l'anticorps est efficace. Elle pourrait être de plus utilisée avec d'autres anticorps (pour cibler d'autres tumeurs) ou bien avec d'autres radioisotopes (pour varier le type de radiation).

V. BIBLIOGRAPHIE

[1] R. Bacon, *J. Appl. Phys.* **1960**, *31*, 283.

[2] A. Oberlin, M. Endo, T. Koyama, *J. Cryst. Growth* **1976**, *32*, 335.

[3] S. Iijima, *Nature* **1991**, *354*, 56.

[4] D. Pantarotto, R. Singh, D. McCarthy, M. Erhardt, J.-P. Briand, M. Prato, K. Kostarelos, A. Bianco, *Angew. Chem. Int. Ed.* **2004**, *43*, 5242.

[5] F. Lu, L. Gu, M. J. Meziani, X. Wang, P. G. Luo, L. M. Veca, L. Cao, Y.-P. Sun, *Adv. Mater.* **2009**, *21*, 139.

[6] K. Kostarelos, A. Bianco, M. Prato, *Nat. Nanotechnol.* **2009**, *4*, 627.

[7] E. Heister, E. W. Brunner, G. R. Dieckmann, I. Jurewicz, A. B. Dalton, *ACS Appl. Mater. Interfaces* **2013**, *5*, 1870.

[8] K. T. Al-Jamal, F. M. Toma, A. Yilmazer, H. Ali-Boucetta, A. Nunes, M.-A. Herrero, B. Tian, A. Eddaoudi, A. Eddaoui, W. T. Al-Jamal, A. Bianco, M. Prato, K. Kostarelo, *FASEB J.* **2010**, *24*, 4354.

[9] J. E. Podesta, K. T. Al-Jamal, M. A. Herrero, B. Tian, H. Ali-Boucetta, V. Hegde, A. Bianco, M. Prato, K. Kostarelos, *Small* **2009**, *5*, 1176.

[10] G. Cellot, E. Cilia, S. Cipollone, V. Rancic, A. Sucapane, S. Giordani, L. Gambazzi, H. Markram, M. Grandolfo, D. Scaini, F. Gelain, L. Casalis, M. Prato, M. Giugliano, L. Ballerini, *Nat. Nanotechnol.* **2009**, *4*, 126.

[11] W. Yang, K. R. Ratinac, S. P. Ringer, P. Thordarson, J. J. Gooding, F. Braet, *Angew. Chem. Int. Ed.* **2010**, *49*, 2114.

[12] P. Singh, S. Campidelli, S. Giordani, D. Bonifazi, A. Bianco, M. Prato, *Chem. Soc. Rev.* **2009**, *38*, 2214.

[13] Z. Zhang, X. Yang, Y. Zhang, B. Zeng, S. Wang, T. Zhu, R. B. S. Roden, Y. Chen, R. Yang, *Clin. Cancer Res.* **2006**, *12*, 4933.

[14] K. T. Al-Jamal, L. Gherardini, G. Bardi, A. Nunes, C. Guo, C. Bussy, M. A. Herrero, A. Bianco, M. Prato, K. Kostarelos, T. Pizzorusso, *Proc. Natl. Acad. Sci. U. S. A.* **2011**, *108*, 10952.

[15] A. Battigelli, J. T.-W. Wang, J. Russier, T. Da Ros, K. Kostarelos, K. T. Al-Jamal, M. Prato, A. Bianco, *Small* **2013**, *9*, 3610.

[16] A. Bianco, K. Kostarelos, M. Prato, *Chem. Commun.* **2011**, *47*, 10182.

[17] K. Kostarelos, *Nat. Biotechnol.* **2008**, *26*, 774.

[18] M. M. Harmsen, H. J. De Haard, *Appl. Microbiol. Biotechnol.* **2007**, *77*, 13.

[19] S. Y. Hong, G. Tobias, K. T. Al-Jamal, B. Ballesteros, H. Ali-Boucetta, S. Lozano-Perez, P. D. Nellist, R. B. Sim, C. Finucane, S. J. Mather, M. L. H. Green, K. Kostarelos, B. G. Davis, *Nat. Mater.* **2010**, *9*, 485.

[20] A. Hirsch, *Angew. Chemie Int. Ed.* **2002**, *41*, 1853.

[21] H. Hu, B. Zhao, M. A. Hamon, K. Kamaras, M. E. Itkis, R. C. Haddon, *J. Am. Chem. Soc.* **2003**, *125*, 14893.

[22] K. S. Coleman, S. R. Bailey, S. Fogden, M. L. H. Green, *J. Am. Chem. Soc.* **2003**, *125*, 8722.

[23] M. Holzinger, J. Abraham, P. Whelan, R. Graupner, L. Ley, F. Hennrich, M. Kappes, A. Hirsch, *J. Am. Chem. Soc.* **2003**, *125*, 8566.

[24] Y. Jiang, C. Jin, F. Yang, X. Yu, G. Wang, S. Cheng, Y. Di, J. Li, D. Fu, Q. Ni, *J. Nanoparticle Res.* **2011**, *13*, 33.

CHAPTER 1

INTRODUCTION

Abstract – Carbon nanomaterials such as nanotubes and graphene arouse great research interest, by virtue of their outstanding properties for different applications. A major concern is the investigation of their behavior in a biological environment and beforehand of their functionalization and thorough characterization. For a better comprehension of the research strategies and experimental investigations that we have undertaken, in the following Introduction chapter we will provide a general description of carbon nanotubes structure, production and chemical modification, along with an overview of the state-of-art of their applications in the biomedical field.

1.1 Structure, Synthesis and Properties

Since immemorial time graphite and diamond have been the only known allotropic forms of carbon. It was only in the late 20th century that the number of carbon allotropes started to increase, thanks to the discovery of many new carbon nanostructures (*e.g.* fullerene, carbon nanotubes, graphene, carbon nanohorns). Since then, these fascinating and unprecedented architectures generated a great research interest among the scientific community. Indeed, the fortunate discovery of fullerene C_{60} in 1985 was internationally recognized by the award of the Nobel Prize to Kroto, Curl and Smalley.[1] Only few years after, in 1991, Iijima remarked the growth of layered microtubular structures made of carbon atoms organized in a honeycomb lattice.[2] Despite observations of hollow carbon fibers in the nanometer scale were reported already in the 60's-70's,[3–5] it was only after Iijima's structural elucidation that scientists started to look at carbon nanotubes (CNTs) as a potential field of research.[6] Since then, carbon nanotube popularity increased remarkably maybe overpassing that of their spherical brother.

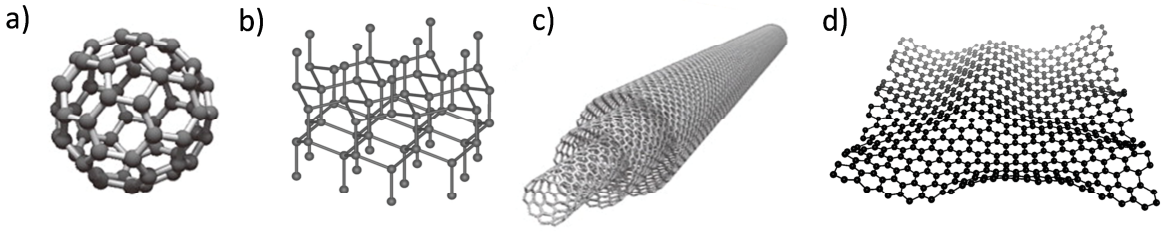

Figure 1.1 Structural representations of some recently discovered carbon allotropes: a) fullerene, b) nanodiamonds, c) carbon nanotubes and d) graphene.

Carbon nanotubes can be described as hollow cylindrical tubes solely made of carbon atoms, with diameters ranging between 1 and 100 nm, and lengths up to the order of millimetres. The carbon atoms in a CNT have a sp^2 hybridization and are arranged in a honeycomb lattice such as in graphite, endowing the whole molecule with extended aromaticity. A single carbon nanotube can be ideally formed by rolling up a sheet of graphene along its length with a certain degree of twist. The way the hexagonal rings are joined together defines the nanotube chirality (*e.g.* armchair, zigzag) and it uniquely determines the tube diameter, curvature and electronic properties, such as their metallic or semi-conducting character.[7] The tips of the tubes can be either open, presenting reactive dangling bonds, or closed by dome-shaped half-fullerene molecules. Carbon nanotubes are generally classified by the number of concentric graphene layers. Single-walled carbon nanotubes (SWCNTs) are constituted by one single cylinder and have diameters ranging from 0.7 to 2 nm, whereas multi-walled carbon nanotubes (MWCNTs) display from 2 to several concentric layers, and they are consequently larger, with external diameter from few to tens of nanometres.

Despite the structural similarity of carbon nanotubes with graphite, which is also constituted of hexagons of sp^2-hybridized carbon atoms, the physico-chemical properties of these two materials are substantially different. Indeed, CNTs possess extraordinary strength, thermal and electrical conduction efficiency, along with unique mechanical, optical and chemical properties.[8] All these attractive features rapidly allowed to propose CNTs as valuable building blocks for the preparation of new materials which have already proved their applicability in different technological fields such as photovoltaics,[9] molecular electronics,[10,11] material science[12] and nanomedicine.[13] Nowadays, we can see that the initial interest of scientists toward carbon nanotubes is being rewarded by their

commercial outlet. In fact, CNTs are already incorporated in some commercial products for daily lives.[14] For example, MWCNTs are used as electrically conductive additive to polymers for electrostatic painting, or integrated into water filters for the removal of bacteria and viruses, or even in sporting goods. Thanks to their electrical conductivity, nanotubes are also currently used in lithium ion batteries and field emission sources for displays, and for the preparation of gas detection transistors. Therefore, nowadays there is a strong need of multi-ton quantities of these compounds in a high purity degree, and lots of research is still dedicated to improving and scaling-up their synthesis and purification. In the following paragraph we will briefly introduce the main methods for the production and purification of CNTs.

1.1.1 PRODUCTION AND PURIFICATION METHODS

CNT production has been largely investigated since their discovery, and several techniques have so far been developed, most of them involving gas phase processes.[8,15,16] Among the most established techniques are arc discharge, laser ablation and chemical vapor deposition (CVD). In the first two methods, CNTs are formed by the rearrangement of carbon atoms vaporized from graphite, therefore very high temperatures are required to sublimate graphite (~3200 °C). In the CVD process instead, the carbon sources are hydrocarbons (like methane, ethane, ethanol, etc.) which are thermally decomposed at temperatures between 700 and 1000 °C in the presence of catalysts.[8] The axial growth of nanotubes initiates from metal particles implanted in a porous substrate affording very long and vertically arranged nanotubes. In most production methods, metallic nanoparticles (*e.g.* Fe, Co, Ni) are employed to catalyse the nanotube growth, and this implies that a purification step is necessary to remove these impurities from the final batch.

The arc discharge method allows the large-scale production of CNTs that generally display few structural defects and good electrical and mechanical properties; hence this technique is sometimes favored for certain material applications.[17] The synthesis of CNTs by laser ablation has the main advantages of affording nanotubes in a relatively high yield and with rather low content of metallic impurities, but this method is overall quite expensive because it encompasses the use of high-purity graphite and high-power lasers.[15] Currently, the CVD technique has been substituting the high temperature methods to synthesize CNTs at the industrial level, since it allows a large-scale and low cost production of CNTs, together with better control of the nanotubes length, diameter, alignment and purity.[16] The fact that by CVD the CNTs growth occurs on pre-designed lithographic surfaces is advantageous for some applications as it enables to produce ordered arrays of CNTs.[16,18] Moreover, CNTs produced by CVD are usually preferred for their application in biological fields because of the lower content of residual catalyst.

All these methods lead to mixtures of CNTs that exhibit different chiralities, diameters and lengths. In addition, variable amounts of impurities and undesired by-products are usually present in the final material, such as amorphous carbon, graphitic particles and metal catalysts (if employed). Hence, the purification and sorting of nanotubes are imperative before their usage, to obtain more homogenous and pure batches of pristine nanotubes. Depending on the production method, there are many different ways for nanotube purification; however it should be noted that the removal of by-products/impurities is generally more costly than the production itself. Purification strategies can involve filtrations, solvent washings for the removal of catalysts and fullerenes, oxidation techniques to eliminate graphitic particles.[19] Some other non-destructive methods for CNT separation include

size-exclusion chromatography, density-gradient ultracentrifugation or simply dispersion in colloidal suspension by use of surfactants, polymers or colloidal particles.[16] Nevertheless, these techniques have been so far only applied on a small scale of CNTs and not at the industrial level.

1.1.2 Properties of Carbon Nanotubes

Depending on the production method, the properties of CNTs can greatly vary. Carbon nanotubes are usually characterized by their diameter, chirality and degree of defects, which are important parameters as they determine their electronic properties, especially for SWCNTs. In fact, the behavior of SWCNTs can vary from metallic to semi-conducting. The electrical conductivity of CNTs is even higher than that of copper as electrons are conducted without dissipation of energy in the form of heat. Furthermore, CNT conductivity can be modulated by doping the carbon lattice with other atoms, such as boron and nitrogen.[15] Compared to their allotropes, nanotubes show an incredibly high tensile strength (up to 100 GPa), which is due to the sp^2 hybridization of the carbon atoms. Indeed, the C-C bond in CNTs is much stronger than the sp^3 bond of diamond and it endows the nanotubes with very interesting mechanical properties. As a result of the bond strength, CNTs are very resistant to high temperatures (up to 750 °C at normal pressure) and are very good thermal conductors.[16] CNTs do also exhibit remarkable elasticity, permitting their axial twist and bend without ruptures. All these properties can differ between single- and multi-walled CNTs. Generally, SWCNTs have a lower degree of defects, but MWCNTs present higher tensile strength due to the multiple layers.

Because of their long fiber-shape and hollow cavity, CNTs are characterized by a very high aspect ratio and large surface area, which render them interesting for many applications. However, the extended aromatic surface of CNTs determines a high polarizability, propelling the formation of strong van der Waals inter-tube interactions and thus facilitating their aggregation into spaghetti-like bundles. This strong tendency toward aggregation severely depletes CNT solubility, hampering their manipulation and limiting their usage. Addition of chemical groups to the nanotube sidewalls, in either a covalent or non-covalent way, disrupts the bundles enhancing the dispersibility of the nanotubes in different solvents. The external modification of CNTs is therefore highly advantageous to their employment, although it can dramatically alter their functional properties, such as the electronic and optical ones, hence limiting their potential for material applications.

1.2 Functionalization

Understanding the properties of CNTs and developing their practical applications have been hindered for a long time by their extremely low solubility in all conventional solvents. Hence, the effort toward the functionalization of CNTs was driven both by the need to circumvent CNT insolubility and difficult manipulation, and by the possibility of modifying their functional properties in a controlled manner. In the past decades, a great slice of nanotube research has been devoted to the development of approaches for CNT functionalization, and much literature can be found on the subject.[10,20–25] Essentially, the modification of CNTs can be achieved by covalent attachment of molecules at the defect sites or at the sidewalls, or by non-covalent interaction of organic or

inorganic molecules (Figure 1.2). A special case of non-covalent functionalization is the endohedral filling of CNTs with atoms or small molecules. By covalent functionalization, functional groups are grafted to the skeleton of CNTs through chemical reactions and this approach generally affords chemically stable conjugates. The non-covalent functionalization is instead based on weak interactions, such as van der Waals forces, charge interaction or π-π stacking, between a molecule and the nanotube surface (internal or external). The main advantages offered by this approach are the fact that it is non-destructive, thus it does not affect the nanotube lattice, and can allow the release of the adsorbed (or encapsulated) molecules.

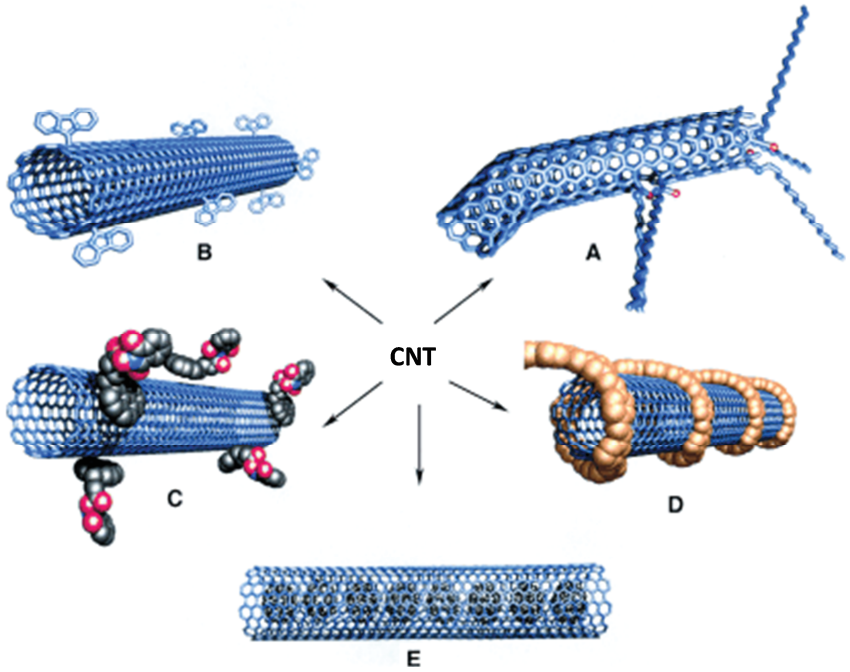

Figure 1.2 Functionalization possibilities for CNTs: A) defect-group functionalization, B) covalent sidewall functionalization, C) non-covalent exohedral functionalization with surfactants, D) non-covalent exohedral functionalization with polymers, and E) endohedral functionalization with, for example, C_{60}. For methods B–E, the tubes are drawn in idealized fashion, but defects are found in real situations. Image adapted from ref. [20].

A largely explored approach is the combination of both covalent and non-covalent functionalization, which consents to impart multimodalities to the CNTs extending the scope of their potential applications.[26] It is now widely recognized that the external modification of carbon nanotubes is necessary for their employment for bioapplications, especially for drug delivery, as CNTs need to meet the basic requirements of water-dispersibility.[27] Moreover, the functionalization of CNTs allows decreasing cytotoxicity and improving biocompatibility, besides giving the opportunity for the conjugation of drug molecules, proteins or genes, for the construction of advanced delivery systems.[28,29] By immobilizing different types of bioactive molecules onto CNTs, in a covalent or non-covalent way, it is possible to impart them targeting, diagnostic and therapeutic abilities, which makes them very appealing as nanocarriers.

It is worth mentioning that in some cases the word *functionalization* is employed to name also other types of CNT modifications, such as in-lattice doping or intercalation, however in this Thesis we will only refer to the conventional functionalization strategies partly portrayed in Figure 1.2. In the following sections we will introduce the main approaches for the covalent and non-covalent functionalization of CNTs, with a bigger emphasis on the covalent strategies. A brief paragraph will be also dedicated to the multi-functionalization of CNTs derived from the combination of covalent

and non-covalent methods, whereas the endohedral functionalization will be addressed in detail in a specific section in Chapter 4.

1.2.1 COVALENT FUNCTIONALIZATION

In the context of chemical reactivity, CNTs can be considered either as extended π-conjugated systems or as electron deficient alkenes. Indeed, the highly aromatic hexagonal network is susceptible of a wide range of chemical reactions.[20,24] A fundamental role in the reactivity of CNTs toward covalent bonding is played by defects on the external surface. Defects introduced during the production method and post processes (*i.e.* purification, separation) are considered topological. They include pentagon–heptagon pairs and can reach around 1-3% of all carbon atoms present.[30] Alternatively, defects can also be created by the covalent attachment of reactive molecules on the nanotube lattice. As CNTs are ideally made of sole sp^2-bonded carbon atoms, the covalent addition of an atom to the exterior of a nanotube would change the hybridization of one or more C atoms to sp^3, engendering a new defect site. In general, these structural imperfections can increment the local reactivity of the CNTs, although they concomitantly compromise their electrical and mechanical properties.[31,32] Furthermore, the presence of discrete amounts of defects destroys the straight shape of CNTs increasing their flexibility, which has an overall significant effect on their toxicological profile.[33,34]

The covalent functionalization of CNTs is usually performed according to two main approaches: (i) derivatization of oxidized CNTs by amidation or esterification, and (ii) sidewall functionalization by addition reactions. The first approach is also known as 'defect-site chemistry', as the anchoring of functionalities to the tubes exploits preexisting, or intentionally created, defects on the CNT scaffold after their oxidation. On the other hand, the sidewall functionalization occurs by addition of a new atom (or molecule) on the π-system of the tubes triggering the rehybridization of the carbon atoms. The two approaches can also be simultaneously performed on the same CNTs (*e.g.* double or triple functionalization), to combine multiple functionalities and tailor different properties, as we will briefly discuss in the following paragraphs.

1.2.1.1 Defect-site functionalization

The defect-site functionalization of CNTs usually consists in amidation or esterification reactions performed at the carboxylic groups of oxidized nanotubes. Generally, oxidation of CNTs is carried out by treatment with oxidizing agents such as nitric/sulfuric acids mixtures,[35,36] piranha solution (H_2O_2/sulfuric acid)[37] or $KMnO_4$,[38] which are the most common methods to process pristine nanotubes. In fact, as received pristine CNTs can contain a discrete amount of impurities, such as catalyst particles and amorphous carbon, depending on the production method. The oxidative treatment is commonly performed as initial step in CNT defect-site functionalization, as it allows to remove these impurities and to obtain shorter open-ended tubes with many oxygenated functions. These groups are mainly carboxylic acids and they are mostly located at the tips of nanotubes, as it was visually demonstrated by Prato and co-workers with scanning tunneling microscopy (STM) images of oxidized CNTs functionalized with alkyl chains by amidation (Figure 1.3).[39]

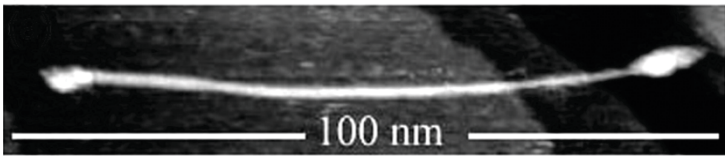

Figure 1.3 STM image of oxidized SWCNTs functionalized with 1-octylamine, showing irregularities at the terminal parts, which were attributed to the functional chains. Image reproduced from ref. [39].

Following oxidation, CNTs become water-soluble and stable in solution, due to the shorter length and the hydrophilicity conveyed by the oxygen-containing groups. Oxidized CNTs are then optimal precursors for the further introduction of desired functionalities through amidation or esterification. Generally, the carboxylic groups are first converted into acyl chlorides by reaction with thionyl or oxalyl chloride, and then reacted with an amine or an alcohol to afford the respective amide or ester (Scheme 1.1). Alternatively, the activation of the carboxylic acid functions can be performed in milder conditions using carbodiimide-based coupling reagents (*e.g.* 1-ethyl-3-(3-dimethylaminopropyl) carbodiimide), as described by Jiang *et al*., who employed this strategy to graft a protein onto the nanotubes.[40]

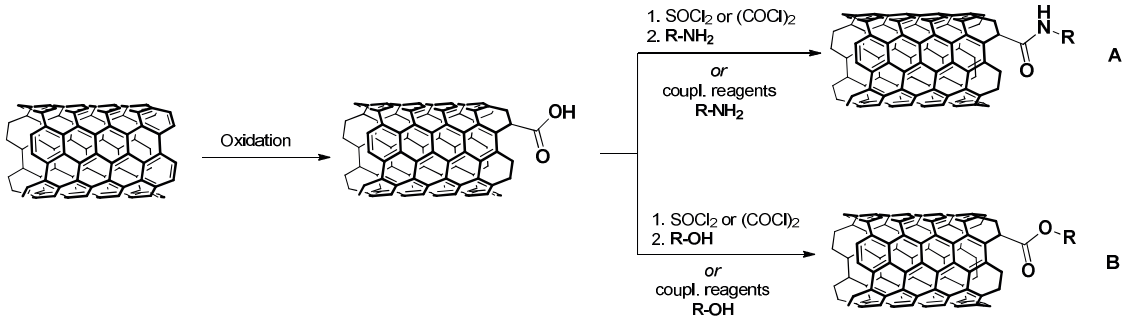

Scheme 1.1 Oxidation of CNTs followed by activation and amidation (A) or esterification (B). For clarity, a SWCNT fragment is represented with only one single added functional group.

Amidation and esterification have been extensively used to append several types of functionalities onto CNTs, like fullerene derivatives[41] and porphyrins,[10] for charge-transfer nanohybrids, or peptides, DNA and drugs, for delivery applications.[25,42]

1.2.1.2 Sidewall functionalization

The covalent functionalization of CNTs by addition chemistry is a very interesting strategy for the appendage of molecules to the nanotubes, especially because it allows their distribution all along the sidewalls. However, these addition reactions usually require very reactive species (*e.g.* carbenes, nitrenes, or halogens) and harsh conditions for the formation of the covalent bonds, so it is difficult to keep control over the chemo- and regioselectivity of the reaction. Two parameters that influence the sidewall reactivity are the degree of defects and the curvature. It has been reported that SWCNTs are generally more reactive than MWCNTs toward the same type of reaction: this accounts to the smaller diameter of SWCNTs and to the layered nature of MWCNTs, which renders the inner layers inaccessible.[43]

Up to date, the fan of possibility for the sidewall functionalization of CNTs is very broad and vary, comprehending reactions such as cycloadditions (Diels-Alder, [2+1] and [3+2]), radical addition, halogenation, electrophilic or nucleophilic additions. Extensive descriptions of these reactions has

been reported in many reviews.[25,44] The aim of the following discussion is to give a panoramic view of the different possibilities and introduce the most commonly used reactions.

1.2.1.2.1 Halogenation

One of the first proposed methods to attain the functionalization of nanotube sidewalls is fluorination, which leads to the attachment of single fluorine atoms to the carbon lattice. Fluorination usually involves elemental fluorine or CF_2 and rather high temperatures (up to 600°C), and can afford high degrees of functionalization.[45] The increased reactivity of fluorinated CNTs can be exploited for further derivatization by nucleophilic substitution of the fluorine atom using Grignard or organolithium reagents. In a similar way, CNTs can be brominated by using Br_2, plasma-based bromine treatment or *N*-bromosuccinimide in milder conditions.[46,47] Nanotube iodination was instead obtained by UV irradiation of oxidized CNTs in the presence of iodosobenzene diacetate by a modified Hunsdiecker reaction.[48]

1.2.1.2.2 Cycloaddition Reactions

Cycloaddition reactions are among the most used strategies for the direct functionalization of CNTs, as they allow to tether chains of variable nature and length onto the nanotube sidewalls, sensibly increasing their dispersibility. By properly selecting the functional groups of the appended chains it is possible to further derivatize the CNTs and possibly graft any type of molecule. The most common cycloaddition reactions performed on CNTs are: i) 1,3-dipolar cycloaddition, ii) Diels-Alder reaction, and iii) [2+1] cycloadditions of nitrenes or carbenes.

The 1,3-dipolar cycloaddition, also known with the name of Prato's reaction, is a [3+2] cycloaddition. It consists in the addition of an azomethine ylide generated *in situ* by the thermal condensation of an α-amino acid and an aldehyde derivative, and leads to the formation of a pyrrolidine ring fused to the C-C bond of CNTs (Scheme 1.2 -a). The reaction can also be performed under solvent-free microwave irradiation,[49] or using different substrates such as aziridine derivatives[49] or zwitterions resulting from the addition of pyridine to acetylene derivatives.[50] The attractiveness of this reaction is represented by the fact that it works efficiently on most CNT types (pristine, oxidized, SW- or MWCNTs), and that a number of different conjugates can be prepared by simply varying the functional groups on the aldehyde or the side chain of the amino acid.[51] 1,3-Dipolar cycloaddition has been widely exploited to covalently attach to nanotubes electron-donors, such as ferrocene,[52] or biologically active molecules, such as peptides, antibodies and drugs.[53]

The reactivity of CNTs toward Diels-Alder reaction is also broad, since the nanotubes can act either as dienophiles or dienes, depending on the reaction partner (Scheme 1.2 -b). In fact, CNTs can react with maleimide derivatives as dienophiles, or with furan as dienes.[54] Fluorinated SWCNTs have shown to be very reactive toward a wide range of dienes due to the activating effect of the electron-withdrawing fluorine atoms.[55] Nevertheless, this [4+2] cycloaddition is not always a suitable method for CNT functionalization because of the reversibility of the reaction.

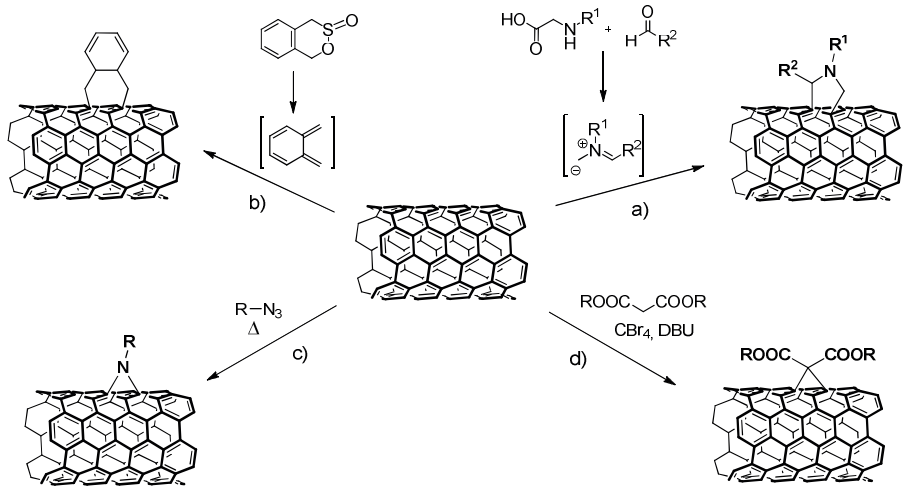

Scheme 1.2 Examples of cycloaddition reactions on CNTs: a) 1,3-dipolar cycloaddition, b) Diels-Alder reaction, c) nitrene and d) Bingel reaction.

CNTs have been also functionalized by [2+1] cycloaddition of nitrenes and carbenes, which leads to the formation of 3-membered rings on the CNT sidewalls. Nitrene reaction is performed starting from azide derivatives, which can generate very reactive nitrene intermediates by thermolysis or photolysis. The electrophilic attack of the nitrene to the π-conjugated system of CNTs occurs with extrusion of N_2 and engenders an aziridine ring involving a C-C bond from the nanotube (Scheme 1.2 -c).[56] In a similar way, *in situ*-generated carbenes can react with nanotubes forming cyclopronane rings.[57] A more common cyclopropanation reaction is the Bingel reaction, which is operated by carbanionic species originated from malonate derivatives (Scheme 1.2 -d).[58] A more detailed discussion about [2+1] reactions will be covered in Chapter 5.

Cycloaddition reactions, but also amidations and esterifications, are often performed employing alkyl chains featuring a protected-amine as terminal group, such as phthalimide- or Boc-protected amines. After cleavage of the protecting group, the amine can be easily quantified by colorimetric tests (*e.g.* Kaiser test), thus allowing the quantification of the degree of functionalization. By using a linker with a terminal alkyne or azide group, it is otherwise possible to further functionalize CNTs by click-chemistry, forming triazole rings on the functional chain. This approach has been exploited to graft molecules that could be sensible to certain cycloaddition reaction conditions, such as polymers, chromophores and nanoparticles.[59,60]

1.2.1.2.3 Radical Additions

Another very common route to functionalize nanotubes and sensibly increase their solubility is the radical addition of aryl diazonium salts, which was first described by Tour's group.[61] On a first instance, they reported the arylation of SWCNTs using diazonium salts obtained *via* electrochemical reduction of aniline derivatives in the presence of $NOBF_4$. The same group later affirmed that arylation of CNTs could be achieved also by direct treatment with aryl diazonium tetrafluoroborate salts in solution or with the corresponding amine, which, in the presence of isoamyl nitrite, is transformed *in situ* into the corresponding diazonium (Scheme 1.3).[62] The reaction between aryl diazonium salts and CNTs probably proceeds *via* highly reactive aryl radical intermediates. Hudson *et al.* devised an interesting way to perform the arylation of SWCNTs in aqueous solution using aniline and triazene derivatives for the *in situ* formation of the diazonium intermediate.[63] Some researchers exploited diazonium-based functionalization strategies to graft photoactive compounds to

CNTs, like phtalocyanines or porphyrins, affording conjugates that exhibit exceptional optical and electron transfer properties and are exploitable for the development of optoelectronic devices.[64,65]

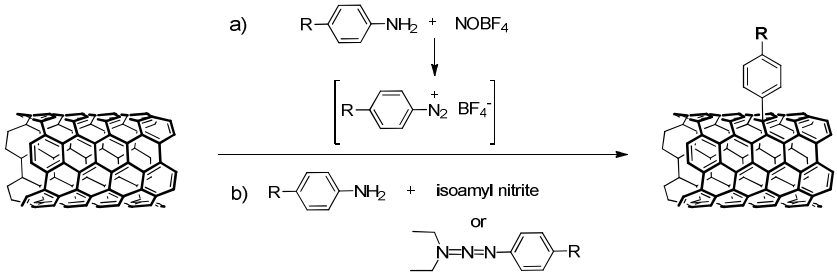

Scheme 1.3 Functionalization of CNTs using (a) preformed diazonium salts or (b) *in situ* generated diazonium salts.

1.2.1.2.4 Electrophilic and Nucleophilic Additions

Alkyl functions can also be introduced on nanotubes by electrophilic or nucleophilic addition reactions. For example, CNTs can undergo Friedel-Craft acylation, as reported by Balaban *et al.*, who prepared polyacylated SWCNTs starting from an acyl chloride derivative and a Lewis acid (Scheme 1.4 -a).[66] Tertiary amines have been introduced on MWCNTs by a deprotonation-carbometalation reaction in the presence of butyl lithium, followed by an electrophilic substitution with bromo-derivatives. Direct alkylation of carbon nanotubes can be as well accomplished by nucleophilic addition of organometallic reagents such as *n*BuLi, EtLi, *t*BuMgCl (Scheme 1.4 -b).[67] This reaction is highly selective toward metallic SWCNTs, and the reactivity is influenced by the steric hindrance of the nucleophile and the nanotube diameter.

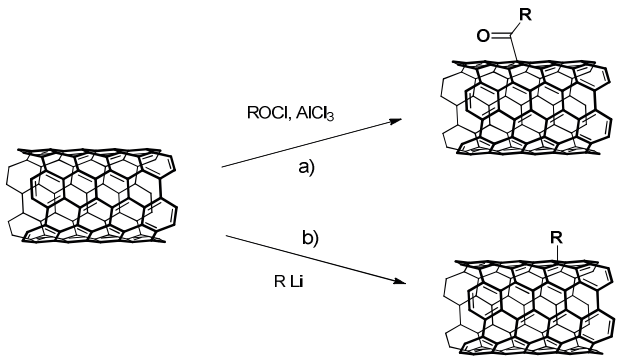

Scheme 1.4 Functionalization of CNTs by (a) Friedel-Craft acylation and (b) nucleophilic addition of an organolithium compound.

1.2.2 NON-COVALENT FUNCTIONALIZATION

Non-covalent functionalization of carbon nanotubes has been widely exploited as a non-destructive method to increase their dispersibility and to tailor specific applications by selecting the appropriate coating compound. Indeed, stable solutions of CNTs can be obtained by dispersing them with amphiphilic surfactants, polymers, polynuclear aromatic compounds or biomolecules. The driving forces for this supramolecular interaction are usually van der Waals forces, π-π stacking, charge-transfer and hydrophobic interactions. Early investigations on CNT non-covalent functionalization

were driven by the need to bring them in solution and disentangle the bundles in order to obtain individualized nanotubes.[68] Nowadays, very stable suspensions of individually dispersed nanotubes can be attained both in aqueous and organic solutions.[69] Typically, the dispersion of nanotubes in solution is assisted by ultrasonication as this triggers the formation of gaps and spaces within the bundles. If these unstable gaps are accessible to the dispersing agent, this one will intercalate between the CNTs impeding their re-aggregation and ultimately separating them into isolate tubes.[70,71] The solubilization of the nanotubes in water is generally based on the non-covalent interactions of amphiphilic molecules (surfactants) with the tube surfaces: while the hydrophilic part interacts with water, the hydrophobic one adsorbs onto the nanotube surface solubilizing them and preventing their aggregation. The structures of the hydrophilic groups of surfactants can be very diverse and their nature defines the efficiency of the CNT dispersion (Figure 1.4). For example, charged surfactants stabilize nanotube dispersions by electrostatic repulsion, while neutral surfactants create a large solvation shell by wrapping around the nanotube.[72,73] Length and shape of the alkyl chains do also play an important role for the efficiency of the interaction between the surfactant and CNTs: longer and more branched chains are more solubilizing than linear and straight ones.[74,75] Nevertheless, many surfactants are stable only at high concentrations, due to their high critical micellar concentration, and this is a drawback when it comes to their employment for biological applications because an excess of surfactant can cause cell membrane lysis or protein denaturation.[76]

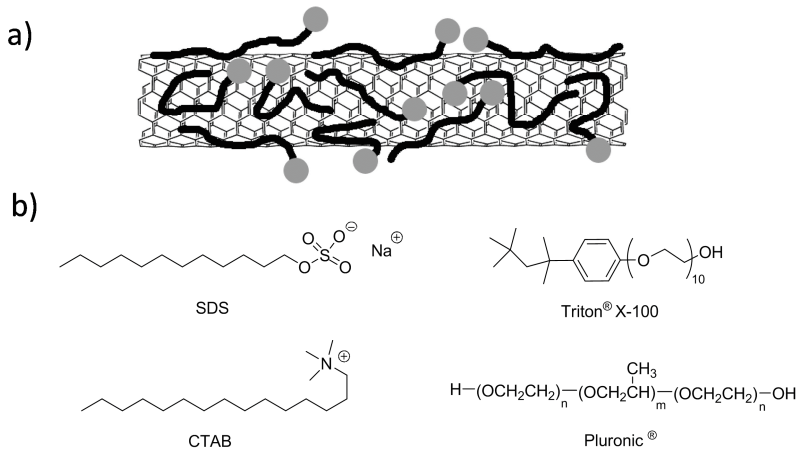

Figure 1.4 (a) Schematic representation of the random adsorption of surfactant molecules onto the SWCNT sidewalls. (b) Chemical structures of some of the most used surfactants and polymers (SDS: sodium dodecyl sulfate; CTAB: hexadecyltrimethylammonium bromide). Figure adapted from ref. [73].

The presence of aromatic moieties within the surfactant can also be helpful due to the formation of π-π stacking interactions with the graphitic nanotube surface. Compounds such as porphyrin and pyrene derivatives proved to efficiently adsorb onto CNTs with large degree of coverage.[72,77] The group of Harada interestingly profited of this capacity to construct a water soluble hybrid conjugate of SWCNTs functionalized with β-cyclodextrins (β-CDs), previously anchored to a molecule of pyrene (Py).[78] The aromatic moiety of pyrene permitted the interaction with the nanotubes, while cyclodextrins added polarity to the system. They then exploited the supramolecular host-guest potential of the appended cyclodextrins to prepare gel-sol switchable SWCNT hydrogels (Figure 1.5).

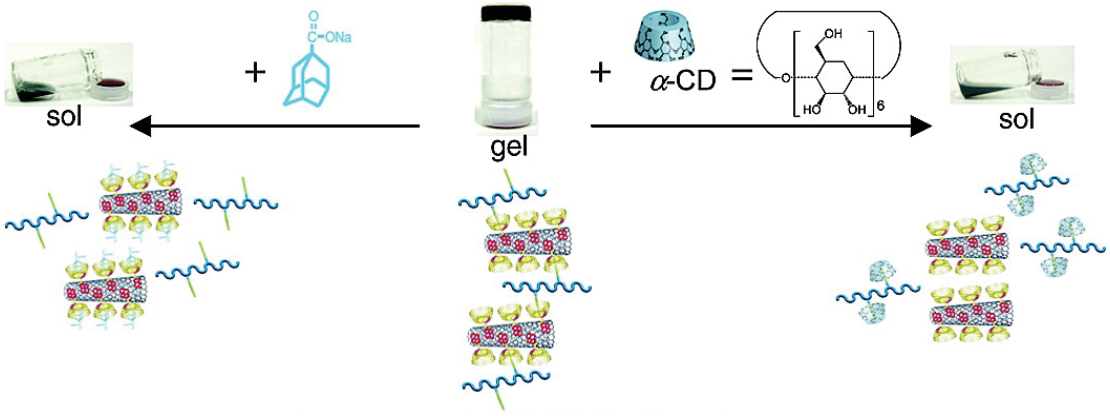

Figure 1.5 Hydrogel of SWCNTs and β-CDs prepared by π−π interaction between pyrene (red) modified β-CDs (yellow) and SWCNTs (center). Gel to sol transition upon addition of a competitive guest such as adamantane carboxylate (left) and α-CDs (right). Figure adapted from ref. [78].

Supramolecular conjugates of CNTs with polymers have been variously investigated with the aim of matching polymer applications with nanotube physical properties.[79] CNT-polymer composites have been prepared with polystyrene, polypropylene, polyphenylene-vinylene (PPV) and many others, and have found application as lightweight reinforcing materials or optoelectronics. Some polymers can even wrap around CNTs with a helical arrangement to overcome the conformational strain imposed by the rigidity of the tubes.[24]

Interestingly, many biological molecules have shown the capability to adsorb onto nanotubes, and this has broadened the range of CNT applications in the biological field. Immobilization of biomolecules onto CNTs has been reported for peptides, proteins, mono- and polysaccharides, phospholipids and nucleic acids.[42,80] For instance, proteins work very well in dispersing nanotubes: the supramolecular interaction between the two is enhanced by the π-π stacking between the graphitic surface and the aromatic amino acid residues of the protein sequence. The adsorption of biomolecules onto CNTs allows the combination of the conducting properties of the latter with the recognition ability of the biomolecule, obtaining new bioelectronic systems exploitable as advanced biosensors.[24] For example, a conjugate of CNT with glucose-oxidase, an enzyme that catalyses the oxidation of glucose, has been integrated into an electrode and this apparatus is now employed in clinical tests for the voltammetric detection of glucose.[81,82]

1.2.3 Multi-functionalization of Carbon Nanotubes

Multiple functionalization of carbon nanotubes has been extensively used as a powerful approach to attach two or more different functionalities and thus endow the final conjugate with multimodal properties. Multi-functionalization strategies relies on the combination of different covalent approaches (*e.g.* arylation and amidation), multiple non-covalent functionalization, or combination of covalent and non-covalent approaches (Figure 1.6). Moreover, up to three or four different functionalization strategies can be performed on the same conjugate, hence the range of possibilities is very broad and allows a great versatility. This synthetic strategy has been particularly exploited to prepare CNT constructs dedicated to bioapplications, as it consents to simultaneously conjugate them with a targeting molecule, a fluorescent probe and a therapeutic agent.[26,42]

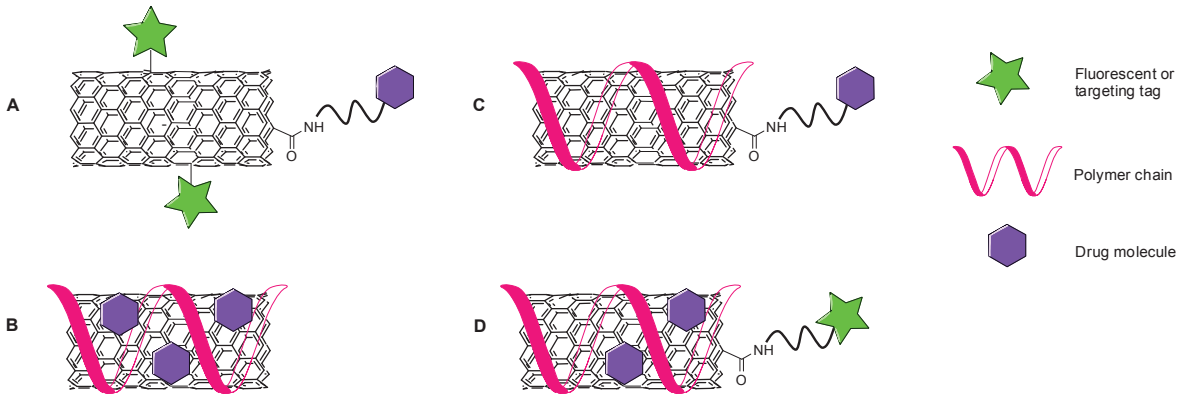

Figure 1.6 Examples of multi-functionalization approaches: A) double covalent approach, B) double non-covalent approach, C) mixed covalent and non-covalent approach, D) mixed triple functionalization.

In 2006 our group reported one of the first examples of double functionalization of CNTs, which were covalently derivatized by 1,3-dipolar cycloaddition with two different functional chains. After selective cleavage of the two orthogonal protecting groups, the free amines were conjugated in one case with a fluorescent probe and in the other with an anticancer molecule.[83] In another example, the anticancer drug doxorubicin (DOX) was adsorbed onto SWCNTs previously functionalized with a phospholipidic PEG (PL-PEG) either by amidation of the carboxylic groups or by non-covalent adsorption.[84] In this report, Liu *et al.* proved that despite the PL-PEG wrapped around the tubes, these were still able to be loaded with a relevant amount of DOX. Many other groups have developed CNT-based nanocarriers for the delivery of different drugs, such as doxorubicin and paclitaxel, usually by loading the molecule onto CNTs previously functionalized with a polymeric chain (*e.g.* polysaccharides, PEG, phospholipids) and/or a targeting agent (*e.g.* antibody, RGD [arginine–glycine–aspartic acid] peptide, folic acid [FA]).[42] An innovative example of multimodal CNT functionalization was reported by Lu *et al.* who developed a magnetic dual-targeted hybrid nanocarrier combining the advantages of MWCNTs and those of magnetic iron oxide nanoparticles (MIONP), and exploited it for drug delivery and chemotherapy (Figure 1.7).[85] MWCNTs were first functionalized with poly(acrylic acid) (PAA) by free radical polymerization, and subsequently decorated with MIONP in a non-covalent way. The targeting ligand folic acid was then grafted by carbodiimide-mediated amidation between the COOH of PAA onto MWCNTs and the NH_2 of FA. A fluorescent probe, fluorescein isothiocyanate (FITC), was also conjugated to the nanocarrier by spontaneous covalent bonds formation with the residual surface amino groups, while DOX was finally loaded *via* both π–π stacking and hydrogen bonding.

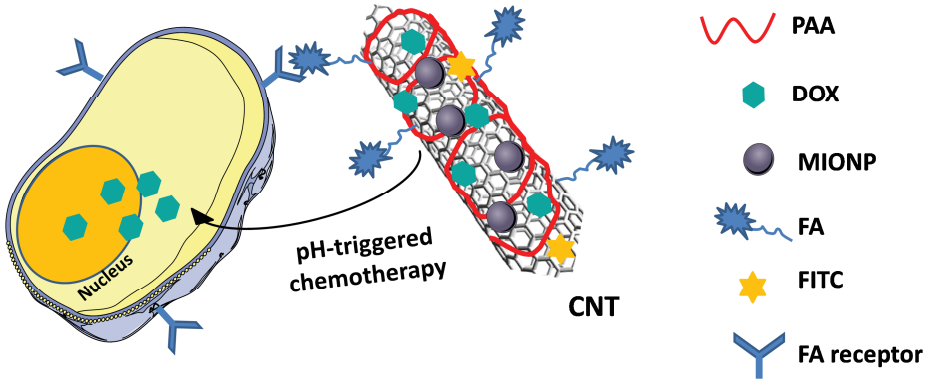

Figure 1.7 Schematic representation of *in vitro* pH-triggered DOX delivery and release using FITC/FA-PAA/MIONP/MWCNT nanohybrids. Adapted from ref. [85].

This interesting multiple synthetic approach provides dual targeted delivery of the anticancer drug to cancer cells under the guidance of a magnetic field and through ligand–receptor interactions. *In vitro* studies allowed to verify that this conjugate was efficiently taken up by U87 glioblastoma cells and the subsequent intracellular release of DOX caused enhanced cytotoxicity compared to the free drug.

1.3 Carbon Nanotube Applications for Therapy and Imaging

It is already consolidated that CNTs can have applications in different fields, spanning from materials science, such as optoelectronic, composites, sensors, to many bio-related areas, like biosensing, imaging, delivery and prosthetics. Because the research of this Thesis is related to the preparation of CNT carriers for cancer therapy, in this section we will give an overview of the major applications of CNTs in the biomedical field, with a particular focus on those destined to cancer therapy. To this purpose, CNT-based constructs have been used as vehicles to deliver drugs, genes, radiotherapy, or as direct tools for hyperthermia or photoacoustic therapy. These applications will be briefly outlined, joined with a few remarkable examples.

1.3.1 Carriers for Cancer Therapy

Why are CNTs good candidates as carriers?

Carbon nanotubes, along with many other nanoparticles, have started to be considered as potential entities exploitable for therapeutic uses thanks to their nanometer size and their tunable surface properties. Indeed, the pharmacokinetics and pharmacodynamics, and thus the efficacy of a therapeutic tool, are highly dependent on its morphological properties (size, shape, surface), together with its ability to induce cell death (into the tumor tissues). Nanoparticles are very attractive from the point of view of their size compared to classic molecular therapeutics or to bigger size particles (> several micrometers). On one hand, nanosized particles (> 10 nm) can escape a too rapid excretion by the blood stream, resulting in longer circulation times. On the other hand, too big particles are not suitable as delivery systems because they can be trapped inside the smallest capillaries before reaching the target, or be engulfed by the phagocytic cells triggering adverse effects for the body. In addition, the nanosize of these particles is suitable to achieve the so-called 'passive targeting'. The vasculature in tumor tissues displays increased fenestration, resulting in an easier percolation and accumulation of these particles (< 500 nm) through the blood vessels by the so-called enhanced permeability and retention (EPR) effect.[86] This phenomenon is in fact widely exploited in the design of drug delivery systems because it allows the selective accumulation of the nanoparticles within the tumor tissues with higher concentration than in the healthy ones.[87] Furthermore, the high aspect ratio of CNTs is, for example, very advantageous for the construction of delivery systems, because high amounts of payloads can be attached to their surface and carried inside the body, thus increasing the drug bioavailability. However, due to this large surface area available, it is important to have a good control over the surface properties of the nanoparticles (surface charge, type and amount of functional groups, structure). Finally, specific targeting ligands can be attached to the nanoparticles, endowing them with site-selectivity and somehow enhancing the cellular uptake, thanks to the ligand interaction with cellular receptors. Overall, the possibility to tune a nanoparticle circulation time by

control of its size and shape, together with the targeting ability, greatly enlarges the potential of nanoparticles for therapeutic use.[87–90]

The pioneer exploration of CNT applicability in the nanomedical field was certainly prompted by their belonging to the nanomaterial family. However, CNTs soon demonstrated to be very valuable candidates thanks to their ability to easily cross the cellular membrane and to vehicle inside the cells various payloads, from small drug molecules to bigger size pharmaceuticals (*e.g.* proteins, genetic material). In fact, upon functionalization, CNTs can be imparted with an amphiphilic character that allows them to be homogeneously dispersed in physiological media and at the same time interact with organic moieties such as the membrane phospholipidic bilayer or water-insoluble drugs. Moreover, the possibility to anchor different functionalities onto CNTs by their multi-functionalization, further raised the interest toward their exploitation in the biomedical field. To this scope, many groups have dedicated intense efforts to design and build CNT-based constructs to be employed as therapeutic platforms, and at present a wide library of these construct has been reported.[28,91–93]

1.3.1.1 CNTs for Drug Delivery

The large surface area of carbon nanotubes offers a great possibility to reach high loading of drug molecules and consequently reduce the required therapeutic dosage. Thanks to their aromatic character, CNTs are an ideal platform to carry inside the cells hydrophobic drugs that are poorly soluble in water. The loading of a drug onto CNTs can be accomplished through several approaches, according to its chemical structure. By a fully covalent approach, the drug can be connected to the nanotube solely by covalent bonds, eventually *via* a spacing chain, elsewise, a drug molecule can be linked to a polymeric chain wrapping the CNTs. Alternatively, it can be directly adsorbed on the backbone by π-stacking or, finally, small size drugs can be encapsulated in the CNT cavity.[26,28,42,93] Up to now, CNTs have been decorated with small anticancer drugs, such as DOX, cisplatin, Paclitaxel (PTX), methotrexate (MTX),[42,93] but also with therapeutic antibodies and antiviral or antibacterial drugs.[42,94] For the efficacy of a drug delivery system, besides the conjugation of the drug to the carrier, it is important that the drug integrity is preserved until the final destination, and that its release and restoration occur in the desired location. For example, most of CNT/DOX constructs exploit the strong π-π interaction between the two moieties to carry DOX inside tumor cells, where the acidic pH triggers its release from the tube surface.[42] Another valuable approach is to anchor the drug to the CNTs through a cleavable linker that can be selectively cleaved in certain environmental conditions (*e.g.* pH) or by specific enzymes (see Chapter 3).[95–97] For example, Liu *et al.* covalently conjugated PTX, a widely used chemotherapeutic drug, to PEG chains on SWCNTs *via* a cleavable ester bond, obtaining a water-soluble SWCNT-PTX construct (Figure 1.8). They demonstrated that the conjugate accumulation into tumor tissues was ten times more than that of the free drug Taxol®, and ascribed this to the EPR effect. Moreover, the intracellular enzymatic cleavage of the ester bond induced the controlled release of the drug, ultimately leading to the successful suppression of the tumor growth in a murine model of 4T1 breast cancer (Figure 1.8 -b).[95]

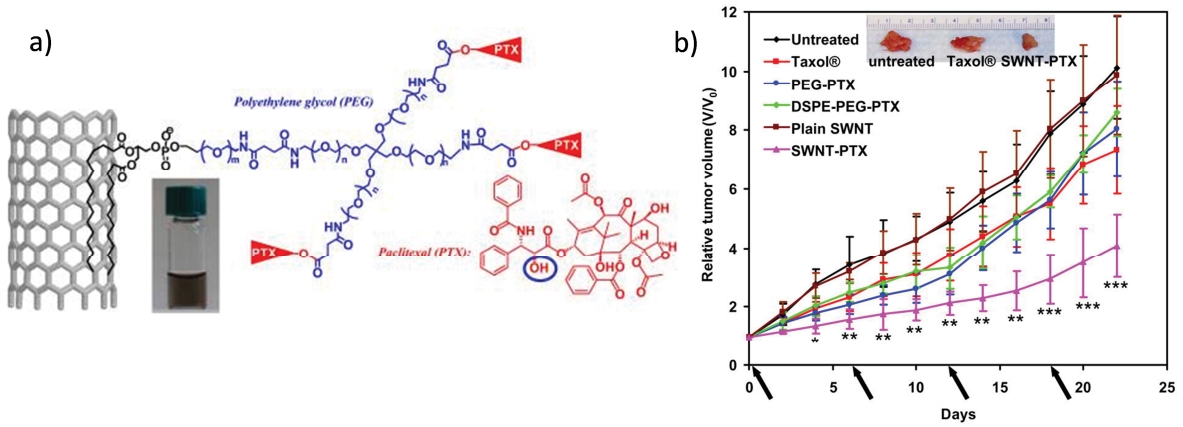

Figure 1.8 Carbon nanotubes for paclitaxel delivery. a) Schematic representation of the SWNT-PTX conjugate. The PTX molecules were connected to PEG at the circled OH site, forming a cleavable ester bond. b) Suppression of tumor growth in 4T1 breast cancer mice model by treatment with different conjugates and control. P values (Taxol® vs SWNT-PTX): * $p<0.05$, ** $p<0.01$, *** $p<0.001$. Inset: photo of tumors coming from sacrificed mice untreated and treated with Taxol® or with SWNT-PTX. Figures adapted from ref. [95].

For the preparation of CNT-based drug delivery systems, most of the approaches feature the functionalization (covalent and non-covalent) of nanotubes with linear or branched PEG chains, or similar derivatives. This accounts for multiple reasons: first, PEGylation significantly improves CNT dispersibility and stability in physiological buffers and it offers the possibility to further derivatize the PEG terminal groups with suitable functionalities.[98] Second, the presence of biocompatible PEG chains on the nanotube surface considerably increases the blood circulation time of the nanocarrier by lowering its immunogenicity and preventing its non-specific phagocytosis by the reticuloendothelial system (RES) (opsonization).[99,100] Dai and co-workers coated SWCNTs with a PL-PEG chain, which was further derivatized with the RGD peptide and with the macrocyclic chelating agent DOTA (1,4,7,10-tetraazacyclododecane-1,4,7,10-tetraacetic acid).[101] The role of RGD was to target integrin $\alpha_v\beta_3$ receptor, which is a marker of tumor angiogenesis and metastasis, while DOTA was used for chelating the positron-emitting radionuclide ^{64}Cu. The biodistribution of these radiolabeled SWCNTs was then investigated in mice by positron emission tomography (PET) and Raman spectroscopy. The so-functionalized SWCNTs were found to be surprisingly stable *in vivo*, exhibiting relatively long blood circulation times and low uptake by the RES. The conjugate showed efficient targeting of integrin-positive tumors in mice, with high tumor accumulation levels and allowed for the *in vivo* imaging of the tumor.

As alternative to the external functionalization, small-size drugs and prodrugs can also be encapsulated within the inner cavity of CNTs to guaranty their protection from external agents and possibly afford a slower and controlled release.[93] In a report by Pastorin and co-workers, the anticancer drug cisplatin was encapsulated inside MWCNTs and the tube ends were capped with gold nanoparticles (AuNP), for a better protection of the drug. While the non-capped MWCNTs showed a rapid release of cisplatin (in less than 1 hour in PBS buffer), the AuNP-MWCNT conjugate allowed a slower release both in the buffer and *in vitro*.[102]

Finally, to the aim of drug delivery, carbon nanotubes have been employed also in other ways than carriers; for instance, they were incorporated in a matrix as additive to improve its properties. Combining the electrical properties of MWCNTs with the electrosensitivity of poly(methylacrylic acid) (PMAA) gels, the group of Kostarelos developed an innovative electroresponsive hydrogel hybrid that showed good potential for *in vivo* pulsatile drug delivery (Figure 1.9).[103] Radiolabeled sucrose was loaded into the MWCNT/PMAA hydrogel and its release upon electrical stimulation was

studied both *in vitro* and *in vivo* after subcutaneous implantation of the device in the mice. It was observed that the drug release profile in blood was slower compared to the free sucrose administration or to a CNT-free matrix, proving that the presence of the CNTs improved the responsiveness of the gel to stimulation, allowing the controlled delivery of the drug under short-time stimulation and low electric voltage.

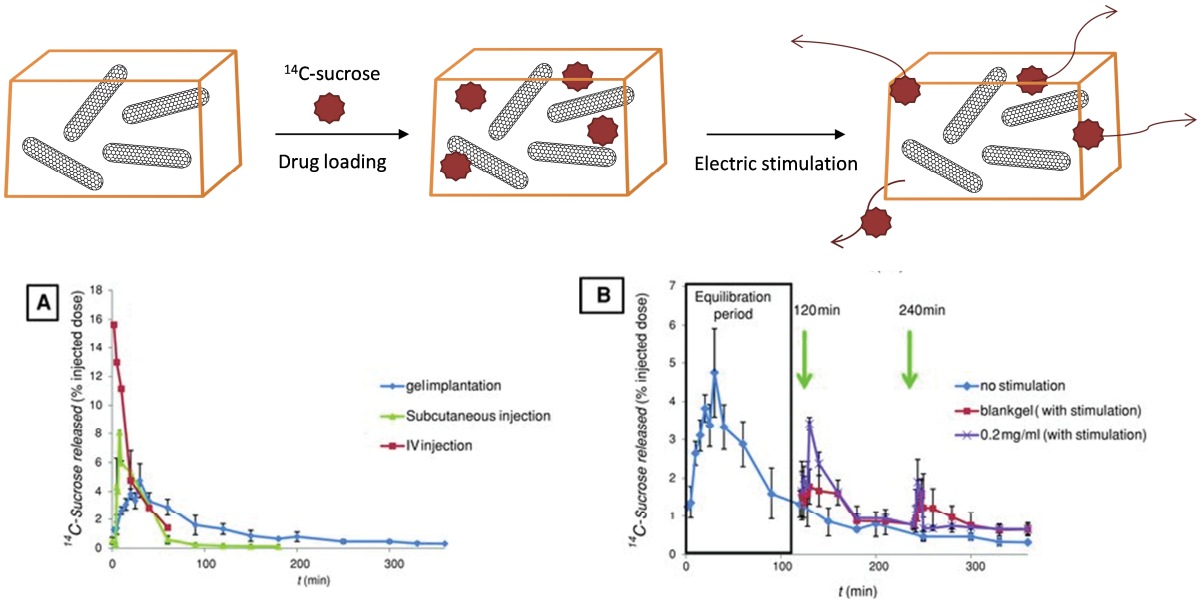

Figure 1.9 (Top) Loading of ^{14}C-sucrose into MWCNT/PMAA hydrogel hybrids and mechanism of drug release upon electrical field application. (Bottom) *In vivo* drug release in systemic circulation. A) Pharmacokinetic profiles of ^{14}C- sucrose release following different routes of administration (subcutaneous gel implantation, intravenous and subcutaneous injection), without stimulation. B) Release profile of ^{14}C-sucrose from hybrid gel in systemic blood circulation: comparison between blank gels and 0.2 mg/mL MWNT hybrid gels upon electric stimulation. Gels were stimulated (10 V for 1 min) at 2 h intervals (vertical arrows). The first stimulation was performed following a 2 h equilibration period. Figure adapted from ref. [103].

1.3.1.2 CNTs for Gene Delivery

Genes are segments of nucleic acids that can be employed for the treatment of genetic disorders and cancer by replacing/silencing the diseased gene responsible for the abnormal phenotype. Despite great advancements in the field of gene therapy, still some challenges needs to be faced, such as the safe and efficient delivery of sufficient amounts of genetic materials inside the cells up to the nucleus, without eliciting adverse immune responses in the host. The ability of CNTs to cross the cellular membranes sounded like an interesting strategy to attain gene transfection, and ultimately achieve cancer treatment. In 2004, our group reported the first successful CNT-assisted transfection of plasmid DNA *in vitro*,[104] and thereafter studies in this field incredibly boosted.[105] Nucleic acids can be tethered onto CNTs either by covalent attachment to a present functionality or through self-assembly driven by charge interaction or by π-π stacking between the nucleobases and the tube sidewalls. Because of the overall negative charge of nucleic acids, the functionalization of CNTs with positively-charged groups is often preferred to favor the efficient complexation between the two components. So far, CNT ability in gene delivery has been tested with many different nucleic acid sequences from plasmid DNA and small-interfering RNA (siRNA), and also with DNA and RNA aptamers.[105] The majority of these studies has been performed *in vitro*; however, in a recent work, a siRNA specific for the proto-oncogene Braf, was delivered topically to a mouse melanoma model

resulting in the successful attenuation of tumor growth.[106] A further insight on the use of CNTs as vehicles for intracellular transfer of genetic material will be provided in Chapter 2.

1.3.2 PHOTOTHERMAL THERAPY

The treatment of a malignant tumor consists in the killing of the diseased cells and tissues. This can be performed either by delivery of a therapeutic molecule or by altering the environmental conditions of the cells. One effective way to do this is by increasing the local temperature of the cancer cells, thus leading to their death by excessive temperature. This approach is at the basis of photothermal therapy (PTT). Because of the strong optical absorbance of CNTs and their propensity toward cellular uptake, they have become good candidates to accomplish the hyperthermic death of cancerous cells. Indeed, CNTs can absorb radiation in the NIR region and efficiently convert it into heat. Moreover, human tissues and biological fluids are relatively transparent to NIR light, which can reach deep penetration. To the aim of hyperthermia therapy, CNTs can either be directly injected into the tumor, if it is superficial or easily reachable, or they can be intravenously injected and actively addressed to cancerous cells by an appropriate targeting molecule. Dai's group was the first to report the use of CNTs for hyperthermia therapy in 2005.[107] SWCNTs functionalized with PL-PEG and folate as targeting agent were incubated with cervical carcinoma HeLa cells overexpressing the folate receptor. Irradiation of the cells with a 808 nm laser for 2 min induced extensive cell death, whereas HeLa cells that did not overexpress the folate receptor were not affected by the same treatment, as they did not internalize the CNTs. Later on, Moon and co-workers explored the ability of PEGylated SWCNTs to destroy solid malignant tumors *in vivo* after intratumoral injection of the nanotubes and NIR irradiation (Figure 1.10).[108] They reported the complete destruction of the tumor in the treated mice, without recurrence for over six months, whereas the tumor in untreated mice continued to grow. Moreover, they observed that most of the nanotubes were excreted within 2 months, *via* the biliary or renal pathway, thus concluding that SWCNT-mediated photothermal therapy could be a very promising approach for cancer therapy. Finally, tumor photothermal ablation with CNTs is possible also by means of radiofrequencies, as it was demonstrated *in vitro* and *in vivo* by treating hepatic tumor-bearing mice.[109]

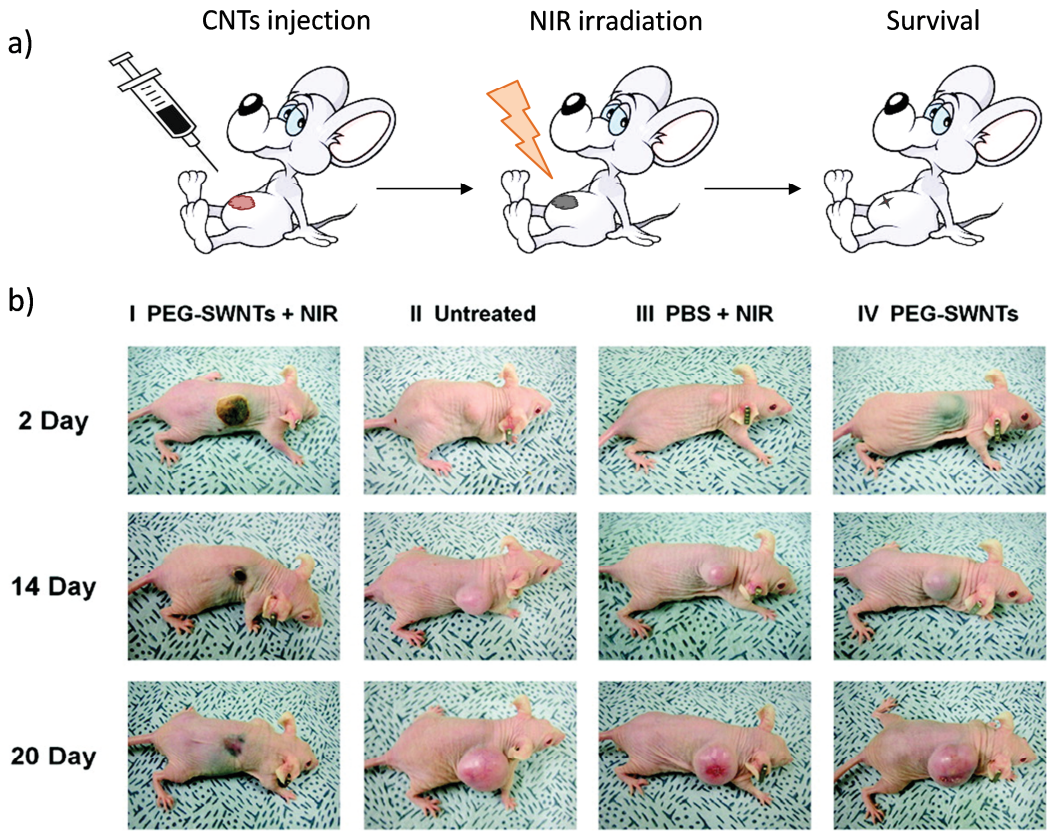

Figure 1.10 (a) Schematic representation of the procedure of photothermal treatment of tumors in mice with PEG-SWCNTs; (b) representative photographs of the mice treated in different ways at various time points after each treatment (I, PEG-SWNTs + NIR; II, untreated; III, PBS + NIR; IV, PEG-SWNTs). Figure adapted from ref. [108].

1.3.3 TISSUE ENGINEERING

The development of biocompatible materials for implants or supports is very important in the field of regenerative medicine to thwart neurodegenerative diseases or traumatic injuries. Tissue engineering refers to the practice of combining scaffolds, cells, and biologically active molecules into functional tissues with the goal of restoring, maintaining or improving damaged tissues or whole organs. Scaffolds for tissue regeneration require properties such as rigidity to resist external forces, biodegradability, ability to promote cell adhesion and proliferation, and ability to be sprayed by blood vessels and body fluids. The integration of CNTs with natural or synthetic polymers for the construction of new scaffolds has attracted great interest, since the CNTs can provide these materials with additional strength and flexibility and with novel properties such as electrical conductivity.[110,111] For example, incorporation of CNTs into collagen, which is the most commonly used scaffold material, significantly improves the mechanical strength of the composite, thus imparting structural support.[112,113] Moreover, CNT-polymer nanocomposites display improved biocompatibility and favorable characteristics toward cell adhesion and proliferation.[110,111] Da Silva *et al.* designed a 3D collagen/nanotube composite for bone regeneration, and beside featuring optimal mechanical rigidity, the composite proved to be bioresorbable and biodegradable, and induced mineralization of hydroxyapatite (the principal component of bones) crystals *in vitro*.[114] In another example, the electrical stimulation of osteoblasts (the bone-forming cells) grown on a CNT-

polylactic acid composite significantly increased bone cell proliferation and extracellular calcium production, demonstrating the potential application for accelerated bone repair.[115] Besides being incorporated in a matrix as additive, CNTs can also act as substrates for cell growth providing the cells with a support to grasp on. So far, a variety of cell phenotypes were reported to have high binding affinity for CNT surfaces, being able to grow and proliferate on their surface (*e.g.* fibroblasts, neurons, stem cells, osteoblasts).[116] In particular, the biocompatibility between CNTs and neurons, combined with CNT electrical conductivity, aroused interest toward their use for neural prosthesis and interfacing.[117,118] The first study in this field was reported in 2000 by Mattson *et al*., who demonstrated that neurons were able to grow on CNTs coated with 4-hydroxynonenal exhibiting multiple neurites and extensive branching. Later on, Ballerini and Prato's groups thoroughly investigated the ability of CNTs to sustain neuronal electrical activity establishing that CNTs can increase spontaneous synaptic activities and improve the responsiveness of neurons by forming entangled neuron-CNT networks.[117,119,120] The majority of these findings are proof-of-principle studies, but some *in vivo* studies already showed that CNTs are very promising as promoter of neuroregeneration and neuroprotection in injured nervous system.[121,122]

1.3.4 Cancer Diagnosis and Imaging

1.3.4.1 CNTs for Imaging

Due to their intrinsic chemico-physical properties, CNTs have started to be largely employed as tools for imaging applications. In fact, CNTs can give rise to unique optical, photoacoustic and Raman signals, thus allowing to exploit the corresponding imaging mode.[123] As alternative, carbon nanotubes can be functionalized with imaging agents, such as quantum dots, metallic nanoparticles or radionuclides, to facilitate conventional imaging techniques such as magnetic resonance imaging (MRI), positron emission tomography (PET) or single photon emission computed tomography (SPECT). The possibility to detect CNTs *in vitro* and *in vivo* is highly interesting both from the point of view of their biodistribution assessment, in order to follow their fate within the cells and the body, and from a diagnostic perspective, since it allows to visualize specific organs or diseases within the body.

After injecting mice with PEGylated SWCNTs, Welsher and co-workers demonstrated whole animal *in vivo* imaging by means of photoluminescence response, while in a following study they could even monitor the nanotube circulation through the mouse anatomy in real-time by dynamic contrast-enhanced imaging in the second NIR window (from 1000 to 1400 nm) (Figure 1.11).[124] Treatment of the acquired data by principal component analysis (PCA) allowed to greatly increase the anatomical resolution of the organs, permitting to visualize also small organs like the pancreas. This technique was later used by the same group and others to achieve the *in vivo* imaging of tumors, showing that CNTs could efficiently work as probes for cancer diagnosis.

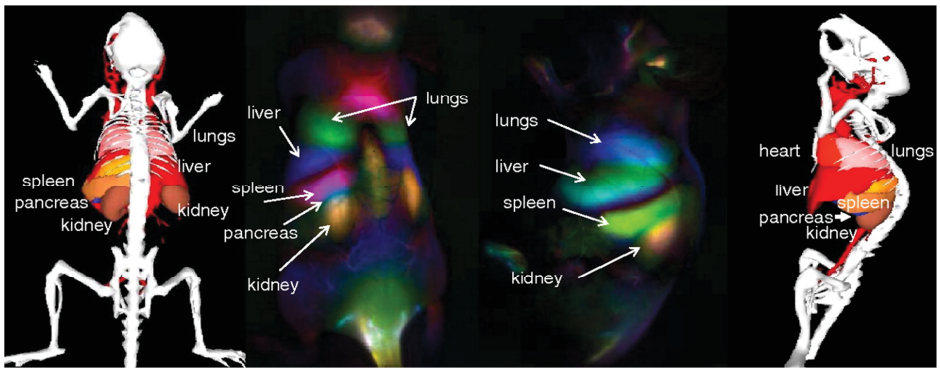

Figure 1.11 Dynamic contrast-enhanced imaging with SWCNTs through PCA. PCA images taken over the first 130 s following injection. Major features observed belong to the lungs, liver, kidney, spleen and pancreas, in the interstitial space between the kidney and spleen. Image reproduced from ref. [124].

In the last few years, CNTs started to be employed as contrast agent also for photoacoustic imaging, a technique that generally offers a higher spatial resolution and deeper tissue penetration compared to other optical imaging techniques. An interesting example was reported by Kim *et al*., who firstly coated SWCNTs with a thin gold layer in order to enhance their NIR absorption, and then they conjugated it to an antibody targeting the lymphatic endothelial receptor.[125] With this approach, they could reduce the required CNT concentration to the femtomolar range, and achieve the *in vivo* mapping of the lymphatic system by using CNTs as photoacoustic and photothermal contrast agent.

Combined ultrasound imaging and drug delivery through CNTs was achieved by Wu and co-workers, who engineered a CNT multifunctional platform by covalently functionalizing MWCNTs with polyethyleneimine (PEI), FITC as fluorescent probe and a monoclonal antibody (mAb) specific toward prostate stem cell antigen (PSCA), which is overexpressed by prostate cancer cells.[126] By ultrasound and confocal luminescence imaging, the researchers confirmed that the conjugate was able to specifically target PSCA-overexpressing cells, and upon loading with DOX it afforded good targeted drug delivery and suppression of tumor growth in mice. By decorating CNTs with contrast agents (exo- or endohedrically), other types of non-optical bioimaging have been accomplished. Carbon nanotubes have been variously functionalized with typical agents for T_1 and T_2 relaxation (*e.g.* Gd^{3+}, Mn^{2+}, magnetic and superparamagnetic iron oxide nanoparticles) for MRI, or with radioactive isotopes for nuclear medicine imaging, such as ^{18}F and ^{64}Cu for PET, and ^{99}Tc for SPECT. For example, Liu *et al.* immobilized superparamagnetic iron oxide nanoparticles (SPION) modified with a targeting lactose–glycine adduct (Lac–Gly) onto oxidized MWCNTs previously coated with poly(diallyldimethylammonium chloride) (PDDA) by electrostatic interaction.[127] These multifunctional magnetic MWCNTs showed low cytotoxicity *in vitro*, and increased T_2 relaxivity compared to the free SPION, due to the ability of the tubes to complex a great extent of clustered NPs. The *in vivo* trials demonstrated the potential of CNT–PDDA–SPION@Lac–Gly as MRI contrast agent with good aqueous dispersibility, high T_2 relaxation time and enhanced tumor/liver contrast ratio (277% enhancement).

1.3.4.2 CNT-based Biosensors

Traditional clinical cancer imaging methods, like X-ray, computed tomography (CT) and MRI, are often inadequate for a precise detection of early stage diseases and cancers, due to their initial asymptomaticity. However, many characteristic biomarkers are often overexpressed by cancer cells, thus providing an open gate for early diagnosis and prognosis. In the last years, the employment of carbon nanotubes for the development of sensors and biosensors has sensibly increased, motivated by

the good conducting properties of CNTs.[128,129] The deposition of CNTs on an electrode increases the exposed surface and the conductivity, thus enhancing the sensitivity of the electrochemical sensor and lowering the detection limits. In addition, the use of suitably functionalized CNTs, or their *in situ* derivatization, can endow the electrode with sensing ability toward a given analyte. This approach has been exploited to probe biological molecules, peptides, enzymes, pollutants, cells and protons (pH sensors), and nowadays much effort is devoted toward the fabrication of CNT-devices for cancer diagnosis and detection. As an example, Shi *et al.* modified an indium tin oxide (ITO) microelectrode with oxidized CNTs, building a microfluidic electrochemical sensor to monitor the release of dopamine from single cells of living rat pheochromocytoma (a neuroendocrine tumor).[130] Several CNT-based sensing devices have been reported for the detection of PSA, one of the most used biomarkers in diagnosis of prostate cancer, consenting detection limits of 4 pg/mL, far below those achieved by commercial immunoassays.[16] At present, the adoption of carbon nanotubes for the preparation of biosensors constitutes a valid alternative to classic methods for cancer biomarkers diagnosis, and it looks like the most realistic, and rapidly implementable, application of CNTs in the biomedical field.

1.4 What about Carbon Nanotube Toxicity?

From the point of view of biomedical and pharmacological applications, CNTs have been regarded as a very controversial subject. Indeed, the literature is split between descriptions of their potential toxicity and praise of their paramount potential for bioapplications. Their structural resemblance with the well-known carcinogenic asbestos fibers has aroused a lot of toxicological concerns since early times,[131,132] and a great number of investigations have been undertaken to reply to the question: are CNTs toxic?[27,133–136] Unfortunately, the answer to this question is not easy and straightforward, since the toxicity of a compound is determined by a great number of parameters and, as with any therapeutic and diagnostic agent, the risk of toxic effects has to be evaluated concomitantly to the potential benefits. What emerges from the massive literature on CNT toxicity is that their toxicological profile is strictly dependent on the nanotube properties and characteristics (structure, length, aspect ratio, degree of defects, extent of aggregation, degree and type of functionalization, manufacturing method), as well as on the experimental setup of the biological tests (protocol, cellular models, administration route, concentration, doses, toxicity assay). As a result, contradictory opinions can be found on the matter of CNT toxicity, internalization mechanisms and biodistribution, so that caution should be taken in drawing any final conclusion. Nevertheless, it is now commonly recognized that some CNT characteristics have a great influence on their toxicity,[116] and these will be briefly explained hereafter.

Purity. The presence and amount of residual metallic particles (from the production process) in the CNT sample can contribute to originate adverse effects in the cellular environment by triggering the production of reactive oxygen species (ROS), responsible of inflammatory symptoms.[137] High-quality purified CNTs are thus overall preferred for bioapplications.

Degree and type of functionalization. It is now established that the external chemical functionalization of CNTs can dramatically improve their biocompatibility and reduce the risk of acute inflammatory response.[27] The amount and type of functionalities present on the nanotube surface do also affect their cytotoxicity as well as their biodistribution and fate within the

organism;[138,139] notably, PEGylated CNTs display lower immunogenicity and higher blood circulation times.[98] It is worthy to note that acid-oxidized CNTs have shown to trigger toxic effects and inflammatory response, which was ascribed to the oxygenated groups and the great amount of reactive defect sites.[140,141]

Agglomeration state. Especially for *in vivo* applications, it is imperative to ensure having stable dispersions of CNTs and to individualize them. In fact, big agglomerates cannot be engulfed by macrophages or they can remain stuck in the smallest capillaries, ultimately engendering toxic effects. Extensive sonication and suitable functionalization are therefore important steps in the preparation process.

Length. Many studies have so far reported that long rigid CNTs should be avoided because, besides being unpractical for drug delivery scopes, they can generate severe adverse effects, in analogy with asbestos fibers. For example, CNTs exceeding 20 μm in length were found to be not completely engulfed by macrophages, leading to frustrated phagocytosis and impeded clearance.[142]

All these parameters can determine a different impact on the *in vitro* and *in vivo* toxicity of CNTs, and this is why both aspects need to be evaluated in parallel. The *in vitro* assessment of toxicity consists in the evaluation of cell proliferation, apoptosis or necrosis, oxidative stress, DNA damage and expression of specific enzymes, which may arouse from the CNT interference. It has been variously demonstrated that pristine CNTs induce a higher cellular toxicity, inducing cell apoptosis and necrosis.[27] Conversely, the external functionalization of CNTs renders them more biocompatible with physiological systems and reduces their toxicity.[27] Some reports show that macrophages can actively ingest significant quantities of SWCNTs without showing toxic effects, and even that functionalized CNTs are not cytotoxic against cells regulating the immune system (*e.g.* lymphocytes).[143,144]

In vivo toxicity regards both the pharmacokinetics of the administrated compound (*e.g.* blood circulation, drug release rate, retention, metabolism, excretion) and its toxicology (*e.g.* physiological and immunological response, biodistribution). One of the main concerns about CNT *in vivo* toxicity is the pulmonary toxicity determined by their inhalation in the occupational environment, and many toxicological studies have been carried out attempting to mimic the possible workplace exposure levels, mainly employing non-functionalized CNTs. In two pioneering studies, the groups of Donaldson and Kanno, have independently explored the carcinogenic risk of CNTs *in vivo* and reported that the abdominal delivery of nanotubes forms granulomas and can induce mesothelioma (cancer of the pleura) in mice, in a similar way of certain asbestos fibers.[142,145] These studies suggested that lung exposure to long rigid non-functionalized CNTs may increase the risk of carcinogenesis, and Donaldson hypothesized that possibly macrophages cannot completely engulf long fibers.[142] Later on, the same group instilled CNTs having different lengths into the pleural cavity of mice.[146,147] They observed that only long CNTs failed to surpass the lung barriers and their retention in those tissues provoked inflammatory response and mesothelial cell damage leading to chronic inflammation and granuloma formation. Contemporaneously to these investigations, many others have been undertaken to study the potential toxic effects of CNTs after functionalization and intravenous injection, which are fundamental conditions for their therapeutic applications.[139] Indeed, the type of functionalization and the administration route greatly influence the CNT biodistribution and clearance, and the overall physiological response. CNT biodistribution profiles have been investigated by different groups exploiting diverse methods. The most used strategy is to radiolabel the materials with radioactive isotopes in order to follow their fate in the body. This method allows for both CNT quantification through gamma scintigraphy and *in vivo* imaging by tomography

techniques such as SPECT or PET. CNT signatures in tissues can also be identified by Raman spectroscopy. As already mentioned, PEGylation is one of the most widely used strategies to increase the blood circulation of CNTs, while their functionalization with a targeting molecule allows to address them to a specific location, modifying the distribution profile. Generally, pristine/non-covalently functionalized CNTs are mainly retained in the RES organs (liver, spleen) or in the lungs, while covalently functionalized CNTs showed a reduced accumulation in the RES organs and a better elimination trough the renal system, thus being more suitable for future biomedical applications.[139]

The nanometer size of CNTs represents one of their major advantages for drug delivery (EPR effect), as well as one of the major drawbacks from the toxicological point of view. In fact, the often bundled state of CNTs increases their overall size, by far outstripping that of some organs vessels and the renal filtration cut-off (ca. 5 nm). As a result, phenomena of obstruction with consequent inflammation episodes, or incomplete metabolization and clearance by the specific organs, with consequent long-term toxicity, are likely to occur. The excretion of intravenously injected CNTs *via* the renal clearance pathway is severely hampered by their length and agglomeration, which do not allow an efficient passage through the endothelium. The other metabolic pathway for the elimination of larger particles is by entering the liver and becoming part of bile and feces. Nevertheless, the biliary excretion is a very slow and less efficient process, which increases the chances of having the CNT trapped inside the liver and spleen and trigger adverse responses. The unfavorable excretion pathways, long retention time and long-term health concerns are to-date the main obstacles in the clinical application of carbon nanotubes.

1.5 Future of Carbon Nanotubes

Nowadays, CNTs have become a commercial good and they have entered in our daily lives as additive for a variety of products, from composites to aeronautics or sporting materials. Besides, thanks to their outstanding physical and electronic properties they have found a broad application in material science and nanotechnology, for the preparation of sensors, batteries, solar cells, capacitors etc. In this perspective, CNTs are in fact a promising and competitive alternative to the present technology. Their remarkable chemical and biological properties have instead fueled much research toward their application in the biological domain. Indeed, CNTs have already been integrated in sensors for the detection of biomolecules and have shown great efficiency also as tools for imaging and tissue engineering. In addition, the ability of CNTs to work as a biomedical carrier for imaging and therapy has been largely investigated, proving their great clinical potential. However, with regard to all the *in vivo* applications of CNTs, optimism should be tempered until thorough understanding of the issues related to their biodegradability and the long-term toxicity. The comprehension of the specific pharmacological and pharmacodynamic profiles of CNTs is in fact imperative for their regulatory compliance and clinical translation. The major concerns of regulatory authorities are typically addressed to the toxicological profile and risk associated with the biopersistence of these material. The latest investigations have been indeed moving in this direction and some reports demonstrated that CNTs can be degraded by intracellular oxidative enzymes (*e.g.* horseradish- and myelo-peroxidase)[148,149] and by some type of leucocytes and granulocytes.[150] Both pristine and oxidized SWCNTs have been shown to undergo degradation *in vitro* and *in vivo*,[151] while the possibility to achieve the complete degradation of MWCNTs is currently being investigated.[149,152,153] This research area is greatly contributing to gain a deeper understanding of CNT fate after

administration and disclosing new possibilities for their biomedical employment. Therefore the hope toward the clinical application of CNTs should be maintained and the investigations in this direction are still of great interest.

1.6 THESIS OBJECTIVES AND OUTLINE

The research described in this Thesis is aimed at exploring new methodologies and solutions to several problems associated to the manipulation and processing of multifunctional carbon nanomaterials, thereby expanding the current horizons in fundamental and applied science fields such as CNT chemical derivatization and CNT bioapplications, including drug delivery. As discussed in this Introduction, carbon nanotubes are potentially an optimal carrier for the targeted delivery of therapeutic and imaging probes with applicability in nanomedicine. The fact that CNTs can be decorated internally and externally with a variety of functionalities widens the range of applications and offers the possibility for multimodal therapy. The researches described in this Thesis have been focused toward the development of new chemical strategies for the preparation of novel CNT carriers for anticancer therapy. Specifically, the modification of pristine CNTs and the conjugation of the therapeutic biomolecule has been explored only by covalent approaches, in order to convey a higher *in vivo* stability to the carrier. The work of this Thesis is divided in three main research projects:

- one was meant to study the possibility to convert carboxylic groups of oxidized CNTs into amino groups in order to prepare amino-functionalized CNT conjugates able to complex siRNA;

- in a second project we have developed new CNT conjugates connected to a therapeutic nanobody (a fragment of antibody) *via* a disulfide cleavable linker;

- finally, the last project has been developed within a Marie Curie network and is focused on the targeted delivery of radiotherapy by means of CNTs filled with radionuclides. In this framework, our group has investigated different synthetic strategies to achieve the functionalization of filled CNTs by [2+1] cycloaddition and the conjugation of a targeting antibody.

This last project is the main one of this Thesis work and has been carried out in strong collaboration with many partners. For a better comprehension of the subject and of the project, its discussion will be preceded by a short introduction chapter.

The Thesis is therefore composed of six Chapters, as outlined:

Chapter 1 gives an overview on the main characteristics of carbon nanotubes, their production and applications in the biomedical field, with a main focus on anticancer therapies.

Chapter 2 discusses different synthetic strategies performed to achieve the conversion of carboxylic groups of oxidized MWCNTs into amino groups, and the investigation of the ability of the obtained conjugates toward siRNA complexation, for gene delivery.

Chapter 3 describes the design and synthesis of CNT-nanobody constructs featuring a cleavable disulfide linker, and reports the main studies to assess their therapeutic efficacy.

Chapter 4 introduces the basis of radiotherapy and reports the state-of-the-art on the use of CNTs for the delivery of radioactive molecules. It then outlines the goal and strategy of the Marie Curie program (named RADDEL), and the task of our group within the network.

Chapter 5 describes the investigations we have carried out within the RADDEL project. Namely, the functionalization of filled and sealed CNTs by [2+1] cycloaddition and the conjugation with imaging and/or targeting molecules.

Chapter 6 reports the conclusive remarks and perspectives of this research work.

Each Chapter is followed by its own list of references, and each experimental Chapter is followed by its own experimental part.

1.7 BIBLIOGRAPHY

[1] H. W. Kroto, J. R. Heath, S. C. O'Brien, R. F. Curl, R. E. Smalley, *Nature* **1985**, *318*, 162.

[2] S. Iijima, *Nature* **1991**, *354*, 56.

[3] R. Bacon, *J. Appl. Phys.* **1960**, *31*, 283.

[4] A. Oberlin, M. Endo, T. Koyama, *J. Cryst. Growth* **1976**, *32*, 335.

[5] R. Baker, *J. Catal.* **1973**, *30*, 86.

[6] M. Monthioux, V. L. Kuznetsov, *Carbon* **2006**, *44*, 1621.

[7] R. Saito, G. Dresselhaus, M. S. Dresselhaus, *Physical Properties of Carbon Nanotubes*, Imperial College Press, London, **1998**.

[8] A. Jorio, G. Dresselhaus, M. S. Dresselhaus, *Carbon Nanotubes - Advanced Topics in the Synthesis, Structure, Properties and Applications*, Springer, Berlin, **2008**.

[9] L. Yang, S. Wang, Q. Zeng, Z. Zhang, L.-M. Peng, *Small* **2013**, *9*, 1225.

[10] V. Sgobba, D. M. Guldi, *Chem. Soc. Rev.* **2009**, *38*, 165.

[11] J. M. Schnorr, T. M. Swager, *Chem. Mater.* **2011**, *23*, 646.

[12] M. T. Byrne, Y. K. Gun'ko, *Adv. Mater.* **2010**, *22*, 1672.

[13] K. Kostarelos, A. Bianco, M. Prato, *Nat. Nanotechnol.* **2009**, *4*, 627.

[14] M. F. L. De Volder, S. H. Tawfick, R. H. Baughman, A. J. Hart, *Science* **2013**, *339*, 535.

[15] M. Terrones, *Annu. Rev. Mater. Res.* **2003**, *33*, 419.

[16] A. Eatemadi, H. Daraee, H. Karimkhanloo, M. Kouhi, N. Zarghami, A. Akbarzadeh, M. Abasi, Y. Hanifehpour, S. W. Joo, *Nanoscale Res. Lett.* **2014**, *9*, 393.

[17] C. Journet, W. K. Maser, P. Bernier, A. Loiseau, M. L. de la Chapelle, S. Lefrant, P. Deniard, R. Lee, J. E. Fischer, *Nature* **1997**, *388*, 756.

[18] E. Dervishi, Z. Li, Y. Xu, V. Saini, A. R. Biris, D. Lupuc, Alexandru S. Biris, *Part. Sci. Technol.* **2009**, *27*, 107.

[19] N. Grobert, *Mater. Today* **2007**, *10*, 28.

[20] A. Hirsch, *Angew. Chemie Int. Ed.* **2002**, *41*, 1853.

[21] J. L. Bahr, J. M. Tour, *J. Mater. Chem.* **2002**, *12*, 1952.

[22] S. Niyogi, M. A. Hamon, H. Hu, B. Zhao, P. Bhowmik, R. Sen, M. E. Itkis, R. C. Haddon, *Acc. Chem. Res.* **2002**, *35*, 1105.

[23] D. Tasis, N. Tagmatarchis, V. Georgakilas, M. Prato, *Chemistry* **2003**, *9*, 4000.

[24] D. Tasis, N. Tagmatarchis, A. Bianco, M. Prato, *Chem. Rev.* **2006**, *106*, 1105.

[25] P. Singh, S. Campidelli, S. Giordani, D. Bonifazi, A. Bianco, M. Prato, *Chem. Soc. Rev.* **2009**, *38*, 2214.

[26] G. Lamanna, A. Battigelli, C. Ménard-Moyon, A. Bianco, *Nanotechnol. Rev.* **2012**, *1*, 17.

[27] A. Bianco, K. Kostarelos, M. Prato, *Chem. Commun.* **2011**, *47*, 10182.

[28] M. Foldvari, M. Bagonluri, *Nanomedicine* **2008**, *4*, 183.

[29] A. Battigelli, C. Ménard-Moyon, T. Da Ros, M. Prato, A. Bianco, *Adv. Drug Deliv. Rev.* **2013**, *65*, 1899.

[30] M. A. Hamon, H. Hu, P. Bhowmik, S. Niyogi, B. Zhao, M. E. Itkis, R. C. Haddon, *Chem. Phys. Lett.* **2001**, *347*, 8.

[31] H. F. Bettinger, *J. Phys. Chem. B* **2005**, *109*, 6922.

[32] X. Lu, Z. Chen, P. v R. Schleyer, *J. Am. Chem. Soc.* **2005**, *127*, 20.

[33] K. Kostarelos, *Nat. Biotechnol.* **2008**, *26*, 774.

[34] K. Kostarelos, *Nat. Mater.* **2010**, *9*, 793.

[35] J. Liu, A. G. Rinzler, H. Dai, J. H. Hafner, R. K. Bradley, P. J. Boul, A. Lu, T. Iverson, K. Shelimov, C. B. Huffman, F. Rodriguez-Macias, Y.-S. Shon, T. R. Lee, D. T. Colbert, Richard E. Smalley*, *Science* **1998**, *280*, 1253.

[36] T. Kyotani, S. Nakazaki, W.-H. Xu, A. Tomita, *Carbon* **2001**, *39*, 782.

[37] K. J. Ziegler, Z. Gu, H. Peng, E. L. Flor, R. H. Hauge, R. E. Smalley, *J. Am. Chem. Soc.* **2005**, *127*, 1541.

[38] J. Zhang, H. Zou, Q. Qing, Y. Yang, Q. Li, Z. Liu, X. Guo, Z. Du, *J. Phys. Chem. B* **2003**, *107*, 3712.

[39] D. Bonifazi, C. Nacci, R. Marega, S. Campidelli, G. Ceballos, S. Modesti, M. Meneghetti, M. Prato, *Nano Lett.* **2006**, *6*, 1408.

[40] K. Jiang, L. S. Schadler, R. W. Siegel, X. Zhang, H. Zhang, M. Terrones, *J. Mater. Chem.* **2004**, *14*, 37.

[41] J. L. Delgado, P. de la Cruz, A. Urbina, J. T. López Navarrete, J. Casado, F. Langa, *Carbon* **2007**, *45*, 2250.

[42] C. Fabbro, H. Ali-Boucetta, T. Da Ros, K. Kostarelos, A. Bianco, M. Prato, *Chem. Commun.* **2012**, *48*, 3911.

[43] C. A. Dyke, J. M. Tour, *Chemistry* **2004**, *10*, 812.

[44] N. Karousis, N. Tagmatarchis, D. Tasis, *Chem. Rev.* **2010**, *110*, 5366.

[45] Y.-S. Lee, *J. Fluor. Chem.* **2007**, *128*, 392.

[46] J.-F. Colomer, R. Marega, H. Traboulsi, M. Meneghetti, G. Van Tendeloo, D. Bonifazi, *Chem. Mater.* **2009**, *21*, 4747.

[47] W. Z. Wang, A. S. Mahasin, P. Q. Gao, K. H. Lim, M. B. Chan-Park, *J. Phys. Chem. C* **2012**, *116*, 23027.

[48] K. S. Coleman, A. K. Chakraborty, S. R. Bailey, J. Sloan, M. Alexander, *Chem. Mater.* **2007**, *19*, 1076.

[49] F. G. Brunetti, M. A. Herrero, J. de M. Muñoz, S. Giordani, A. Díaz-Ortiz, S. Filippone, G. Ruaro, M. Meneghetti, M. Prato, E. Vázquez, *J. Am. Chem. Soc.* **2007**, *129*, 14580.

[50] W. Zhang, T. M. Swager, *J. Am. Chem. Soc.* **2007**, *129*, 7714.

[51] N. Rubio, M. A. Herrero, A. de la Hoz, M. Meneghetti, M. Prato, E. Vázquez, *Org. Biomol. Chem.* **2010**, *8*, 1936.

[52] D. M. Guldi, M. Marcaccio, D. Paolucci, F. Paolucci, N. Tagmatarchis, D. Tasis, E. Vázquez, M. Prato, *Angew. Chem. Int. Ed.* **2003**, *42*, 4206.

[53] A. Bianco, K. Kostarelos, C. D. Partidos, M. Prato, *Chem. Commun.* **2005**, 571.

[54] C.-M. Chang, Y.-L. Liu, *Carbon* **2009**, *47*, 3041.

[55] L. Zhang, J. Yang, C. L. Edwards, L. B. Alemany, V. N. Khabashesku, A. R. Barron, *Chem. Commun.* **2005**, 3265.

[56] M. Holzinger, O. Vostrowsky, A. Hirsch, F. Hennrich, M. Kappes, R. Weiss, F. Jellen, *Angew. Chem. Int. Ed.* **2001**, *40*, 4002.

[57] H. Hu, B. Zhao, M. A. Hamon, K. Kamaras, M. E. Itkis, R. C. Haddon, *J. Am. Chem. Soc.* **2003**, *125*, 14893.

[58] K. S. Coleman, S. R. Bailey, S. Fogden, M. L. H. Green, *J. Am. Chem. Soc.* **2003**, *125*, 8722.

[59] G. Clavé, S. Campidelli, *Chem. Sci.* **2011**, *2*, 1887.

[60] T. Palacin, H. Le Khanh, B. Jousselme, P. Jegou, A. Filoramo, C. Ehli, D. M. Guldi, S. Campidelli, *J. Am. Chem. Soc.* **2009**, *131*, 15394.

[61] J. L. Bahr, J. Yang, D. V. Kosynkin, M. J. Bronikowski, R. E. Smalley, J. M. Tour, *J. Am. Chem. Soc.* **2001**, *123*, 6536.

[62] J. L. Bahr, J. M. Tour, *Chem. Mater.* **2001**, *13*, 3823.

[63] J. L. Hudson, H. Jian, A. D. Leonard, J. J. Stephenson, J. M. Tour, *Chem. Mater.* **2006**, *18*, 2766.

[64] S. Campidelli, B. Ballesteros, A. Filoramo, D. D. Díaz, G. de la Torre, T. Torres, G. M. A. Rahman, C. Ehli, D. Kiessling, F. Werner, V. Sgobba, D. M. Guldi, C. Cioffi, M. Prato, J.-P. Bourgoin, *J. Am. Chem. Soc.* **2008**, *130*, 11503.

[65] Z. Guo, F. Du, D. Ren, Y. Chen, J. Zheng, Z. Liu, J. Tian, *J. Mater. Chem.* **2006**, *16*, 3021.

[66] T. S. Balaban, M. C. Balaban, S. Malik, F. Hennrich, R. Fischer, H. Rösner, M. M. Kappes, *Adv. Mater.* **2006**, *18*, 2763.

[67] D. Wunderlich, F. Hauke, A. Hirsch, *J. Mater. Chem.* **2008**, *18*, 1493.

[68] C. Richard, F. Balavoine, P. Schultz, T. W. Ebbesen, C. Mioskowski, *Science* **2003**, *300*, 775.

[69] T. Premkumar, R. Mezzenga, K. E. Geckeler, *Small* **2012**, *8*, 1299.

[70] M. S. Strano, V. C. Moore, M. K. Miller, M. J. Allen, E. H. Haroz, C. Kittrell, R. H. Hauge, R. E. Smalley, *J. Nanosci. Nanotechnol.* **2003**, *3*, 81.

[71] L. Vaisman, H. D. Wagner, G. Marom, *Adv. Colloid Interface Sci.* **2006**, *128-130*, 37.

[72] D. A. Britz, A. N. Khlobystov, *Chem. Soc. Rev.* **2006**, *35*, 637.

[73] B. White, S. Banerjee, S. O'Brien, N. J. Turro, I. P. Herman, *J. Phys. Chem. C* **2007**, *111*, 13684.

[74] W. Wenseleers, I. I. Vlasov, E. Goovaerts, E. D. Obraztsova, A. S. Lobach, A. Bouwen, *Adv. Funct. Mater.* **2004**, *14*, 1105.

[75] M. F. Islam, E. Rojas, D. M. Bergey, A. T. Johnson, A. G. Yodh, *Nano Lett.* **2003**, *3*, 269.

[76] L. Dong, K. L. Joseph, C. M. Witkowski, M. M. Craig, *Nanotechnology* **2008**, *19*, 255702.

[77] H. Li, B. Zhou, Y. Lin, L. Gu, W. Wang, K. A. S. Fernando, S. Kumar, L. F. Allard, Y.-P. Sun, *J. Am. Chem. Soc.* **2004**, *126*, 1014.

[78] T. Ogoshi, Y. Takashima, H. Yamaguchi, A. Harada, *J. Am. Chem. Soc.* **2007**, *129*, 4878.

[79] P. Liu, *Eur. Polym. J.* **2005**, *41*, 2693.

[80] C. Ménard-Moyon, K. Kostarelos, M. Prato, A. Bianco, *Chem. Biol.* **2010**, *17*, 107.

[81] H. Tang, J. Chen, S. Yao, L. Nie, G. Deng, Y. Kuang, *Anal. Biochem.* **2004**, *331*, 89.

[82] S. H. Lim, J. Wei, J. Lin, Q. Li, J. Kuayou, *Biosens. Bioelectron.* **2005**, *20*, 2341.

[83] G. Pastorin, W. Wu, S. Wieckowski, J.-P. Briand, K. Kostarelos, M. Prato, A. Bianco, *Chem. Commun.* **2006**, 1182.

[84] Z. Liu, X. Sun, N. Nakayama-Ratchford, H. Dai, *ACS Nano* **2007**, *1*, 50.

[85] Y.-J. Lu, K.-C. Wei, C.-C. M. Ma, S.-Y. Yang, J.-P. Chen, *Colloids Surf. B. Biointerfaces* **2012**, *89*, 1.

[86] Y. Matsumura, H. Maeda, *Cancer Res.* **1986**, *46*, 6387.

[87] D. Peer, J. M. Karp, S. Hong, O. C. Farokhzad, R. Margalit, R. Langer, *Nat. Nanotechnol.* **2007**, *2*, 751.

[88] M. Ferrari, *Nat. Rev. Cancer* **2005**, *5*, 161.

[89] M. E. Davis, Z. G. Chen, D. M. Shin, *Nat. Rev. Drug Discov.* **2008**, *7*, 771.

[90] B. Wang, X. He, Z. Zhang, Y. Zhao, W. Feng, *Acc. Chem. Res.* **2013**, *46*, 761.

[91] Y. Zhu, S. Murali, W. Cai, X. Li, J. W. Suk, J. R. Potts, R. S. Ruoff, *Adv. Mater.* **2010**, *22*, 3906.

[92] W. Zhang, Z. Zhang, Y. Zhang, *Nanoscale Res. Lett.* **2011**, *6*, 555.

[93] B. S. Wong, S. L. Yoong, A. Jagusiak, T. Panczyk, H. K. Ho, W. H. Ang, G. Pastorin, *Adv. Drug Deliv. Rev.* **2013**, *65*, 1964.

[94] C. Klumpp, K. Kostarelos, M. Prato, A. Bianco, *Biochim. Biophys. Acta* **2006**, *1758*, 404.

[95] Z. Liu, K. Chen, C. Davis, S. Sherlock, Q. Cao, X. Chen, H. Dai, *Cancer Res.* **2008**, *68*, 6652.

[96] J. Chen, S. Chen, X. Zhao, L. V. Kuznetsova, S. S. Wong, I. Ojima, *J. Am. Chem. Soc.* **2008**, *130*, 16778.

[97] P.-C. Lee, Y.-C. Chiou, J.-M. Wong, C.-L. Peng, M.-J. Shieh, *Biomaterials* **2013**, *34*, 8756.

[98] M. Bottini, N. Rosato, N. Bottini, *Biomacromolecules* **2011**, *12*, 3381.

[99] S.-T. Yang, K. A. S. Fernando, J.-H. Liu, J. Wang, H.-F. Sun, Y. Liu, M. Chen, Y. Huang, X. Wang, H. Wang, Y.-P. Sun, *Small* **2008**, *4*, 940.

[100] N. Kotagiri, J.-W. Kim, *Int. J. Nanomedicine* **2014**, *9 Suppl 1*, 85.

[101] Z. Liu, W. Cai, L. He, N. Nakayama, K. Chen, X. Sun, X. Chen, H. Dai, *Nat. Nanotechnol.* **2007**, *2*, 47.

[102] J. Li, S. Q. Yap, S. L. Yoong, T. R. Nayak, G. W. Chandra, W. H. Ang, T. Panczyk, S. Ramaprabhu, S. K. Vashist, F.-S. Sheu, A. Tan, G. Pastorin, *Carbon* **2012**, *50*, 1625.

[103] A. Servant, L. Methven, R. P. Williams, K. Kostarelos, *Adv. Healthc. Mater.* **2013**, *2*, 806.

[104] D. Pantarotto, R. Singh, D. McCarthy, M. Erhardt, J.-P. Briand, M. Prato, K. Kostarelos, A. Bianco, *Angew. Chem. Int. Ed.* **2004**, *43*, 5242.

[105] K. Bates, K. Kostarelos, *Adv. Drug Deliv. Rev.* **2013**, *65*, 2023.

[106] K. S. Siu, D. Chen, X. Zheng, X. Zhang, N. Johnston, Y. Liu, K. Yuan, J. Koropatnick, E. R. Gillies, W.-P. Min, *Biomaterials* **2014**, *35*, 3435.

[107] N. W. S. Kam, M. O'Connell, J. A. Wisdom, H. Dai, *Proc. Natl. Acad. Sci. U. S. A.* **2005**, *102*, 11600.

[108] H. K. Moon, S. H. Lee, H. C. Choi, *ACS Nano* **2009**, *3*, 3707.

[109] C. J. Gannon, P. Cherukuri, B. I. Yakobson, L. Cognet, J. S. Kanzius, C. Kittrell, R. B. Weisman, M. Pasquali, H. K. Schmidt, R. E. Smalley, S. A. Curley, *Cancer* **2007**, *110*, 2654.

[110] H. Haniu, N. Saito, Y. Matsuda, T. Tsukahara, Y. Usui, N. Narita, K. Hara, K. Aoki, M. Shimizu, N. Ogihara, S. Takanashi, M. Okamoto, S. Kobayashi, N. Ishigaki, K. Nakamura, H. Kato, *J. Nanomater.* **2012**, *2012*, DOI doi:10.1155/2012/343747.

[111] B. S. Harrison, A. Atala, *Biomaterials* **2007**, *28*, 344.

[112] R. A. MacDonald, B. F. Laurenzi, G. Viswanathan, P. M. Ajayan, J. P. Stegemann, *J. Biomed. Mater. Res. A* **2005**, *74*, 489.

[113] Y. Cao, Y. M. Zhou, Y. Shan, H. X. Ju, X. J. Xue, *J. Nanosci. Nanotechnol.* **2007**, *7*, 447.

[114] E. E. da Silva, H. H. M. Della Colleta, A. S. Ferlauto, R. L. Moreira, R. R. Resende, S. Oliveira, G. T. Kitten, R. G. Lacerda, L. O. Ladeira, *Nano Res.* **2010**, *2*, 462.

[115] P. R. Supronowicz, P. M. Ajayan, K. R. Ullmann, B. P. Arulanandam, D. W. Metzger, R. Bizios, *J. Biomed. Mater. Res.* **2002**, *59*, 499.

[116] E. Heister, E. W. Brunner, G. R. Dieckmann, I. Jurewicz, A. B. Dalton, *ACS Appl. Mater. Interfaces* **2013**, *5*, 1870.

[117] A. Fabbro, M. Prato, L. Ballerini, *Adv. Drug Deliv. Rev.* **2013**, *65*, 2034.

[118] A. Nunes, K. Al-Jamal, T. Nakajima, M. Hariz, K. Kostarelos, *Arch. Toxicol.* **2012**, *86*, 1009.

[119] V. Lovat, D. Pantarotto, L. Lagostena, B. Cacciari, M. Grandolfo, M. Righi, G. Spalluto, M. Prato, L. Ballerini, *Nano Lett.* **2005**, *5*, 1107.

[120] G. Cellot, E. Cilia, S. Cipollone, V. Rancic, A. Sucapane, S. Giordani, L. Gambazzi, H. Markram, M. Grandolfo, D. Scaini, F. Gelain, L. Casalis, M. Prato, M. Giugliano, L. Ballerini, *Nat. Nanotechnol.* **2009**, *4*, 126.

[121] H. J. Lee, J. Park, O. J. Yoon, H. W. Kim, D. Y. Lee, D. H. Kim, W. B. Lee, N.-E. Lee, J. V Bonventre, S. S. Kim, *Nat. Nanotechnol.* **2011**, *6*, 121.

[122] J. A. Roman, T. L. Niedzielko, R. C. Haddon, V. Parpura, C. L. Floyd, *J. Neurotrauma* **2011**, *28*, 2349.

[123] G. Hong, S. Diao, A. L. Antaris, H. Dai, *Chem. Rev.* **2015**, DOI 10.1021/acs.chemrev.5b00008.

[124] K. Welsher, S. P. Sherlock, H. Dai, *Proc. Natl. Acad. Sci. U. S. A.* **2011**, *108*, 8943.

[125] J.-W. Kim, E. I. Galanzha, E. V Shashkov, H.-M. Moon, V. P. Zharov, *Nat. Nanotechnol.* **2009**, *4*, 688.

[126] H. Wu, H. Shi, H. Zhang, X. Wang, Y. Yang, C. Yu, C. Hao, J. Du, H. Hu, S. Yang, *Biomaterials* **2014**, *35*, 5369.

[127] Y. Liu, T. C. Hughes, B. W. Muir, L. J. Waddington, T. R. Gengenbach, C. D. Easton, T. M. Hinton, B. A. Moffat, X. Hao, J. Qiu, *Biomaterials* **2014**, *35*, 378.

[128] W. Yang, K. R. Ratinac, S. P. Ringer, P. Thordarson, J. J. Gooding, F. Braet, *Angew. Chem. Int. Ed.* **2010**, *49*, 2114.

[129] Z. Liu, S. Tabakman, K. Welsher, H. Dai, *Nano Res.* **2009**, *2*, 85.

[130] B.-X. Shi, Y. Wang, K. Zhang, T.-L. Lam, H. L.-W. Chan, *Biosens. Bioelectron.* **2011**, *26*, 2917.

[131] A. A. Shvedova, V. Castranova, E. R. Kisin, D. Schwegler-Berry, A. R. Murray, V. Z. Gandelsman, A. Maynard, P. Baron, *J. Toxicol. Environ. Health. A* **2003**, *66*, 1909.

[132] H. Nagai, S. Toyokuni, *Cancer Sci.* **2012**, *103*, 1378.

[133] X. Li, L. Wang, Y. Fan, F. Cui, *J. Nanomater.* **2012**, *2012*, 548389.

[134] J.-P. Kaiser, M. Roesslein, T. Buerki-Thurnherr, P. Wick, *Curr. Med. Chem.* **2011**, *18*, 2115.

[135] S. Lanone, P. Andujar, A. Kermanizadeh, J. Boczkowski, *Adv. Drug Deliv. Rev.* **2013**, *65*, 2063.

[136] C. Bussy, H. Ali-Boucetta, K. Kostarelos, *Acc. Chem. Res.* **2013**, *46*, 692.

[137] K. Pulskamp, S. Diabaté, H. F. Krug, *Toxicol. Lett.* **2007**, *168*, 58.

[138] K. T. Al-Jamal, A. Nunes, L. Methven, H. Ali-Boucetta, S. Li, F. M. Toma, M. A. Herrero, W. T. Al-Jamal, H. M. M. ten Eikelder, J. Foster, S. Mather, M. Prato, A. Bianco, K. Kostarelos, *Angew. Chem. Int. Ed.* **2012**, *51*, 6389.

[139] H. Ali-Boucetta, K. Kostarelos, *Adv. Drug Deliv. Rev.* **2013**, *65*, 2111.

[140] H. Tong, J. K. McGee, R. K. Saxena, U. P. Kodavanti, R. B. Devlin, M. I. Gilmour, *Toxicol. Appl. Pharmacol.* **2009**, *239*, 224.

[141] O. Vittorio, V. Raffa, A. Cuschieri, *Nanomedicine* **2009**, *5*, 424.

[142] C. A. Poland, R. Duffin, I. Kinloch, A. Maynard, W. A. H. Wallace, A. Seaton, V. Stone, S. Brown, W. Macnee, K. Donaldson, *Nat. Nanotechnol.* **2008**, *3*, 423.

[143] P. Cherukuri, S. M. Bachilo, S. H. Litovsky, R. B. Weisman, *J. Am. Chem. Soc.* **2004**, *126*, 15638.

[144] H. Dumortier, S. Lacotte, G. Pastorin, R. Marega, W. Wu, D. Bonifazi, J.-P. Briand, M. Prato, S. Muller, A. Bianco, *Nano Lett.* **2006**, *6*, 1522.

[145] A. Takagi, A. Hirose, T. Nishimura, N. Fukumori, A. Ogata, N. Ohashi, S. Kitajima, J. Kanno, *J. Toxicol. Sci.* **2008**, *33*, 105.

[146] F. A. Murphy, C. A. Poland, R. Duffin, K. T. Al-Jamal, H. Ali-Boucetta, A. Nunes, F. Byrne, A. Prina-Mello, Y. Volkov, S. Li, S. J. Mather, A. Bianco, M. Prato, W. Macnee, W. A. Wallace, K. Kostarelos, K. Donaldson, *Am. J. Pathol.* **2011**, *178*, 2587.

[147] F. A. Murphy, A. Schinwald, C. A. Poland, K. Donaldson, *Part. Fibre Toxicol.* **2012**, *9*, 8.

[148] V. E. Kagan, N. V Konduru, W. Feng, B. L. Allen, J. Conroy, Y. Volkov, I. I. Vlasova, N. A. Belikova, N. Yanamala, A. Kapralov, Y. Y. Tyurina, J. Shi, E. R. Kisin, A. R. Murray, J. Franks, D. Stolz, P. Gou, J. Klein-Seetharaman, B. Fadeel, A. Star, A. A. Shvedova, *Nat. Nanotechnol.* **2010**, *5*, 354.

[149] J. Russier, C. Ménard-Moyon, E. Venturelli, E. Gravel, G. Marcolongo, M. Meneghetti, E. Doris, A. Bianco, *Nanoscale* **2011**, *3*, 893.

[150] F. T. Andón, A. A. Kapralov, N. Yanamala, W. Feng, A. Baygan, B. J. Chambers, K. Hultenby, F. Ye, M. S. Toprak, B. D. Brandner, A. Fornara, J. Klein-Seetharaman, G. P. Kotchey, A. Star, A. A. Shvedova, B. Fadeel, V. E. Kagan, *Small* **2013**, *9*, 2721.

[151] G. P. Kotchey, Y. Zhao, V. E. Kagan, A. Star, *Adv. Drug Deliv. Rev.* **2013**, *65*, 1921.

[152] Y. Zhao, B. L. Allen, A. Star, *J. Phys. Chem. A* **2011**, *115*, 9536.

[153] L. Zhang, E. J. Petersen, M. Y. Habteselassie, L. Mao, Q. Huang, *Environ. Pollut.* **2013**, *181*, 335.

CHAPTER 2

DIRECT AMINO-FUNCTIONALIZATION OF OXIDIZED MWCNTS FOR SIRNA COMPLEXATION AND DELIVERY

Abstract – In the present chapter we will relate about the preparation of amino-functionalized MWCNTs as potential carriers for the delivery of siRNA. Several studies have shown promising results exploiting functionalized CNTs for the delivery of genomic material *in vitro* and *in vivo*. Our study was designed to elucidate further the possible relationship between the CNT surface functionalization strategy and the siRNA complexation ability. We had previously observed that the type of chemical functionalization used to surface-modify oxMWCNTs led to significant differences in nanotube cellular uptake and delivery ability. In those studies, amino-functionalized CNTs were obtained by cycloaddition reactions. This time we focused on the direct conversion of the carboxylic groups present on oxMWCNTs into amines and we attempted different synthetic strategies in order to directly tether the amines to the CNTs, without extending the lateral chain. The prepared compounds were characterized by XPS, FT-IR and TEM, and few of them were selected for siRNA complexation and cellular uptake, on the basis of their water dispersibility.

2.1 INTRODUCTION

Small interfering RNA (siRNA) is a synthetic double-strand sequence of RNA which can interfere with the expression of specific genes within the mechanism of RNA interference (RNAi). Since the discovery of RNAi in mammalian cells, great interest has been devoted to the exploration of this pathway of gene silencing because the possibility to knock down a specific gene holds a high potential in the treatment of several diseases.[1–3] So far, a number of clinical trials have investigated the mechanism of gene silencing by delivery of naked siRNA.[4,5] However, unmodified siRNA is unstable in the bloodstream, can be immunogenic and does not readily cross cellular membranes. These problematics limit the broad potential of siRNA-based therapeutics, therefore chemical modifications and/or delivery carriers are required to bring siRNA to its site of action, protecting it from nuclease degradation along the way. A variety of materials have been already explored to achieve efficient *in vivo* delivery, including polymers, lipids, peptides, antibodies, aptamers and small molecules.[3] In most of these cases, the carrier was designed to display a positive charge, for a better interaction with the siRNA payload.

CNT-mediated siRNA delivery

The ability of carbon nanotubes to penetrate mammalian cells and deliver a cargo (*e.g.* proteins, small peptides, nucleic acids), has been widely demonstrated along the past decades.[6–8] In 2004, our group has shown that covalently functionalized CNTs are able to translocate the plasma membrane and achieve the intracellular delivery of genomic material such as plasmid DNA.[9] Soon after, the group of Hongjie Dai reported for the first time the CNT-mediated siRNA delivery by a novel strategy based on SWCNTs functionalized with siRNA *via* a cleavable bond.[10] These first examples disclosed the promising potential of CNTs as a carrier for gene delivery and stimulated a lot of research in this direction. Since then, our and other groups, have reported several studies on the efficacy of CNTs as transfecting agents for siRNA, *in vitro* and *in vivo*.[11–13] We have shown that CNTs functionalized with terminal amino groups can form stable complexes with siRNA, thanks to the electrostatic interaction between the positively charged ammonium groups and the negatively charged phosphate groups of the nucleic acids. Amino-functionalized MWCNTs (MWCNT-NH_3^+) were used to deliver a toxic siRNA sequence to a human lung tumor xenograph model by intratumoral injection, leading to tumor growth inhibition and prolonged animal survival.[14] In another study from our group, the same type of amino-functionalized MWCNTs were able to achieve therapeutic gene silencing in neuronal tissues by delivery of siRNA in an induced stroke model, affording the functional rehabilitation of the rodent.[12] The ability of these CNT-based cationic conjugates to silence cytotoxic genes suggests they could become promising tools for gene therapy.

In light of the previous findings, we wanted to investigate more in detail the structure-delivery relationship, by preparing a novel type of amino-MWCNT carrier for siRNA. Specifically, our aim has been to achieve the direct conversion of the carboxylic groups of oxidized MWCNTs (oxMWCNTs) into amino groups, without extension of the alkyl chain (Scheme 2.1). In all our previous reports in fact, aminated CNTs were prepared either by cycloaddition or by amidation of the -COOH (or a combination of the two), these approaches foreseeing the attachment of an amine-terminating linker and thus extending the distance between the amino groups and the CNT surface.[9,12–17]

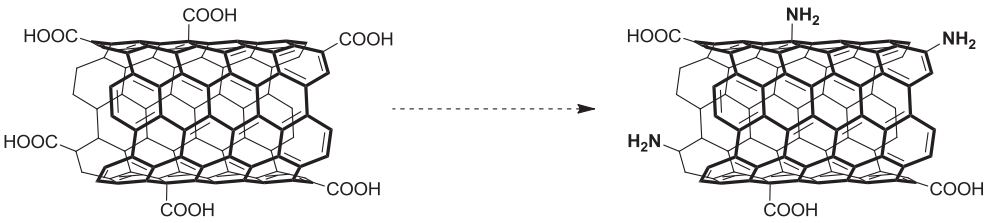

Scheme 2.1 Direct conversion of carboxylic groups into amino groups.

Moreover, in one of our recent studies, we observed that oxidized MWCNTs can trigger a sustained inflammatory response in brain tissues, whereas ammonium-functionalized MWCNTs are better tolerated.[17] Therefore increasing the amount of positively charged groups (*i.e.* ammonium over carboxylic groups) on the nanotubes could remarkably modify and improve the toxicity profile of the carrier. It seemed interesting to explore further the relationship between surface chemistry, delivery and cellular uptake, and carry out investigations for the preparation of different CNT-based carriers for siRNA delivery.

Amino-functionalized Carbon Nanotubes

To date, reports concerning carbon nanotubes directly modified with amino groups are very few due to the relative difficulty of the modification. In contrast to the rather 'rich' side-wall chemistry of CNTs, the chemistry at the tips of nanotubes has been limited only to few reactions, mainly based on derivatization of the carboxylic groups generated after oxidative treatment.[18–20] Only few reports have so far investigated the possibility of directly tethering to the CNT ends heteroatoms different from oxygen.[21–24] Previous attempts to directly convert carboxylic terminal groups into amines have been reported for SWCNTs by the group of Campbell.[22] They applied for the first time in nanotube chemistry the Hofmann rearrangement of primary amides and the Curtius rearrangement of acyl azides, achieving in both ways the preparation of SWCNTs with amino groups directly attached to the tube structure. Brinson and co-workers described the transformation of carboxyl groups of SWCNTs into aminomethyl groups through a different multistep synthetic path, involving a phthalimide intermediate.[21] However, the final step of their procedure suffers from an inappropriate protocol to remove the phthalimide protecting group, which requires hydrazine, and not trifluoroacetic acid as reported.[21] All mentioned studies were performed only on SWCNTs, and similar experiments have so far not been carried out on MWCNTs, nor envisaging any bioapplication. Therefore, further investigations are undoubtedly needed and could help to achieve a better understanding of the surface chemistry of oxMWCNTs. This work aims at investigating the chemical conversion of carboxylic groups of MWCNTs into amino groups through different synthetic strategies. Amino-functionalized MWCNTs were characterized by X-ray photoelectron spectroscopy (XPS), transmission electron microscopy (TEM) and Fourier transform infra-red spectroscopy (FT-IR). In collaboration with the group of Kostas Kostarelos (University of Manchester), we have then investigated the behavior of these amino-functionalized MWCNTs toward siRNA complexation and evaluated the uptake of these complexes by lung cancer cells.

2.2 Results and Discussion

Herein we will first describe the different synthetic strategies attempted to achieve the conversion of carboxylic groups of oxMWCNTs into amino groups, and successively we will discuss the characterization of the final compounds altogether. Finally, the biological assays on siRNA complexation and cellular uptake will be presented and discussed.

2.2.1 Chemical Modifications

As outlined in the general introduction of this Thesis (Chapter 1), most approaches for covalent functionalization of CNTs depart from their preliminary oxidation through acid treatment. This process introduces a large number of carboxylic groups, mainly at the CNT tips, and concurrently increases their dispersibility. This treatment also shortens and introduces defects on the aromatic honeycomb structure. Based on a thorough literature research, we designed and explored different strategies to achieve the conversion of the –COOH groups of oxMWCNTs into $–NH_2$ groups, without introducing any linker between the amines and the CNTs. Combining different synthetic steps, we selected six strategies (**Scheme 2.2**):

I. Hofmann rearrangement
II. Curtius rearrangement
III. *via* cyanide
IV. Hunsdiecker reaction
V. *via* phthalimide coupling
VI. *via* mesylation

The first three approaches are based on the activation of the carboxyl group into acyl chloride. Hofmann and Curtius rearrangements (strategy I and II) occur *via* an isocyanate intermediate, which is afterward hydrolyzed into amine.[25] Path III involves instead the decarbonylation of an acyl cyanide derivative and the subsequent reduction of the cyanide group. The fourth strategy (IV) features a halodecarboxylation (Hunsdiecker reaction), subsequent substitution of the halide by an azide and reduction into an amine. In the last two approaches instead, we proceeded first with the reduction of the carboxyl functions and continued towards the amination through introduction of phthalimide (V), or through sequential mesylation, azidation and reduction (VI). The overview of all synthetic routes is presented in **Scheme 2.2**, and they will be explained in detail in the following paragraphs.

We proceeded with the complete characterization only for the final compounds and the relevant stable intermediates. All compounds in the schemes are named by intuitive acronyms (*e.g.* MWCNT-COCN stands for acyl-cyanide-functionalized multi-walled carbon nanotubes). By this nomenclature we intend to highlight the functional group taking part in the reaction and the expected transformation. However, we do not assume that all functional groups of that type are converted upon reaction.

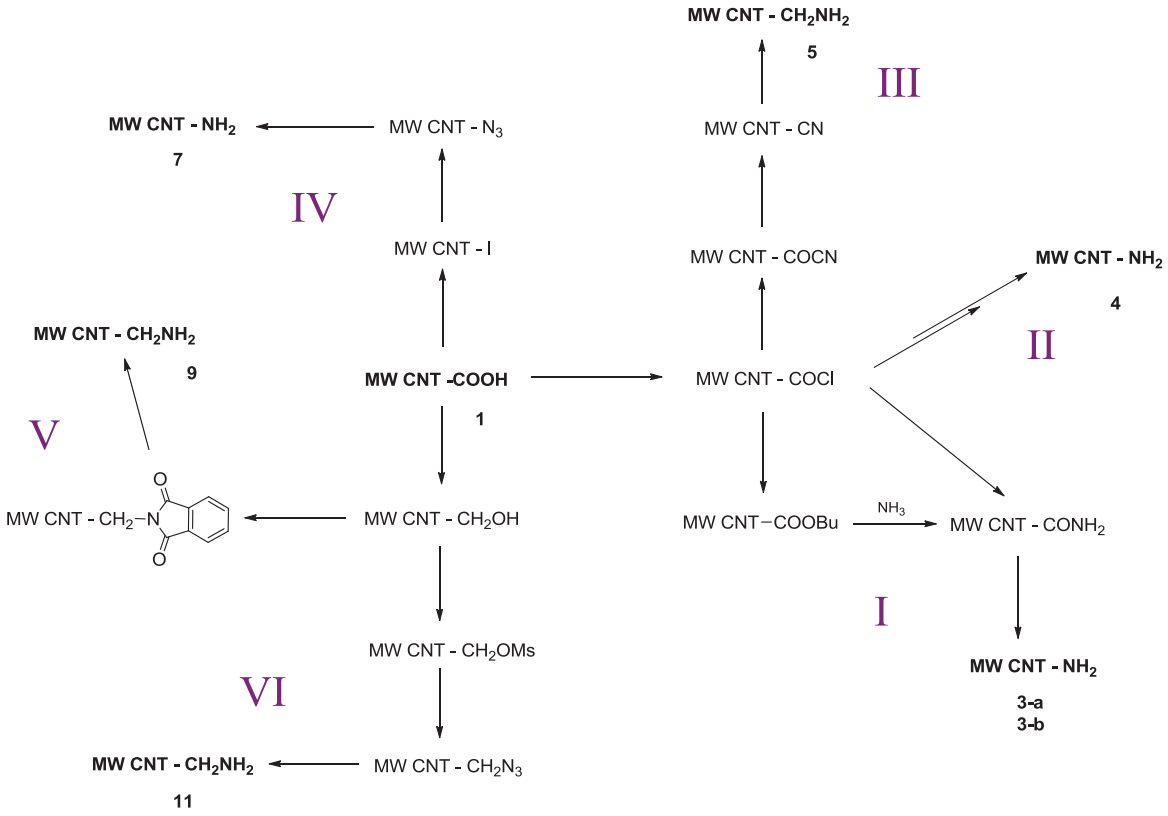

Scheme 2.2 Panoramic representation of the synthetic pathways performed to achieve the conversion of –COOH into –NH_2.

Oxidation of pristine MWCNTs and acylation

Commercially available MWCNTs were firstly oxidized by acid treatment with a HNO_3/H_2SO_4 (1:3) mixture under sonication (Scheme 2.3), following a common reported procedure.[26] This oxidation method allows for the further purification of pristine nanotubes and yields shortened oxMWCNTs highly functionalized with oxygen-containing groups, like carboxylic acids, located mainly at the ending tips.[27]

Scheme 2.3 Oxidation of pristine MWCNTs and activation with oxalyl chloride.

The average length distribution of oxMWCNTs (**1**) assessed by TEM is 381 nm, and the amount of oxygen-containing groups estimated by thermogravimetric analysis (TGA) is 1.4 mmol/g. The atomic percentage of carbon assessed by elemental analysis varies from 97.1% for pristine CNTs to 83.6% for the oxidized sample, while the percentage of hydrogen increases from 0 to 0.7%, accounting for the hydrogen atom of the –COOH groups. These values are in good agreement with the atomic percentage obtained by XPS analysis of oxMWCNTs **1**: 84.2% of carbon and 15.8% of oxygen (Table 2.1 and Figure 2.7 in the Exp. Part).

	pMWCNTs			oxMWCNTs		
	C	H	O	C	H	O
Elemental analysis	97.1	0	-	83.6	0.7	-
XPS	96.9	-	2.9	84.2	-	15.8

Table 2.1 Comparison between the atomic percentages of carbon, hydrogen and oxygen for pristine and oxidized MWCNTs, measured by elemental analysis and XPS.

To proceed with the first three strategies, the carboxylic functions were converted into acyl chlorides by treating oxMWCNTs **1** with neat oxalyl chloride (Scheme 2.3).[26] Because of the poor stability of acyl chlorides toward humidity, MWCNT-COCl were immediately used in the next step.

Strategy I: Hoffman Rearrangement

The Hofmann rearrangement is a well-known reaction that allows to convert an unsubstituted amide into a primary amine bearing one carbon atom less than the starting amide.[25] By rearrangement of the alkyl/aryl moiety, an isocyanate is formed, which is usually hydrolyzed under normal reaction conditions, with extrusion of carbon dioxide (Scheme 2.4).

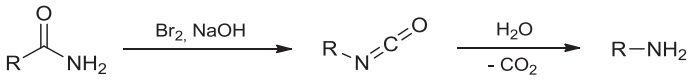

Scheme 2.4 General representation of the Hofmann rearrangement.

Gromov and co-workers have employed this rearrangement on SWCNTs to achieve the direct conversion of carboxyl into amino group.[22] They first prepared amide-functionalized SWCNTs following two different pathways, and finally proceeded with the Hofmann reaction. We decided to repeat their approach on oxMWCNTs aiming to achieve similar conversion results; hence we reproduced their procedures starting from activated MWCNT-COCl. We prepared MWCNT-$CONH_2$ in two different ways: (a) by esterification of the acyl chloride and subsequent amidation with aqueous ammonia, and (b) by one-step amidation with ammonium carbonate (Scheme 2.5).

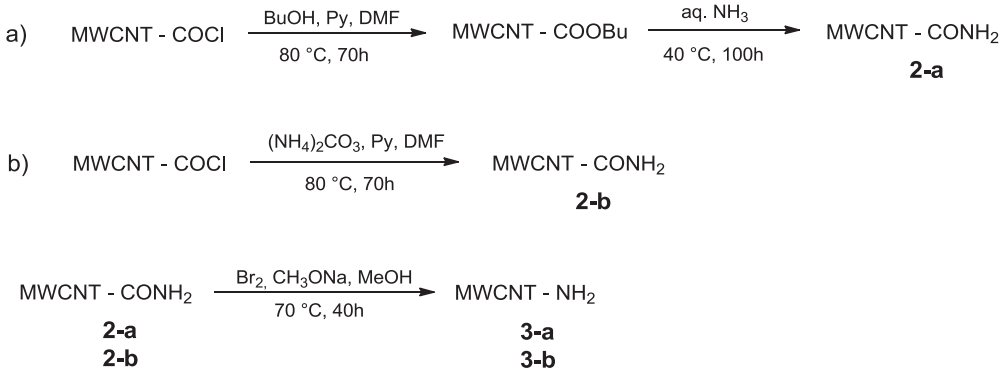

Scheme 2.5 Preparation of amide-functionalized MWCNTs *via* esterification (a) and *via* amidation (b), and Hofmann rearrangement of the amide (strategy I).

In the following step, the Hofmann rearrangement of MWCNT-$CONH_2$ (**2-a** and **2-b**) was carried out with bromine in basic and dry conditions. The hydrolysis of the isocyanate intermediate occurred *in situ* affording the primary amine (compounds **3a** and **3-b**).

Strategy II: Curtius Rearrangement

The second strategy starting from MWCNT-COCl involves the derivatization of the acyl chloride into acyl azide, which gives an isocyanate intermediate by Curtius rearrangement.[25] This is a general procedure that can be applied to almost any carboxylic acid. Gromov and co-workers already reported the application of Curtius rearrangement on oxidized SWCNTs, to prepare amino-functionalized SWCNTs.[22] The same procedure was employed by us for MWCNTs (Scheme 2.6). The formation of the acyl azide was carried out at room temperature. The temperature was then increased to allow the pyrolysis of the acyl azide and concomitant rearrangement. The so-formed isocyanate undergoes acid hydrolysis into primary amine (compound **4**).

Scheme 2.6 Amination of activated MWCNTs *via* Curtius rearrangement (strategy II).

Strategy III: via cyanide

Georgin *et al.* described a method for the ^{14}C-labeling of oxMWCNTs which features the conversion of the carboxylic acid group into a labeled nitrile, finally hydrolyzed into labeled carboxylic acid.[28] Inspired by their approach, we designed a similar route for the functionalization oxMWCNTs with nitrile groups, to be then reduced into amines. Freshly prepared MWCNT-COCl were reacted with CuCN to form acyl cyanides, which were secondarily decarbonylated into nitrile groups by a Pd-catalyzed reaction (Scheme 2.7).[28] The following reduction of the nitrile group with lithium aluminium hydride yields a methylene amine. Hence, in this case, the amine functions of compound **5** are linked to the aromatic nanotube structure through a methylene moiety, differently from the previous compounds.

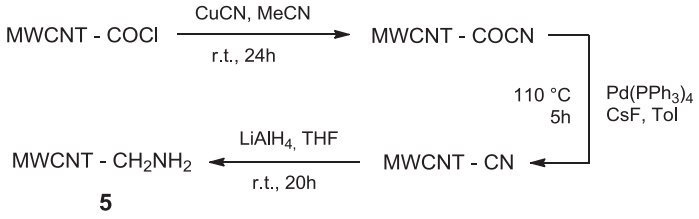

Scheme 2.7 Amination of activated MWCNTs *via* cyanide (strategy III).

Strategy IV: Hunsdiecker reaction

The Hunsdiecker reaction is a well-known method to form an alkyl or aryl halide starting from a carboxylic acid, decreasing the length of the alkyl chain by one carbon unit (Scheme 2.8Scheme 2.8).[29] Several variations and modifications of the original Hunsdiecker reaction have been so far investigated to avoid the employment of the very sensitive silver salts.[30–32] Although bromine is the mostly used halogen, chlorine and iodine have also been employed.

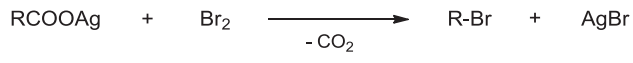

Scheme 2.8 General representation of the Hunsdiecker reaction.

One example of a modified Hunsdiecker reaction has been reported for the iodination of oxidized SWCNTs by Coleman and co-workers.[24] In their procedure they achieved the iodo-decarboxylation of oxidized SWCNTs by reacting them with iodosobenzene diacetate under broadband UV irradiation. We decided to apply to MWCNTs a variation of the Hunsdiecker reaction, which was reported by Roy's group to work efficiently with unsaturated carboxylic acids.[31] oxMWCNTs **1** were reacted with *N*-iodosuccinimide and a catalytic amount of LiOAc to afford iodinated MWCNTs **6** (Scheme 2.9). Characterization of this compound by XPS proved that iodine was present, although in a very low percentage (see Figure 2.1 in the Exp. Part). The nucleophilic substitution of iodine into azide was followed by azide reduction with $LiAlH_4$ to give amino-functionalized MWCNTs **7**.

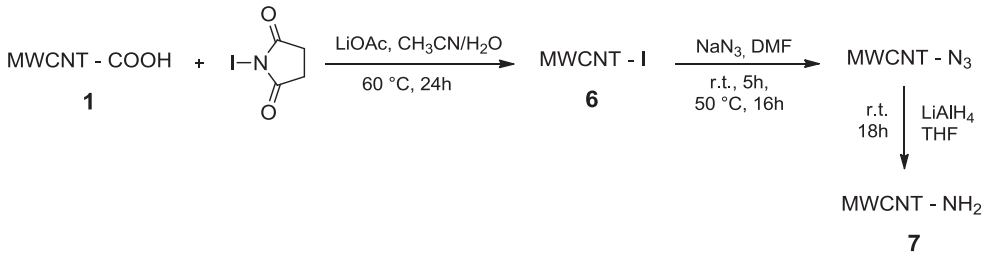

Scheme 2.9 Conversion of carboxyl to amino group by Hunsdiecker reaction (strategy IV).

Strategy V: via phthalimide coupling

In this approach we reproduced a modified version of the strategy reported by Brinson and co-worker for the preparation of amino-functionalized SWCNTs.[21] This consists of two main steps: first the reduction of the carboxyl group into hydroxyl, and second the derivatization of the hydroxyl with phthalimide followed by hydrazine-mediated deprotection to afford an aminomethyl group (Scheme 2.10). The reduction of –COOH was carried out by treating oxMWCNTs **1** with lithium aluminium hydride, and the resulting compound **8** was characterized by XPS and IR (see Figure 2.10 in Exp. Part) and then submitted to the subsequent coupling with phthalimide. The phthalimide group was then cleaved by treating the CNTs with hydrazine, differently by what reported by Brinson.[21] With this synthetic strategy, amino-functionalized MWCNTs **9** would finally feature the amine group detached from the aromatic nanotube structure by one carbon unity, the methylene group, in analogy with compound **5**, which was obtained by reduction of the nitrile group.

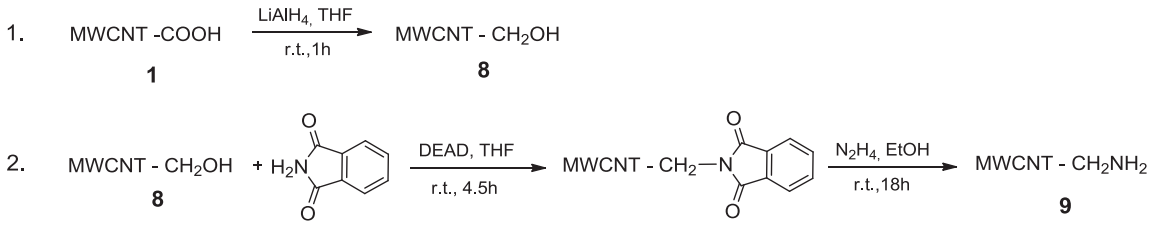

Scheme 2.10 (Step 1) reduction of oxMWCNTs; (step 2) derivatization of MWCNT-CH_2OH with phthalimide and subsequent deprotection (strategy V).

Strategy VI: via mesylation

The last strategy for the conversion of the carboxylic groups starts from hydroxyl-functionalized MWCNTs, as well as strategy V. Hence, the first step was the reduction of COOH, as described in the previous paragraph (step 1. of Scheme 2.10). The hydroxyl group of compound **8** was then converted into a mesylate by reaction with methanesulfonyl chloride, and further derivatized into azido group (Scheme 2.11). Reduction of the azide with $LiAlH_4$ affords a methylene amine (compound **11**). Also in this case, the amino groups are not directly tethered to the CNT structure, but interspaced from it by a methylene moiety.

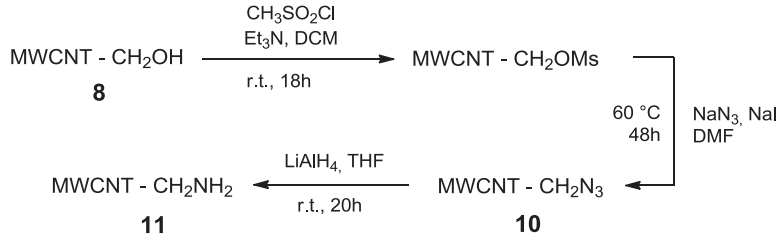

Scheme 2.11 Derivatization of compound **8** by successive mesylation, azidation and finally reduction of azide into amine (strategy VI).

2.2.2 CHARACTERIZATION

Rigorous characterization of the surface composition of modified carbon nanotubes is critical to their further employment, both for material and bio applications. To achieve a thorough characterization of CNTs after functionalization, it is essential to match different techniques, because of the intrinsic limitations presented by both the material and the instrumental techniques. For the characterization of the final amino-functionalized MWCNTs, we had to exclude thermogravimetric analysis because of minor weight loss difference with the starting oxMWCNTs. Generally, the quantification of primary amines on nanotubes is accomplished by Kaiser test, which is a colorimetric test based on the generation of a ninhydrin chromophore.[33] For the surface characterization of carbon nanotubes, XPS and FT-IR represent powerful tools for the detection of nitrogen atoms and amine-containing groups, respectively. Below we will discuss both surface and morphological characterization of the final aminated compounds.

2.2.2.1 Colorimetric tests

Kaiser test is the most popular colorimetric assay for the quantification of primary aliphatic amines in solid-phase organic synthesis. This assay is based on the reaction of ninhydrin with amine groups, and the violet color of the solution (Ruhemann's purple) is indicative of the presence of amines.[33,34] The color intensity measured at 570 nm by UV-Vis spectroscopy is correlated to the amount of amino groups, therefore allowing their quantification. The use of this assay in carbon nanomaterial characterization has been extensively reported.[26] Because of the involved mechanism, Kaiser test represents a valid assay only for the quantification of primary aliphatic amines. In our final compounds, the direct bond between the amino group and the nanotube structure likely results in a high percentage of aromatic amines, except for the case of compounds **5**, **9** and **11**, which display aminomethylene groups. We carried out Kaiser test for all compounds, to investigate the possibility

of detecting the introduced amines, but results were very low or negligible for all compounds. This was in agreement with the expectations for aminated MWCNTs with directly bonded amines (compounds **3-a**, **3-b**, **4**, **7** and **9**), but in contrast with what was expected for MWCNT-CH_2NH_2 **5**, **9** and **11**. For this set of samples, we can speculate that either the proximity of the aromatic structure affects the amine reactivity, or the location of the amino groups next to the nanotubes hampers the reaction with ninhydrin.

2.2.2.2 XPS analysis

X-ray photoelectron analysis allows to investigate the surface chemical composition of carbon nanomaterials and to obtain information about the nature of the functional groups. In Table 2.2 are reported the atomic concentrations of C, O and N for the different samples, obtained from the averaged peak areas of two measurements. After the chemical modification to introduce amino groups, nitrogen was detected in all samples, and a concomitant variation in the atomic percentage of carbon was registered. This variation accounts for the different synthetic steps involved in the six approaches, which can modify the relative ratio between the different elements. In the samples of aminated MWCNTs, the concentration of nitrogen ranges between 1.1 and 2.1%, while the content of oxygen remains still high. We thus think that only a small amount of carboxylic groups were efficiently converted into amino groups.

Compound	Synthetic Strategy	Atom %		
		C	O	N
oxMWCNTs **1**		84.6	15.4	-
MWCNTs – NH_2 **3-a**	I (Hofmann)	76.5	22.0	1.6
MWCNTs – NH_2 **3-b**	I (Hofmann)	82.4	15.7	1.8
MWCNTs – NH_2 **4**	II (Curtius)	76.1	21.7	2.1
MWCNTs – CH_2NH_2 **5**	III (*via* cyanide)	81.9	16.9	1.1
MWCNTs – NH_2 **7**	IV (Hunsdiecker)	77.4	21.2	1.4
MWCNTs – CH_2NH_2 **9**	V (Phthalimide)	84.8	13.9	1.3
MWCNTs – CH_2NH_2 **11**	VI (mesylate)	76.1	22.6	1.3

Table 2.2 Atomic percentages of carbon, oxygen and nitrogen in oxMWCNTs and aminated MWCNTs calculated from XPS experimental data.

By deconvolution of the C1s experimental curve of oxidized MWCNTs **1** we could identify the contributions given by the different functional groups (Figure 2.1). Aside from the main peak at 284.5 eV due to sp^2 C-C bonds, additional features due to sp^3 C, -*C*-O (alcohol) and O-*C*=O (carboxyl and ester) were present in all compounds (see example in Figure 2.1).[35] Around 291.5 eV appears the π- π^* satellite band, which is typical of the aromatic structures of carbon nanotubes.[36] De-composing the C1s curves of the aminated compounds, a good fitting was possible only including the component of the *C*-N bond, which has energy between 284.9-285.9 eV, and whose intensity varies around 4-7% among the different samples. However, the peak attributed to *C*OOH (at 288 eV) is still present after the reaction. The N1s spectra of the MWCNT-NH_2 samples were also registered and display the respective nitrogen peak centred at 400 eV (see example in Figure 2.1), which is in agreement with the expected value for primary amines.[21,37] To avoid data redundancy, the XPS

spectra of all MWCNT-NH_2 compounds are not reported herein, however a representative example referred to compound **3-a** is presented below.

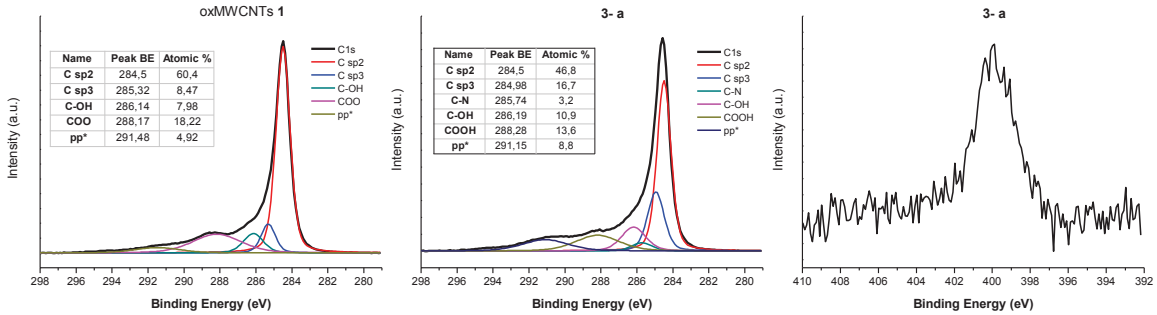

Figure 2.1 XPS spectra: C1s with fitting for oxMWCNTs **1** and aminated MWCNTs **3-a** (left and center), N1s for MWCNTs **3-a** (right).

2.2.2.3 Infra-red spectroscopy

In the FT-IR spectrum of oxMWCNTs **1** (Figure 2.2) we can clearly recognize the typical features of oxidized nanotubes: the broad band at 3430 cm^{-1} and the peak at 1584 cm^{-1} are respectively determined by the stretching vibration of OH and C=O of the carboxylic groups, while the C-C bendings are originating bands between 1700 and 1500 cm^{-1}.[38–40] The C-O stretching is also responsible for the peak at 1205 cm^{-1}. In the aminated MWCNTs **3-a** (Hofmann strategy) the presence of amine groups is confirmed by the appearance of an intense band at 1365 cm^{-1}, due to the C-N stretching, and smaller peaks at 841 and 701 cm^{-1}, from the NH_2 bending out-of-plane. The shoulder band at 1668 cm^{-1} can also be attributed to the scissoring of primary amines. For compound **3-b** instead, the absorption spectra does not present substantial changes compared to the starting material, which might be interpreted as a very low conversion. The FT-IR spectra of MWCNT-NH_2 **4** (Curtius strategy) exhibits new bands at 1709 cm^{-1} from NH_2 scissoring, and 1085 cm^{-1} from the C-N stretching vibrations. Compound **5** (*via* cyanide) displays an intense band between 1200 and 1000 cm^{-1}, which can be attributed to the C-N stretching vibrations. Concomitantly, the carbonyl peak (1580 cm^{-1}) appears less intense than in oxMWCNTs. What is more remarkable is the appearance of two intense new bands at 2921 and 2848 cm^{-1}: these are originated by the C-H stretching of the methylene moiety, which was introduced upon chemical conversion, and this is in accordance with previous reports.[21] The IR absorption of MWCNT-NH_2 **7** (Hunsdiecker strategy) displays again changes in the range between 1250 and 950 cm^{-1}, which are determined by the C-N stretching. The spectra of compound **9** (*via* phthalimide coupling) exhibits several bands associated with the C-N stretching vibrations (1588, 1423 and 1049 cm^{-1}), while the peak at 2919 cm^{-1} accounts for the stretching of C-H, thus confirming the presence of the methylene moiety. Similarly, MWCNT-NH_2 **11** (*via* mesylation) also presents a band at 2916 cm^{-1} associated with the methylene group, and relevant absorption at 1426 and 1110 cm^{-1} from the C-N vibration. A significant decrease in the intensity of the carbonyl band (1607 cm^{-1}) is also to be remarked, and could be explained by the reducing action of $LiAlH_4$.

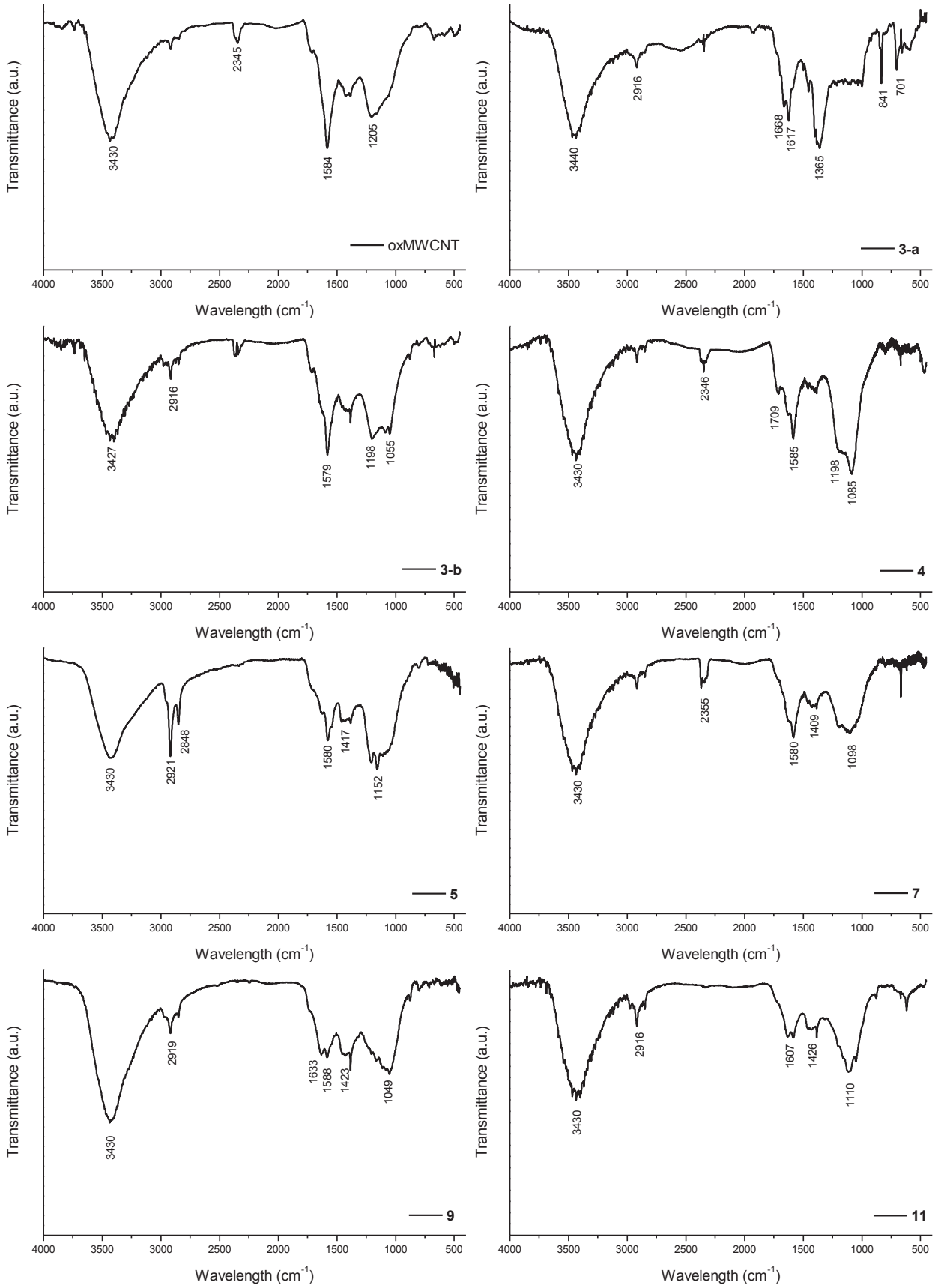

Figure 2.2 FT-IR spectra of oxMWCNTs and aminated MWCNTs.

In general, by IR spectroscopy we could observe major changes in the spectra of many of the amine-functionalized MWCNTs obtained by direct conversion of the COOH. The spectral features of the new compounds are relatively similar between each other, and those compounds featuring the aminomethylene group (**5**, **9**, and **11**) do display the expected corresponding absorbance in the spectra. The changes in the IR spectra of aminated compounds compared to oxMWCNTs are a proof of the structural modification that occurred upon reaction, and together with XPS data they evidence the covalent introduction of nitrogen-containing groups, which are likely to be amine groups. Nevertheless, the IR characterization of these materials is of difficult interpretation and certainly not straightforward, therefore we prefer not to enter in further speculations.

2.2.2.4 Morphological characterization

The average length distribution of oxMWCNTs was assessed by TEM and corresponds to 381 nm. By TEM we could also observe that oxMWCNTs are predominantly individualized and they generally display a curved shape, which is due to the defects present along the honeycomb structure. In Figure 2.3 are reported TEM pictures of some of the final amino-functionalized compounds as a proof that the nanotube morphology is unchanged after derivatization.

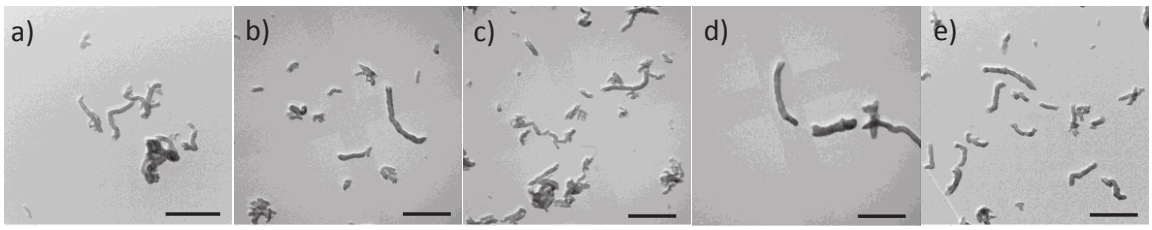

Figure 2.3 TEM images of oxMWCNTs **1** (a) and aminated MWCNTs **3-a** (b), **4** (c), **7** (d) and **9** (e). Scale bars correspond to 500 nm.

For the employment of CNTs in bioapplications and for their further use as carriers, it is imperative that the CNT conjugates display good dispersibility in aqueous solutions. By the various synthetic strategies, no solubilizing functions have been added to the CNTs (*e.g.* polyethylene glycol chains), and moreover, oxMWCNTs have been subjected to several reactions, in some cases with strong reducing agents. By these treatments the surface properties of the starting material might have been severely modified and the good dispersibility of oxMWCNTs reduced. We tested the water dispersibility of the amino-functionalized MWCNTs by preparing 0.2 mg/mL dispersions of each compound in ddH_2O, and compared it to that of oxMWCNTs **1** (Figure 2.4).

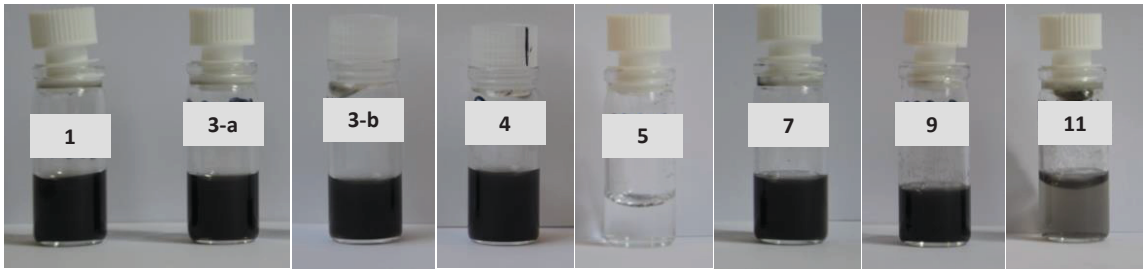

Figure 2.4 Dispersibility of oxMWCNTs and aminated MWCNTs in ddH_2O at a concentration of 0.2 mg/mL.

Most of the amino-functionalized MWCNTs maintained a good water-dispersibility after derivatization, except for compounds **5** (*via* cyanide) and **11** (*via* mesylation). Both compounds feature the aminomethylene group, and underwent a synthetic step involving $LiAlH_4$ reduction: this

might have resulted in the concomitant reduction of some carboxylic groups and/or side-reactions with the graphenic walls. These compounds are therefore not be suitable for further applications, as it was not possible to obtain a good dispersion, also by extensive sonication. In the following table are listed the synthesized compounds and their key characterizations.

Compound	Synthetic Strategy	N atomic % [1]	Water dispersibility
oxMWCNTs **1**		-	good
MWCNTs – NH_2 **3-a**	I (Hofmann)	1.6	good
MWCNTs – NH_2 **3-b**	I (Hofmann)	1.8	good
MWCNTs – NH_2 **4**	II (Curtius)	2.1	good
MWCNTs – CH_2NH_2 **5**	III (*via* cyanide)	1.1	none
MWCNTs – NH_2 **7**	IV (Hunsdiecker)	1.4	good
MWCNTs – CH_2NH_2 **9**	V (Phthalimide)	1.3	good
MWCNTs – CH_2NH_2 **11**	VI (mesylate)	1.3	low

Table 2.3 Summary of the key characterizations of the synthesized compounds. [1]Atomic percentage estimated by XPS.

2.2.3 BIOLOGICAL INVESTIGATIONS

In collaboration with the group of Kostas Kostarelos, we studied the ability of these newly-synthesized aminated MWCNT constructs to bind siRNA and transport it inside cells. These studies include gel electrophoresis analysis, to assess the complexation ability of aminated MWCNTs toward siRNA, and cellular uptake into lung cancer cells. The experiments showed hereafter were performed by our partner.

2.2.3.1 Electrophoretic mobility of siRNA:MWCNT-NH_2 complexes

Electrophoresis in agarose gel is one of the mostly used techniques to assess the complexation between nucleic acids and nanoparticles. The principle is that if siRNA forms strong complexes with the nanoparticles, CNTs in our case, upon application of a potential, only unbound siRNA will migrate through the gel, while the complex will not move from the loading well (because CNTs cannot enter it and migrate). By incubating siRNA with CNTs at different mass ratios, it is then possible to evaluate the extent of the electrostatic complexation.

To perform this experiment we selected only the sample that appeared more valuable from the characterization. We thus discarded those that did not fulfil the dispersibility requirement (compounds **5** and **11)**; and we also ruled out compound **3-b**, whose FT-IR spectra did not show relevant changes compared to oxMWCNTs. The final pool of aminated MWCNTs for the complexation experiment consisted of MWCNT-NH_2 **3-a**, **4** and **7**, and MWCNT-CH_2NH_2 **9**. A fixed concentration (0.25 μg) of non-coding siRNA (siRNAneg) was mixed with increasing concentrations of aminated MWCNTs, and then allowed to electrostatically interact for 30 min at room temperature.

The siRNA:CNT complexes were then loaded into the wells of a pre-formed 1% agarose gel and an electrical current was applied. The bright spots visible at the bottom of the gel indicate the free (uncomplexed) siRNA that was free to migrate (Figure 2.5). For compounds **3-a** and **7**, we can notice that the intensity of the siRNA bands sensibly decreases for higher concentrations of CNTs. The less intense the band appears, the more siRNA was complexed by the CNTs, leaving only a small amount of unbound siRNA free to migrate. Therefore, MWCNTs **3-a** and **7** show the best complexation ability toward siRNA, whith the highest complexation ratio being 1:16. In fact at higher ratios there are no more significant changes in the band intensities. MWCNTs **4** showed a limited capacity to bind siRNA, while MWCNTs **9** were not at all effective, since the band of siRNA appears as intense for the complexes as for the control (1:0 mass ratio).

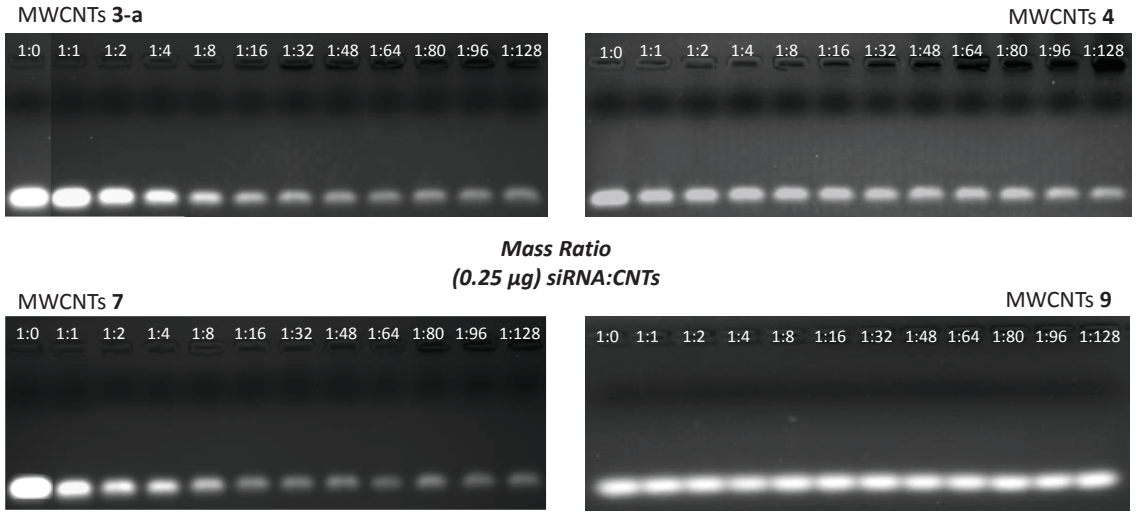

Figure 2.5 Electrophoretic mobility agarose gels obtained by loading non-coding siRNA:MWCNT complexes at increasing mass ratio of nanotubes. Mass ratio 1:0 corresponds to siRNA migrating alone (control). Decreasing of the intensity of the siRNA band in the gel indicates complexation with carbon nanotubes.

2.2.3.2 Cellular uptake of siRNA:MWCNT complexes

To evaluate whether the aminated MWCNTs were able to efficiently deliver the siRNA payloads into cells, we performed a cellular uptake experiment with compound **3-a**, which is the conjugate that showed the best complexation capacity toward siRNA, by gel electrophoresis. Using confocal laser microscopy we investigated if a fluorescently labeled siRNA (siRNA-AF546, siRNA-AlexaFluor546-labeled) was internalized by A549 lung cancer cells following complexation with aminated MWCNTs **3-a**. To this purpose, the cells were incubated for 4 h and 24 h in the presence of pre-formed complexes of siRNA-AF546 with **3-a**, at 1:16, 1:48 and 1:96 mass ratios. In the first raw of Scheme 2.5, we can see that the uptake of siRNA alone (uncomplexed) is very poor, even after 24 hours of incubation. The siRNA-AF546:**3-a** complexes were instead substantially taken up by the A549 cells after 4 h, which is proved by the increased intensity of the red signal co-localized with the cytosolic compartments surrounding the nuclei (Figure 2.6). The accumulation of siRNA-AF546 into the cytosol increased when cells were treated with increasing ratios of MWCNTs. The cellular uptake at 24 h shows that the delivery of siRNA can be sustained over time by using MWCNTs **3-a** as vector, without leading to significant differences in the intensity of the signals, likely because after 4 h the amount of internalized siRNA reached the maximum.

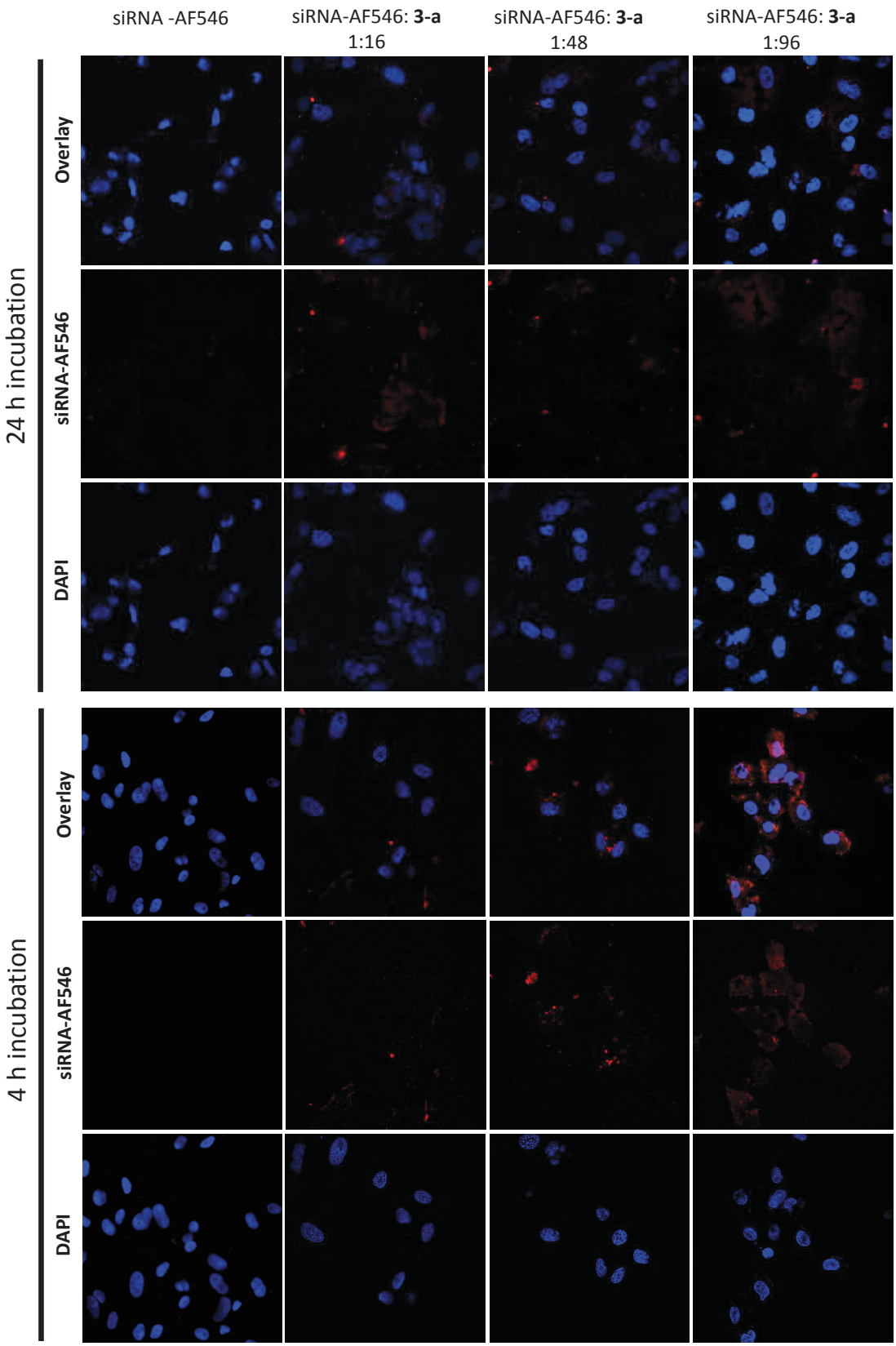

Figure 2.6 Cellular uptake of siRNA-AF546 and siRNA-AF546:**3-a** complexes in A549 cells. Pictures were obtained by confocal microscopy after exposing A549 cells for 4h and 24 h to pre-formed siRNA-AF546:**3-a** complexes at a fixed concentration of siRNA-AF546 (0.25 µg) and at increasing concentrations of MWCNT **3-a**, as indicated by mass ratios in the figure. Cellular uptake can be visualized by the presence of red signal corresponding to AlexaFluor546-labeled siRNA entering the cytosol of the cells. Cell nuclei were stained by DAPI (blue).

Remarkably, the observed cellular uptake is rather relevant compared to the relatively low concentrations of the CNT complexes to which the cells were exposed to. In fact, mass ratios of 1:16, 1:48 and 1:96 correspond to 4, 12 and 24 μg of nanotubes, respectively. In addition, the morphology of the cells was preserved after the uptake of the complexes and this can be considered a good indication of non toxicity. From these results we can affirm that the aminated MWCNT conjugate **3-a** is able to efficiently deliver siRNA into this specific tumor cell line (A549), in an extent comparable to that of ammonium-functionalized nanotubes reported in our previous works.[13–15]

2.3 CONCLUSIONS

In this study we have designed and explored six different synthetic strategies to achieve the direct conversion of the carboxylic group of oxMWCNTs into amino groups, without extending the lateral chain. The surface and morphological characterization of all the final compounds was carried out by different techniques. The quantification of amino groups by the classical ninhydrin colorimetric assay was not possible, probably because of the aromatic character of the introduced amines. However, by XPS analysis we were able to detect the presence of nitrogen in all the samples, with a percentage between 1.1 and 2.1%. FT-IR spectroscopy allowed to identify the changes in the chemical bonding of the aminated MWCNTs compared to oxMWCNTs (except for compound **3-b**), and the characteristic absorption bands of amino groups were recognizable. Furthermore, the compounds featuring aminomethyl groups (**5**, **9**, and **11**) displayed the typical absorbance of methylene around 2900 cm^{-1}, confirming the effectiveness of the synthetic strategy. The morphology of the samples was preserved after chemical modification, according to TEM imaging, whereas some of the compounds (**5** and **11**) presented a significantly reduced water-dispersibility, compared to oxMWCNTs. On the basis of the performed characterization it is clear that structural modifications have occurred for almost all samples (except maybe **3-b**), and nitrogen has been introduced onto MWCNTs. However, the degree of conversion of –COOH into $–NH_2$ is not very high, meaning that a consistent amount of carboxylic groups are still present. Furthermore, it was not possible to achieve the straightforward assessment of the amount and type of functionalities introduced, although it is reasonable to believe that they are amino groups. The ability of four of the aminated MWCNTs to complex siRNA has been assessed by gel electrophoresis using different mass ratios. MWCNTs **3-a** and **7** have shown the best complexation ability, reaching the highest complexation at 1:16 ratio siRNA:MWCNTs. We then evaluated the efficacy of the siRNA:**3-a** complexes to transfect the genetic material inside a tumor cell line, and proved that the cells were able to uptake the complexes already after 4 hours, without showing any sign of toxicity.

By this study we confirmed the importance of surface chemistry and its impact on the behavior of MWCNTs in a biological context. In fact, not all compounds displayed the necessary water-dispersibility, and only two were able to efficiently complex siRNA. Clearly, the presence of positively charged groups on the surface plays a major role for the siRNA complexation/delivery, but further investigations are undoubtedly needed. In particular, we would like to stress on the importance of thorough characterization of the CNT conjugates, which is mandatory for their possible application as vectors of genetic material.

2.4 EXPERIMENTAL PART

2.4.1 COMPOUNDS SYNTHESIS AND CHARACTERIZATION

Materials and Methods

The chemicals and solvents were obtained from commercial suppliers and used without further purification. MWCNTs were purchased from Nanostructured & Amorphous Materials Inc. (Stock # 1240 XH), and they were produced by catalytic carbon vapor deposition (CCVD). The solvents used for synthesis were analytical grade. When anhydrous conditions were required, high quality commercial dry solvents were used. Water was purified using a Millipore filter system MilliQ®. When stated, suspensions were sonicated in a water bath (20 W, 40 kHz). For CNTs filtration, PTFE membrane from Millipore were employed. Membranes for dialysis (MWCO 12000-14000 Da) were purchased from Spectrum Laboratories, Inc. FT-IR spectra were measured on a Perkin Elmer Spectrum One ATR-FT-IR spectrometer. TGA was performed on a TGA1 (Mettler Toledo) apparatus from 30 °C to 900 °C with a ramp of 10 °C min-1 under N2 using a flow rate of 50 mL/min and platinum pans. For the loading estimation, values of weight loss were picked at 500 °C. XPS analyses were performed on one of the following spectrometers. A MULTILAB 2000 (THERMO) spectrometer equipped with an anode using Al Kα radiation (hν = 1486.6 eV), with 10 min of acquisition in order to achieve a good signal-to-noise ratio. A Thermo Scientific K-Alpha X-ray photoelectron spectrometer equipped with a Al anode as the X-ray source (x-ray radiation of 1486 eV) and with a basic chamber pressure of ~10.8 – 10.9 mbar. Spot sizes of 400 μm were used. Survey spectra are an average of 10 scans with a pass energy of 200.00 eV and a step size of 1eV. High-resolution spectra are an average of 10 scans with a pass energy of 50.00 eV and a step size of 0.1 eV. TEM analysis was performed on a Hitachi H7500 microscope (Tokyo, Japan) with an accelerating voltage of 80 kV, equipped with a AMT Hamamatsu camera (Tokyo, Japan). The samples were dispersed in water/MeOH (1:1) at a concentration of 0.05 mg/mL and the suspensions were sonicated for 15 min. Ten microliters of the suspensions were drop-casted onto carbon-coated copper grids (Formvar/Carbon 300 Mesh, Cu from Delta Microscopies) and left for evaporation under ambient conditions.

Oxidation of MWCNTs

500 mg of pristine MWCNTs were treated with a solution of H_2SO_4/HNO_3 (75 mL, 3:1 v/v, 98% and 65% respectively) at 0 °C, and the mixture was sonicated for 24 h in a water bath (20 W, 40 kHz). The mixture was then carefully diluted with distilled water (300 mL) and filtered through a PTFE membrane (0.45 μm). The black material on the filter membrane was re-suspended in water by sonicating for 15 min and filtered again, and this sequence was repeated until neutrality of the aqueous solution. The CNTs were then further purified by dialysis against deionized water for 48 h and finally lyophilized.[26] Shortened oxidized MWCNTs (oxMWCNTs **1**) were obtained with a yield of 98% w/w. The average length distribution of oxMWCNTs was assessed to be 381 nm by TEM. The amount of carboxylic acids introduced corresponds to 1.4 mmol/g and was calculated on the base of the weight loss difference with the pristine MWCNTs obtained by TGA.

XPS: C1s (285.2 eV) 84.6%, O1s (532.5 eV) 15.4%; FT-IR (KBr, ν /cm^{-1}): 3430, 2345, 1584, 1205.

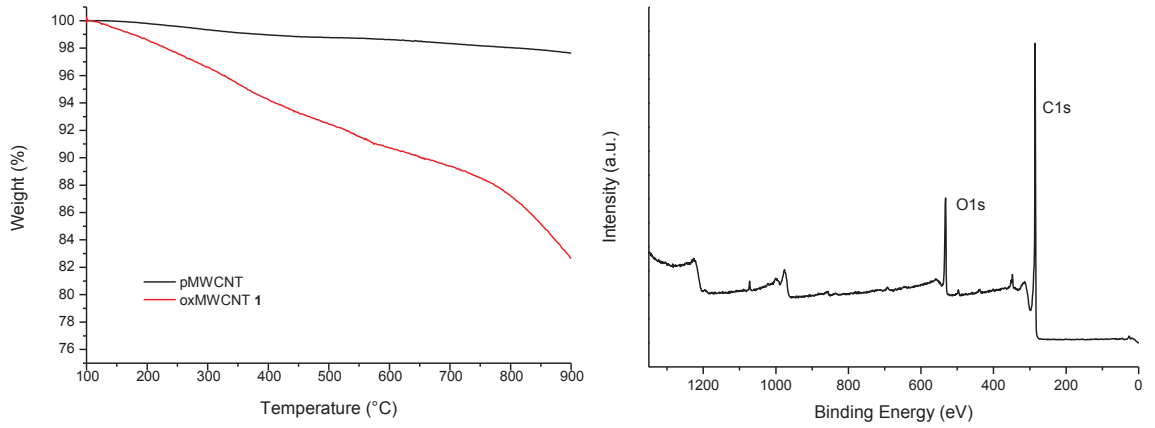

Figure 2.7 Thermogravimetric curves of pMWCNTs and oxMWCNTs **1** (left), and XPS spectrum of oxMWCNTs **1**.

Activation of oxMWCNTs

oxMWCNTs **1** (160 mg) were dispersed in oxalyl chloride (80 mL) by shortly sonicating, and the mixture was then refluxed for 24 h stirring under argon.[26] The solvent was removed under reduced pressure and the resulting activated nanotubes (MWCNT-COCl) were used straightaway for the following step (strategy I, II or III).

Strategy I: Hoffmann reaction

Synthesis of MWCNT-CONH$_2$ **2-a** via *esterification (a)*

Activated ox-MWCNTs (160 mg) were dispersed in dry DMF (26 mL) by sonicating 5 min. A solution of BuOH/Py 1:2 (3 mL) was then slowly added to the dispersion at r.t. and the reaction mixture was stirred at 80 °C for 70 h, under argon. The mixture was filtered through a PTFE membrane (0.45 μm), and the CNTs were re-dispersed in EtOH by sonicating 10 min and filtered again. This washing sequence was repeated twice, finally affording MWCNT-COOBu. The molar loading of –COOBu estimated by TGA is of 135 μmol/g.

MWCNTs-COOBu were dispersed in 25% aq. NH_3 (250 mL) by sonicating for 10 min, and the reaction mixture was stirred at 40 °C for 100 h.[22] CNTs were then recovered by filtration (0.1 μm) and washed by dispersing them in water, sonicating for 10 min and filtrating. This sequence was repeated with H_2O, EtOH (x 2) and the CNTs were dried, affording 131 mg of MWCNT-CONH$_2$ **2-a** (yield of 82% w/w).

Synthesis of MWCNT-CONH$_2$ **2-b** via *amidation (b)*

20 mg of MWCNT-COCl were added to a dispersion of $(NH_4)_2CO_3$ in dry DMF (10 mL), and gently sonicated for few minutes. Pyridine (10 mL) was then dropped on the mixture at r.t., and

this was stirred at 70 °C for 40h, under argon. CNTs were filtrated over a PTFE membrane (0.1 μm), washed with H_2O and EtOH and dried.[22]

Synthesis of MWCNT-NH$_2$ **3-a** *and* **3-b**

Br_2 (2.7 mL, 53 mmol) was slowly added to a solution of CH_3ONa (4.06 g, 75 mmol) in dry MeOH (150 mL) at 0 °C, while vigorously stirring under argon. After 5 min, MWCNT-CONH$_2$ **2-a** or **2-b** (125 mg) were added to the solution, this was gently sonicated for few minutes and then refluxed (70 °C) overnight under argon. An additional aliquot of Br_2 (1.2 mL) was further added, and the mixture was stirred at 70 °C for additional 20 h.[22] The product was recovered by filtration, washed with sat. $NaHCO_3$ (x 3), H_2O, EtOH and acetone, and finally dried *in vacuo,* affording aminated MWCNTs **3-a** (yield of 98% w/w) and **3-b** (yield of 70% w/w).

Compound **3-a**: NH_2 loading (by K.T.) = nil; XPS: C1s (285.3 eV) 76.5%, O1s (533.0 eV) 22.0%, N1s (400.4 eV) 1.6%; FT-IR (KBr, ν /cm^{-1}): 3440, 2916, 1668,1617, 1365, 841, 701.

Compound **3-b**: NH_2 loading (by K.T.) = 11 μmol/g; XPS: C1s (284.7 eV) 82.5%, O1s (532.9 eV) 15.7%, N1s (400.2 eV) 1.8%; FT-IR (KBr, ν /cm^{-1}): 3427, 2916, 1579, 1198, 1055.

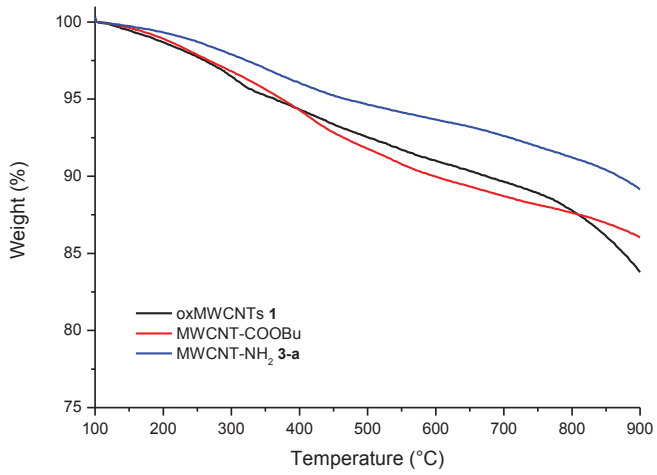

Figure 2.8 Thermogravimetric graph showing the weight loss of oxMWCNTs **1**, MWCNT-COOBu and MWCNT-NH$_2$ **3-a**.

Strategy II: Curtius rearrangement

Synthesis of MWCNT-NH$_2$ **4**

Sodium azide (26 mg) was added to a dispersion of MWCNT-COCl (10 mg) in dry DMF (10 mL), and the mixture was stirred at r.t. for 45 h, and then at 100 °C for 20 h, under argon. The mixture was then filtered through a PTFE membrane (0.45 μm), and the CNTs were washed with DMF by sonication for 10 min and filtration, and successively treated with conc. HCl for 60 h.[22] Aminated CNTs were recovered by filtration, and washed by dispersing them in water, sonicating for 10 min and filtrating. This washing sequence was then repeated with MeOH (x 2) and acetone, and MWCNTs **4** were finally dried *in vacuo*.

NH_2 loading (by K.T.) = 29 μmol/g; XPS: C1s (285.3 eV) 84.4%, O1s (533.9 eV) 13.9%, N1s (400.9 eV) 1.3%; FT-IR (KBr, ν /cm^{-1}):3430, 2346, 1709, 1585, 1198, 1085.

Strategy III: via cyanide

Synthesis of MWCNT-CH_2NH_2 **5**

CuCN (14.4 mg) was added to a dispersion of MWCNT-COCl (16 mg) in dry MeCN (7.5 mL) and the mixture was stirred at r.t. for 24 h, under argon. The mixture was then diluted with acetone (10 mL) and centrifuged (5000 r/min, 5 min), the supernatant was removed and the CNTs were re-dispersed in fresh acetone. This sequence was repeated 4 times and the so-obtained MWCNTs were dried *in vacuo*.

For the decarbonylation of acyl cyanide, nanotubes were suspended in dry toluene (7 mL) by sonicating for 10 min. Cesium fluoride (10.5 mg, 1 eq.) and $Pd(PPh_3)_4$ (7.5 mg, 0.1 eq.) were added to the mixture and this was stirred at 110 °C for 5 hours.[28] The reaction was stopped by centrifuging the mixture (5000 r/min, 5 min) and removing the liquid phase. The CNTs were re-dispersed in toluene by sonication (15 min), centrifuged and the solvent removed. This washing procedure was repeated with 0.1M KOH, aq. NH_3 (20% v/v), 0.01 M HCl, EtOH and Et_2O, and MWCNT-CN were finally dried under vacuum.

In a flamed round-bottom flask, MWCNT-CN (7 mg) were dispersed in freshly dried THF (10 mL) by sonicating for 20 min, under argon. A 2.2 M solution of $LiAlH_4$ in freshly dried THF (0.8 mL) was slowly added to the CNTs solution *via* syringe, and stirred vigorously at r.t. for 20 h. The mixture was quenched in a beaker with cold water, stirred for few minutes and filtrated. The black residue was treated with conc. HCl (3-4 mL) to dissolve the lithium salts, filtrated (0.1 μm), washed with H_2O, EtOH and acetone, and MWCNT-CH_2NH_2 **5** were recuperated by precipitation and dried.

NH_2 loading (by K.T.) = 10 μmol/g; XPS: C1s (284.7 eV) 81.9%, O1s (532.5 eV) 16.9%, N1s (400.3 eV) 1.1%; FT-IR (KBr, ν /cm^{-1}): 3430, 2921, 2848, 1580, 1417, 1152.

Strategy IV: Hunsdiecker reaction

Synthesis of MWCNT-I **6**

oxMWCNTs 1 (17 mg) were dispersed in MeCN/H_2O 97:3 (8 mL) by sonicating for 15 min. LiOAc (6 mg) and *N*-iodosuccinimide (150 mg) were then added to the mixture and this was stirred at 60 °C for 24 h. The CNTs were recovered by filtration (0.1 μm), and washed with MeCN, MeOH, acetone (x 2), and finally dried *in vacuo* obtaining iodinated MWCNTs **6**.

XPS: C1s (285.3 eV) 83.3%, O1s (532.5 eV) 16.6%, I3d (620.5 eV) 0.06%; FT-IR (KBr, ν /cm^{-1}): 3437, 1580, 785.

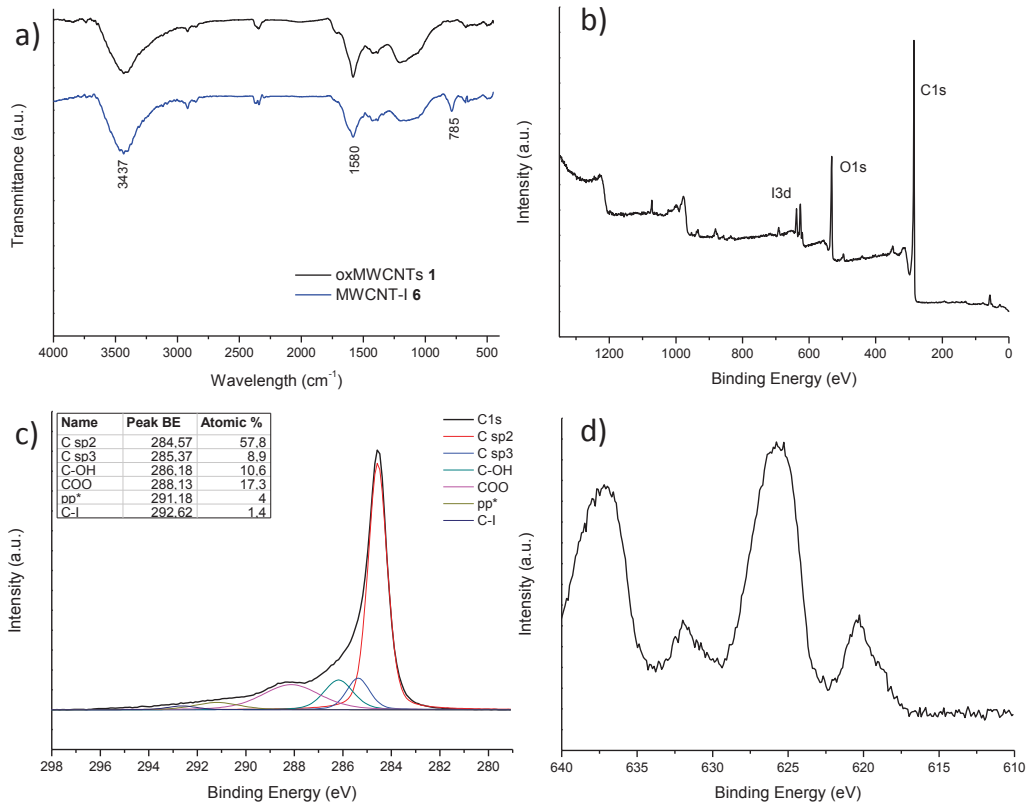

Figure 2.9 Characterization of compound **6**. FT-IR (a) and XPS spectra: general survey (b), C1s (c), I3d (d).

Synthesis of MWCNT-NH_2 **7**

MWCNTs **6** (13 mg) were sonicated in dry DMF (6 mL) for 10 min under argon. NaN_3 (40 mg) was added to the dispersion and this was stirred at r.t. for 5 h and at 50 °C for 16 h. The CNTs were then recovered by filtration (0.1 μm) and washed with DMF (x 2), MeOH (x 2) and acetone (x 2), and finally dried *in vacuo*. Right afterwards, the so-obtained MWCNTs were dispersed in freshly dried THF (10 mL) inside a flamed vessel by sonicating for 20 min. A 2.2 M solution of $LiAlH_4$ in dry THF (0.8 mL) was slowly added by syringe to the CNTs dispersion, and this was vigorously stirred overnight at r.t. The reaction was stopped by carefully pouring the mixture into a beaker with cold water (60 mL) while stirring. Few drops of conc. HCl were added to the mixture to dissolve the lithium salts, and the CNTs were recovered by filtration (0.1 μm), re-dispersed in H_2O and precipitated by centrifugation. The supernatant was removed away and CNTs were further washed once with EtOH and once with acetone recovering them by centrifugal precipitation. MWCNT-NH_2 **7** were finally dried *in vacuo*.

NH_2 loading (by K.T.) = 34 μmol/g; XPS: C1s (285.4 eV) 77.4%, O1s (533.3 eV) 21.2%, N1s (401.2 eV) 1.4%; FT-IR (KBr, ν /cm^{-1}): 3430, 2355, 1580, 1409, 1098.

Synthesis of MWCNT-CH_2OH **8**

oxMWCNTs **1** (19 mg) were dispersed in dry THF (10 mL) by sonicating for 30 min under argon. A 1 M solution of $LiAlH_4$ in THF (0.4 mL) was carefully added by syringe to the dispersion and

this was stirred at r.t. for 1 h. The mixture was sonicated for 10 min and then slowly poured onto a 2 M HCl solution (30 mL), while stirring vigorously. The CNTs were then recovered by filtration (0.1 μm), washed with H_2O, EtOH, acetone and dried *in vacuo*, obtaining MWCNTs-CH_2OH **8**.

XPS: C1s (285.2 eV) 84.8%, O1s (532.8 eV) 15.2%; FT-IR (KBr, ν /cm^{-1}): 3430, 2917, 631, 1579, 1210, 1077, 798.

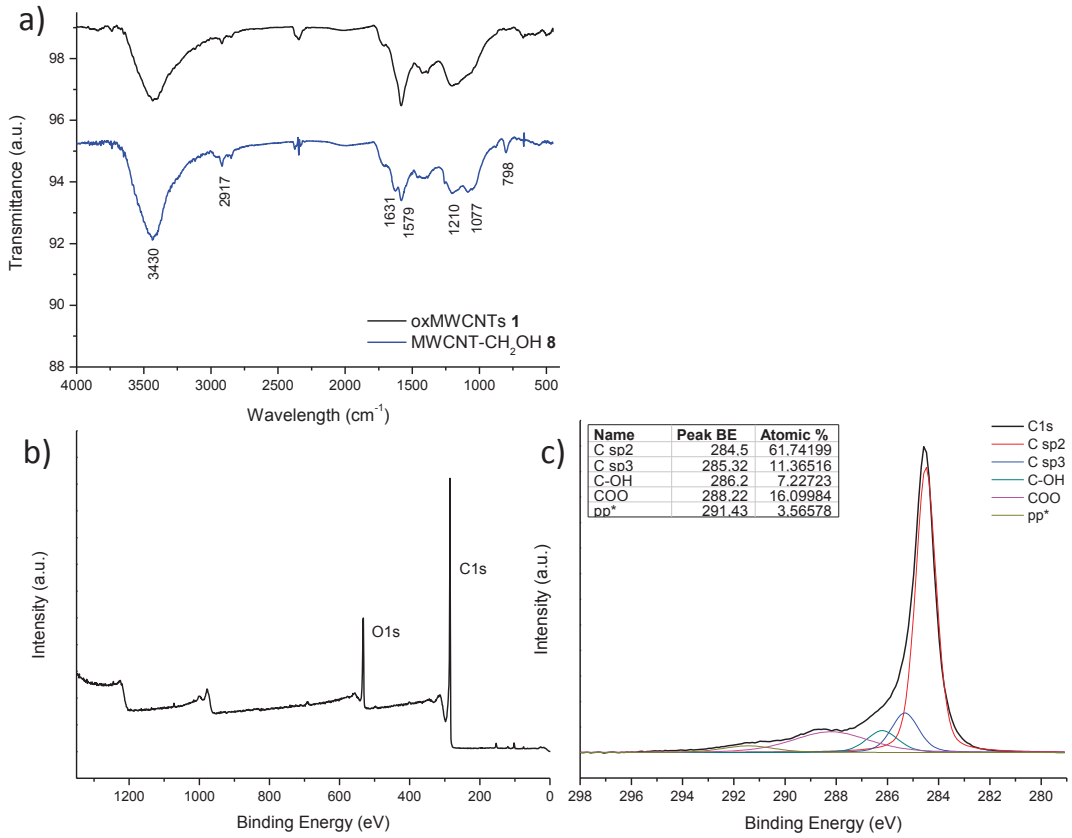

Figure 2.10 Characterization of compound **8**. FT-IR (a) and XPS spectra: general survey (b), C1s (c).

Strategy V: via phthalimide coupling

Synthesis of MWCNT-CH_2NH_2 **9**

MWCNTs **8** (12 mg) were dispersed in THF (10 mL) by sonicating for 30 min under argon. Phthalimide (14 mg) and DEAD (2 mL) were then added, and the mixture was sonicated for 2 h and further stirred for 2.30 h. The mixture was then diluted with MeOH (50 mL), filtered (0.1 μm) and the recovered CNTs were re-dispersed in MeOH (20 mL) by sonication, filtered again and dried *in vacuo*. The so-obtained Pht-functionalized CNTs were suspended in a small volume of DCM (2 mL) by sonication, and the dispersion was then treated with trifluoroacetic acid (7 mL) and sonicated for 3 h. Aminated CNTs **9** were recovered by filtration, washed twice with DCM and dried.

NH_2 loading (by K.T.) = 16 μmol/g; XPS: C1s (285.2 eV) 84.8%, O1s (533.0 eV) 13.9%, N1s (401.1 eV) 1.3%; FT-IR (KBr, ν /cm^{-1}): 3430, 2919, 1633, 1588, 1423, 1049.

Strategy VI: via mesylation

Synthesis of MWCNT-CH_2N_3 **10**

MWCNT-CH_2OH **8** (9 mg) were suspended in dry DCM by sonicating for 30 min under argon. Methanesulfonyl chloride (6.5 mL) and then Et_3N (0.5 mL) were added to the mixture at 0 °C, and this was further sonicated at 0 °C for 30 min and stirred at r.t. overnight. The CNTs were recovered by filtration (0.1 μm), washed with DCM (x 2) and vacuum dried. The so-obtained CNTs were dispersed in dry DMF by sonicating 15 min under argon. Sodium azide (10 mg) and sodium iodide (catalytic amount) were added and the mixture was sonicated for additional 15 min and then left to react at 60 °C for 48 h, under argon. After filtration (0.1 μm), CNTs were washed with DMF, MeOH (x 2), acetone (x 2) and dried under vacuum, affording compound **10**.

FT-IR (KBr, ν /cm^{-1}): 3430, 2912, 1580, 1014.

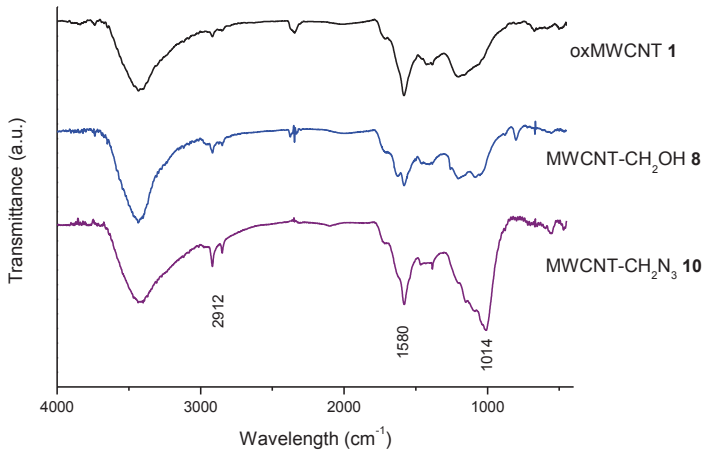

Figure 2.11 FT-IR spectrum of compounds **1**, **8** and **10**.

Synthesis of MWCNT-CH_2NH_2 **11**

In a flamed round-bottom flask, MWCNT-CH_2N_3 **10** (6 mg) were dispersed in freshly dried THF (10 mL) by sonicating for 20 min, under argon. A 2.2 M solution of $LiAlH_4$ in freshly dried THF (0.8 mL) was slowly added to the CNTs solution by syringe, and stirred vigorously at r.t. for 20 h. The reaction was quenched by carefully pouring the mixture in a beaker with cold water, and stirring stirred for few minutes. The slurry was then filtrated (0.1 μm) and the black residue was treated with conc. HCl (3-4 mL) to dissolve the lithium salts, filtrated, washed with H_2O, EtOH and acetone, and MWCNT-CH_2NH_2 **11** were finally recuperated by precipitation and dried.

NH_2 loading (by K.T.) = 26 μmol/g; XPS: C1s (284.7 eV) 76.1%, O1s (533.0 eV) 22.6%, N1s (400.4 eV) 1.3%; FT-IR (KBr, ν /cm^{-1}): 3430, 2916, 1607, 1426, 1110.

2.4.2 BIOLOGICAL INVESTIGATIONS

Gel electrophoresis mobility assay

Dilutions of non-coding siRNA (siRNAneg, Qiagen, MW= 14857 g/mol) in RNAse-free water (20 μM) were prepared according to the manufacturer protocols. Dilutions were prepared in milli-Q water in order to have a final concentration of 0.25 μg of siRNAneg in 15 μL of solution. Dilutions of aminated MWCNTs were prepared according to each mass ratio required for the complexation with siRNAneg from a 1 mg/mL dispersion in milli-Q RNAase-free water after sonication for few minutes. Final volumes of MWCNT dilutions were set to be at 15 μL. The siRNA solution was added to the CNTs dispersion and the two were mixed by rapidly pipetting. After an incubation of 30 min at r.t., each siRNA:CNT dispersions was added with 8 μL of Green Orange DNA loading dye (Fermentas, Thermo Scientific) and then loaded into 1% agarose gel (final volume 38 μL). Gels were run for 45 min at 70 mV before visualization using the GeneSnap software under the UV light. Gel was prepared by using TBE buffer (Tris-Borate-EDTA) added of 1% agarose. Briefly, Trizma base (108 g), boric acid (55 g), EDTA (9.3 g) and NaOH (1 g) were dissolved in 1 L of distilled water by vigorously stirring. The buffer was diluted 20x with distilled water, and the same buffer used for the 1% agarose gel preparation (30 min) as well as running buffer.

Cellular uptake in A459 cells

A459 lung cancer cells were maintained in complete F12-Ham's (Gibco, LifeTechnologies) media complemented with 10% FBS (foetal bovine serum) on non-coated Petri's dishes, and media renewed every 3 days until cells were at confluence. The day before the experiment, the cells were seeded at $5x10^3$ cells/well density on a Millipore-microscope slide multi well support (Ezslides, Millipore) in the presence of complete media. Non-coding AlexaFluor546-labeled siRNAneg (siRNA-AF546) (5'-3': UGCGCUACGAUCGACGAUG) (Eurogentec, UK) was used to complex with aminated MWCNTs, mixing equal volumes to obtain a mass ratio of 16:1, 48:1 and 96:1. To obtain siRNA-AF546 at final concentration of 40 nM corresponding to 0.25 μg of siRNA on each well, 75 μL of siRNA-AF546 (20 μM) was diluted in of RNAse free sterile water. One hundred μL of this solution ware mixed with 100 μL of aminated MWCNTs diluted in sterile/RNAse free milli-Q water. These dilutions were thus mixed together by rapidly pipetting and let interact for 30 min prior being added to each well containing cells and 400 μL of FBS free complete media. Treatments at 4h were stopped by removing the media, washing several time with sterile water, fixing cells in 4% paraformaldehyde for 15 min, removing by washing and adding 5 μL of DAPI staining for the cell nuclei. The same procedure was repeated for the 24 h treatments, but after 4 h incubation in the presence of the complexes, the medium was complemented with 10% of FBS to preserve the cell growth. Cells were then visualized under confocal microscopy by mounting the coverslip to each microscopy slide. Images were acquired on a confocal laser scanning LSM 710 microscope (Carl Zeiss) or on a Mp-OPO SP8 (Leica) used in the confocal mode.

2.5 BIBLIOGRAPHY

[1] A. J. Hamilton, D. C. Baulcombe, *Science* **1999**, *286*, 950.

[2] G. J. Hannon, *Nature* **2002**, *418*, 244.

[3] R. Kanasty, J. R. Dorkin, A. Vegas, D. Anderson, *Nat. Mater.* **2013**, *12*, 967.

[4] A. de Fougerolles, H.-P. Vornlocher, J. Maraganore, J. Lieberman, *Nat. Rev. Drug Discov.* **2007**, *6*, 443.

[5] A. Akinc, A. Zumbuehl, M. Goldberg, E. S. Leshchiner, V. Busini, N. Hossain, S. A. Bacallado, D. N. Nguyen, J. Fuller, R. Alvarez, A. Borodovsky, T. Borland, R. Constien, A. de Fougerolles, J. R. Dorkin, K. Narayanannair Jayaprakash, M. Jayaraman, M. John, V. Koteliansky, M. Manoharan, L. Nechev, J. Qin, T. Racie, D. Raitcheva, K. G. Rajeev, D. W. Y. Sah, J. Soutschek, I. Toudjarska, H.-P. Vornlocher, T. S. Zimmermann, R. Langer, D. G. Anderson, *Nat. Biotechnol.* **2008**, *26*, 561.

[6] N. W. S. Kam, H. Dai, *J. Am. Chem. Soc.* **2005**, *127*, 6021.

[7] M. Foldvari, M. Bagonluri, *Nanomedicine* **2008**, *4*, 183.

[8] K. Bates, K. Kostarelos, *Adv. Drug Deliv. Rev.* **2013**, *65*, 2023.

[9] D. Pantarotto, R. Singh, D. McCarthy, M. Erhardt, J.-P. Briand, M. Prato, K. Kostarelos, A. Bianco, *Angew. Chem. Int. Ed.* **2004**, *43*, 5242.

[10] N. W. S. Kam, Z. Liu, H. Dai, *J. Am. Chem. Soc.* **2005**, *127*, 12492.

[11] Z. Zhang, X. Yang, Y. Zhang, B. Zeng, S. Wang, T. Zhu, R. B. S. Roden, Y. Chen, R. Yang, *Clin. Cancer Res.* **2006**, *12*, 4933.

[12] K. T. Al-Jamal, L. Gherardini, G. Bardi, A. Nunes, C. Guo, C. Bussy, M. A. Herrero, A. Bianco, M. Prato, K. Kostarelos, T. Pizzorusso, *Proc. Natl. Acad. Sci. U. S. A.* **2011**, *108*, 10952.

[13] A. Battigelli, J. T.-W. Wang, J. Russier, T. Da Ros, K. Kostarelos, K. T. Al-Jamal, M. Prato, A. Bianco, *Small* **2013**, *9*, 3610.

[14] J. E. Podesta, K. T. Al-Jamal, M. A. Herrero, B. Tian, H. Ali-Boucetta, V. Hegde, A. Bianco, M. Prato, K. Kostarelos, *Small* **2009**, *5*, 1176.

[15] K. Kostarelos, L. Lacerda, G. Pastorin, W. Wu, S. Wieckowski, J. Luangsivilay, S. Godefroy, D. Pantarotto, J.-P. Briand, S. Muller, M. Prato, A. Bianco, *Nat. Nanotechnol.* **2007**, *2*, 108.

[16] K. T. Al-Jamal, A. Nunes, L. Methven, H. Ali-Boucetta, S. Li, F. M. Toma, M. A. Herrero, W. T. Al-Jamal, H. M. M. ten Eikelder, J. Foster, S. Mather, M. Prato, A. Bianco, K. Kostarelos, *Angew. Chem. Int. Ed.* **2012**, *51*, 6389.

[17] G. Bardi, A. Nunes, L. Gherardini, K. Bates, K. T. Al-Jamal, C. Gaillard, M. Prato, A. Bianco, T. Pizzorusso, K. Kostarelos, *PLoS One* **2013**, *8*, e80964.

[18] A. Hirsch, *Angew. Chemie Int. Ed.* **2002**, *41*, 1853.

[19] S. Niyogi, M. A. Hamon, H. Hu, B. Zhao, P. Bhowmik, R. Sen, M. E. Itkis, R. C. Haddon, *Acc. Chem. Res.* **2002**, *35*, 1105.

[20] C.-H. Andersson, H. Grennberg, *European J. Org. Chem.* **2009**, *2009*, 4421.

[21] T. Ramanathan, F. T. Fisher, R. S. Ruoff, L. C. Brinson, *Chem. Mater.* **2005**, *17*, 1290.

[22] A. Gromov, S. Dittmer, J. Svensson, O. A. Nerushev, S. A. Perez-García, L. Licea-Jiménez, R. Rychwalski, E. E. B. Campbell, *J. Mater. Chem.* **2005**, *15*, 3334.

[23] L. Wang, S. Feng, J. Zhao, J. Zheng, Z. Wang, L. Li, Z. Zhu, *Appl. Surf. Sci.* **2010**, *256*, 6060.

[24] K. S. Coleman, A. K. Chakraborty, S. R. Bailey, J. Sloan, M. Alexander, *Chem. Mater.* **2007**, *19*, 1076.

[25] M. Smith, J. March, in *March's Adv. Org. Chem. React. Mech. Struct.*, John Wiley & Sons Inc., New Jersey, **2007**, pp. 1607–1609.

[26] C. Samorì, R. Sainz, C. Ménard-Moyon, F. M. Toma, E. Venturelli, P. Singh, M. Ballestri, M. Prato, A. Bianco, *Carbon* **2010**, *48*, 2447.

[27] D. Bonifazi, C. Nacci, R. Marega, S. Campidelli, G. Ceballos, S. Modesti, M. Meneghetti, M. Prato, *Nano Lett.* **2006**, *6*, 1408.

[28] D. Georgin, B. Czarny, M. Botquin, M. Mayne-L'hermite, M. Pinault, B. Bouchet-Fabre, M. Carriere, J.-L. Poncy, Q. Chau, R. Maximilien, V. Dive, F. Taran, *J. Am. Chem. Soc.* **2009**, *131*, 14658.

[29] M. Smith, J. March, in *March's Adv. Org. Chem. React. Mech. Struct.*, John Wiley & Sons Inc., New Jersey, **2007**, pp. 994–996.

[30] D. Naskar, S. Chowdhury, S. Roy, *Tetrahedron Lett.* **1998**, *39*, 699.

[31] D. Naskar, S. Roy, *Tetrahedron* **2000**, *56*, 1369.

[32] S. Chowdhury, S. Roy, *J. Org. Chem.* **1997**, *62*, 199.

[33] E. Kaiser, R. L. Colescott, C. D. Bossinger, P. I. Cook, *Anal. Biochem.* **1970**, *34*, 595.

[34] V. K. Sarin, S. B. H. Kent, J. P. Tam, R. B. Merrifield, *Anal. Biochem.* **1981**, *117*, 147.

[35] V. Datsyuk, M. Kalyva, K. Papagelis, J. Parthenios, D. Tasis, A. Siokou, I. Kallitsis, C. Galiotis, *Carbon* **2008**, *46*, 833.

[36] C. Moreno-Castilla, M. V. López-Ramón, F. Carrasco-Marín, *Carbon* **2000**, *38*, 1995.

[37] S. Biniak, G. Szymański, J. Siedlewski, A. Świątkowski, *Carbon* **1997**, *35*, 1799.

[38] G. Ovejero, J. L. Sotelo, M. D. Romero, A. Rodríguez, M. A. Ocaña, G. Rodríguez, J. García, *Ind. Eng. Chem. Res.* **2006**, *45*, 2206.

[39] S. Goyanes, G. R. Rubiolo, A. Salazar, A. Jimeno, M. A. Corcuera, I. Mondragon, *Diam. Relat. Mater.* **2007**, *16*, 412.

[40] U. J. Kim, C. A. Furtado, X. Liu, G. Chen, P. C. Eklund, *J. Am. Chem. Soc.* **2005**, *127*, 15437.

CHAPTER 3

FUNCTIONALIZATION OF CNTS *VIA* A CLEAVABLE DISULFIDE BOND FOR DELIVERY OF A THERAPEUTIC NANOBODY

Abstract – In this Chapter, we will present the design and synthesis of novel CNT conjugates for anticancer therapy, obtained by connecting a therapeutic nanobody to oxidized CNTs *via* cleavable linkers. These particular nanobodies are antibody-derived therapeutic proteins from camel that display the typical antibody advantages, such as high affinity for the target and low inherent toxicity, and are easy to manufacture. The CNT constructs were designed to contain a hydrophilic chain (TEG) for water dispersibility, and a disulfide cleavable linker, to access the controlled release of the therapeutic intracellularly. The disulfide bond can in fact be cleaved by enzymes in lysosomal compartments or once exposed to the reducing environment (*e.g.* by glutathione) of the cytosol. The as-prepared nanobody-CNT conjugates have been characterized by several techniques, including TGA, gel electrophoresis and surface plasmon resonance, and their therapeutic efficiency was investigated on a carcinoma cell line, and on tumor-bearing mice.

3.1 INTRODUCTION

Antibodies are large Y-shaped proteins used by the immune system to identify and neutralize foreign objects like bacteria and viruses. Each antibody recognizes a specific antigen with high selectivity, and this has contributed to the large success of antibodies as tools for the analysis of biomolecules in research, diagnostics and therapy. The use of monoclonal antibodies has indeed revolutionized both cancer therapy and cancer imaging.[1] Antibodies have been used to directly inhibit tumor cell proliferation or to target drugs to tumors. However, antibodies are big size biomolecules (150 kDa) and are not functional within a living cell due to the reducing environment of the cytoplasm. Furthermore, their distribution within tumors is hampered by their size, leading to insufficient efficacy of cancer treatment and irregular imaging.[2] An attractive alternative to monoclonal antibodies are nanobodies. Nanobodies are constituted by the variable domain of heavy-chain antibodies (*i.e.* VHHs) and are considered the smallest naturally derived fragments retaining antigen-binding specificity (Figure 3.1).[3] Nanobodies were first discovered in 1993 in animals from the Camelidae family, which exhibit a high ratio of heavy-chain antibodies to conventional antibodies.[4] Because of their size in the nm range, the term 'nanobody' was coined by the Belgian company Ablynx®. Nanobodies offer many advantages over full antibodies such as size reduction, high solubility and stability and very low immunogenicity in humans. Moreover, nanobodies are easy to clone and can efficiently enter into cells and specifically bind antigens that typically cannot be reached by conventional intact antibodies. All these desirable properties stimulated a lot of research around nanobodies for their application in biomedical imaging, as well as targeting and therapy of specific diseases.[2,5]

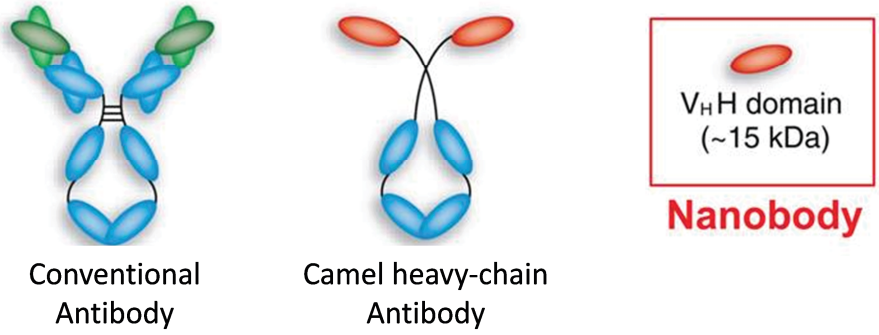

Figure 3.1 Schematic representation of a conventional antibody, heavy-chain antibody and nanobody (VHH). Adapted from ref. [6].

Since it was demonstrated that VHHs can bind antigens on the surface of tumor cells and their immunogenicity is low, they are under intensive scrutiny as potential therapeutic tools, and among the most studied are VHHs with anti-cancer activity. To date, VHHs recognizing antigens that are expressed by cells of different cancers have been obtained, and many of them reveal prospective therapeutic values.[3,7,8]

One of our collaborators, UCB (UK), modified a VHH scaffold to prepare a therapeutic nanobody able to selectively target β-catenin, a protein implicated in the endogenous Wnt signalling pathway. Mutations and overexpression of β-catenin are associated with many cancers, including hepatocellular carcinoma, colorectal carcinoma, lung cancer, malignant breast tumors, ovarian and endometrial cancer.[9] Due to its involvement in cancer development, inhibition of β-catenin continues to receive significant attention. The VHH synthesized by UCB is able to target and hinder the transcriptional

activity of the β-catenin, thus blocking the expression of tumor-associated genes. We found it interesting to match the potential of this therapeutic nanobody toward cancer treatment, with nanotube ability to cross cellular membranes and carry molecules inside the cells. Indeed, the aptitude of CNTs to work as intracellular transporters can be exploited in this case to facilitate the internalization of VHH. Furthermore, we decided to introduce a cleavable linker between the CNT structure and the biomolecule, in order to induce the release of the nanobody in the cytoplasm and to preserve its therapeutic activity. The use of cleavable linkers is quite common in the synthesis of drug delivery systems because it allows a controlled release of the drug, which is triggered only under specific conditions (pH, enzymes, oxidizing/reducing agents, etc.).[10] Among cleavable bonds, disulfides are appealing because of their straightforward synthesis, relative stability in plasma and because they can be efficiently and rapidly cleaved by intracellular reducing agents, such as glutathione (GSH), thioredoxin, glutaredoxin, etc.[11] However, there are only few reports describing the use of disulfides associated with carbon nanotubes. In 2005, the group of H. Dai firstly described the preparation of a CNT vector for gene delivery based on a disulfide linker.[12] SWCNTs were non-covalently functionalized with phospholipidic chains featuring terminal amino groups, a disulfide linker was connected to the latter, and thiolated DNA or siRNA were finally conjugated to the CNTs *via* the linker. They proved that so-functionalized CNTs were able to transport their cargo inside mammalian cells and release it within the lysosomal compartment due to enzymatic reduction of the disulfide bond. Analogously, Delogu *et al.* functionalized PEGylated SWCNTs with the same disulfide linker in order to deliver antisense oligonucleotides inside immune cells (Figure 3.2). These nucleotide sequences can achieve the knockdown of protein tyrosine phosphatase N22, which is an important drug target for autoimmune diseases.[13] Following a similar synthetic pathway, Chen *et al.* built a CNT construct employing a siRNA sequence inhibiting murine double minute clone 2 (MDM2), and they could efficiently transfect breast cancer cells with this construct, achieving inhibition of cell proliferation.[14] All these examples are based on the non-covalent functionalization of CNTs with a solubilizing polymer, followed by the conjugation with the biomolecule.

Figure 3.2 Schematic representation of oligonucleotide-S-S-CNT conjugates used in ref. [12] and [13].

You *et al.* were the first to report the covalent functionalization of CNTs with a disulfide linker.[15,16] They derivatized oxidized CNTs with pyridylthio functionalities and then attached to these a long-chain polymer[15] or BSA,[16] through thiol-disulfide exchange. Later on, the group of I. Ojima prepared an interesting SWCNT-based drug delivery system consisting of tumor-targeting functionalities (biotin) and a cytotoxic drug warhead (i.e. taxoid) attached to the CNTs through a strategically designed cleavable linker.[17] The biotin moieties enhanced the internalization of the conjugate by tumor cells, and once inside the cells, the reducing activity of endogenous thiols (glutathione and/or thioredoxin) triggered the cleavage of the disulfide bond, releasing the taxoid in its active form.

The aim of our study was to design a novel VHH-CNT conjugate bearing a disulfide cleavable linker in order to control the release of the nanobody. To the best our knowledge, no example of

functionalization of CNTs with nanobodies has been so far reported, hence investigations on this area could open a new area of interest in the use of CNTs for cancer therapy.

3.2 Results and Discussion

For the preparation of the VHH-CNT conjugate we used oxidized multi-walled carbon nanotubes as starting material. As mentioned in Chapter 2, the oxidation of MWCNTs by acid treatment shortens and functionalizes the tubes with oxygen-containing groups, substantially increasing their water dispersibility. We studied a fully covalent approach to tether the VHH nanobody to the CNTs, in order to avoid the premature detachment of the nanobody from the nanotubes, which can likewise occur in case of non-covalent functionalization. We designed a linker constituted of a triethylene glycol (TEG) chain as solubilizing spacer, a disulfide-containing moiety, and a maleimide terminal group for the further conjugation of the nanobody. Maleimide is often used in the preparation of bioconjugates since proteins display a number of cysteine residues that can react very easily and in mild conditions with the maleimide double bond.[18–20] The VHH provided by UCB displays in its structure free thiol groups that could be exploited to tether it onto CNTs *via* the maleimido group. The designed conjugate is presented in Scheme 3.1 and it features four main building blocks:

1) the MWCNT
2) the TEG spacer
3) the linker containing the disulfide moiety
4) the maleimide functionality

Connection between these blocks can be easily achieved by amide bonds (Scheme 3.1). We decided to use cystamine as starting material for the disulfide linker and we designed our synthetic strategy accordingly.

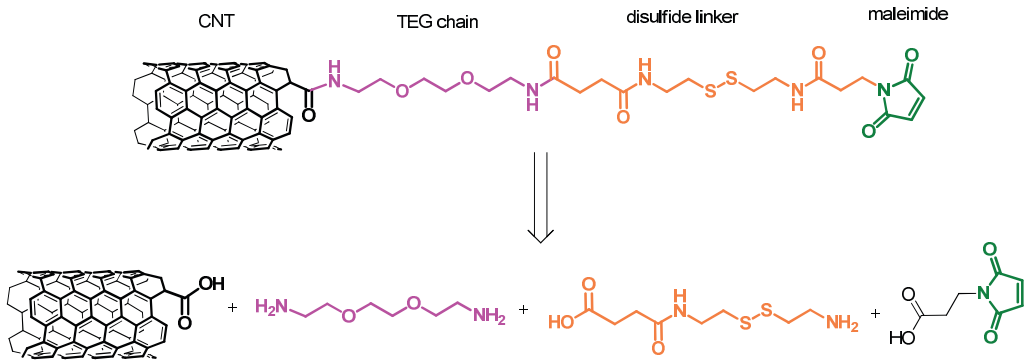

Scheme 3.1 Retrosynthetic analysis for the preparation of the CNT conjugate with a cleavable linker.

Various synthetic solutions can be foreseen to bind the four blocks together and build the desired conjugate (Scheme 3.1). The attachment of amine-terminating chains to the CNTs is commonly one of the favored strategy for the preparation of CNT-functionalized compounds, as the degree of functionalization can be easily monitored by colorimetric Kaiser test. Therefore, we opted for the initial derivatization of oxMWCNTs with amine-terminating TEG. For the combination of the two remaining synthons, it is possible either to attach one after the other to the aminated-CNTs, or to combine them before, and then bind the whole linker to the CNTs. We chose this second strategy as it

appeared synthetically more practical. The final step is the conjugation with the nanobody through Michael addition to the double bond of the maleimide. In this conjugate, named CNT-SS-mal-VHH, the site of cleavage is detached from the nanobody by a short organic chain (ca. 10 atoms), which would remain with the nanobody when the disulfide bond is cleaved. As a consequence, the structure and efficacy of VHH could be affected by this pendant. For comparison, we therefore designed a second CNT-nanobody conjugate bearing no spacer between the nanobody and the cleavage site (Scheme 3.2). To ensure this direct connection, the disulfide bond has to involve a sulfur atom coming from the nanobody itself. This can be achieved by thiol-disulfide exchange between a thiol of VHH and a pyridylthio functionality on the CNTs, in similarity with the above-mentioned examples.[15,16] We used a commercial linker containing a pyridyl disulfide and connected it to amino-functionalized CNTs *via* an amide bond. After attachment of the VHH, the resulting compound was named CNT-SS-VHH, differently from the previous CNT-SS-mal-VHH, to mark the absence of spacer between the disulfide bond and the nanobody.

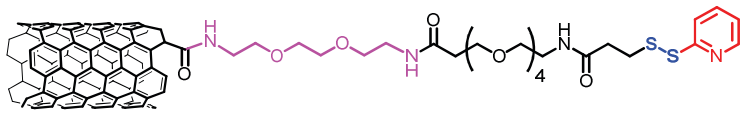

Scheme 3.2 Representation of the precursor for the second conjugate, featuring the pyridylthio group.

Starting from amino-functionalized CNTs, we finally prepared a last conjugate (CNT-VHH), devoid of cleavable linker, to compare its biological behavior with the previous two. In the following paragraph, the synthesis and characterization of the three conjugates will be described in detail. First, we will illustrate the synthesis of amino-functionalized MWCNTs, which is the precursor of all three final conjugates. We will then describe the preparation of each conjugate, followed by its characterization. Finally, the biological investigation performed by us and our partners will be presented and discussed.

3.2.1 SYNTHESIS OF AMINO-FUNCTIONALIZED MWCNTS

MWCNTs were first oxidized and then reacted with previously prepared Boc-mono-protected TEG amine. Commercially available MWCNTs were sonicated in a HNO_3/H_2SO_4 (1:3) mixture for 24 hours, obtaining oxidized MWCNTs **1** (cf. Chapter 2 for a detailed characterization).[21] The functionalization of oxMWCNTs with the amine-terminating TEG chain was obtained by amidation between the carboxylic groups of CNTs and the free amine groups of the TEG spacer. Boc-mono-protected TEG diamine **8** was previously synthesized by reacting triethylene glycol diamine with di-*tert*-butyl dicarbonate (Boc_2O) in 1,4-dioxane. For the amidation reaction, oxidized MWCNTs **1** were refluxed for 24 hours in neat oxalyl chloride under argon, to allow the formation of the acyl chloride intermediate (compound **2**). As this compound is unstable, after evaporation of the reagent the CNTs were dispersed in dry THF and immediately subjected to the reaction with TEG amine **8** (Scheme 3.3). The amidation was conducted for 48 hours at reflux, forming derivative **3**, which displays a Boc-protected amine group as terminus of the TEG chain. The Boc protecting group was removed by treating the CNTs with HCl in 1,4-dioxane, affording amino-functionalized CNTs **4**, which were used as precursors for the preparation of all nanobody-CNT conjugates.

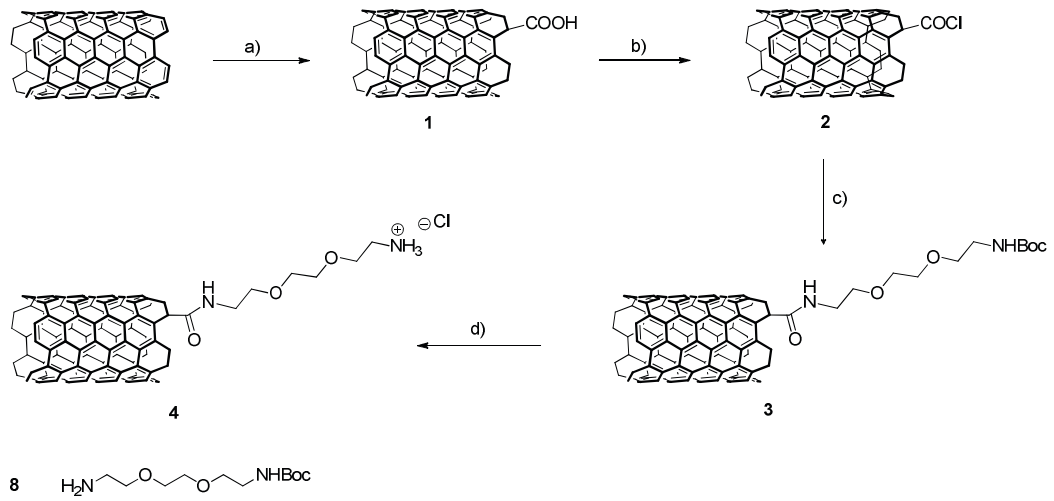

Scheme 3.3 Synthesis of amino-functionalized MWCNTs **4**. a) H_2SO_4/HNO_3 (3:1), sonication, 24 h; b) $(COCl)_2$, reflux, 24 h; c) **8**, THF, reflux, 48 h; d) HCl in 1,4-dioxane, overnight.

The loading achieved by amidation was estimated by TGA under inert atmosphere and by colorimetric Kaiser test. Thermogravimetric analysis is a technique widely used to quantify the degree of functionalization of CNTs and the thermal stability of the conjugates. This analytical technique allows to study the decomposition of the derivatives as a function of the temperature. Pristine CNTs are stable up to 700 °C, while organic functions start to degrade around 200-300 °C. Generally, between 350 °C and 500 °C all organic groups attached to carbon nanotubes are burnt. Above 500°C there is the possibility of a contribution of the oxidation of carbon nanotubes. For the loading calculation we chose to take weight loss values at 500 °C to be sure that all functional groups are removed and that the nanotubes are not degraded. In this way, by correlating the weight loss percentage of two different derivatives at 500 °C, it is possible to obtain the degree of functionalization of the material.

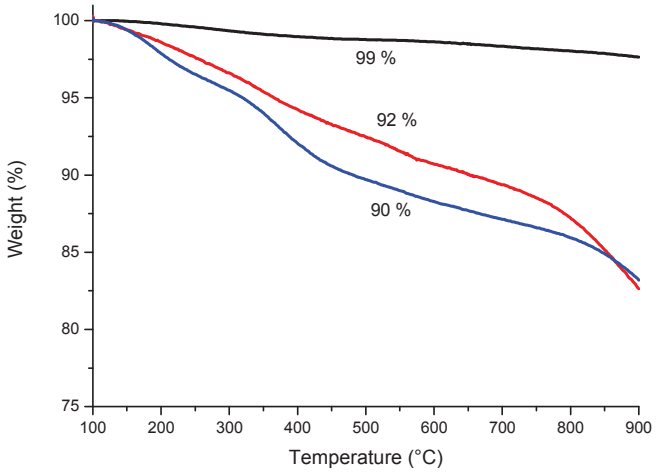

Figure 3.3 TG curves of pMWCNTs (black), oxMWCNTs **1** (red) and MWCNTs **3** (blue).

For oxidized MWCNTs, TGA showed a weight loss of 7.0% compared to pMWCNTs, corresponding to an amount of carboxylic groups of 1.4 mmol/g. By difference between the weight loss of compound **3** and oxMWCNTs, we estimated the loading of Boc-amine TEG to be 100 µmol/g (Figure 3.3). Moreover, after cleavage of the Boc protecting group, it is possible to estimate the amount of free amines (or ammonium) on CNTs by Kaiser test. For compound **4**, the amine loading resulted 182 µmol/g. The discrepancy between the loadings obtained by TGA and Kaiser test

accounts for the intrinsic difference of the technique. Nevertheless, the calculated values are in the same order of magnitude and the estimated divergence is considered acceptable.

3.2.2 SYNTHESIS OF CNT-SS-MAL-VHH

Synthesis of the disulfide linker

For the preparation of the first nanobody-CNT derivative (Scheme 3.1), we synthesized the disulfide-containing linker, which is the intermediate module between amino-functionalized CNTs and VHH. As previously explained, we selected cystamine as starting material because of its commercial availability and synthetic versatility. Cystamine is a symmetric molecule presenting a disulfide bridge and two terminal amino groups. According to our synthetic strategy, one amino group has to be derivatized with the maleimide moiety, which is the reactive site for the successive conjugation of VHH, while the other amino group needs to be modified into a carboxylic group, suitable for the amidation with amino-functionalized CNTs **4** (Scheme 3.5). A common protocol to introduce the maleimide group in a molecule is by reaction with compound **9**, which is a hetero-bifunctional cross-linker. This was prepared by coupling maleic anhydride with β-alanine and *N*-hydroxysuccinimide in the presence of *N,N'*-dicyclohexylcarbodiimide (DCC) (Scheme 3.4).[22]

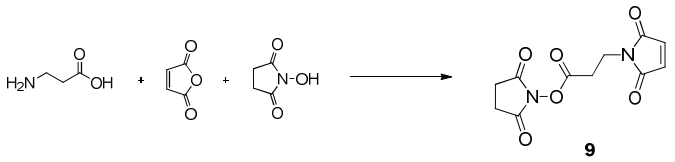

Scheme 3.4 Synthesis of maleimide linker **9**: DCC, DMF, r.t., 4 h.

Before connecting maleimide linker **9** to cystamine, one amino group of cystamine needs to be protected. Following a reported procedure,[23,24] we reacted cystamine dihydrochloride with Boc anhydride in the presence of Et_3N, obtaining Boc-mono-protected cystamine **10** (Scheme 3.5). The remaining free amino group was then derivatized with maleimide linker **9**, and the Boc protecting group was successively removed by treating **11** with TFA in DCM.

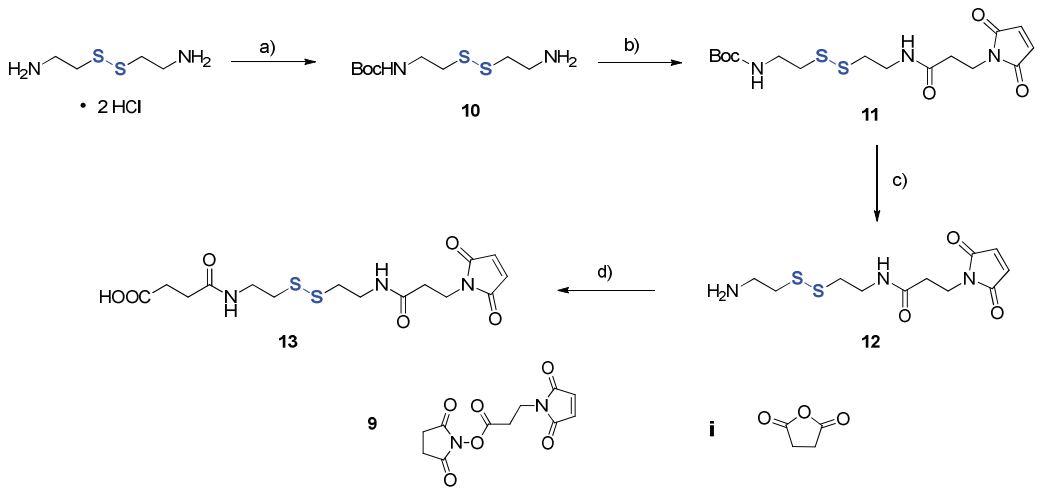

Scheme 3.5 Synthesis of the disulfide linker **13**: a) Boc_2O, Et_3N, MeOH r.t., 1 h; b) **9**, Et_3N, DCM, r.t., 3.5 h; c) TFA/DCM 2:8; d) **i**, DMAP, r.t. 24 h, 40 °C, 7 h.

Finally, as the disulfide linker is meant to be connected to amino-functionalized CNTs **4** *via* amidation, a terminal carboxylic group on the linker is required. To this purpose, compound **12** was reacted with succinic anhydride and catalytic 4-dimethylaminopyridine (DMAP), slightly modifying a reported procedure.[25] Flash-chromatography purification of the reaction mixture afforded compound **13** (Scheme 3.5).As compounds **11**, **12** and **13** were never reported in the literature, to confirm their identity we performed a thorough characterization by proton and carbon NMR, mass spectrometry and FT-IR (data reported in the Exp. Part).

Synthesis of the CNT-nanobody conjugate

Disulfide linker **13** was attached to amino-functionalized CNTs **4** by amidation reaction in the presence of coupling reagents such as 1-ethyl-3-(3-dimethylaminopropyl) carbodiimide (EDC) and hydroxybenzotriazole (HOBt) (Scheme 3.6). The so-obtained compound **5** was extensively dialyzed against deionized water to remove non-reacted compounds, especially the linker which can possibly be absorbed onto the CNTs.

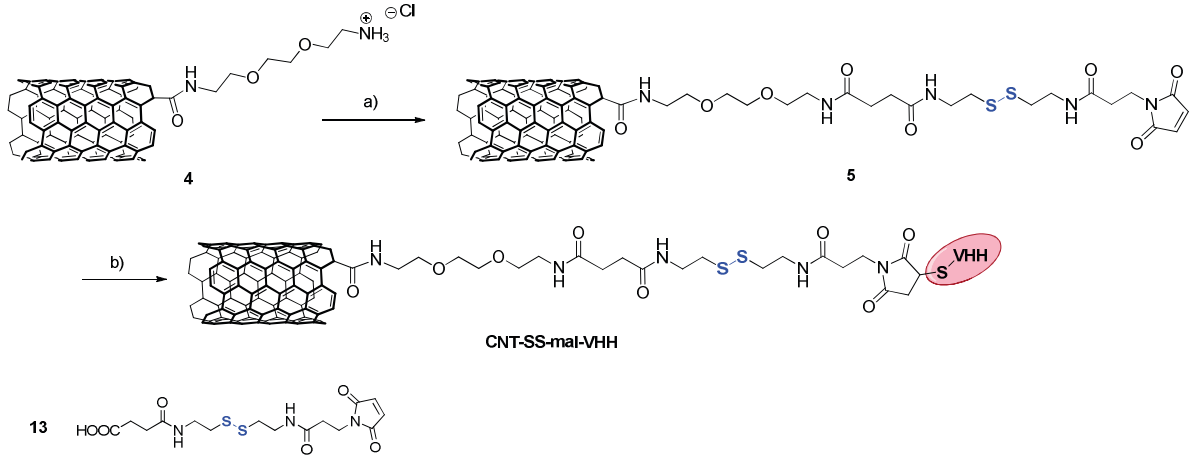

Scheme 3.6 Synthesis of conjugate CNT-SS-mal-VHH: a) **13**, DIEA, HOBt, EDC, DMF, r.t., 56 h; b)VHH, EDTA/PBS pH 6.4, r.t., 6 h.

By Kaiser test it is possible to estimate the residual non-reacted ammonium functions on compound **5**, and deduce the degree of functionalization by difference with the starting MWCNTs **4** (182 μmol/g). The free amine loading calculated by Kaiser test is 12 μmol/g, which corresponds to a degree of functionalization of 170 μmol/g. By TG analysis we obtained a loading value of 120 μmol/g, which is in good agreement with the Kaiser test (Figure 3.4).

The coupling reaction between MWCNTs **5** and VHH was performed in EDTA/PBS buffer at slightly acidic pH (Scheme 3.6), monitoring the reaction by UV-Vis.[26] Small aliquots of the reaction mixture were collected at different time points (0, 5 and 6 hours), centrifuged, and the absorbance of the supernatant was measured to follow the disappearance of the VHH peak. After 6 hours there was no more absorbance of the VHH in the supernatant, therefore we stopped the coupling by centrifuging the mixture and removing the supernatant. As VHH can adsorb onto nanotubes, CNT-SS-mal-VHH was thoroughly washed through repeated centrifugation/redispersion cycles in PBS buffer, and finally subjected to extensive dialysis. By thermogravimetric analysis, we observed a 10% increase of the weight loss compared to the CNT precursor, which corresponds to a loading of VHH of 9.9 μmol/g (Figure 3.4).

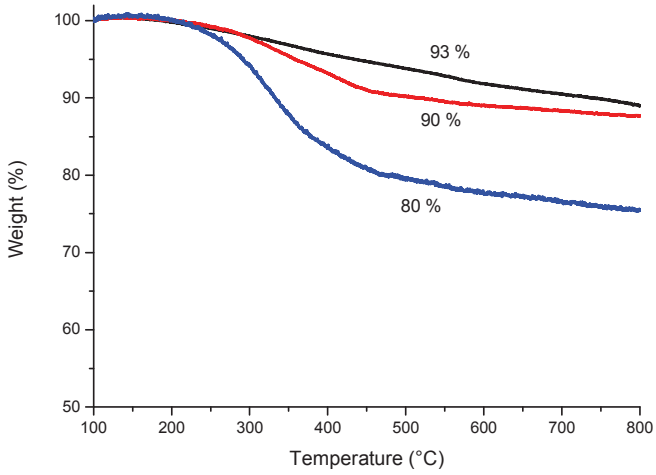

Figure 3.4 TG curves of oxMWCNT **1** (black), MWCNT **5** (red) and CNT-SS-mal-VHH (blue).

3.2.3 SYNTHESIS OF CNT-SS-VHH

For the preparation of the second CNT-nanobody conjugate displaying no organic spacer between the disulfide bridge and the nanobody, we employed a commercially available linker, 2-pyridylthiol-tetraoxatetradecane-*N*-hydroxysuccinimide (PEG_4-SPDP, compound **14** in Scheme 3.7). PEG_4-SPDP is a heterobifunctional cross-linker for protein conjugation that contains a cleavable disulfide bond and a 4-unit PEG group, which confers greater solubility to the cross-linker compared to those having only hydrocarbon spacers. SPDP-type reagents have an amine-reactive *N*-hydroxysuccinimide (NHS) ester at one end and a sulfhydryl-reactive 2-pyridyldithiol group at the opposite end. Amino-functionalized MWCNTs **4** were mixed with the PEG_4-SPDP linker **14** in the presence of a base to afford derivative **6** (Scheme 3.7). The amount of residual free amines calculated by Kaiser test is 61 µmol/g, which corresponds to a degree of functionalization of 121 µmol/g, while the value obtained by TG analysis corresponds to 90 µmol/g.

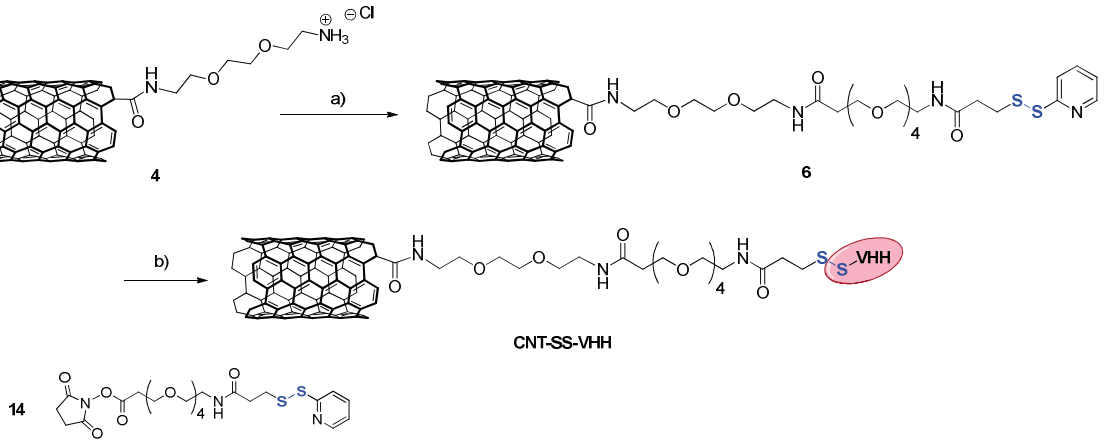

Scheme 3.7 Synthesis of conjugate CNT-SS-VHH: a) **14**, DIEA, DMF, r.t., 48 h; b) VHH, EDTA, PBS, r.t., 6 h.

The terminal pyridylthiol group in MWCNTs **6** is reactive toward thiols and resulting in the displacement of pyridine-2-thione, with formation of a new disulfide linkage with the peptide. Following the above described protocol, we conjugated VHH to MWCNTs **6** affording compound

CNT-SS-VHH. The weight loss difference with the precursor is 9%, which corresponds to a loading of VHH of 5.3 μmol/g.

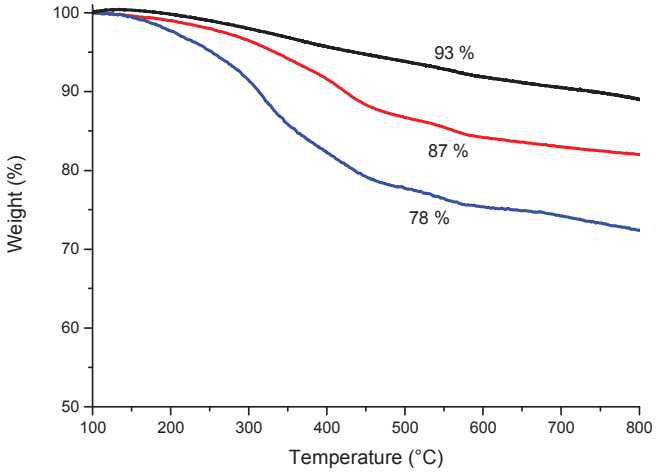

Figure 3.5 TG curves of oxMWCNTs **1** (black), MWCNT **6** (red) and CNT-SS-VHH (blue).

3.2.4 Synthesis of CNT-VHH

Finally, we synthesized a CNT-nanobody conjugate devoid of any cleavable linker to compare its biological behavior with that of the two disulfide-containing conjugates. Amino-functionalized CNTs **4** were derivatized with the previously synthesized maleimide linker **9** by amidation reaction (Scheme 3.1). By Kaiser test we estimated the amount of residual ammonium groups to be 65 μmol/g, which by difference corresponds to a loading of 95 μmol/g. This value is in very good agreement with that obtained by thermal analysis, which is 92 μmol/g.

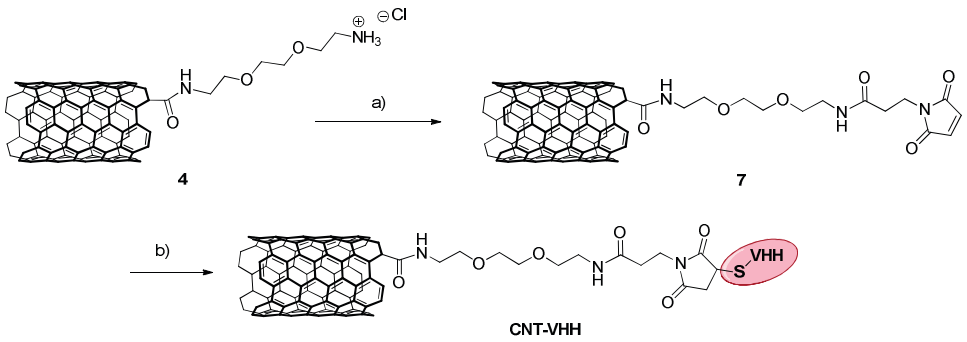

Scheme 3.8 Synthesis of conjugate CNT-VHH: a) **9**, DIEA, DMF, r.t., 48 h; b) VHH, EDTA, PBS, r.t., 6 h.

MWCNTs **7** were reacted with VHH in PBS buffer for 6 hours and then extensively washed and dialyzed to eliminate the non-covalently attached nanobody. The loading of VHH estimated from the TG analysis amounts to 8.1 μmol/g (Figure 3.6).

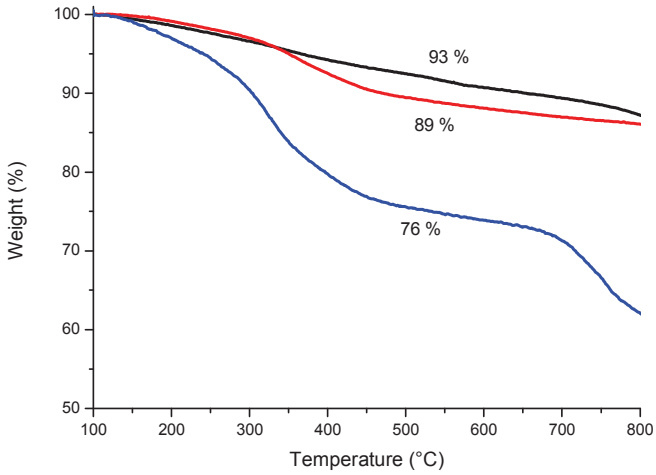

Figure 3.6 TG curves of oxMWCNTs **1** (black), MWCNT **7** (red) and CNT-VHH (blue).

3.2.5 CHARACTERIZATION

In addition to TG analysis, the three final CNT-nanobody conjugates were further characterized by transmission electron microscopy, gel electrophoresis (GE) and surface plasmon resonance (SPR).

3.2.5.1 Electron microscopy

As we stated in Chapter 2, the average length distribution of MWCNTs after the oxidative process corresponds to 381 nm, and the tubes are predominantly individualized and with a curved shape (Figure 3.7). From the TEM pictures of the final conjugates, we can observe that no significant morphological change occurred upon functionalization.

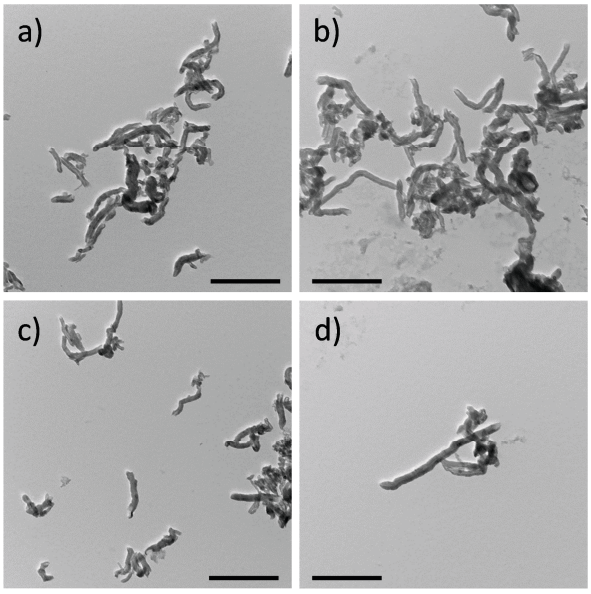

Figure 3.7 TEM images of oxMWCNTs **1** (a), CNT-VHH (b), CNT-SS-VHH (c), and CNT-SS-mal-VHH (d). Scale bars correspond to 500 nm.

3.2.5.2 Gel electrophoresis

Gel electrophoresis is a useful technique for the analysis of macromolecules such as DNA and proteins, since it allows their separation by charge and/or size. The migration of a protein within the gel is driven by its total charge, which is dependent on its size. Hence, it is possible to attest the presence of a certain protein in a sample and verify its integrity by knowing its size. CNTs cannot penetrate the agarose gel because of their big size, therefore they remain at the top of the loading well. When a protein is covalently bound to the CNTs, it will not be able to migrate through the gel, and no protein band will be seen in the lane. However, if a certain amount of protein is absorbed on the CNT sidewalls, it will migrate and the corresponding band will appear at the proper size.

As previously mentioned, the adsorption of macromolecules on CNTs is a phenomenon that can likewise occur during bioconjugation. By extensively washing and dialysis of the CNT-nanobody conjugates, we expect to remove most of the adsorbed nanobody. Neveretheless, TG analysis does not allow to discriminate between covalently and non-covalently attached nanobody. To have an idea of the extent of adsorbed VHH, parallely to the covalent conjugation we performed a control reaction that excluded any possible covalent interaction between VHH and CNTs. To this purpose, we stirred together VHH and MWCNTs **3** (Boc-protected amino-functionalized MWCNTs), which are devoid of the maleimide function, therefore only non-covalent interactions can occur (Scheme 3.9). The reaction mixture was submitted to the same work-up as for the covalent conjugation (washings and dialysis), and the obtained material was analyzed by gel electrophoresis as well as the covalent CNT-nanobody conjugates.

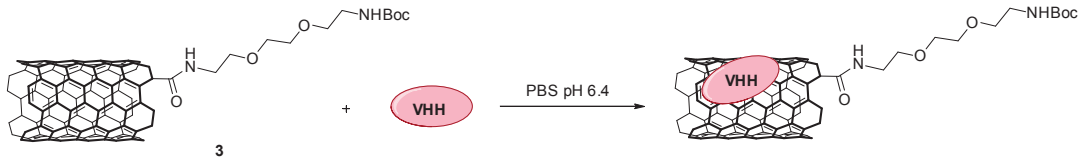

Scheme 3.9 Schematic representation of the control reaction.

The four samples and native VHH were analyzed by gel electrophoresis in non-reducing conditions and the gel was stained with Coomassie blue to visualize the bands. In the second lane of Figure 3.8 we can see an intense band at ~17 kDa, which accounts for the VHH nanobody (MW ca. 17 kDa), while the less intense bands at higher MW are attributed to VHH dimers.

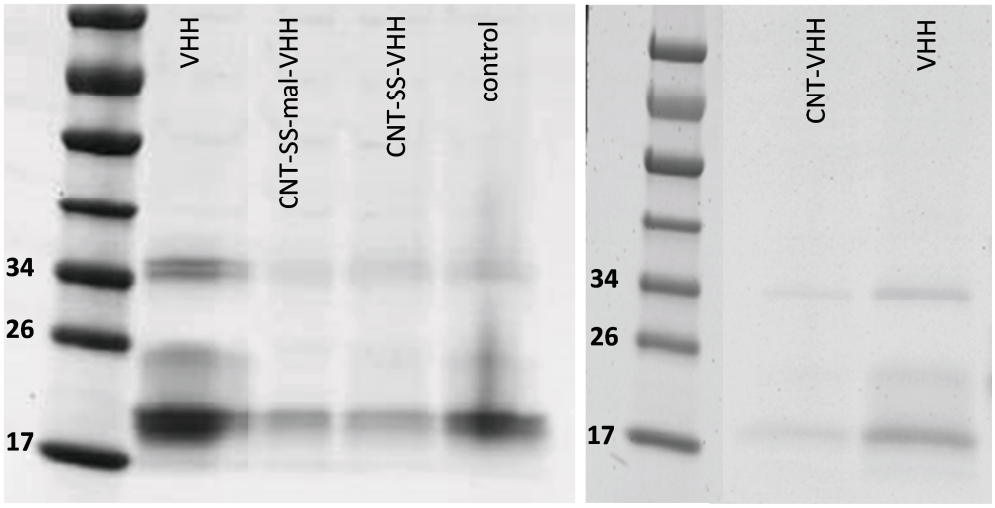

Figure 3.8 Gel electrophoresis run under non-reducing conditions at 150 kV. Gel stained with Coomassie blue. Protein size expressed in kDa. Left and right panels correspond to gels performed in different moments.

We can notice that for the control reaction (lane 5), the intensity of the nanobody band is rather high, due to the presence of adsorbed VHH. In the lanes of the three covalent conjugates (CNT-SS-mal-VHH, CNT-SS-VHH, CNT-VHH) low intense bands are visible in correspondence with VHH, meaning that a small amount of the nanobody is possibly still adsorbed onto the CNTs. We tried to further wash the conjugates and repeat the electrophoresis, but the outcome was similar. In other experiments with VHH previously carried out in our laboratory,[26] we indeed experienced the same behavior concerning gel electrophoresis of CNT-VHH conjugates. Accounting for this reason, we decided to evaluate the stability of the conjugates *in vitro* and *in vivo*.

3.2.5.3 Surface Plasmon Resonance

The biological affinity of a coupled antibody towards its antigen can be assessed by surface plasmon resonance (SPR). SPR is a physical process that can occur when plane-polarized light hits a metal film under total internal reflection conditions. If the metal film is modified by chemical immobilization of molecules/biomolecules, its refractivity changes accordingly.[27] By exploiting this technique in the field of biosensors, it is possible to measure the specific interaction between an antibody and its antigen in real time. The principle is to immobilize the antigen on a sensor chip surface while the antibody is allowed to continuously flow over this surface.[28] As the antibody/antigen binding occurs, the reflection properties of the chip surface change, and the reflected light detected as a function of time originates a sensorgram. Because of the continuous flow, the interactions between the analytes are dynamic: there will be an initial association step, when the antibody binds to the antigen, followed by a dissociation and regeneration step, where the antibody dissociates from the antigen and is recovered in the liquid phase, while the antigens on the surface of the chip are again available (Figure 3.9). From the registered sensorgram it is possible to calculate the kinetic parameters of the antibody/antigen interaction, *i.e.* the association and dissociation rate constants (k_a and k_d, respectively).

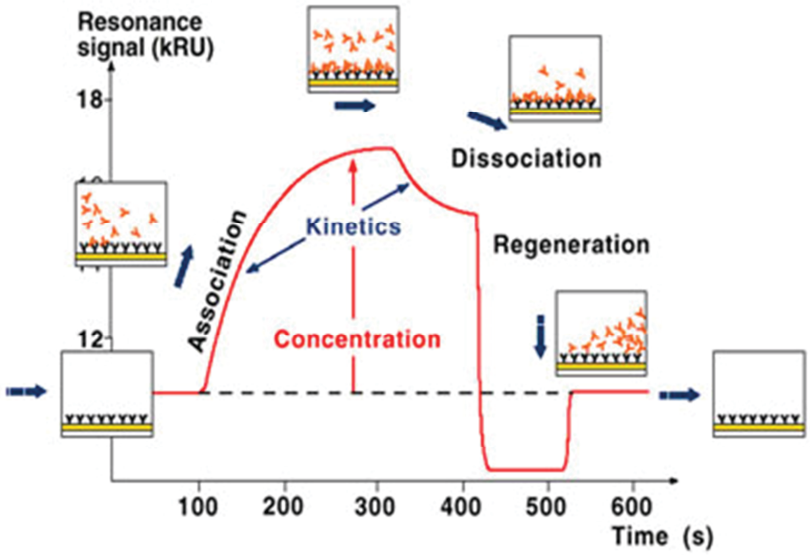

Figure 3.9 Sensorgram showing the interaction between an analyte in the flow and the ligand on the chip surface. Figure adapted from ref. [29].

In collaboration with Dr. Olivier Chaloin in our laboratory, we performed SPR analysis of the CNT-nanobody conjugates to verify that the VHH affinity for β-catenin was not affected by the covalent conjugation with the CNTs. To immobilize the antigen on the chip surface, we exploited a bioaffinity

approach based on the streptavidin-biotin interaction. Streptavidin molecules were bound onto the pre-activated chip surface, while biotin was already present on the peptide sequence of the β-catenin antigen provided by UCB. Biotinylated-catenin was allowed to interact with streptavidin and was thus immobilized on the chip. Alternatively, for the immobilization of the antigen on the chip, β-catenin without biotin was directly linked to the activated chip surface by amidation. Afterwards, the three CNT conjugates and VHH alone were separately injected onto the sensor chip at different concentrations (6-100 μg/mL).

As we can observe in Figure 3.10-a, the VHH nanobody recognizes the antigen in a concentration-dependent manner. From the sensorgrams registered at different VHH concentrations, we determined the equilibrium dissociation constant K_D ($K_D=k_d/k_a$), which is a measure of the binding strength (affinity). The calculated value is 4.8 x 10^{-10} M, indicating a great affinity between VHH and the antigen. Graphs b), c) and d) of Figure 3.10 show the sensorgrams of the three CNT conjugates, and is evident that all conjugates display recognition ability towards the antigen on the chip and their response is concentration-dependent. Therefore, the nanobody's recognition ability was preserved after conjugation with the different CNTs. However, the quantification of the dissociation constant cannot be pursued for CNT conjugates because of the limitations posed by the CNTs themselves. In fact, for the calculation of the K_D it is necessary to know the precise molecular weight of the injected sample, which cannot be determined for CNTs due to their heterogeneous length distribution. Moreover, the antigen binding capacity might be affected by the uneven distribution of the nanobody along the CNTs.

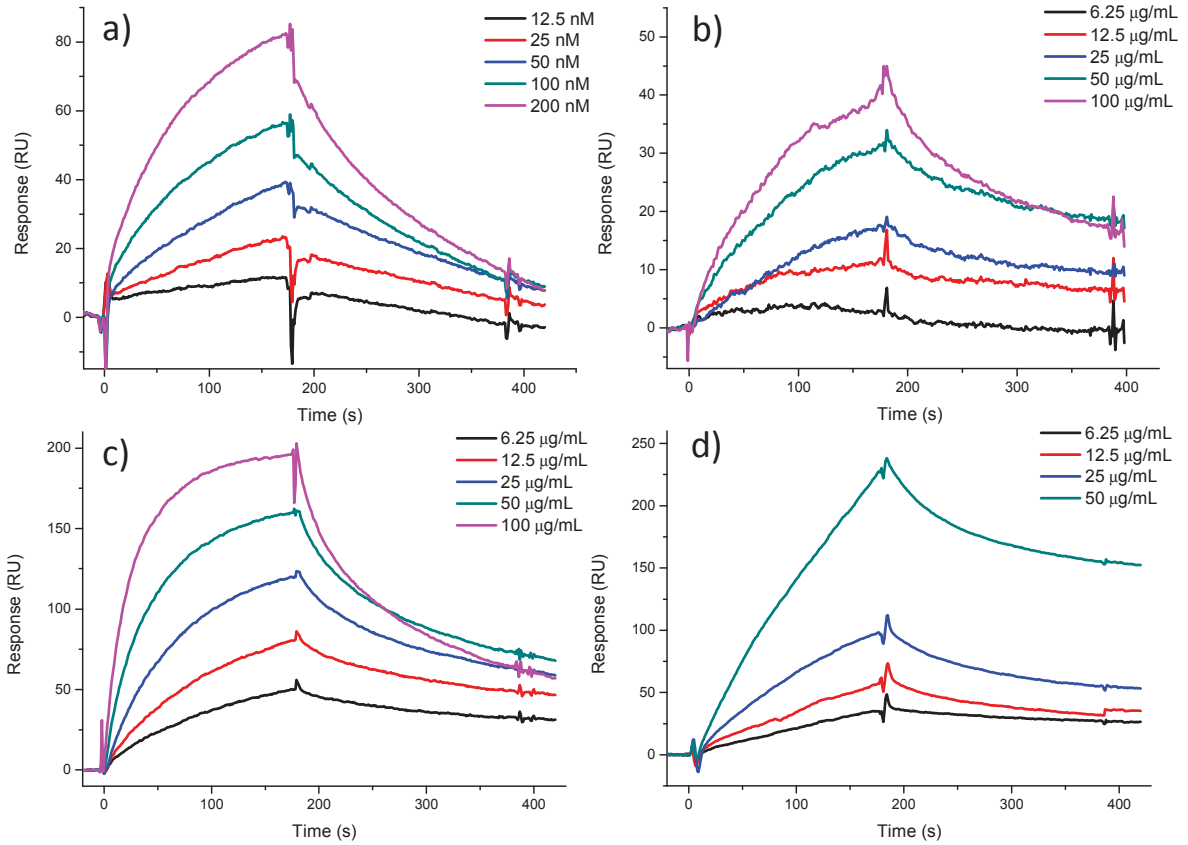

Figure 3.10 Sensorgrams showing the specific binding of: a) therapeutic nanobody (VHH), b) CNT-SS-mal-VHH, c) CNT-SS-VHH and d) CNT-VHH to the antigen β-catenin at different concentrations. Sensorgrams a) and d) were performed with catenin immobilized via amidation on the chip, while b) and c) were registered with biotinylated-catenin immobilized *via* streptavidin.

3.2.6 CLEAVAGE OF THE DISULFIDE BOND

As explained in the Introduction of this Chapter, the interest of inserting cleavable bonds between the drug and the carrier is justified by the possibility to induce a controlled release of the therapeutic agent. Among cleavable bonds, disulfide bonds are appealing because they can be thorn by reducing conditions, usually present inside the cells. The efficacy of such a stimuli-sensitive delivery system depends not only on its tumor-targeting specificity, but also on the efficiency of the cleavable linker to release the anticancer drug inside the cells. The main intracellular reducing agent is glutathione (GSH), a thiolated tripeptide. Concentrations of GSH are typically 1-2 μM in circulating human blood plasma and extracellular environment, but are in the range of 2-8 mM in tumor tissues.[30,31] These intracellular concentrations are sufficient to break the disulfide bond, thereby releasing the biological molecules from the surface of the delivery vehicle; whereas, the lower glutathione concentration outside the cell has a minimal effect.[32] Treating the CNT-nanobody conjugates with GSH, the cleavage of the disulfide bond should occur by disulfide exchange reaction.[30] To identify the smart release property of our conjugates, CNT-SS-VHH and CNT-SS-mal-VHH (Conc. ~ 1 mg/mL) were separately treated with 20 mM GSH for 36 hours (Scheme 3.10). We observed that CNTs aggregated, leaving a rather clear solution, which may account for the detachment of the protein. Nevertheless, by measuring the UV-Vis absorbance of the supernatant of the CNT dispersion, it was not possible to assess the occurrence of the cleavage because glutathione absorbs in the same range of VHH (210-280 nm). We then tried to analyze both the supernatants and the precipitated CNTs by gel electrophoresis, along with the original conjugates, but this attempt was not successful, as no evident proof of the VHH cleavage was discernible (data not shown). Even by treating the CNT conjugates with higher GSH concentration (55 mM), we could not observe the band of cleaved VHH by gel electrophoresis. We therefore decided to verify the occurrence of the release by investigating the intracellular behavior of the three CNT-nanobody conjugates.

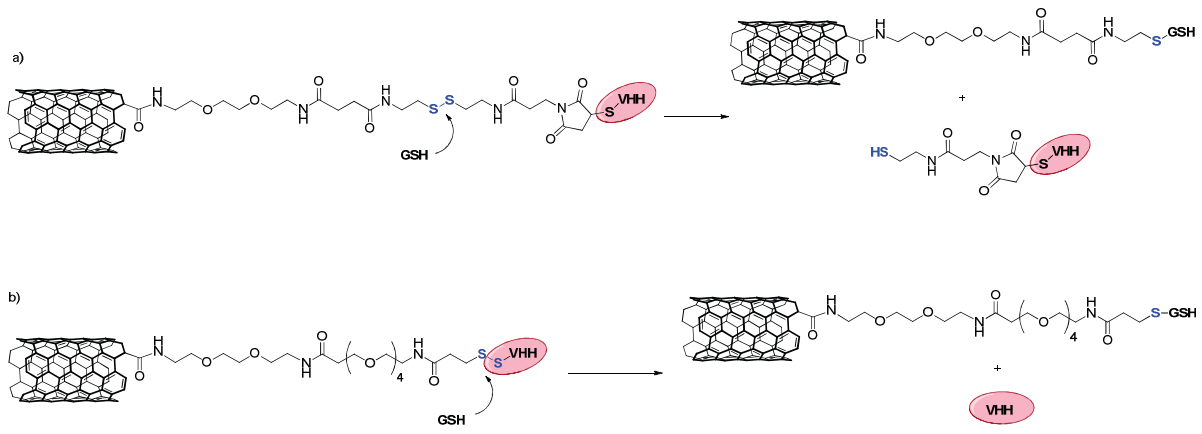

Scheme 3.10 Representation of the mechanism of GSH-induced disulfide cleavage for the two conjugates featuring the cleavable S-S bond, CNT-SS-mal-VHH (a) and CNT-SS-VHH (b).

3.2.7 BIOLOGICAL STUDIES

In order to study the potential of these conjugates as antitumoral therapeutics, we carried out *in vitro* cellular uptake and *in vivo* experiments in tumor-bearing mice in collaboration with the group of Prof. K. Kostarelos in Manchester (UK) and the main results are reported below.

Cell Viability

In order to check the efficacy of the CNT-VHH conjugates a cell viability experiment was carried out on colorectal cancer HCT116 cells, which overexpress β-catenin. The cells were incubated with CNT **4**, CNT-VHH, CNT-SS-VHH and CNT-SS-mal-VHH for 24 and 48 hours at two different CNT concentrations (5 and 50 μg/ml). We can observe that after 24 hours, the cells treated with the CNT conjugates show a good level of viability, compared to the positive control DMSO (Figure 3.11). After 48 hours, the viability of cells treated with the CNT-VHH conjugates is instead significantly reduced compared to the CNTs without nanobody. This suggests that the conjugates have been taken up by the cells and that the VHH is exerting its activity toward β-catenin blocking the corresponding survival pathway. A reduction in cell viability is only observed after 48 h, which can be explained by the fact that the sequestration of β-catenin and consequent cell death is induced only by a slow release of VHH from the conjugates. In addition, no significant difference in the cell viability can be revealed between the three different conjugates, although we could expect an enhanced efficacy for the conjugates with the cleavable linker. It seems also that increasing the concentration of the conjugates does not clearly lead to a higher cell mortality. These *in vitro* experiments were necessary to design the following tests using the tumor-bearing mouse model.

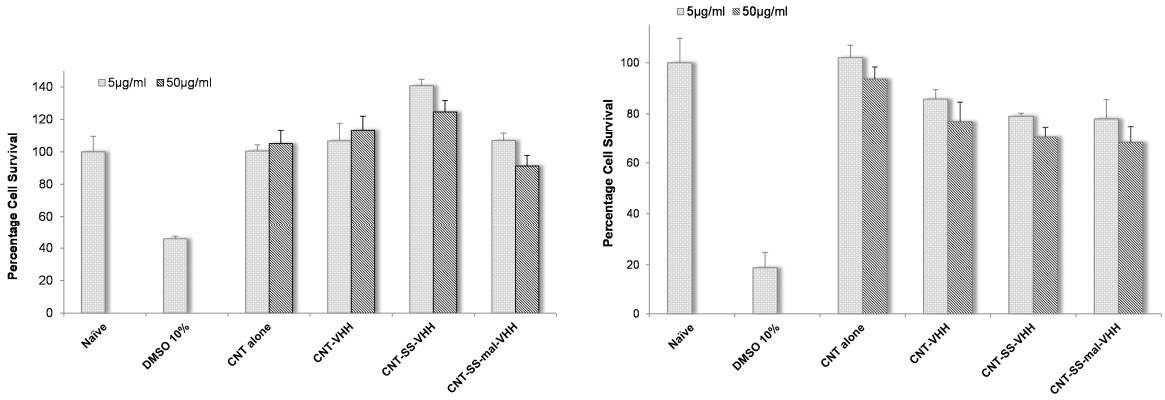

Figure 3.11 Cell viability of colorectal cancer HCT116 cells after (A) 24 h and (B) 48 h incubation with MWCNT **4** (named CNT alone in the graphs), CNT-VHH, CNT-SS-VHH and CNT-SS-mal-VHH at 5 and 50μg/ml. DMSO (10%) was used as a positive control.

In vivo experiments

The therapeutic effect of the conjugates was then investigated *in vivo* on tumor-bearing mice previously inoculated with the HCT116 carcinoma. For this experiment, CNTs were injected intratumorally, to avoid their circulation and accumulation in other parts of the body, and to have a proof of principle of their efficacy. After injection, the tumor volume variation was monitored over time. We can observe that all the three VHH conjugates afford a reduction of the tumor size compared to the CNT precursor (without nanobody) and the non-treated mice (Figure 3.12). Looking at the mice survival rate after tumor implantation (Figure 3.12), it results that CNT-SS-VHH showed the longest survival compared to the other groups, followed by CNT-VHH and then CNT-SS-mal-VHH. Furthermore, in the case of CNT-SS-VHH and CNT-VHH the mice survival is significantly better than for untreated mice (naïve) or mice treated with CNT alone (compound **3**), which is a very encouraging result. Like *in vitro* experiments, it seems that the presence of the linker is not really beneficial to the anticancer activity.

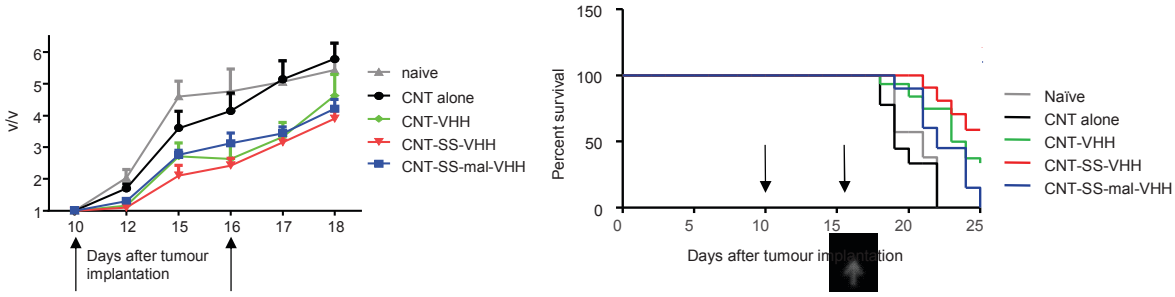

Figure 3.12 (Left) Change in tumour growth and (right) mice survival after intratumoral administration of MWCNT **4** (CNT alone in the graphs) and CNT-VHH conjugates in HCT116 xenograft (n= 5-8 mice; arrows indicate the days of injection).

We then performed a western blot, which is an analytical technique used to detect a specific protein in a sample of tissue homogenate. The proteins are separated by gel electrophoresis, transferred to a nitrocellulose membrane and then stained with a specific antibody. Our goal in doing this was to see whether there was a reduction of β-catenin in the tumors 48 hours after their treatment with the CNT conjugates. In the image of the gel (Figure 3.13), we can observe that the intensity of the band corresponding to β-catenin is decreased in the case of CNT-SS-VHH and CNT-SS-mal-VHH, while it does not vary for CNT-VHH and CNT alone. This proves that the constructs featuring the cleavable linker are more efficient in delivering the VHH nanobody against β-catenin.

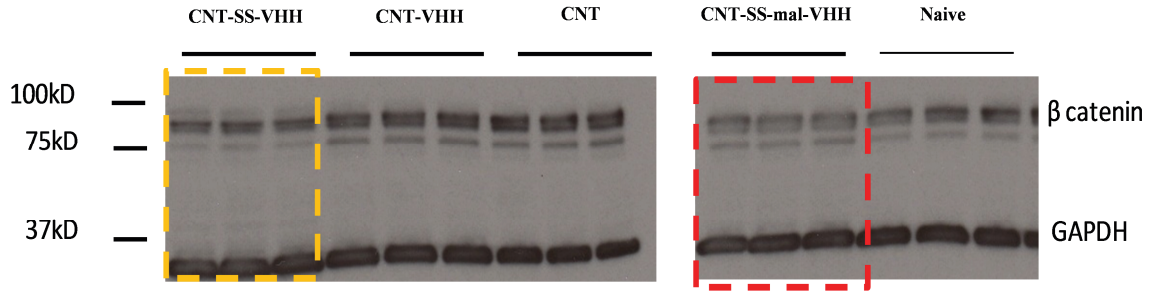

Figure 3.13 Western blot of HCT116 tumors 48 hours after treatment. GAPDH was used as internal reference gene (MWCNTs **4** are named 'CNT' in the figure).

The histology of the sectioned tumors evidenced that CNT alone do not trigger any toxicity in the tumor tissues, whereas extended necrosis in the areas around the nanotubes is revealed in the case of tumors treated with the CNT-VHH constructs (Figure 3.14). These results are in good correlation with the cell viability and western blot analyses.

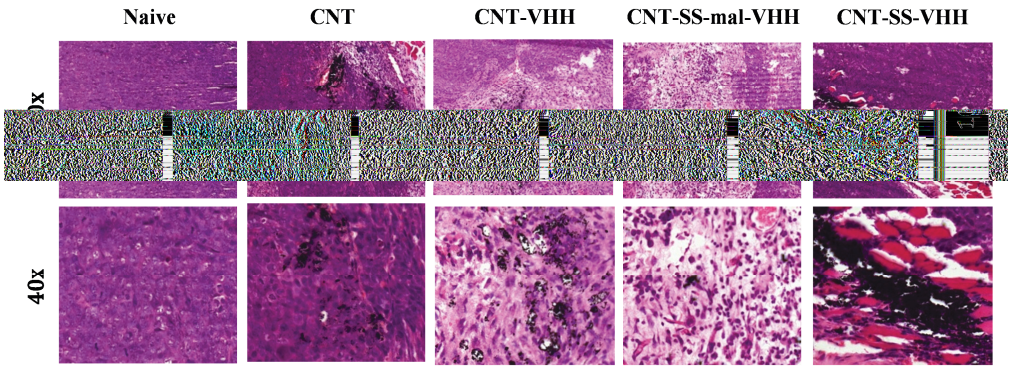

Figure 3.14 Haematoxylin and eosin tissue histology (MWCNTs **4** are named 'CNT' in the figure).

The performed biological investigations suggest that the synthesized conjugates were effective in delivering VHH into tumor cells, and that toxic effects are only provoked by the presence of VHH and not by the nanotubes themselves. Among the three conjugates, CNT-SS-VHH seems to have the highest therapeutic effect, according to histology and mice survival. From the *in vitro* test and the evaluation of the tumor size and mice survival, the presence of the cleavable linker on the CNT conjugate does not seem to play a determinant role. However, by Western blot, CNT-SS-VHH and CNT-SS-mal-VHH appear to be the conjugates that induced the higher reduction of β-catenin in the tumor.

3.3 CONCLUSIONS

In this Chapter we have described the preparation of three novel CNT conjugates functionalized with VHH, a therapeutic nanobody. Two of these conjugates were designed to feature a disulfide cleavable bond, in order to provide the conjugate with smart-release properties. For the synthesis of the first conjugate (CNT-SS-mal-VHH), we have derivatized TEG-amine functionalized CNTs with a previously synthesized disulfide linker, and further bound the VHH through a maleimide linker. The second conjugate (CNT-SS-VHH) has been prepared by derivatizing TEG-amine functionalized CNTs with PEG_4-SPDP, a linker featuring a terminal pyridylthio group. In this case, the VHH was linked to the conjugate by disulfide exchange with the pyridylthio group, and was therefore directly attached to the cleavage site (the disulfide bond), without any spacing moiety, such as the maleimide. Finally, for comparison, we synthesized a CNT-VHH conjugate devoid of cleavable linker. All compounds were characterized by TGA to assess the degree of loading, by TEM and gel electrophoresis to verify their morphology and composition. The possibility to induce the cleavage of the disulfide bond and thus VHH release was investigated by treating CNT-SS-mal-VHH and CNT-SS-VHH with GSH, but we could not draw any conclusion due to experimental limitations. For all the three constructs, surface plasmon resonance analysis proved that the nanobody affinity toward β-catenin was still preserved after conjugation to the CNTs. The efficacy of conjugates was then evaluated through cell viability tests and *in vivo* experiments on tumor-bearing mice. The three conjugates were able to trigger toxic effect on a carcinoma cell line overexpressing β-catenin after 48 hours. They were moreover effective in reducing the tumor size and prolonging survival of tumor mice, suggesting that the VHH on the CNTs is still able to exert its therapeutic effects, and that the CNTs alone do not display evident toxicity. The *in vivo* experiments did not provide a clear proof of the better efficacy of the conjugates presenting the disulfide linker. However, the obtained results showed the efficacy of our CNT-VHH constructs against tumors, both *in vivo* and *in vivo*. These results are overall encouraging and suggest that CNT-VHH conjugates could represent a promising tool for the delivery of therapeutic nanobodies.

3.4 EXPERIMENTAL PART

3.4.1 COMPOUNDS SYNTHESIS AND CHARACTERIZATION

Materials and Methods

The chemicals and solvents were purchased from commercial suppliers and used without purification. MWCNTs were purchased from *Nanostructured & Amorphous Materials Inc. (*Stock # 1240 XH), and they were produced by catalytic carbon vapor deposition (CCVD). VHH was provided by UCB (UK). PEG_4-SPDP linker **14** was purchased by Thermo Scientific Pierce. The solvents used for synthesis were analytical grade. When anhydrous conditions were required, high quality commercial dry solvents were used. Water was purified using a Millipore filter system MilliQ®. When stated, suspensions were sonicated in a water bath (20 W, 40 kHz). The filtration and dialysis membranes were purchased from Millipore and Spectrum Laboratories, Inc., respectively. If not differently specified, dialysis of CNT compounds was carried out employing membrane with MWCO 12000-14000 Da. Thin layer chromatography (TLC) was conducted on pre-coated aluminum plates with 0.25 mm Macherey-Nagel silica gel with fluorescent indicator UV254. Chromatographic purifications were carried out with silica gel (Merck Kieselgel 60, 40-60 μm, 230-400 mesh ASTM). ^{1}H-NMR and ^{13}C-NMR spectra were recorded in deuterated solvents using Bruker spectrometers (Avance III - 400 MHz and Avance I - 500 MHz). Chemical shifts are reported in ppm using the residual signal of deuterated solvent as reference. The resonance multiplicity is described as *s* (singlet), *t* (triplet), *qt* (quintuplet), *m* (multiplet), *bs* (broad singlet), and *bt* (broad triplet). Coupling constants (*J*) are given in Hz. The UV–Vis analysis were performed on a Varian Cary 5000 spectrophotometer and the Kaiser test was performed according to reported procedures [21,33]. FT-IR spectra were measured on a Perkin Elmer Spectrum One ATR-FT-IR spectrometer. MS experiments were performed on a Bruker Daltonics microTOF spectrometer (Bruker Daltonik GmgH, Bremen, Germany) equipped with an orthogonal electrospray (ESI) interface. Calibration was performed using Tunning mix (Agilent Technologies). Sample solutions were introduced into the spectrometer source with a syringe pump (Harvard type 55 1111: Harvard Apparatus Inc., South Natick, MA, USA) with a flow rate of 5 μL/min. TGA was performed on a TGA1 (Mettler Toledo) apparatus from 100 °C to 900 °C with a ramp of 10 °C min^{-1} under N_2 using a flow rate of 50 $mL \cdot min^{-1}$ and platinum pans. For TGA of the CNT-nanobody conjugates, an aliquot of the conjugate in PBS was previously dialyzed against deionized water to remove the buffer salts and lyophilized. TEM analysis was performed on a Hitachi H7500 microscope (Tokyo, Japan) with an accelerating voltage of 80 kV, equipped with a AMT Hamamatsu camera (Tokyo, Japan). oxMWCNT were dispersed in MeOH at a concentration of ~50 $\mu g \cdot mL^{-1}$ and the suspension was sonicated for 15 min. Ten microliters of the suspension were drop-casted onto a carbon-coated copper grids (Formvar/Carbon 300 Mesh, Cu from Delta Microscopies) and left for evaporation under ambient conditions. In the case of nanobody-CNT samples, 10 microliters of the final PBS suspension were drop-cast on the TEM grid at a concentration of ~50 $\mu g \cdot mL^{-1}$; after drying, the grid was washed 3 times with deionized water to remove the buffer salts.

Surface Plasmon Resonance (SPR)

The BIACORE 3000 system, sensor chip CM5, surfactant P20, amine coupling kit containing *N*-hydroxysuccinimide and 1-ethyl-3-(3-dimethylaminopropyl)carbodiimide, were from BIACORE

(Upsala, Sweden). All biosensor assays were performed with HEPES-buffered saline (HBS-P) as running buffer (10 mM HEPES, 150 mM sodium acetate, 3 mM magnesium acetate, 0.005% surfactant P20, pH 7.4). The different compounds were dissolved in the running buffer. The surface of a sensor chip CM5 was activated by EDC/NHS. Samples CNT-SS-mal-VHH and CNT-SS-VHH were passed on a sensor chip functionalized with biotynilated-catenin by streptavidin/biotin interaction. Immobilization of streptavidin (Sigma-Aldrich) was performed by injecting 40 µL of streptavidin (100 µg/ml in formate buffer, pH 4.3), which gave a signal of approximately 2000 RU, followed by 20 µL of ethanolamine hydrochloride (pH 8.5), to saturate the free activated sites of the matrix. Biotinylated β-catenin (10 µM in formate buffer, pH 4.3) was allowed to interact with streptavidin until a response of 2000 RU was obtained. Analysis of pure VHH and CNT-VHH were carried out on a chip modified with β-catenin, without biotin, by amidation. Immobilization of β-catenin *via* the free amino groups was performed by injecting onto the activated surface of a sensorchip CM5, 35 µL of β-catenin (50 µg/ml in acetate buffer buffer, pH 4.9) which gave a signal of 2000 RU, followed by 20 µL of ethanolamine hydrochloride (pH 8.5). All the binding experiments were carried out at 25 °C with a constant flow rate of 20 µl/min. Different concentrations of the samples were injected for 3min, followed by a dissociation phase of 3 min. The sensor chip surface was regenerated after each experiment by injection of 10 µL of 10 mM HCl. The kinetic parameters were calculated using the BIAeval 4.1 software. Analysis was performed using the simple Langmuir binding model or separate k_a/k_d (k_{on}/k_{off}). The specific binding profiles were obtained after subtracting the response signal from the channel control (activated/deactivated) and from blank buffer injection. The fitting of each model was evaluated by the reduced chi square and randomness of residue distribution compared to the theoretical model.

Synthesis of organic precursors

Synthesis of 2-[2-(2-aminoethoxy)-ethoxy]ethyl}-carbamic acid tert-*butyl ester* **8**

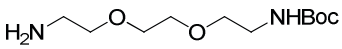

A solution of Boc_2O (2.21g , 10.1 mmol) in 1,4-dioxane (45 mL) was dropped on a solution of 2,2'-(ethylenedioxy)bis(ethylamine) (15 mL, 101 mmol) in 1,4-dioxane (75 mL) over 2 h, and the resulting mixture was stirred for 24 h. The solvent was then evaporated, the residue was diluted with DCM (40 mL), washed with water (60 mL x 3), dried over $MgSO_4$ and the resulting oil was purified by FC (eluant DCM/MeOH 95:5 and then DCM/MeOH/Et_3N 87:10:3), affording the mono-protected product as a yellow oil (1.66 g, 65% yield).

^1H NMR ($CDCl_3$, 300 MHz) δ (ppm): 5.21 (1H, br s), 3.59-2.84 (12H, m), 2.03 (2H, s), 1.43 (9H, s). All structural assignments were in agreement with previously reported data.[34]

Synthesis of N-*succinimidyl 3-meleimidopropionate* **9**

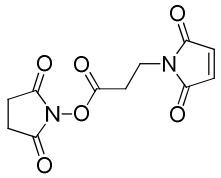

Maleic anhydride (3.36 g, 34 mmol) and β-alanine (3.0 g, 34 mmol) were dissolved in dry DMF (50 mL) and the mixture was stirred for 1h under argon, until complete solubilization of β-alanine. *N*-hydroxysuccinimide (4.92 g, 34 mmol) and DCC (14 g, 68 mmol) were then added to the mixture, at 0 °C. After 10 min the ice bath was removed and the yellowish suspension was stirred for 4h at r.t., under argon. The mixture was then filtered with a Buchner to remove the precipitated dicyclohexylurea and the solution was diluted with 4-5 volumes of H_2O, and extracted with DCM. The organic phases were washed with water, dried over $MgSO_4$ and concentrated. The resulting solid was dissolved in few DCM and further precipitated from *n*-hexane. The organic layer was decanted away, and the solid was recrystallized twice from MeOH affording the product as white crystals (3.56 g, 40% yield).

^{1}H NMR ($CDCl_3$, 400 MHz) δ (ppm): 6.73 (2H, s), 3.93 (2H, t, J = 7.0 Hz), 3.01 (2H, t, J = 7.0 Hz), 2.82 (4H, s). All structural assignments were in agreement with previously reported data.[22]

Synthesis of N-(*t-butyloxycarbonyl)cystamin* **10**

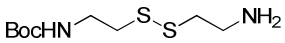

A solution of Boc_2O (1.97 g, 9 mmol) in MeOH (20 mL) was added dropwise to a solution of cystamine dihydrochloride (2.03 g, 1 eq.) and Et_3N (3.73 mL, 3 eq.) in MeOH (25 mL) and the mixture was then stirred for 1 h at r.t. The solvent was removed under reduced pressure and the resulting oil was treated with 1 M aq. $NaHPO_4$ (20 mL) and extracted with Et_2O (2 x 15 mL) to remove the di-protected by-product. The aqueous phase was treated with 1 M aq. NaOH until pH~9 and extracted twice with EtOAc (20 mL). The combined organic phases were washed with H_2O, dried over $MgSO_4$ and concentrated, yielding compound **10** as colorless oil (1.11 g, 49% yield).

^{1}H NMR ($CDCl_3$, 400 MHz) δ (ppm): 4.97 (1H, br s), 3.44-3.42 (2H, m), 3.00 (2H, t, J = 6.1 Hz), 2.79-2.74 (4H, m), 1.43 (9H, s). All structural assignments were in agreement with the data available from the literature.[23]

Synthesis of compound **11**

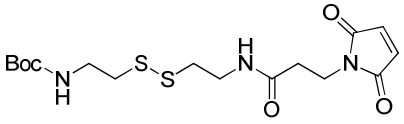

N-succinimidyl-3-maleimidopropionate **9** (0.95 g, 3.56 mmol) and Boc-cystamine **10** (0.92 g, 3.60 mmol) were dissolved in DCM (25 mL). Et_3N (0.74 mL, 5.34 mmol) was then added and the solution was stirred for 3.30 h at r.t. The reaction crude was washed with 1M HCl (15 mL), H_2O (2 x 20 mL),

and the organic layers were then separated, dried over $MgSO_4$ and concentrated under reduced pressure, affording quantitatively **11** as white solid (1.41 g, 98% yield).

^{1}H NMR ($CDCl_3$, 500 MHz) δ (ppm): 6.70 (2H, s), 6.60 (1H, br s), 4.95 (1H, br s), 3.85 (2h, t, *J* = 7.0 Hz), 3.55 (2H, q, *J* = 5.9 Hz), 3.43 (2H, q, *J* = 6.0 Hz), 2.82 (2H, t, *J* = 5.8 Hz), 2.76 (2H, t, *J* = 6.9 Hz), 2.57 (2H, t, *J* = 7.0 Hz), 1.44 (9H, s). ^{13}C NMR ($CDCl_3$, 125 MHz) δ (ppm): 170.5, 170.5, 155.9, 155.8, 134.2, 134.2, 79.8, 38.4, 37.9, 37.5, 34.7, 34.3, 34.3, 28.3. MS (ESI, *m/z*): 426.1 $[M+Na]^+$, 829.2 $[2M+Na]^+$. HR-MS (ESI): *m/z* = 426.1157 $[M+Na]^+$ (calcd for $C_{16}H_{25}N_3O_5S_2Na$ *m/z* = 426.1128). FT-IR (neat, *v* /cm^{-1}): 3312, 1696, 1638, 1527, 1408, 1274, 1173, 948, 839, 698.

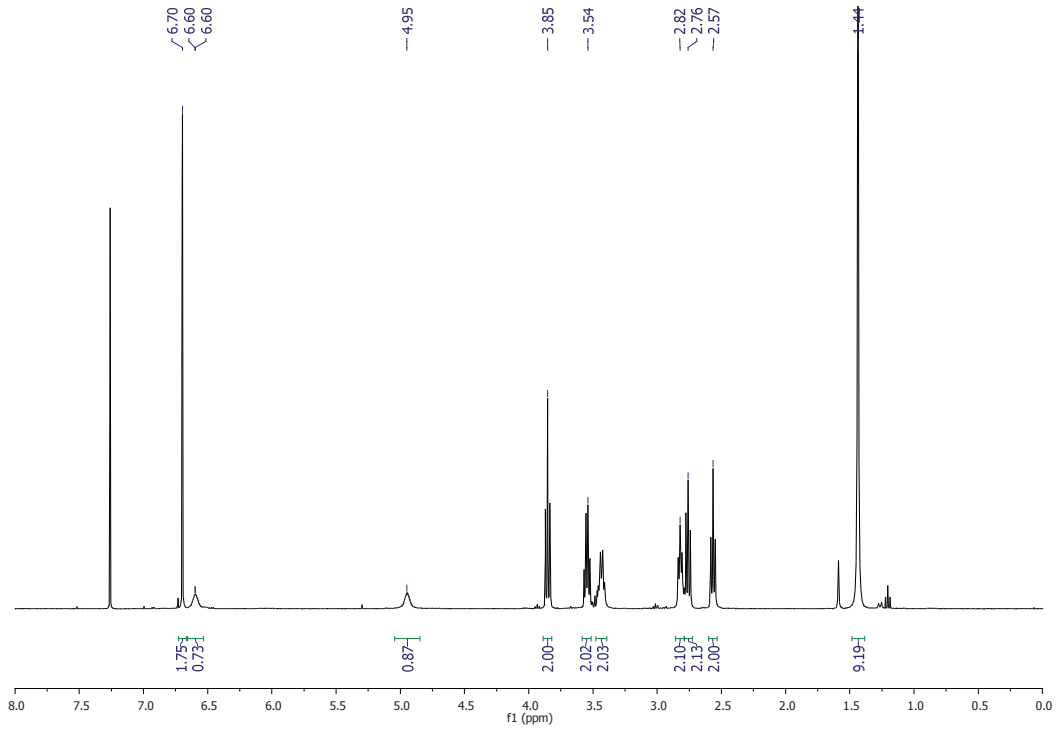

Synthesis of compound **12**

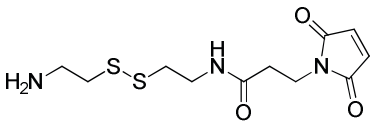

Deprotection of compound **11** (1.41 g, 3.49 mmol) was achieved by treatment with a solution of TFA/DCM 2:8 (8 mL) for 7 h at r.t. The solvents were evaporated and the residual orange oil was dissolved in acidic water (20 mL), and the organic impurities were removed by extraction with cyclohexane (15 mL). The water phase was treated with NH_3 and NaOH until pH ~8-9 and the organic compound was successively extracted with DCM (3 x 20 mL). The organic layers were dried over $MgSO_4$ and concentrated to quantitatively afford **12** as yellow oil, which was immediately used for the following step, due to its poor stability. NMR characterization was in agreement with the expected molecular structure.

^{1}H NMR (CD_3OD, 500 MHz) δ (ppm): 6.74 (2H, s), 3.70 (2h, t, *J* = 6.8 Hz), 3.38 (2H, t, *J* = 6.7 Hz), 3.21 (2H, t, *J* = 6.8 Hz), 2.90 (2H, t, *J* = 6.8 Hz), 2.73 (2H, t, *J* = 6.6 Hz), 2.39 (2H, t, *J* = 6.8 Hz). ^{13}C NMR (CD_3OD, 125 MHz) δ (ppm): 173.4, 172.3, 135.5, 39.5, 38.2, 35.8, 35.6, 35.5, 27.8.

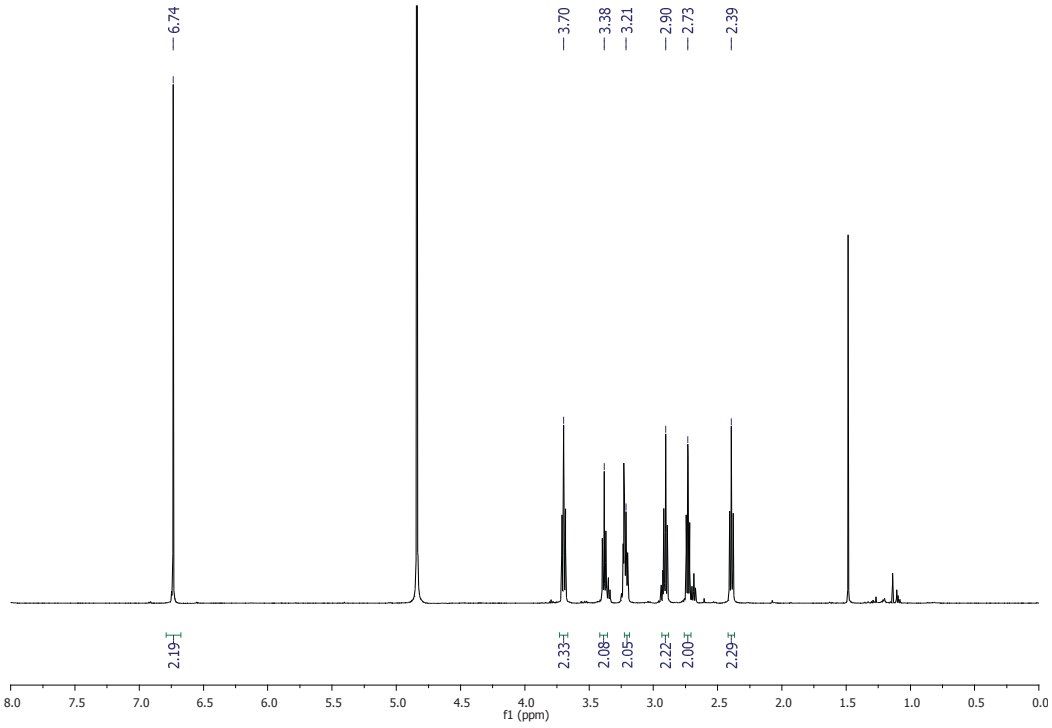

Synthesis of compound **13**

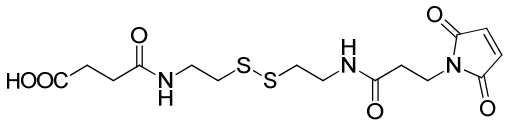

Succinic anhydride (0.124 g, 1.23 mmol) and a catalytic amount of DMAP were added to a solution of **12** (0.68 g, 1.23 mmol) in DMF/DCM (1:6 v/v, 35 mL), and the mixture was stirred for 24 h at r.t. and 7 h at 40 °C. After 6, 12 and 24 hours additional aliquots of succinic anhydride (0.10 g) and DMAP were added. The crude mixture was concentrated by rotary evaporation and purified by FC (eluant DCM/MeOH in gradient from 95:5 to 80:20), affording **13** as pale yellow oil (0.37 mg, 73% yield).

^{1}H NMR (CD_3OD, 500 MHz) δ (ppm): 6.81 (2H, s), 3.77 (2H, t, *J* = 6.8 Hz), 3.47 (2H, t, *J* = 6.8 Hz), 3.44 (2h, t, *J* = 6.6 Hz), 2.80 (2H, t, *J* = 6.8 Hz), 2.78 (2H, t, *J* = 6.6 Hz), 2.60-2.57 (2H, m), 2.49-2.46 (4H, m). ^{13}C NMR (CD_3OD, 125 MHz) δ (ppm): 176.3, 176.2, 174.7, 173.3, 172.2, 135.5, 39.8, 39.5, 38.4, 35.9, 35.5, 31.5, 30.3, 29.9. MS (ESI, *m/z*): 426.1 $[M+Na]^+$. HR-MS (ESI): *m/z* = 426.0782 $[M+Na]^+$ (calcd for $C_{15}H_{21}N_3O_6S_2Na$ *m/z* = 426.0764). FT-IR (neat, *v* /cm^{-1}): 2926, 1683, 1638, 1545, 1408, 1193, 1108, 915, 796, 693.

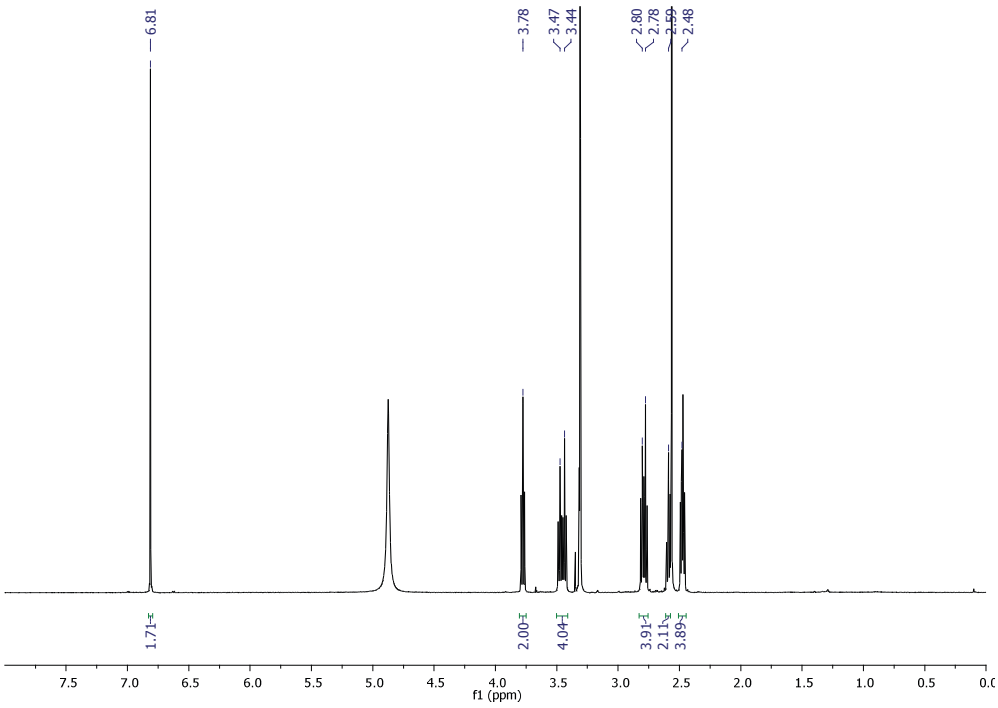

Synthesis of CNT conjugates

Oxidation of MWCNTs

500 mg of pristine MWCNTs were treated with a solution of H_2SO_4/HNO_3 (75 mL, 3:1 v/v, 98% and 65% respectively) at 0 °C, and the mixture was sonicated for 24 h in a water bath (20 W, 40 kHz). The mixture was then carefully diluted with distilled water (300 mL) and filtered through a PTFE membrane (0.45 μm). The black material on the filter membrane was re-suspended in water by sonicating for 15 min and filtered again, and this sequence was repeated until neutrality of the aqueous solution. The CNTs were then further purified by dialysis against deionized water for 48 h and finally lyophilized. Shortened oxidized MWCNTs (oxMWCNTs **1**) were obtained with a yield of 98% w/w. The average length distribution of oxMWCNTs was assessed to be 381 nm by TEM. The amount of carboxylic acids introduced corresponds to 1.4 mmol/g and was calculated on the base of the weight loss highlighted by TGA graphs (see Figure 3.3).

Activation of oxMWCNTs

oxMWCNTs **1** (160 mg) were dispersed in oxalyl chloride (80 mL) by shortly sonicating, and the mixture was then refluxed for 24 h stirring under argon. The solvent was removed under reduced pressure and the resulting activated nanotubes (MWCNT-COCl) were used straightaway for the following step.

Synthesis of f-MWCNTs **3**

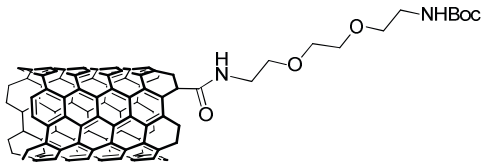

A dispersion of ox-MWCNTs **1** (20 mg) in oxalyl chloride (10 mL) was shortly sonicated (5 min) and then refluxed for 24 h under argon, stirring vigorously. Afterwards the solvent was removed under reduced pressure and the resulting activated MWCNTs **2** were immediately used for the amidation step. CNTs **2** were dispersed in a solution of Boc-mono-protected TEG-diamine **8** (240 mg) in dry THF (10 mL) and refluxed for 48 h, under argon. The crude mixture was filtered through a PTFE membrane (0.1 μm), and the CNTs recovered on the membrane were washed by dispersing them in DMF, sonicating for 10 min and filtrating. This washing sequence was further repeated with MeOH (x 2) and with acetone (x 2). The CNTs powder was finally dried under vacuum to give *f*-MWCNTs **3**. The degree of functionalization estimated from the weight loss comparison with oxMWCNTs **1** is 2.7 %, corresponding to a loading of 100 μmol/g.

Synthesis of f-MWCNTs **4**

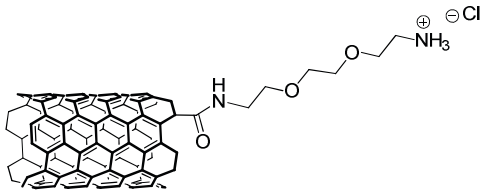

Amidated CNTs **3** (20 mg) were sonicated for 10 min in a 2 M solution of HCl in 1,4-dioxane (20 mL), and the mixture was stirred overnight at r.t. The reaction mixture was then filtered (0.1 μm) and the CNTs were washed with DMF, MeOH (x 2) and acetone (x 2). Finally the CNTs were dialyzed against deionized water for 2 days, and lyophilized affording compound **4**. From the Kaiser test, the amount of free amine results to be 182 μmol/g.

Synthesis of f-MWCNTs **5**

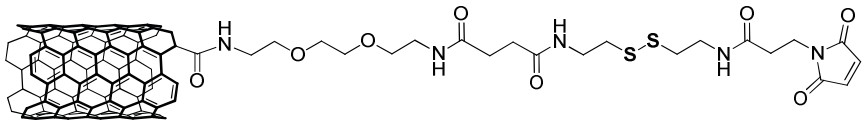

Aminated CNTs **4** (15 mg, 2.7 μmol of amine functions calculated by Kaiser test) were dispersed in dry DMF (8 mL) by sonicating for 10 min under argon. DIEA (47.7 μL, 100 eq.) was added and the mixture was further sonicated for 5 min. In parallel, disulfide linker **13** (55 mg, 50 eq.) was dissolved in a solution of HOBt (37 mg, 100 eq.) and EDC (43 mg, 100 eq.) in dry DMF (7 mL), and stirred for 1 h under argon. This solution was then added to the CNTs dispersion, briefly sonicated and left to react for 56 h at r.t. The reaction mixture was filtered over a PTFE membrane (0.1 μm) and the CNTs were washed with DMF (x 2), MeOH (x 2) and DCM (x 1), dialyzed against deionized water and finally lyophilized. The free amine loading calculated by Kaiser test is 12 μmol/g, which corresponds

to a degree of functionalization of 170 μmol/g. The estimation of the degree of functionalization obtained from TG analysis corresponds to 120 μmol/g and is in good agreement with the Kaiser test value.

*Synthesis of **CNT-SS-mal-VHH***

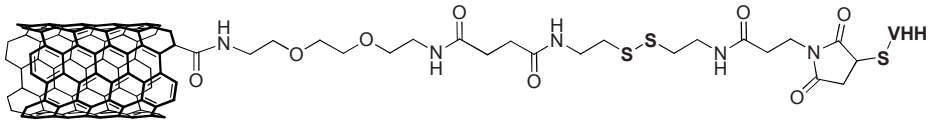

Maleimide-functionalized CNTs **5** (7 mg) were dispersed in a VHH solution in 2 mM EDTA/PBS (150 μg/mL, 14 mL, pH 6.4), sonicated in cold water for 1 min, and shaken for 6 h at r.t. Conjugation of the nanobody

was checked at time points 0, 5 and 6 h by measuring the UV-Vis absorbance of the supernatant of the reaction mixture. After 6 h incubation, the CNT-VHH conjugate was recovered by centrifugation (4500 rpm, 4 °C, 5 min), supernatant was removed and the CNTs were re-dispersed in PBS buffer pH 7.4 by sonicating 30 sec in cold water. Centrifugation and re-dispersion in fresh PBS were repeated 3 times, and the final dispersion was dialyzed (MWCO 300000 Da) against PBS buffer pH 7.4 for 48 h at 4 °C. CNT-SS-mal-VHH were characterized by TGA, TEM and GE and stored at 4 °C in a PBS solution (5.5 mg/mL). The loading of VHH estimated from the TG analysis amounts to 9.9 μmol/g.

Synthesis of f-MWCNTs **6**

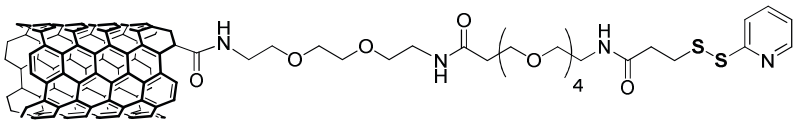

PEG_4-SPDP **14** (15 mg) and DIEA (50 μL) were added to a dispersion of CNTs **4** (15 mg) in dry DMF (15 mL) under argon. The mixture was sonicated for 15 min and then stirred for 48 h at r.t. The functionalized CNTs were recovered by filtration (0.1 μm), washed with DMF (x 2), MeOH (x 2) and DCM (x 1), and further purified by dialysis against deionized water. The free amine loading calculated by Kaiser test is 61 μmol/g, which corresponds to a degree of functionalization of 121 μmol/g. The estimation of the degree of functionalization obtained from TG analysis corresponds to 90 μmol/g and is in good agreement with the Kaiser test value.

*Synthesis of **CNT-SS-VHH***

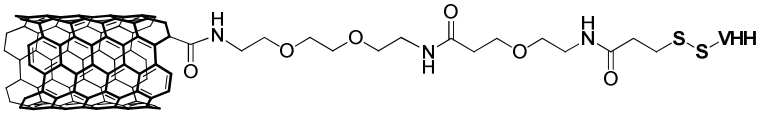

Compound **6** (7 mg) was dispersed in a VHH solution in 2 mM EDTA/PBS (150 μg/mL, 14 mL, pH 6.4), sonicated in cold water for 1 min, and shaken for 6h at r.t. Conjugation of the nanobody was checked at time point 0, 5 and 6 h by measuring the UV-Vis absorbance of the supernatant of the

reaction mixture. After 6 h incubation the CNT-VHH conjugate was recovered by centrifugation (4500 rpm, 4 °C, 5 min), supernatant was removed and the CNTs were re-dispersed in PBS buffer pH 7.4 by sonicating 30 sec in cold water. Centrifugation and re-dispersion in fresh PBS were repeated 3 times, and the final dispersion was dialyzed (MWCO 300000 Da) against PBS buffer pH 7.4 for 48 h at 4 °C. CNT-SS-VHH were characterized by TGA, TEM and GE and stored at 4 °C in PBS solution (4.2 mg/mL). The loading of VHH estimated from the TG analysis amounts to 5.3 μmol/g.

Synthesis of f-MWCNTs **7**

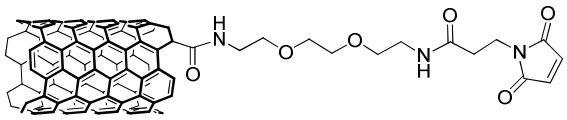

Amidated CNTs **4** (13 mg) and *N*-succinimidyl-3-meleimidopropionate **9** (78 mg) were dispersed in dry DMF by sonicating for 15 min under argon. DIEA (0.7 mL) was then added by syringe and the mixture was left to react for 48 h at r.t. After filtration over a PTFE membrane (0.1 μm), the recovered CNTs were washed with DMF (x 2), MeOH (x 2) and acetone (x 1), and finally dried *in vacuo*. The free amine loading of meleimido-functionalized CNTs calculated by Kaiser test is 65 μmol/g, which corresponds to a degree of functionalization of 95 μmol/g. The estimation of the degree of functionalization obtained from TG analysis corresponds to 92 μmol/g and is in good agreement with the Kaiser test value.

Synthesis of ***CNT-VHH***

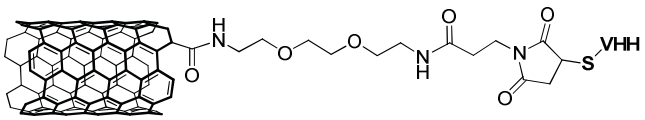

Compound **7** (7 mg) was dispersed in a VHH solution in 2 mM EDTA/PBS (150 μg/mL, 14 mL, pH 6.4), sonicated in cold water for 1 min, and shaken for 6h at r.t. Conjugation of the nanobody was checked at time point 0, 5 and 6 h by measuring the UV-Vis absorbance of the supernatant of the reaction mixture. After 6 h incubation the CNT-VHH conjugate was recovered by centrifugation (4500 rpm, 4 °C, 5 min), supernatant was removed and the CNTs were re-dispersed in PBS buffer pH 7.4 by sonicating 30 sec in cold water. Centrifugation and re-dispersion in fresh PBS were repeated 3 times, and the final dispersion was dialyzed (MWCO 300000 Da) against PBS buffer pH 7.4 for 48 h at 4 °C. CNT-VHH were characterized by TGA, TEM and GE and stored at 4 °C in PBS solution (3.7 mg/mL). The loading of VHH estimated from the TG analysis amounts to 8.1 μmol/g.

3.4.2 BIOLOGICAL EVALUATIONS

Gel Electrophoresis

Gel electrophoresis were performed on Mini-PROTEAN® TGX™ 4-15% Tris-glycine gels purchased from Bio-Rad Laboratories (Hercules, California). Tris-glycine buffer was used to fill the

tank. Prior to loading, the samples were added with Laemmli buffer for non-reducing conditions or reducing conditions (Laemmli buffer supplemented with 5% β-mercaptoehtanol). The first well was always loaded with a protein ladder. Loaded amounts of samples are ca. 7 μg for VHH (in left-side gel, Figure 3.8), ca. 25 μg for CNT-SS-mal-VHH and CNT-SS-VHH; ca. 20 μg for CNT-VHH and ca. 3 μg for VHH (in right-side panel). The amounts of VHH loaded in the gel (in the two cases) correspond to the amount of VHH on the CNT conjugates based on TGA. The gel was run at a voltage of 150 V for ca. 60 min and then stained overnight with Coomassie blue. Finally, the staining solution was removed and the gel extensively washed with distilled water to allow the visualization of the proteins bands.

Cell Cultures

Human colorectal carcinoma HCT116 were maintained in MCoys 5A media and supplemented with 10% fetal bovine serum (FBS), 50 U/ml penicillin, 50 μg/ml streptomycin, 1% L-glutamine at 37°C in 5% CO_2. Cells were passaged when they reached 80% confluence in order to maintain exponential growth. HCT116 cells used for tumor inoculation were passaged two times in antibiotic-free media to ensure the line was free of contaminants prior to implantation.

Cellular Proliferation Studies

HCT 116 Cells (7500 cells/well) were subcultured into 96-well plates. Twenty-four hours later, the cells were treated with 5 and 50 μg/ml of CNT alone, CNT-VHH, CNT-SS-VHH and CNT-SS-mal-VHH conjugates. DMSO 10% was used as a positive control. After 24 and 48 h incubation at 37°C and 5% CO_2, the modified lactate dehydrogenase (LDH) assay was performed. In brief, the Promega Cytotox 96® Non-radioactive cytotoxicity assay (Promega UK Ltd) was used according to the manufacturer instructions. The assay was modified to avoid interference with CNT in which the LDH of healthy cells that survived treatment was assessed by artificially lysing the cells instead of looking at the LDH released due to cytotoxicity. Cells were lyzed with 10 μl of lysis buffer (9% Triton X100 in water) and 100 μl of serum free medium and left for 45-60 min at 37 °C. After centrifugation (13000 rpm, 5 min), 50 μL of cell lysate were mixed with 50 μl of the substrate mix in a microtiter plate and incubated for 15 min at room temperature. Absorbance was read at 490 nm using an FLUOstar Omega plate reader. The amount of LDH released was an indication of the number of cells that survived treatment. The percentage cell survival was expressed as:

$$Percentage\ Cell\ Survival = \frac{LDH\ Released\ from\ Treated\ Cells}{LDH\ Released\ from\ Control\ Cells} \times 100$$

Tumor Xenograft Implantation and Animal Survival Studies

Five to six-weeks old male CD1 nude mice (Charles River Laboratories) were caged in individually vented cages in groups of four to five with free access to food and water. The mice were inoculated subcutaneously with 5x106 HCT116 human colorectal carcinoma cells in 50 μl on the left leg. Intratumoral injections were performed when the tumor volume reached 200 mm^3. Anesthetized mice were injected with 50 μl of the dispersion (the CNT alone or the complex in 5% dextrose). Injections

were carried out on day 10 and 16 for all groups. Mice were sacrificed by cervical dislocation when tumor area reached 800-1000 mm^3.

Western Analysis of β-Catenin

Tumors were homogenized using lysis buffer (50 mM Tris-Cl, pH 8.0, 150 mM NaCl, 0.1% SDS, 1% Nonidet P-40 and 0.5% sodium deoxycholate). The tumor homogenates were left on ice for 30 min and mixed by vortex in between. Samples were then cleared by centrifugation at 13000 rpm for 30 min at 4 °C and the supernatants containing proteins were collected. Protein concentrations were examined using BCA assay kits (Pierce BCA protein assay kit, Thermal Scientific) and 20 µg of protein from each sample was resolved in 10% SDS-PAGE gels and transferred to Hybond ECL nitrocellulose membranes (GE Healthcare). After blocking in 3% BSA at room temperature for 1 h, the blots were incubated with rabbit monoclonal β-catenin antibody (Cell Signalling Technology) at 1:1000 overnight as per the manufacturer instructions. The blots were then incubated with the secondary antibody, horseradish peroxidase linked anti-mouse antibody (Cell Signalling Technology) at 1:1000 dilution for 1 h at room temperature. The specific bands were detected using chemiluminescent kits (Immun-Star Chemiluminescent Kit, BioRad), imaged and quantitatively analysed using ChemiDoc MP imaging system and Image Lab software (BioRad). GAPDH was used as an internal reference (house-keeping) gene.

Haematoxylin/Eosin Tissue Histology

For histological analysis, tumors were fixed in 10% buffered formalin and processed for routine histology with haematoxylin and eosin stain by Human Biomaterials Resource Centre (College of Medical and Dental Sciences, University of Birmingham). Microscopic observation of tissues was carried out with Nikon Microphot-FXA microscope coupled with Infinity 2 digital camera.

3.5 BIBLIOGRAPHY

[1] A. M. Scott, J. D. Wolchok, L. J. Old, *Nat. Rev. Cancer* **2012**, *12*, 278.

[2] S. Oliveira, R. Heukers, J. Sornkom, R. J. Kok, P. M. P. van Bergen En Henegouwen, *J. Control. Release* **2013**, *172*, 607.

[3] M. M. Harmsen, H. J. De Haard, *Appl. Microbiol. Biotechnol.* **2007**, *77*, 13.

[4] C. Hamers-Casterman, T. Atarhouch, S. Muyldermans, G. Robinson, C. Hammers, E. Bajyana Songa, N. Bendahman, R. Hammers, *Nature* **1993**, *363*, 446.

[5] R. Chakravarty, S. Goel, W. Cai, *Theranostics* **2014**, *4*, 386.

[6] "BioLegend — Camelid Antibodies," can be found under http://biolegend.tumblr.com/post/101934444434/camelid-antibodies, n.d.

[7] S. Muyldermans, T. N. Baral, V. C. Retamozzo, P. De Baetselier, E. De Genst, J. Kinne, H. Leonhardt, S. Magez, V. K. Nguyen, H. Revets, U. Rothbauer, B. Stijlemans, S. Tillib, U. Wernery, L. Wyns, G. Hassanzadeh-Ghassabeh, D. Saerens, *Vet. Immunol. Immunopathol.* **2009**, *128*, 178.

[8] D. Smolarek, O. Bertrand, M. Czerwinski, *Postep. Hig Med Dosw* **2012**, *66*, 348.

[9] P. J. Morin, *Bioessays* **1999**, *21*, 1021.

[10] G. Leriche, L. Chisholm, A. Wagner, *Bioorg. Med. Chem.* **2012**, *20*, 571.

[11] G. Saito, J. A. Swanson, K.-D. Lee, *Adv. Drug Deliv. Rev.* **2003**, *55*, 199.

[12] N. W. S. Kam, Z. Liu, H. Dai, *J. Am. Chem. Soc.* **2005**, *127*, 12492.

[13] L. G. Delogu, A. Magrini, A. Bergamaschi, N. Rosato, M. I. Dawson, N. Bottini, M. Bottini, *Bioconjug. Chem.* **2009**, *20*, 427.

[14] H. Chen, X. Ma, Z. Li, Q. Shi, W. Zheng, Y. Liu, P. Wang, *Biomed. Pharmacother.* **2012**, *66*, 334.

[15] Y.-Z. You, C.-Y. Hong, C.-Y. Pan, *Macromol. Rapid Commun.* **2006**, *27*, 2001.

[16] Y.-Z. You, C.-Y. Hong, C.-Y. Pan, *J. Phys. Chem. C* **2007**, *111*, 16161.

[17] J. Chen, S. Chen, X. Zhao, L. V. Kuznetsova, S. S. Wong, I. Ojima, *J. Am. Chem. Soc.* **2008**, *130*, 16778.

[18] T. Miyadera, E. M. Kosower, *J. Med. Chem.* **1972**, *15*, 534.

[19] M. Brinkley, *Bioconjug. Chem.* **1992**, *3*, 2.

[20] M. E. Gindy, S. Ji, T. R. Hoye, A. Z. Panagiotopoulos, R. K. Prud'homme, *Biomacromolecules* **2008**, *9*, 2705.

[21] C. Samorì, R. Sainz, C. Ménard-Moyon, F. M. Toma, E. Venturelli, P. Singh, M. Ballestri, M. Prato, A. Bianco, *Carbon* **2010**, *48*, 2447.

[22] A. Battigelli, Cationic Carbon Nanotubes for Nucleic Acids Delivery, Ph.D. Thesis, University of Trieste and University of Strasbourg, **2012**.

[23] K. A. Jacobson, B. Fischer, X. Ji, *Bioconjug. Chem.* **1995**, *6*, 255.

[24] R. S. Shirazi, K. K. Ewert, C. Leal, R. N. Majzoub, N. F. Bouxsein, C. R. Safinya, *Biochim. Biophys. Acta* **2011**, *1808*, 2156.

[25] S. Li, D. Zeng, *Angew. Chem.* **2007**, *119*, 4835.

[26] E. Venturelli, Antibody-Functionalized Carbon Nanotubes towards a Targeted Anticancer Therapy, University of Strasbourg, **2011**.

[27] J. Homola, S. S. Yee, G. Gauglitz, *Sensors Actuators B Chem.* **1999**, *54*, 3.

[28] B. Johnsson, S. Löfås, G. Lindquist, *Anal. Biochem.* **1991**, *198*, 268.

[29] "Surface Plasmon Resonance Applications," can be found under http://www.alvtechnologies.com.ph/index.php?option=com_content&view=article&id=298:spr-applications&catid=11:news&Itemid=6, n.d.

[30] A. Meister, M. E. Anderson, *Annu. Rev. Biochem.* **1983**, *52*, 711.

[31] Z.-B. Zheng, G. Zhu, H. Tak, E. Joseph, J. L. Eiseman, D. J. Creighton, *Bioconjug. Chem.* **2005**, *16*, 598.

[32] G. T. Zugates, D. G. Anderson, S. R. Little, I. E. B. Lawhorn, R. Langer, *J. Am. Chem. Soc.* **2006**, *128*, 12726.

[33] E. Kaiser, R. L. Colescott, C. D. Bossinger, P. I. Cook, *Anal. Biochem.* **1970**, *34*, 595.

[34] A. Battigelli, J. Russier, E. Venturelli, C. Fabbro, V. Petronilli, P. Bernardi, T. Da Ros, M. Prato, A. Bianco, *Nanoscale* **2013**, *5*, 9110.

CHAPTER 4

CNTS FOR DELIVERY OF RADIOACTIVITY - *INTRODUCTION TO THE RADDEL PROJECT*

Abstract – The Marie Curie ITN program RADDEL in which I have been involved, deals with the targeted delivery of radioactivity. The general purpose is the development of sealed carbon nano-capsules filled with radioactive material in their interior, and externally decorated with targeting biomolecules in order to specifically address radioactivity to carcinogenic organs. To this purpose carbon nanotubes (CNTs) are highly suitable because they can host small molecules (e.g. $SmCl_3$, NaI) inside their hollow interior, and be externally functionalized with biologically active molecules in order to impart specific targeting properties and enhance their biocompatibility.
In this chapter we will describe the fundamentals of radiotherapy and provide an overview on the use of nanoparticles, and in particular CNTs, for the delivery of radioisotopes for cancer treatment and diagnosis. We will then explain the overall goals of the researches developed within the RADDEL program and the choice of the strategy. Because of the strong interconnection between the tasks of the numerous partners participating to the program, we will also outline the articulation of the project in order to provide an understanding of our work within the network.

4.1 General Introduction

The human kind has always been prompted toward the research of efficient solutions to health-related complicacies, and among all diseases, the treatment of cancer has been always considered with great apprehension. Cancer is one of the most deadly diseases, and current treatment modalities suffer from many deficits such as the inability to completely destroy all cancerous cells as well as from severe toxic side effects. The most common treatment methodologies usually consist in surgical tumor ablation, chemotherapy or radiotherapy, or in a combination of multiple treatments. Besides, there still exists a great demand for imaging techniques that allow the detection and visualization of tumors at the different stages, especially at the early-stage. The exploitation of high-energy radiations is indeed valuable for both scopes, and many investigations are nowadays focusing on its development for cancer therapy and diagnosis.

4.1.1 Fundamentals of Radiation Therapy

Radiation therapy employs high-dose ionizing radiation to kill cancer cells and to prevent progression and recurrence of the tumor, and it is very effective especially for radiation-sensitive tumors.[1] Radiotherapy can be applied to the patient in three ways: externally, internally or by systemic radiation. *External radiation therapy* consists in directing high-energy x-rays or electron or proton beams to a tumor from outside the body. This approach is very practical but has its main disadvantages in the destruction of healthy tissues along the beam path, and in the need of high radiation doses to achieve deep penetration and treat large volume tumors. By *internal radiation therapy* (or brachytherapy), a sealed radiation source is positioned within or near the tumor by means of an implant so that the radiation only affects the surrounding tissues. *Systemic radiation therapy* instead, delivers the radiation energy by oral or intravenous administration of a formulation consisting of a radioisotope and a tumor-targeting carrier (*e.g.* antibodies, liposomes, nanoparticles). This method offers similar advantages of drug delivery systems, such as allowing a site-specific delivery and a reduction of the needed doses and the side effects. Furthermore, it consents tracking and quantification of the isotope by imaging techniques and tunability of the radioisotope/carrier pair. For these reasons, systemic radiotherapy is considered a promising approach for personalized oncology. However, to effectively employ this methodology it is essential to carefully select and combine the radioisotope (with suitable half-life), the carrier and the tumor biomarker.[2,3]

4.1.1.1 Radioisotopes

Almost all elements of the periodic table have at least one radioactive isotope, which can be naturally occurring or artificially produced. However, not all radioisotopes are suitable for bioapplications and for oncology in particular, as the type of emission and the time of decay are two fundamental parameters. Generally, radionuclides that are employed for therapeutic applications are those that emit radiation in the form of α, β or Auger particles (Figure 4.1). In addition, γ-emitters and positron (β^+) emitters are commonly employed in nuclear medicine for diagnostic purposes. *Y-emitters* for instance, release γ-ray photons with energy between 130 and 370 keV and allow tumor imaging by scintigraphy or single photon emission computed tomography/computed tomography (SPECT/CT).[4]

However, because of the long penetration range of γ-radiation, these radionuclides can cause severe adverse effects on the cells and are therefore usually employed at very low doses.

α-emitters deliver α-particles, which are positively charged helium nuclei ($^{4}_{2}He^{2+}$) with high energies (5000-8000 keV) and a range of 50-80 μm. Their penetration depth is thus very short and cell death occurs only when α-particles reach the cell nucleus, which makes these particles suitable for the treatment of small-volume tumors, micrometastasis or residual tumors. Notable examples of α-emitters used for therapeutic purposes are actinium-225 (^{225}Ac) and bismuth-213 (^{213}Bi).[5]

β-emitters release electrons having a lower energy than α-particles, but because of their much lower mass, they have longer penetration ranges and can thus penetrate the tissues deeper. Generally, β-particles are divided into low-energy particles (0.15 MeV) and high-energy particles (1.7 MeV). The first type has shorter ranges (0.4-0.9 mm) and is best suited for small tumors, whereas the second type can penetrate up to 5.0 mm and it is thus more indicated for large tumors.[2] β-emitters are the most widely used radioisotopes in cancer therapy, and among the most known there are iodine-131 (^{131}I), yttrium-90 (^{90}Y), copper-67 (^{67}Cu) and lutetium-177 (^{177}Lu).

Auger emitters release low energy (< 1.6 keV) electrons derived from inner-shell electron transitioning. Most of these electrons have a very short range (< 1 μm) and are therefore effective when the radioisotope decay occurs inside the nucleus, or very close to it. This requirement has somehow limited the exploitation of Auger emitters for radiotherapy, however some of them such as indium-111 (^{111}In) and iodine-125 (^{125}I) have already shown promising effects against cancer.[6]

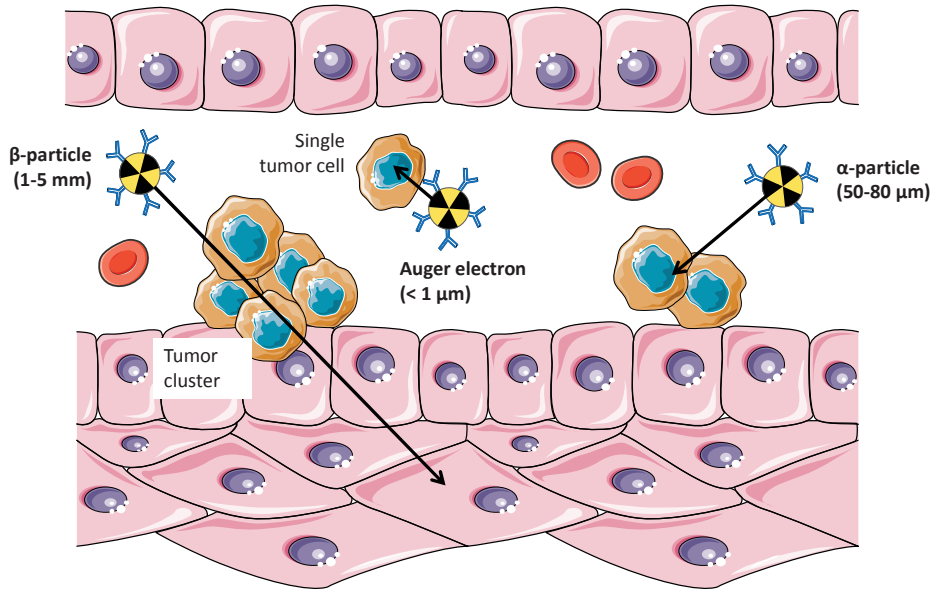

Figure 4.1 Schematic representation of tissue penetration range by β-particles (0.1–2.2 MeV, 1–10 mm range), Auger electron (0.1–2 keV, < 1 μm) and α-particles (5–8 MeV, 50–80 μm range) emitters. Adapted from ref. [4].

Some of these radionuclides are not pure emitters and they concomitantly release γ-radiation during the decay. This can be very advantageous to achieve simultaneous diagnosis and therapy. The choice of a radioisotope over another is determined by several parameters, such as physico-chemical properties, half-life, type of emission and radiation energy. As a general criterion, the half-life of the radionuclide should not be shorter than few hours to allow preparation and administration, but not longer than 2-3 weeks to avoid systemic side effects. In addition, nuclides that release a high abundance of secondary γ-radiation are generally not suitable because this heavily contributes to the

whole-body dose and can dramatically enhance the overall toxicity of the radioconjugate. Not to forget are also the stability of any daughter nuclide formed and the radionuclide route of production and availability. The production methods do in fact play an important role in the achievable specific activity of the nuclide and in its radiochemical purity. The radioisotope characteristics have then to be matched to the cellular distribution of the carrier molecule, namely localization on the surface (β), in the cytoplasm (β/α) or in the nucleus (Auger). Overall, the selection of a good candidate for radiotherapy has to take into account the specific cancer type, characteristic of the tumor, toxicity and safety of the radioisotope, availability and production, and the chemistry involved in the preparation of the delivery system.

4.1.2 Delivery of Radioactivity mediated by Nanoparticles

Among the main obstacles in the delivery of radioisotopes (free or chelated to small molecules), there are their rapid elimination from the bloodstream and their widespread distribution in healthy organs and tissues. One common solution to the rapid elimination has been the administration of large doses of the radioactive agent to the patients, but this approach is rather expensive and often results in undesired toxic effects. The association of a radioisotope to a suitable carrier can instead enable its targeted delivery and avoid the free circulation of the radioisotope in the body and the related toxicity. Most of currently used radiopharmaceuticals involve monoclonal antibodies (mAb) and chelators labeled with radionuclides.[5] However, the use of antibodies as carriers for radiotherapy has shown some limitations, such as inefficient targeting, low accumulation in the tumor site and irradiation of normal tissues caused by the long circulation of the antibody. In addition, mAbs have only few sites of anchoring for the radioisotope and they can trigger undesired immune responses, or undergo protease degradation. The use of nanomaterials for the delivery of radiotherapy showed instead good promises to overcome these limitations, besides offering the possibility for multimodality and multiple loading. Indeed, nanoparticle (NP) carriers represent an ideal theranostic tool with the radioisotope providing both therapeutic and imaging modalities, or combining its therapeutic effect with the imaging capability of the NP. Moreover, the intrinsic properties of the NP can provide additional therapeutic functionalities to the carrier, such as the ability to induce hyperthermia or increase the tumor retention by magnetization. Different examples of radiotherapeutic delivery systems based on nanoparticles have already been published, using materials such as micelles, SPION, polymers, dendrimers.[7,8] Often, these delivery systems are built by conjugating the nanoparticle to a tumor-targeting antibody cross-linked with therapeutic radioisotopes or radioisotope chelates. The tumor therapeutic efficacy and diagnostic quality are determined by the targeting selectivity of the delivery system and by the characteristics of the radioisotope.[7,9] Hence an optimal combination of the two is fundamental to its efficacy and possible future exploitation.

4.1.3 State-of-the-Art of CNTs for Delivery of Radio Isotopes

In contrast with the numerous and varied reports of CNT-conjugates for drug and gene delivery, only few studies exploring CNTs as carriers of radionuclides, either for imaging or therapeutic purposes, have been published. One of the first reports of a radiolabeled CNT construct to study *in vivo*

biodistribution was developed by our group, who built a CNT radiotracer by attaching ^{111}In (γ-emitter) to functionalized CNTs *via* the chelating agent DTPA (diethylenetriamine pentaacetic acid).[10] Soon after, McDevitt and co-workers employed a similar approach to radiolabel a CNT-antibody (CNT-Ab) conjugate for the targeting and treatment of a lymphoma.[11] Specifically, SWCNTs functionalized by 1,3-dipolar cycloaddition were appended with the chelating agent DOTA (tetraazacyclododecane tetraacetic acid) and with the monoclonal antibody Rituximab, which targets the CD20 epitope on human Burkitt lymphoma cells. Indium-111 was then loaded by chelation with DOTA, and the ability of the CNT construct to deliver the radionuclide to the tumor was assessed both *in vivo* and *in vitro*. In a subsequent report, the group of McDevitt radiolabeled with ^{225}Ac (α-emitter) a similar CNT construct functionalized with an antibody targeting the tumor neovasculature.[12] They employed this nanocarrier for targeted radioimmunotherapy in a murine xenograft model and achieved the reduction of the tumor volume and enhanced survival of the tumor mice compared to the control (Figure 4.2). The chelation of a different radionuclide to the construct, namely ^{89}Zr (positron emitters), allowed to perform PET radioimaging of the tumor vessels and study the pharmacokinetic profile of the CNT radioimmuno-carrier in the mice, proving its specific accumulation into the tumor and rapid blood clearance.[12]

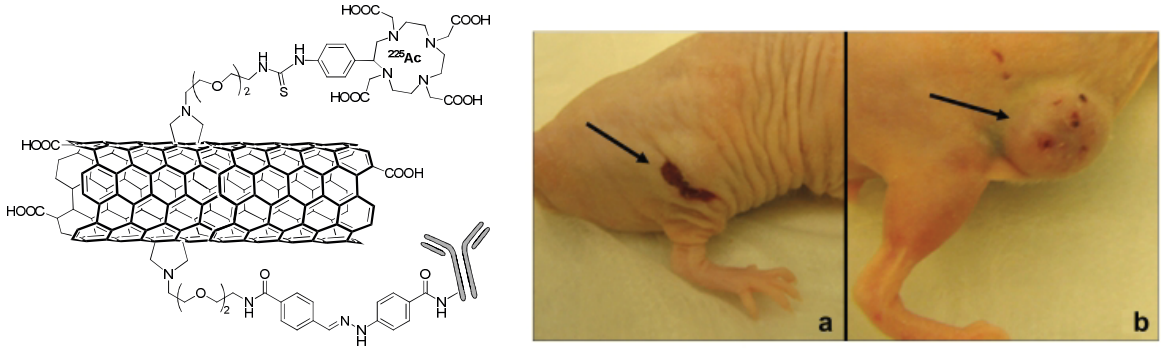

Figure 4.2 (Left) Schematic representation of the radiotherapeutic CNT construct reported by McDevitt *et al.* in ref. [12], featuring a targeting antibody and ^{225}Ac attached to the CNT through the DOTA chelator. (Right) Images of xenograft mice 10 days after treatment with the CNT construct: a) a mouse treated with a high radioactive dose, b) mouse treated with low radioactive dose. Figure adapted from ref. [12].

Other investigations on CNT biodistribution and tumor targeting abilities by radioimaging have been carried out by decorating the nanotubes with other radionuclides such as ^{86}Y, ^{125}I, ^{14}C, ^{64}Cu or ^{99m}Tc,[13–17] generally by coordination with a chelating agent covalently attached to the CNTs. An interesting example was reported by Jain and co-workers, who designed a sophisticated multimodal labeled CNT platform for the targeted delivery of a theranostic prodrug.[18] Oxidized MWCNTs were concomitantly decorated with a fluorochrome (Alexa-Fluor), a γ-emitting radionuclide (^{99m}Tc), a tumor-targeting module (folic acid) and the anticancer drug methotrexate (MTX). The latter was tethered to the nanotubes *via* a cleavable ester bond to afford a controlled intracellular release, while the fluorescent and radiolabeling of the construct was aimed at tracking its biodistribution and intracellular trafficking through combined optical and radioimaging. The conjugate showed a high traceability by both methods, and displayed elevate tumor binding affinity and augmented therapeutic efficacy compared to free MTX. Al-Jamal and co-workers recently reported the synthesis of magnetically decorated MWCNTs for dual MRI and SPECT imaging.[17] The hybrids of SPION and MWCNTs were radiolabeled with technetium-99m through a functionalized bisphosphonate and enabled the quantitative analysis of the biodistribution in mice by SPECT/CT imaging and γ-scintigraphy. The most innovative example of a CNT-based radiotracers has been reported by our collaborators in 2010 in *Nature Materials*.[19] Instead of using traditional chelation chemistry to obtain radiolabeled CNTs, Hong *et al.* engineered a totally new approach by exploiting the hollow

interior of the tubes to enclose the radionuclide.[19] Sodium iodide-125, a Auger and γ-emitter, was encapsulated inside SWCNTs by molten-phase capillary wetting at high temperature, and the tubes were sealed during the cooling step, affording a sealed cage with the metal halide trapped inside ($Na^{125}I$@SWCNTs). The external surface of the nanotubes was then covalently functionalized by 1,3-dipolar cycloaddition and appended with a biantennary glycoconjugate ($GlcNAc^D$), which provided enhanced dispersibility and biocompatibility to the construct (Figure 4.3-a). Hong *et al*. investigated the fate and biodistribution of the glycosylated $Na^{125}I$@SWCNT *in vivo* by SPECT/CT imaging of the whole animal. Whereas free $Na^{125}I$ rapidly accumulated in the thyroid as expected, the $GlcNAc^D$-$Na^{125}I$@SWCNTs accumulated in the lung with no signal from the thyroid, stomach or bladder (Figure 4.3-b,c). Despite the consistent accumulation and retention of the conjugate in the lungs, tissue histology 30 days after administration indicated no particular necrosis or fibrosis of the corresponding tissues, revealing no acute toxic effect determined by the persistence of the CNTs. Moreover, the traceability of radioactivity in the lungs after 30 days was a proof of the excellent *in vivo* stability of the glycosylated $Na^{125}I$@SWCNTs, with essentially no leakage of isotopes to other organs. Furthermore, the confinement of the radionuclide inside the carrier consented the localized and safe delivery of a high radioactive dose (800% ID/g; ionizing dose/gram), which is greater than the uptake achievable in the thyroid using ^{125}I alone (70% ID/g) so far.

The idea of this work was taken up by a network of several partners and constitutes the root of the Marie Curie ITN RADDEL, which will be detailed below.

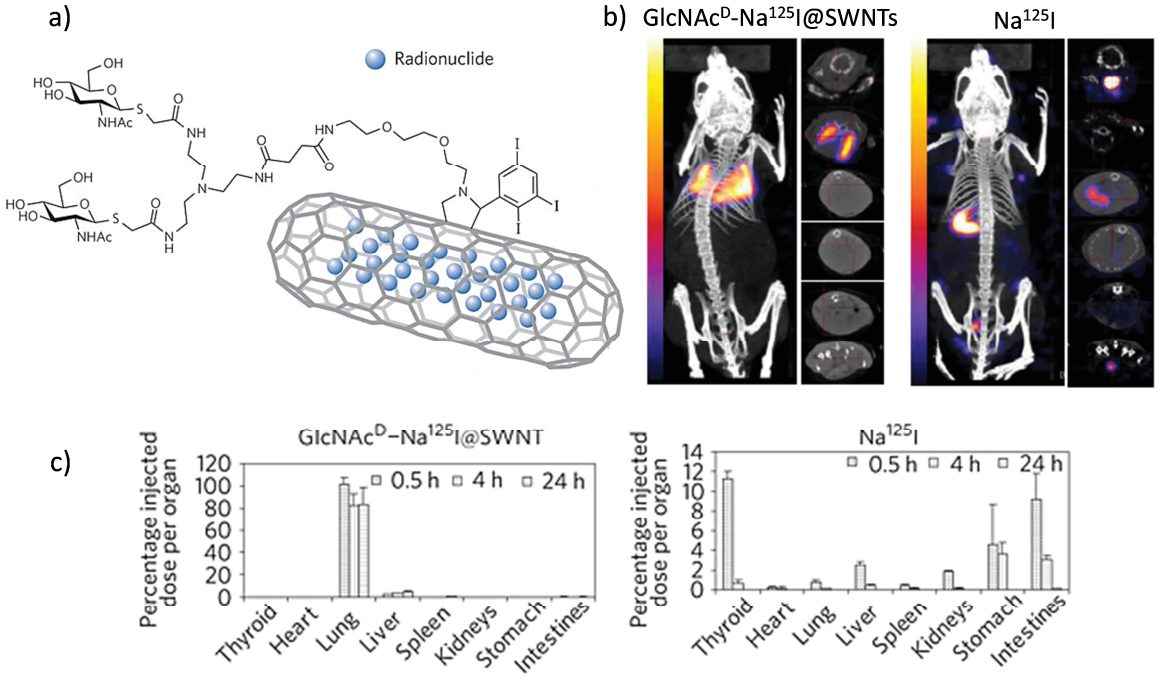

Figure 4.3 a) Schematic representation of $GlcNAc^D$-$Na^{125}I$@SWNTs, showing the radionuclide encapsulated within the nanotubes. b) Whole body SPECT/CT imaging at 4 h after i.v. injection of $GlcNAc^D$-$Na^{125}I$@SWNTs (250 µg, 1.0 MBq) and $Na^{125}I$ (1.8 MBq); cross sections of the thyroid, lung, stomach, liver, kidney and bladder at equivalent time points (top to bottom). c) Tissue biodistribution of $GlcNAc^D$-$Na^{125}I$@SWNTs and $Na^{125}I$ in mice at different time points after i.v. injection. Adapted from ref. [19].

4.1.4 ENDOHEDRAL CNTS

The encapsulation of molecules inside CNTs has been receiving increasing attention in the biomedical field, since the inner cavity of the nanotubes can be filled with a therapeutic or imaging cargo, while the outer surface can be modified to convey dispersibility, biocompatibility and site-selectivity.[20] Although less explored than the external functionalization, the internal loading approach confers the possibility to confine the diagnostic or therapeutic agent, protecting it from degradation or inactivation and providing it with additional stability. After Pederson and Broughton first report on the filling of CNTs,[21] a large variety of both organic and inorganic materials have been encapsulated inside single- and multi-walled CNTs.[20] Typically, SWCNTs have diameters ranging from 0.7 to 2.0 nm, while MWCNTs can reach internal diameters of tens of nm: as a consequence, a wide variety of molecules can be located in the interior cavity of the nanotubes, going from small gas atoms like He to bigger molecules, such as $Gd_2@C_{92}$ (gadolinium metallofullerene).[22,23] Because of the deep potential well inside the tubes, molecules can in principle enter very easily inside nanotubes, provided that they have sufficient energy to move toward the tube open ends and overcome the small energy barrier for entrance.[24] The filling process can be performed either during the CNT synthesis, or after synthesis, if CNTs are open-ended. The latter process is by far the most employed, especially for the inclusion of molecules that are temperature- or catalyst-sensitive. Methodologies for the post-synthesis filling of CNTs are generally classified in two categories: gas-route and liquid-route.[25] In the former strategy, the CNTs are placed in a sealed ampoule under vacuum and the material to be enclosed enters into the CNTs in the gas phase, which is either its natural phase or is obtained by sublimation. By the liquid-route, the filling material is liquid, or is heated above its melting temperature, and the CNTs are filled by capillary wetting. For molecules in the liquid phase, the entry into the interior cavity has a small barrier and is quite spontaneous if the surface tension of the liquid is not too high.[24] Techniques to achieve the CNT filling have been so-far widely explored, as endohedral CNTs can be exploited for a wide range of applications, spanning from molecular electronics,[26] nanothermometry,[27] nanoscale reaction vessels[24] and biomedicine.[20] In the biomedical field, compounds of interest are mainly organic molecules (small drugs, proteins, enzymes) and inorganic compounds, in quality of contrast agents. Many different constructs have been prepared for drug delivery, by encapsulating bioactive molecules such as DNA, RNA, peptides, or anticancer drugs (*e.g.* doxorubicin, gemcitabine, cisplatin). Imaging tools have instead been obtained by filling the tubes with iodine and metal salts ($Na^{125}I$, $^{211}AtCl$, Bi_2O_3) for SPECT/CT, or with MRI contrast agents such as gadolinium salts and Fe_3O_4.[20] The approach of confining the drug or imaging agent inside the carrier can certainly offer some advantages such as its concentration in one sole location, protection from the external environment and eventually controlled release, when the tube ends are left opened. On the other hand, sealing of the nanotube ends after filling can guarantee the complete isolation of the encapsulated material and its entrapment, which is advisable when the free circulation of the material is undesirable.

4.2 RADDEL – NANO-CAPSULES FOR TARGETED DELIVERY OF RADIOACTIVITY

4.2.1 GENERAL PURPOSE

RADDEL (RADioactivity DELivery) is an inter-sectorial network of 11 partners that has been awarded with a Marie Curie Initial Training Network (ITN) grant by the European Commission. The research project is aimed at the development of novel nanomaterials for biomedical applications in the areas of cancer diagnosis and therapy. Specifically, the program focuses on the design, synthesis, characterization and pharmacological studies of carbon nanocapsules that seal in their interior radioactive materials. After sealing the chosen radionuclides, the external walls of the closed-ended filled carbon nanotubes can be decorated with biologically active molecules in order to convey specific targeting properties and enhance their biocompatibility. The general idea of this project has been suggested and developed from a research study performed by a team involving most of the partners in the present consortium, and published in 2010 in *Nature Materials*.[19] As already mentioned above, in this report they described the preparation of carbohydrate-functionalized CNTs filled with ^{125}I radioisotopes for nuclear imaging purposes (cf. Section 4.1.3 and Figure 4.3). It was demonstrated that this CNT conjugate allowed the delivery of an unprecedented radiodosage and remained stable within the biological milieu *in vitro* and *in vivo* without leakages of radionuclides. This initial study cast a new light on the potential of CNTs as tools for the development of novel cancer therapeutics and diagnostics. It appeared thus interesting to carry out further investigations by exploring different filling materials, functionalizations and/or targeting molecules. Indeed, the choice of the filling radionuclide will allow to tailor a specific radiation, cancer type and therapy. In parallel, the functionalization of the external surface offers versatility towards the appendage of multiple functionalities, thus enabling to modulate the biodistribution of the carrier. Since the delivery of radioactivity takes place through the walls of the nanotubes, the release of the encapsulated radionuclides is not needed (and not desired). In the RADDEL project, we propose that the encapsulation of therapeutic or imaging radioisotopes within CNTs and subsequent surface functionalization with targeting ligands could offer a stable and efficient way for the selective delivery of radioisotopes at ultrasensitive doses for therapeutic or diagnostic purposes.

4.2.2 OVERVIEW ON THE CONSORTIUM

Due to the many scientific areas covered by the research program, the RADDEL project is highly multidisciplinary and involves partners with expertise in different fields, from physics and materials science, to chemistry, pharmacology and radiology. Furthermore, the nature of the project implies a strong interconnection and collaboration between the partners, and each of them was assigned with specific tasks, according to their expertise (Table 4.1). The list of partners involved in the consortium and their respective expertise and/or task within the network is presented here below. In summary, the group of Dr. Tobias in Barcelona was in charge of the purification, filling and sealing of the nanotubes with the selected radionuclides. Samples of pristine CNTs were then characterized by different techniques by the groups of Dr. Ballesteros and Dr. Kalbáč (Barcelona and Prague, respectively), and initial toxicological studies were performed *in vivo* and *in vitro* by the groups of

Prof. Al-Jamal and Prof. Kostarelos (London and Manchester). The groups of Prof. Davis, Prof. Prato and Dr. Bianco (Oxford, Trieste and Strasbourg) had the task to explore the external covalent functionalization of the provided pristine CNTs and the further conjugation of a targeting molecule. The prepared samples were characterized by multiple techniques by Dr. Ballesteros and Dr. Kalbáč, and the toxicological and pharmacological profile of *f*-CNTs was assessed *in vivo* and *in vitro* in Strasbourg, London and Manchester. The group of Al-Jamal had also the role of developing suitable cellular and animal tumor models for therapeutic and biodistribution investigations. IBA, the industrial partner, assisted in the choice of radioisotopes, tumor models and preparation strategies; they further provided the radionuclides for the filling and the facilities for the irradiation of the cold isotopes (non-radioactive). Dosimetry calculations on the radiation dosage to be used for specific tumor cell lines and consequent effects were performed by Dr. Emfietzoglou (Ioannina). Prof. Van Tendeloo provided high-resolution microscopic facilities for the characterization of the most relevant samples.

Partner	Institute	Location	Expertise/ Task
Dr. Gerard Tobias	Institut de Ciència de Materials de Barcelona (ICMAB-CSIC)	Bellaterra (Spain)	CNT purification, filling and sealing with metal halides
Prof. Benjamin G. Davis	University of Oxford (UOX)	Oxford (UK)	CNT filling, functionalization, synthesis of sugar-based targeting molecules
Prof. Kostas Kostarelos	University of Manchester (UNIMAN)	Manchester (UK)	Biology, pharmacology and therapeutic efficiency
Dr. Khuloud Al-Jamal	King's College London (KCL)	London (UK)	Biology, pharmacology and therapeutic efficiency
Dr. Tatiana Da Ros Prof. Maurizio Prato	Università degli Studi di Trieste (UNITS)	Trieste (Italy)	CNT covalent functionalization
Dr. Cécilia Menard-Moyon Dr. Alberto Bianco	Centre National de la Recherche Scientifique (CNRS)	Strasbourg (France)	CNT covalent functionalization, conjugation of biomolecules, *in vitro* toxicity studies
Dr. Belén Ballesteros	Catalan Institute of Nanotechnology (ICN 2)	Bellaterra (Spain)	Microscopic characterization: HRTEM and STEM
Dr. Dimitris Emfietzoglou	University of Ioannina (UOI)	Ioannina (Greece)	Dosimetry, radiology, toxicity simulations
Dr. Martin Kalbáč	Ustav Fyzikalni Chemie J. Heyrovskeho AV CR (HIPC)	Prague (Czech Republic)	Spectroscopic characterization (Raman, Vis-NIR, photoluminescence)
Dr. Jean-Claude Saccavini	Cis Bio International Ion Beam Applications SA (IBA)*	Saclay (France)	Radiology, radionuclide supply and irradiation
Prof. Gustaaf Van Tendeloo	Electron Microscopy for Materials Science, Universiteit Antwerpen (EMAT-UA)	Antwerp (Belgium)	Microscopic characterization by HRTEM

Table 4.1 List of partners involved in the RADDEL consortium and respective location and expertise, or task within the project. *Industrial partner.

4.2.3 SYNOPSIS

In the following section we will outline the development of the RADDEL project and illustrate the selected strategies, the goals and the methodologies employed to achieve them. An explanation of the overall organization and articulation of the project within the network is fundamental to understand the research aims, choices and work that our group undertook and that will be presented in detail in Chapter 5.

In the design of the final conjugates and the synthetic procedures, the network had to take into account several procedural issues and satisfy the necessary clinical requirements for radiopharmaceuticals. For instance, the nature and half-life of the radioisotope are determinant for the whole preparation setup and for the final applications. On the advice of the industrial partner, from a panel of possible radionuclides, we selected the following three for our investigations:

Radionuclide	Radiaton type (MeV)	Half-life	Penetration Range
^{153}Sm	β (0.8), γ (0.103)	1.95 d	3.0 mm
^{177}Lu	β (0.497), γ (0.208)	6.7 d	1.6 mm
^{131}I	β (0.6), γ (0.364)	8.04 d	2.0 mm

Table 4.2 Selected radionuclides and respective key characteristics.[3]

This choice was dictated by several considerations, such as availability of the radioisotope, in its hot and cold state, irradiation process, radiochemical purity, radiation type, energy and half-life. The selected radionuclides are essentially all β and γ emitters, which enables to concomitantly accomplish therapy and imaging of the tumor. Considering the half-life of the three isotopes, the whole bench preparation of the radioactive nanocarrier should be completed in maximum two, seven or eight days (for Sm, Lu and I, respectively), in order to have in the injectable formulation an amount of radioactivity sufficient for therapeutic purposes. We reasoned that the most convenient approach was to first perform the filling and sealing of nanotubes with the suitable non-radioactive isotopic precursor, and proceed with its radio-activation in a second instance (Figure 4.4). This strategy would allow to carry out the filling and subsequent washing steps in normal laboratory facilities and without consuming the radioactive life of the isotope. It would have been desirable to carry out also the external functionalization prior to the radio-activation, however, the conditions and energies employed in this process are drastic and the appended organic functionalities would not resist. In fact, the irradiation is performed in specific industrial reactors at elevate temperature and pressure. By adopting this sequence, radio-activation followed by external functionalization, it is crucial that the latter does involve simple and 'short' steps (reactions and work-up), shorter than the half-life of the radioisotope (Figure 4.4).

We decided that the CNT functionalization and derivatization with the bioactive target should be performed only by a covalent approach, in order to ensure the *in vivo* stability of the final conjugate. Besides, the chemical reactions for the CNT functionalization must preserve their closed ends and avoid the formation of big defects (holes) in the structure, which could result in the leakage of the radionuclides along time. As a consequence, the CNT covalent modification had to be restricted to sidewall functionalization, ruling out the reactions that require too harsh conditions, long times, addition of metallic catalyst, or long purification steps. The panel of possibilities thus comprehended: 1,3-dipolar cycloaddition, radical addition, Bingel and nitrene reactions. In order to avoid

overlapping researches, the group of Prof. Prato investigated over the first two reactions, whereas our group focused on the last two (see Chapter 5).

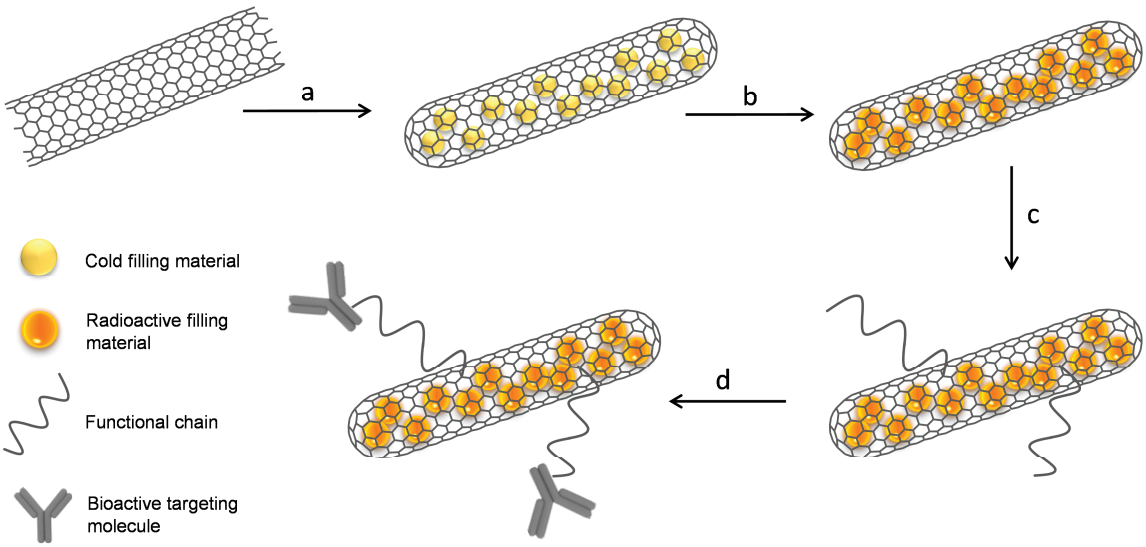

Figure 4.4 General representation of the procedures for the preparation of *f*-X@CNTs (X = general metal) for the delivery of radioactivity. a) Filling and sealing of purified CNTs with non-radioactive isotopes, b) irradiation of X@CNTs, c) covalent functionalization, d) conjugation of the bioactive target.

As a general guideline, we decided to investigate the covalent functionalization of CNTs starting from TEG or PEG derivatives, in order to introduce on the sidewalls water-soluble moieties that could enhance the dispersibility and biocompatibility of the carrier. The terminations of the functional chains should also be suitable for further derivatization with an imaging probe and/or targeting biomolecule (Figure 4.4). To this purpose, investigations were focused on sugar building blocks and antibodies, as targeting agents, and on fluorescent probes, for imaging. The biological and pharmacological profile of the prepared filled and functionalized conjugates (*f*-X@CNTs) was then assessed both *in vitro* and *in vivo*. Different human and murine cell lines were employed to evaluate the cellular uptake, intracellular trafficking and internalization mechanisms. The targeting and therapeutic efficacy of *f*-X@CNTs was studied with specific cancer cell lines and tumor xenograft models. The tissue distribution, pharmacokinetics, body excretion profile were also investigated, following *in vivo* administration both in normal and tumor-bearing mice.

Because of the safety requirements associated with the manipulation of radioactive materials, the costs and the required radio-lab facilities, experiments with radioactive material were only envisaged at the final step of the project, with optimized protocols. Preliminary investigations on the feasibility of the whole procedure were indeed needed to setup any experiment involving radioactivity. The group of Dr. G. Tobias in Barcelona has been providing the other partners with CNTs filled with model compounds (non-radioactive analogues of the radioactive candidates), and at the same time exploring and improving the methodologies to purify, fill and seal SWCNTs and MWCNTs. This allowed the other groups to carry on investigations on the reactivity of the model X@CNTs toward covalent functionalization, biological behavior, characterization, etc. The most promising approaches were selected and optimized preparation protocols were set up to be tested with the radioactive compounds.

4.3 CONCLUSIONS

The RADDEL project is aimed at investigating new strategies and methodologies for the preparation of novel CNT conjugates for the delivery of radioactivity. The multidisciplinarity of the network allowed to develop all investigations in a synergistic way, by matching the expertise and facilities of each partner. Our task within this macro-project has been to explore the reactivity of different types of purified CNTs toward [2+1] cycloaddition reactions (Bingel and nitrene) and the subsequent derivatization with targeting/imaging molecules. All functionalization procedures were conceived in order to achieve the final conjugates within a short time (few days), avoiding long purification steps and harsh reaction conditions that might engender leakages of the filling material. Because in the final scenario we expect to functionalize radioactive filled CNTs, the total synthetic pathway after irradiation up to the injectable formulation should be as simple and rapid as possible. In the next chapter we will describe the researches carried out by our group to achieve these goals and the final results.

4.4 BIBLIOGRAPHY

[1] E. C. Easson, in *Radiother. Malig. Dis.* (Ed: R.C.S. Pointon), Springer London, London, **1991**, pp. 111–129.

[2] J. Zweit, *Phys. Med. Biol.* **1996**, *41*, 1905.

[3] P. A. Schubiger, R. Alberto, A. Smith, *Bioconjug. Chem.* **1996**, *7*, 165.

[4] G. Ting, C.-H. Chang, H.-E. Wang, T.-W. Lee, *J. Biomed. Biotechnol.* **2010**, *2010*, 1.

[5] D. M. Goldenberg, *J. Nucl. Med.* **2002**, *43*, 693.

[6] M. Steiner, D. Neri, *Clin. Cancer Res.* **2011**, *17*, 6406.

[7] L. Zhang, H. Chen, L. Wang, T. Liu, J. Yeh, G. Lu, L. Yang, H. Mao, *Nanotechnol. Sci. Appl.* **2010**, *3*, 159.

[8] M. Muscarella, Y. Pathak, in *Antibody-Mediated Drug Delivery Systems: Concepts, Technol. Appl.* (Eds: Y. Pathak, S. Benita), John Wiley & Sons, Inc., Hoboken, NJ, USA, **2012**.

[9] W. Zhang, T. M. Swager, *J. Am. Chem. Soc.* **2007**, *129*, 7714.

[10] R. Singh, D. Pantarotto, L. Lacerda, G. Pastorin, C. Klumpp, M. Prato, A. Bianco, K. Kostarelos, *Proc. Natl. Acad. Sci. U. S. A.* **2006**, *103*, 3357.

[11] M. R. McDevitt, D. Chattopadhyay, B. J. Kappel, J. S. Jaggi, S. R. Schiffman, C. Antczak, J. T. Njardarson, R. Brentjens, D. A. Scheinberg, *J. Nucl. Med.* **2007**, *48*, 1180.

[12] A. Ruggiero, C. H. Villa, J. P. Holland, S. R. Sprinkle, C. May, J. S. Lewis, D. A. Scheinberg, M. R. McDevitt, *Int. J. Nanomedicine* **2010**, *5*, 783.

[13] M. R. McDevitt, D. Chattopadhyay, J. S. Jaggi, R. D. Finn, P. B. Zanzonico, C. Villa, D. Rey, J. Mendenhall, C. A. Batt, J. T. Njardarson, D. A. Scheinberg, *PLoS One* **2007**, *2*, e907.

[14] X. Deng, S. Yang, H. Nie, H. Wang, Y. Liu, *Nanotechnology* **2008**, *19*, 075101.

[15] H. Wang, J. Wang, X. Deng, H. Sun, Z. Shi, Z. Gu, Y. Liu, Y. Zhaoc, *J. Nanosci. Nanotechnol.* **2004**, *4*, 1019.

[16] Z. Liu, W. Cai, L. He, N. Nakayama, K. Chen, X. Sun, X. Chen, H. Dai, *Nat. Nanotechnol.* **2007**, *2*, 47.

[17] J. T.-W. Wang, L. Cabana, M. Bourgognon, H. Kafa, A. Protti, K. Venner, A. M. Shah, J. K. Sosabowski, S. J. Mather, A. Roig, X. Ke, G. Van Tendeloo, R. T. M. de Rosales, G. Tobias, K. T. Al-Jamal, G. Van Tendeloo, R. T. M. de Rosales, G. Tobias, K. T. Al-Jamal, *Adv. Funct. Mater.* **2014**, *24*, 1880.

[18] M. Das, S. R. Datir, R. P. Singh, S. Jain, *Mol. Pharm.* **2013**, *10*, 2543.

[19] S. Y. Hong, G. Tobias, K. T. Al-Jamal, B. Ballesteros, H. Ali-Boucetta, S. Lozano-Perez, P. D. Nellist, R. B. Sim, C. Finucane, S. J. Mather, M. L. H. Green, K. Kostarelos, B. G. Davis, *Nat. Mater.* **2010**, *9*, 485.

[20] M. Martincic, G. Tobias, *Expert Opin. Drug Deliv.* **2015**, *12*, 563.

[21] M. R. Pederson, J. Q. Broughton, *Phys. Rev. Lett.* **1992**, *69*, 2689.

[22] W. Teizer, R. B. Hallock, E. Dujardin, T. W. Ebbesen, *Phys. Rev. Lett.* **1999**, *82*, 5305.

[23] K. Suenaga, R. Taniguchi, T. Shimada, T. Okazaki, H. Shinohara, S. Iijima, *Nano Lett.* **2003**, *3*, 1395.

[24] D. A. Britz, A. N. Khlobystov, *Chem. Soc. Rev.* **2006**, *35*, 637.

[25] M. Monthioux, E. Flahaut, *Mater. Sci. Eng. C* **2007**, *27*, 1096.

[26] M. del C. Giménez-López, F. Moro, A. La Torre, C. J. Gómez-García, P. D. Brown, J. van Slageren, A. N. Khlobystov, *Nat. Commun.* **2011**, *2*, 407.

[27] A. Vyalikh, A. U. B. Wolter, S. Hampel, D. Haase, M. Ritschel, A. Leonhardt, H.-J. Grafe, A. Taylor, K. Krämer, B. Büchner, R. Klingeler, *Nanomedicine UK* **2008**, *3*, 321.

CHAPTER 5

DESIGN AND SYNTHESIS OF FUNCTIONALIZED RADIOACTIVITY-DELIVERY NANOCARRIERS

Abstract – In the present Chapter we will relate about the work we have accomplished within the RADDEL framework. We have synthesized the organic precursors for Bingel and nitrene cycloadditions and investigated the functionalization of various empty and filled CNTs by these two reactions. Later, investigations on the further derivatization with a targeting antibody have been carried out in order to obtain a targeting CNT-carrier of radioactivity. The principal constraints in the design of the preparation steps have been the preservation of the sealed CNT structure and the employment of short reaction times. To this purpose, different conditions have been attempted and optimization screenings have been carried out. We have succeeded in the functionalization of CNTs by nitrene reaction and further derivatized these conjugates with a tagging molecule, fluorescent probes or a targeting antibody. The Ab-conjugates have been thoroughly chemically characterized and their toxicological and targeting properties have been assayed both *in vitro* and *in vivo*.

Although less popular than [3+2] cycloadditions, [2+1] cycloadditions have also been largely explored for the functionalization of carbon nanotubes. This type of reactions lead to the formation of 3-membered rings on the CNT sidewalls and they typically require highly reactive species (carbenes, nitrenes), and/or harsh reaction conditions. In this Chapter we will describe the investigations that we carried out within the RADDEL project, to achieve the functionalization of filled CNTs by [2+1] cycloaddition, and the further derivatization with a targeting antibody. We started our investigations in parallel on Bingel reaction and the nitrene reaction but, for the sake of clarity, we will first introduce and discuss about Bingel reaction and afterwards about nitrene one. In the last section of this Chapter, the strategies adopted for the conjugation of the targeting antibody will be presented, followed by the biological experiments performed on the final conjugates. All investigations were carried out on pristine CNTs provided by our partner in Barcelona. For more information about the purifications and filling methods of CNTs, we refer to the final Annex (a preliminary reading of this Annex at page 159 could be beneficial to a better understanding of the following discussion).

5.1 BINGEL REACTION

Bingel reaction is a cyclopropanation reaction, which is formally considered as a [2+1] cycloaddition between a carbon double bond and a halo-malonate derivative, usually obtained *in situ* in the presence of a mixture of a base and tetrabromomethane (or iodine). In terms of mechanism, the reaction can be described as a nucleophilic addition operated by the malonyl carbanion (obtained by basic proton abstraction) towards an electrophilic double bond, followed by intramolecular aliphatic substitution into a closed ring, with elimination of the halide anion. This reaction was named after C. Bingel, who first reported the cyclopropanation of C_{60} using a bromomalonate derivative and NaH, in 1993.[1] The reaction has then been widely used in fullerene chemistry, due to the high reactivity under mild conditions, and because it consents to prepare multiple-substituted fullerene adducts. The first application of the Bingel reaction on CNTs was reported in 2003 by Coleman *et al*., who employed diethylbromomalonate as nucleophile and diazabicyclo[5.4.0]undec-7-ene (DBU) as a base, achieving a good degree of functionalization under mild conditions (*i.e.* room temperature for 24 h). The authors then further derivatized the SWCNTs with a tagging moiety (*i.e.* 2-(methylthio)ethanol followed by binding of gold particles) to be able to visually assess the functionalization by spectroscopic techniques. A modified version of the reaction, called Bingel-Hirsch, employs non-halogenated malonate, DBU and CBr_4 as halogenating agent, bypassing the need for isolation/purification of the bromomalonate precursors.[2] Applying this procedure, Ashcroft *et al.* performed the *in situ* functionalization of ultra-short SWCNTs by reacting them with malonic acid bis-(3-*tert*-butoxycarbonylaminopropyl) ester overnight.[3] The sidewall functionalization of oxidized SWCNTs by Bingel reaction has been also reported to occur successfully under microwave (MW) irradiation, with reduced reaction time (up to 30 min) and degrees of functionalization controllable by changing the microwave output power.

From an applicative point of view, Bingel reaction is rather appealing because it allows the introduction of two terminal groups on one grafting side, thus doubling the overall amount of available functionalities. In addition, by a proper asymmetric synthesis of the malonate precursor, it is possible to have two

different head-groups, which would ultimately enable the selective derivatization of so-functionalized CNTs with two diverse molecules (for example a targeting molecule and a tag).

5.1.1 RESULTS AND DISCUSSION

5.1.1.1 First approach: Bingel reaction using a malonate

Several malonate precursors have so-far been employed to carry out the Bingel reaction either on fullerenes or nanotubes.[4,5] Symmetric malonate derivatives are rather easy and quick to prepare as they can be obtained by simple esterification of malonyl chloride with an alcohol-terminating functionality, in the presence of a base. For the initial investigation on Bingel reaction, we designed a simple malonate precursor that can be prepared in few steps: we decided to use a bi-functional TEG chain, featuring at one terminus the hydroxyl group, and at the other a protected-amino group. Though TEG is a short chain, its hydrophilic character can enhance the nanotube water-dispersibility upon functionalization. Furthermore, the use of shorter ethylene glycol chains offers the advantage of minimizing the adsorption phenomena and facilitates the thorough removal of unreacted precursor by dialysis. We selected [(chloroethoxy)ethoxy]ethanol as starting material, which is a commercially available and not expensive compound. Firstly, the chlorine atom was substituted with phthalimide,[6] in order to introduce a terminal protected amine (Scheme 5.1). Secondly, the so-obtained phthalimide-TEG-alcohol was reacted with malonyl chloride in the presence of pyridine, reproducing a procedure reported for the preparation of a similar malonate.[7] Malonate derivative **2** was obtained in 53% yield and was then employed as precursor for the Bingel reaction.

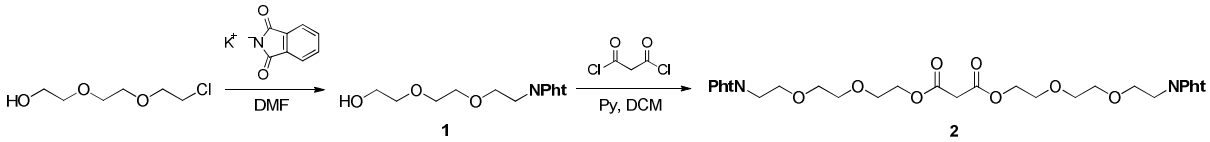

Scheme 5.1 Preparation of malonate derivative **2**.

For the preliminary assessment of the reactivity of the nanotubes provided by our collaborator toward both Bingel and nitrene reaction, we decided to perform all reactions on a batch of empty SWCNTs, whose preparation was faster and more affordable for our partner. The first trial of Bingel reaction on these tubes was carried out following the procedure reported by Imahori and co-workers.[8] A *o*-dichlorobenzene (ODCB) dispersion of SWCNTs was treated with malonate **2**, iodine and DBU, and reacted overnight at r.t. (Scheme 5.2). The work-up of the reaction consisted in several washing steps with different solvents, followed by dialysis against deionized H_2O to ensure removal of absorbed precursor. After cleavage of the phthalimide group by hydrazine, the amine loading calculated by Kaiser test was negligible, and this negative result was supported by TGA. The same reaction was then attempted at higher temperatures (80 and 120 °C), but the loading resulted either negligible or very low (Table 5.1). It is to be noticed that Imahori's attempts of Bingel reaction were not very successful with pristine and oxidized SWCNTs, while they worked efficiently on oxidized SWCNTs after functionalization with alkyl chains using an amidation reaction. Thus a non-optimal dispersion and individualization of CNTs in the solvent could possibly account for these negative results.

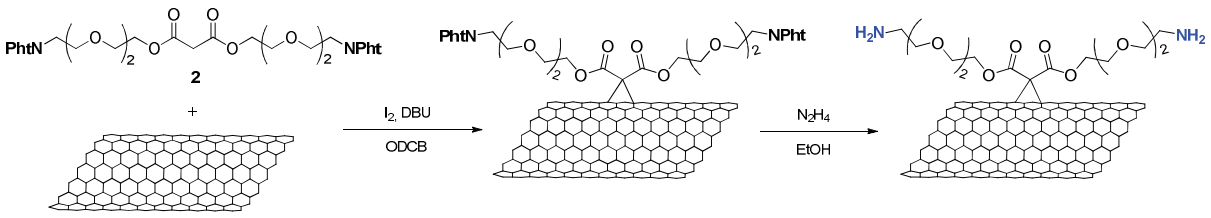

Scheme 5.2 Bingel reaction with malonate derivative **2**, followed by hydrazine-mediated phthalimide cleavage.

We then carried out the reaction substituting the iodine with CBr_4, according to the procedure employed by Ashcroft *et al.* on ultra-short pristine SWCNTs,[3] but the loading assessed by the Kaiser test and TGA was again very low, indicating no functionalization. A table summarizing the trials we attempted is presented below.

Entry	Reactants	Temperature	Time	K.T. loading (μmol/g)
1	I_2, DBU	r.t.	24 h	nd
2	I_2, DBU	80 °C	24 h	12
3	I_2, DBU	120 °C	24 h	20
4	CBr_4, DBU	r.t.	24 h	12

Table 5.1 List of the different reaction conditions employed to achieve the Bingel cyclopropanation of empty SWCNTs, and amine loading determined by Kaiser test (K.T.).

Raman spectroscopy was performed on some of these samples, to control whether the electronic structure of the graphenic network had been modified by the reaction, with re-hybridization of some carbon atoms from sp^2 into sp^3 and consequent variation of the D/G band intensity ratio (Figure 5.1). This technique also proved that the Bingel reaction was not successful.

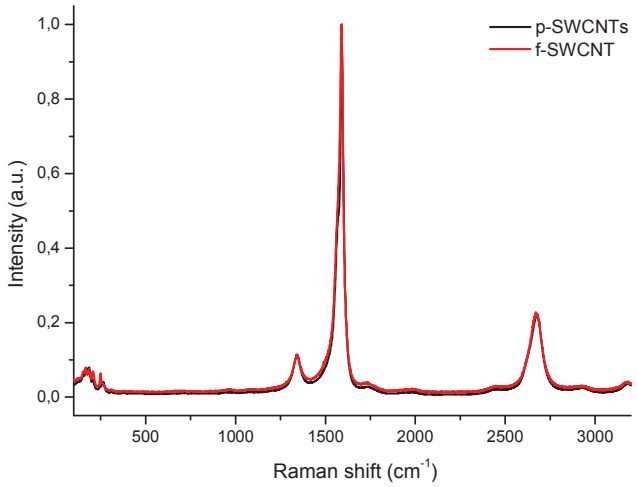

Figure 5.1 Raman spectra of SWCNTs before (p-SWCNTs) and after (f-SWCNTs) performing Bingel reaction at r.t. The spectra is the average of measurements on two areas, and values were normalized on the G band maximum value. No variation in the intensity of the D band can be noticed.

5.1.1.2 Second approach: Bingel reaction using a bromomalonate

We hypothesized that the employed malonate derivative could possibly be not very reactive and that the *in situ* formation of the halogenated intermediate may not have occurred. We therefore synthesized the bromomalonate and performed the Bingel reaction according to the procedure of Coleman and co-workers.[9] After a few attempts to halogenate malonate **2** in the α-position, the corresponding bromomalonate **3** was finally obtained by reaction of **2** with CBr_4 and DBU at -78 °C, under argon (Scheme 5.3).[10]

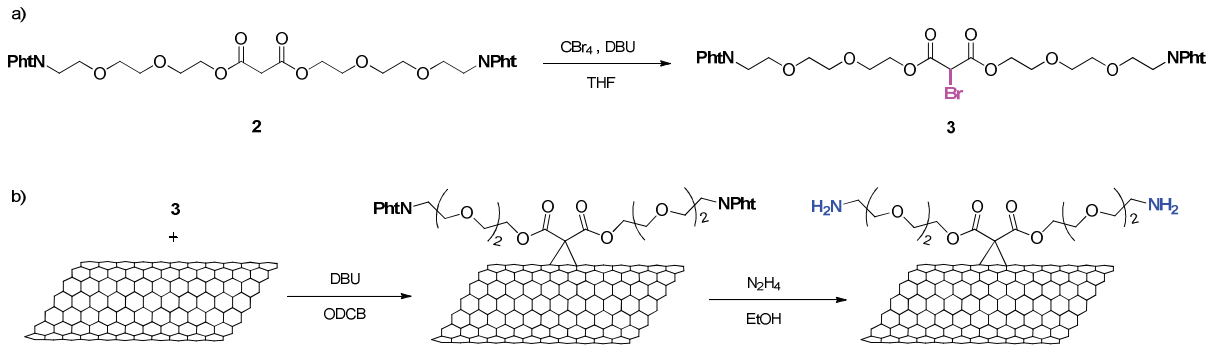

Scheme 5.3 a) Synthesis of bromomalonate precursor **3**; b) Bingel reaction followed by phthalimide cleavage.

Using bromomalonate **3** we performed the Bingel cyclopropanation and the following phthalimide cleavage on three pristine CNT samples (empty SW, $SmCl_3$@SW and empty MW), also exploring different reaction temperatures and times, but the different characterization techniques showed that no functionalization occurred (Table 5.2).

Entry	CNT type	Reactants	Temperature	Time	K.T. loading (μmol/g)
1	empty SWCNTs	DBU	80 °C	24 h	8
2	$SmCl_3$@SWCNTs	DBU	r.t.	18 h	nd
4	MWCNTs	DBU	r.t.	18 h	nd

Table 5.2 List of the different reaction conditions employed to achieve the Bingel cyclopropanation with malonate precursor **3**.

5.1.1.3 Third approach: microwave-assisted Bingel reaction

Imahori and co-workers reported that they could accomplish the functionalization of CNTs by Bingel reaction with good loading degrees by applying microwave irradiation instead of classical heating.[8] They performed the reaction at fixed temperature (120 °C) for 30 min, and observed that the loading degree was enhanced when using higher MW power. Their approach appeared interesting to us and was explored on our CNTs, in order to test whether the MW could improve the low reactivity toward the Bingel reaction. Indeed, many organic reactions, cycloadditions in particular, have shown improved yields when performed under microwave irradiation.[11,12] Furthermore, the very short reaction time reported by Imahori is valuable in the perspective of using functionalized CNTs as carriers of short half-life radioisotopes. However, we were primarily concerned by the effect of MW treatment on the structure of sealed CNTs, which would be the ones finally used for the purpose of the project. Would MW treatment

damage the structure of CNTs compromising the hermetic sealing? Can the internal filling leak out after MW treatment due to possible generation of holes? Our partner at ICMAB - CSIC carried out few experiments to address these questions: they irradiated $LuCl_3$@SWCNTs and $EuCl_3$@SWCNTs at 120 °C with 100 W power during 60 min and characterized the samples by TGA, elemental analysis, STEM and Raman spectroscopy. For both samples they observed that the encapsulated metal halide was preserved inside the nanotubes and there was no significant variation in the filling yield, nor in the amounts of defects (I_D/I_G ratio). Hence the microwave irradiation did not induce any leakage and the conditions used were therefore suitable for the functionalization of filled CNTs.

We thus investigated the Bingel reaction by MW irradiation employing malonate precursor **2** and following the protocol reported in Imahori's paper.[8] A dispersion of SWCNTs, malonate **2**, iodine and DBU in *N*-methylpyrrolidone (NMP) was irradiated with MW (60 W) at 120 °C for 30 min. The amine loading determined by Kaiser test after deprotection resulted to be 48 μmol/g, which, though higher than the previous results, it is considered still low. The thermogravimetric analysis of the sample after nitrene reaction (Pht-functionalized SWCNTs) shows a significant weight loss (18%) compared to that of the pristine SWCNTs, yet the TG curve of the sample after phthalimide cleavage does not significantly differ from the previous (Figure 5.2). Normally, after deprotection the weight loss of the amino-functionalized SWCNTs (SW-NH_2) is lower than that of the precursor (SW-Pht), due to the lower weight of the functional chain after the loss of phthalimide (see Figure 5.5 for example). This incongruence, together with the previous unsuccessful results, prompted us to speculate that the hydrazine employed in the deprotection step, could possibly interfere with the two ester groups causing their cleavage. To solve this doubt we thus decided to prepare a different malonate precursor featuring a Boc protecting group in place of the phthalimide one.

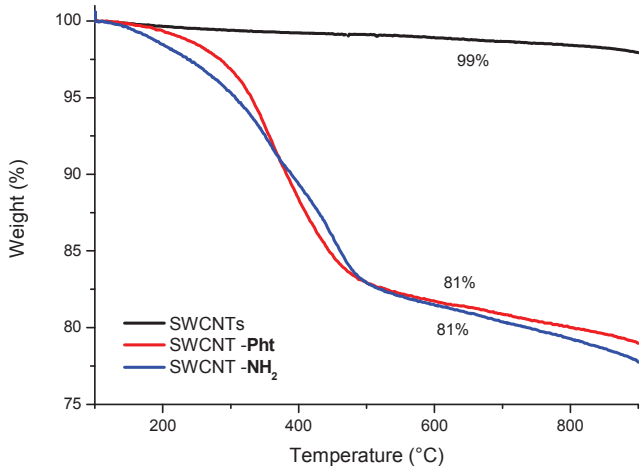

Figure 5.2 TG curves of pristine SWCNTs, phthalimide-functionalized SWCNTs and amino-functionalized SWCNTs.

5.1.1.4 Fourth approach: Bingel reaction using a Boc-protected malonate

Rather than deprotecting and reprotecting the amino group of compounds **1** or **2** (Scheme 5.1), we thought it more convenient to synthesize *ab initio* a new malonate precursor and, by a literature research, we selected a short and 'easy' synthetic strategy. The hydroxyl group of the previously-employed starting

material, [(chloroethoxy)ethoxy]ethanol, was readily converted into azide group by reaction with NaN_3 and catalytic amount of NaI and compound **4** was obtained in 81% yield without need of purification (Scheme 5.4).[13] The Boc protecting group was then inserted by copper-catalyzed click-reaction between the azido group of **4** and the alkyne of previously synthesized Boc-propargyl amine. This type of click reaction, also known as Huisgen 1,3-dipolar cycloaddition, results in the formation of 1,2,3-triazoles and it is particularly interesting because it works very efficiently in mild conditions and it is compatible with almost any functional group. We reacted together compound **4** and Boc-propargyl amine in a water-based solution, in the presence of $CuSO_4$ and sodium ascorbate, attaining compound **5**.[14] By double esterification of malonyl chloride, we finally obtained the desired malonate precursor for Bingel reaction (**6**).

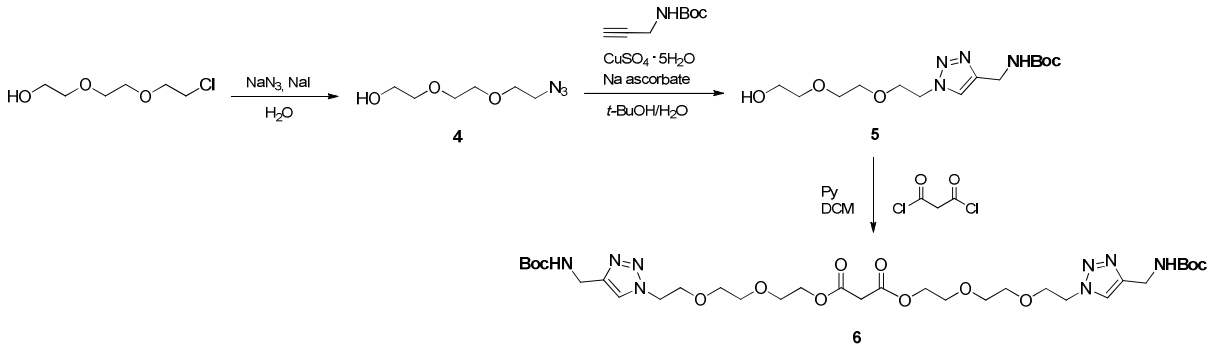

Scheme 5.4 Synthesis of Boc-protected malonate precursor **6**.

The Bingel reaction with precursor **6** was performed by the aid of MW irradiation, using three different power settings: 40, 50 and 60 W, as in the procedures reported by Imahori (Scheme 5.1).[8] After dialysis against water, the Boc protecting group was cleaved by treatment with HCl in dioxane, and the amine loading was assessed by the Kaiser test, but for all three samples the values were almost zero. Moreover, TGA performed before and after deprotection gave incongruent results, as the loading appears to be increased after the Boc cleavage. This could be eventually explained assuming that there might be some solvent absorbed on CNTs, although this phenomenon was never observed in the previous cases.

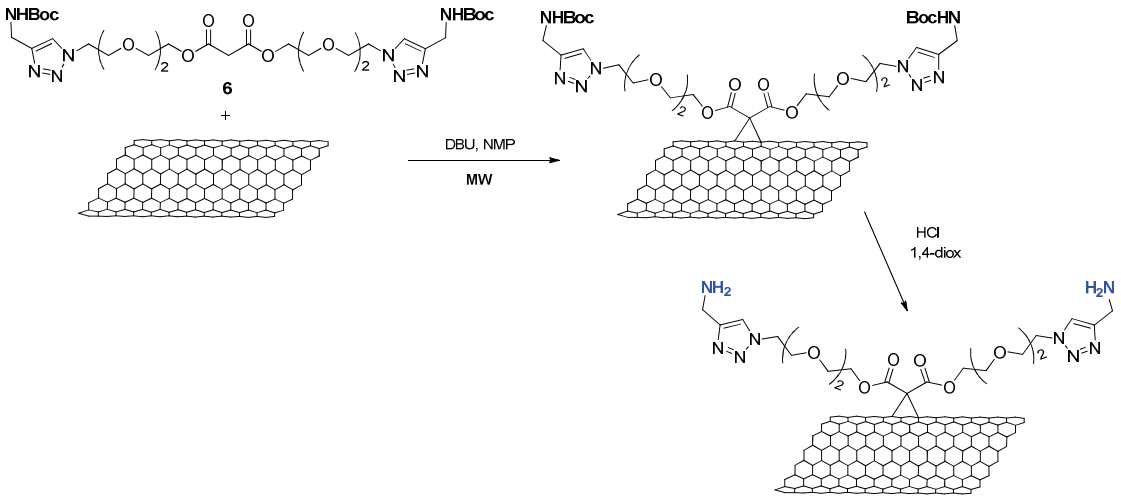

Scheme 5.5 Microwave-assisted Bingel reaction with malonate precursor **6**, followed by Boc cleavage.

5.1.2 CONCLUSIONS

We have accomplished the synthesis of three different malonate precursors (phthalimide-protected malonate and bromomalonate, and Boc-protected malonate), and investigated the Bingel reaction on a few types of pristine CNT trying different procedures and reaction conditions (time, temperature, MW, etc.). The samples were characterized by a combination of techniques (Kaiser test, TGA and Raman spectroscopy) but for all our attempts the degree of functionalization was very low or negligible. As during the course of these unsuccessful attempts, we were obtaining much more satisfying results with the functionalization by nitrene reaction, we focused our efforts toward the latter reaction.

5.2 NITRENE REACTION

Nitrenes are uncharged, electron deficient molecular species which can be considered as the nitrogen analogue of carbenes, where the nitrogen atom behaves like an electrophile. These reactive intermediates cannot be isolated and are formed *in situ* either by thermolysis or photolysis of azides (with N_2 extrusion), or from isocyanates (with CO extrusion).[15] The most commonly applied approach is to generate nitrenes from alkyl azides or azidocarbonates. The thermal or light induced extrusion of nitrogen results in the formation of single-state or triple-state nitrenes. The first types have two p-orbitals, each filled with two electrons, and they can either attack the nanotube sidewall in an electrophilic [2+1] cycloaddition or undergo a transition into a triple-state by inter-system crossing (ISC) (Scheme 5.6).[16] The triple-state nitrenes are biradicals and can therefore react with the π-system of the nanotubes. In both ways, aziridine rings are formed, with two carbon atoms belonging to the nanotubes, and one nitrogen atom from the azide.

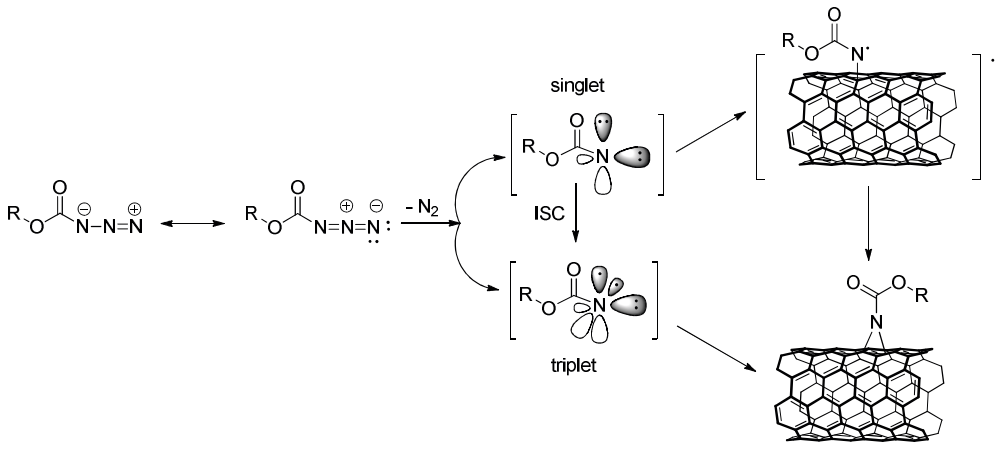

Scheme 5.6 Generation of nitrene species from azidocarbonate and possible pathways for the reaction with nanotubes forming aziridine rings: radical addition or electrophilic cycloaddition. Adapted from ref. [17].

The group of Hirsch has been among the first to explore the functionalization of SWCNTs with reactive species such as nitrenes, carbenes and radicals.[18] In 2003 they published a detailed study of nitrene

reaction onto CNTs by using a range of (R-)oxycarbonyl nitrenes generated from the corresponding azidocarbonates.[19] By this reaction approach the authors managed to covalently functionalize SWCNTs with different alkyl and aryl groups and proved the binding by means of multiple characterization techniques (AFM, XPS, TEM and UV-Vis), also remarking a significant improvement in the CNT dispersibility after reaction. Holzinger *et al*. employed some di-azidocarbonate precursors to achieve the cross-linking of SWCNTs.[17] Gao and co-workers reported a methodology for the large-scale production of *f*-CNTs by using nitrene chemistry, paving the way for its possible conversion at industrial scale.[20] In place of azidocarbonates, they performed the nitrene reaction starting from alkyl azides featuring different terminal groups (*i.e.* -OH, -NH_2, -COOH and -Br), demonstrating that different functional CNTs could be prepared by a one-step reaction. In another report, SWCNTs were successfully functionalized with nitrenes derived from *p*-toluensulfonyl, methylsulfonyl and trimethylsilyl azides.[21] Yet the authors reasoned that the interpretation of the type of bond formed upon reaction is not always straightforward, as nitrenes could react with aromatic moieties also in other ways than the expected [2+1] cycloaddition. Indeed, the formation of 5-membered rings (*i.e.* oxoazoles or triazoles) or of open 6,5-aza-annulenes have been reported in the case of fullerene,[22–25] while the possible rearrangement of aziridines cannot be excluded.[26,27] Finally, MW-assisted nitrene reactions have been reported to achieve the functionalization of carbon nanohorns (conical-shaped nanotubes) in a very short time,[28] representing a good alternative to the classical heating, also from the environmental point of view.

Despite the incertitude on the reaction mechanism and on the exact bonding after reaction, nitrene reaction still represents an interesting approach for the functionalization of CNTs, as good levels of loading have been reported with consequent increased dispersibility. Besides, by changing the alkyl substituent on the nitrogen atom, different organic functionalities can be tethered to the CNTs, allowing the further extension of the lateral chains with molecules of interest.

5.2.1 RESULTS AND DISCUSSION

The use of azidocarbonates as precursors of (R-)oxycarbonyl nitrenes is very common and is indeed the most reported strategy for the functionalization of CNTs.[17,19] However, the synthesis of azidocarbonates involves the preparation of a chlorocarbonate precursor from the reaction of the desired alcohol with phosgene (or its substitutes, diphosgene or triphosgene). Although this can be purchased in 'diluted' solutions (*e.g.* 20% w/w in toluene), it still remains a very toxic and hazardous compound, hence we preferred to avoid this strategy and perform the nitrene reaction with normal alkyl azides, which has been reported as well.[20] We started the synthesis of the azide precursor from the same starting material previously used for the preparation of the malonate derivatives. Indeed, the hydroxyl group of the previously synthesized compound **1** (Scheme 5.1) can be conveniently transformed into an azide by preliminary conversion into the corresponding tosylate. By following a reported procedure,[29] we accomplished the synthesis of compound **8**, which features the reacting azide group at one terminus, and a phthalimide-protected amino group at the other one (Scheme 5.7). We then used this precursor to perform our first trial of nitrene reaction on empty SWCNTs.

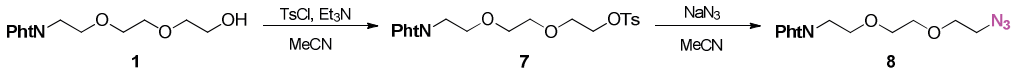

Scheme 5.7 Synthesis of the precursor for nitrene reaction by tosylation of compound **1** and subsequent azidation.

SWCNTs were dispersed in dry ODCB by sonication under inert atmosphere, and after addition of a 20-fold mass excess of azide **8**, the mixture was reacted at 160 °C for 18 hours (Scheme 5.8).[20] As nitrene reaction can proceed also by radical addition, it is important to ensure an inert atmosphere within the reaction vessels, to prevent the highly reactive species from reacting with oxygen.[30]

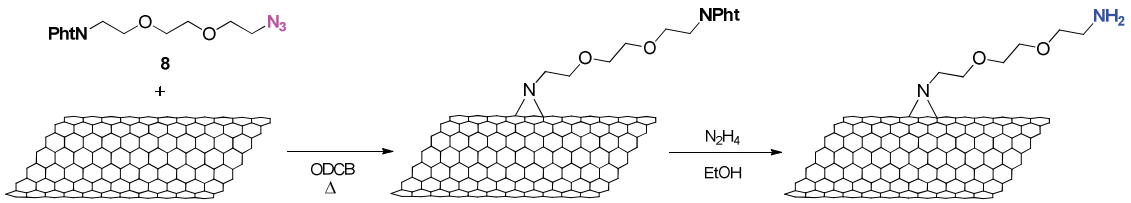

Scheme 5.8 Nitrene reaction on empty SWCNTs followed by phthalimide cleavage.

The nitrene reaction was followed by thorough washing steps, dialysis against ddH_2O (to remove the absorbed TEG chain), and finally the phthalimide protecting group was cleaved by hydrazine (Scheme 5.8). The amine loading determined by Kaiser test was 104 μmol/g, which was rather satisfactory. We then explored the reaction under the same conditions on different types of CNTs provided by our ICMAB partner (MWCNTs, $SmCl_3$@SWCNTs and $LuCl_3$@SWCNTs) to assess their reactivity. We could confirm, by both Kaiser test and TGA (Figure 5.3), that the nitrene reaction worked successfully for all CNT batches, with K.T. showing higher loadings for filled CNTs (Table 5.3). For the estimation of the degree of functionalization by TGA, we decided to take weight loss values at 650 °C, because up to 600 °C strong weight losses were still occurring. As also mentioned in other Chapters of this Thesis, there is a discrepancy between the loading obtained by Kaiser test and TGA due to the intrinsic difference between the two techniques.

Sample Name	p-CNTs	K.T. loading † (μmol/g)	TGA loading † (μmol/g)
9	SWCNTs –**B1**	104	246
10	MWCNTs	81	924
11	$SmCl_3$@SWCNTs –**B1**	204 (250)	801 (981)
12	$LuCl_3$@SWCNTs	179 (213)	683 (811)

Table 5.3 Functionalization loading determined by Kaiser test and TGA for nitrene reaction performed on different types of pristine CNTs (p-CNTs). † In parenthesis, loading values expressed as μmol/g of carbon, calculated on the basis of the filling yield. (Details on the specific CNT batch employed for each reactions are reported in Table 5.10 in the Annex. In the CNT name, **B1** indicates the employed batch).

In general, the loading values are expressed as μmol of organic function per gram of sample. However it is worth to remark that in filled CNTs the total carbon percentage is less than in empty CNTs, therefore the effective loading is higher. In Table 5.3, loadings expressed as μmol/g of carbon are shown in parenthesis for the filled CNTs for the sake of comparison, taking into account the filling yield of the specific CNT batch (see Table 5.10 for specifications). Remarkably, filled CNTs display higher degrees

of loading than empty CNTs. All experiments here presented were carried out considering the total sample weight, regardless of the atomic composition, and along the following discussion we will report the degrees of functionalization as μmol/g of sample (and not of carbon).

5.2.1.1 Microscopic visualization of functional groups

In order to have a further proof of the presence of free amines on the CNTs and of their availability for further derivatization, we decided to couple the amines with a tagging molecule featuring a heavy-element, which would enable atomic-scale detection by electron microscopy, in analogy with what was reported by our partners.[31,32] In their study, a 2,3,5-triiodophenyl motif was introduced on the nanotube sidewall functionalities as a substituent of the pyrrolidine ring generated by 1,3-dipolar cycloaddition. They were then able to detect the iodine tag along the CNTs by *Z*-contrast STEM imaging coupled with energy-dispersive X-ray spectroscopy (EDX). The principle of *Z*-contrast STEM is that the image is strongly dependent on the atomic number *Z* of the observed atoms, thus a heavy-element such as iodine will appear with higher contrast compared to the carbon background of the nanotubes. In addition, the EDX detector associated with the STEM allows to obtain the elemental composition of the imaged area, providing a further characterization proof.

We linked a 2,3,4-triiodophenyl motif to the free amine functions of CNTs **9**, **10**, **11** and **12** by EDC-assisted amidation with 2,3,4-triiodobenzoic acid (Scheme 5.9). Characterization of the new conjugates by Kaiser test proved that the amount of free amines sensibly decreased, meaning that most of the amino groups have reacted with the tagging molecule (Table 5.4), and that the tag is covalently attached to the CNTs. In addition, by comparing the reaction yield obtained by the Kaiser test values for the different types of nanotubes, we can conclude that there is no significant difference in the reactivity of the amino groups toward further functionalization.

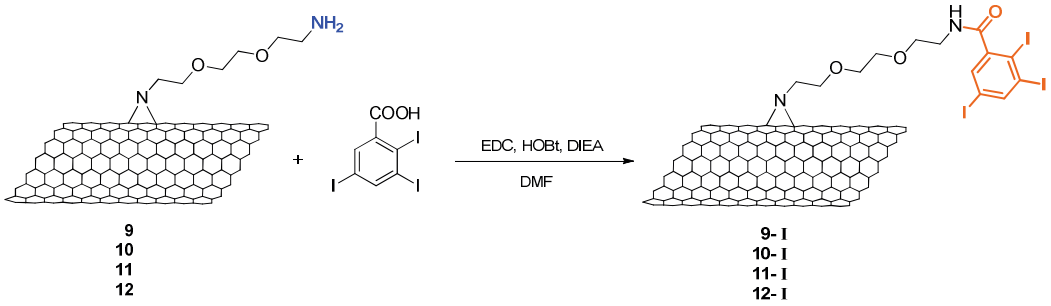

9
10
11
12

9- I
10- I
11- I
12- I

Scheme 5.9 Tagging of amino groups with the 2,3,4-triiodophenyl motif. CNT structure is representative of all types of pristine CNTs (empty, filled, SW and MW).

Sample name	p-CNTs	-NH_2 loading before tagging (μmol/g)	-NH_2 loading after tagging (μmol/g)	Conversion yield (%)
9	SWCNTs –**B1**	104	12	88
10	MWCNTs	81	17	79
11	$SmCl_3$@SWCNTs –**B1**	204	34	83
12	$LuCl_3$@SWCNTs	179	37	79

Table 5.4 Amine loading values obtained by K.T. before and after tagging by amidation, and conversion yield calculated as *(x-y)/x*100*, where *x* is the loading value before tagging, and *y* the value after tagging.

The functionalization was as well confirmed by TGA, comparing the thermogravimetric curves of the amino-functionalized CNTs (CNT-NH_2) with that of the tag-functionalized CNTs (CNT-I) (Figure 5.3). The weight loss corresponding to CNT-I is higher than that of CNT-NH_2, as expected, since there was an increase in molecular weight upon reaction. As examples, we report below the TG curves relative to $SmCl_3$@SWCNTs and $LuCl_3$@SWCNTs after the two functionalization steps. Similar profiles were obtained also for the other compounds.

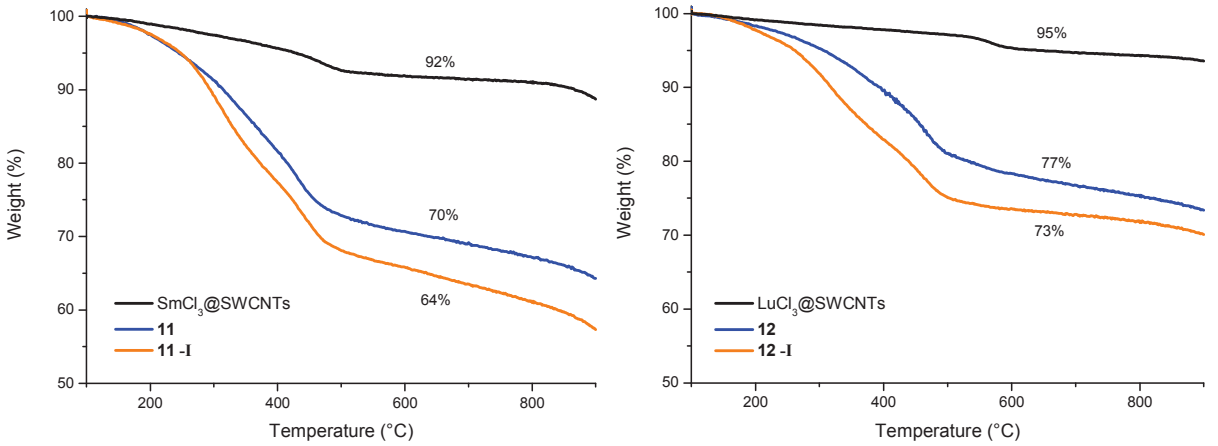

Figure 5.3 TG curves of pristine, amino-functionalized and tag-functionalized $SmCl_3$@SWCNTs (left) and $LuCl_3$@SWCNTs (right).

The obtained tag-functionalized CNTs were then characterized by high-resolution STEM and EDX by our partner at ICN 2 (Barcelona). By microscopy imaging of CNT-I, it was possible to visualize many randomly distributed bright dots along the CNT sidewalls, which were not observed in the amino-functionalized CNT precursors (Figure 5.4). These bright dots were attributed to the iodine atoms of the tag molecule, and the elemental analysis of specific imaged areas performed by EDX gave a further proof of the presence of iodine (Figure 5.4). The same results were observed for all set of samples (**9-12**), but, for simplicity, we report here only the images referred to compounds **12** and **12-I**. By STEM coupled with EDX it was possible to simultaneously detect the filling material (for samples **11** and **12**) and the iodine tag.

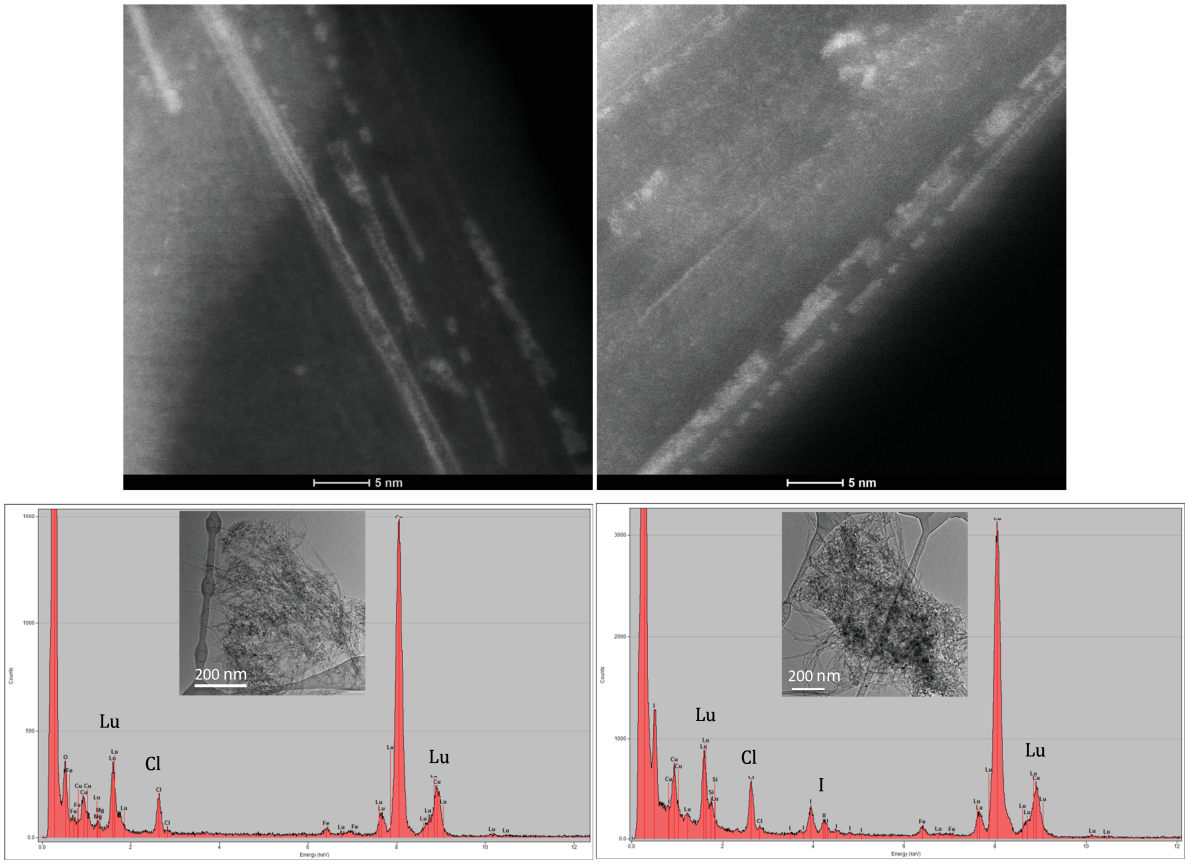

Figure 5.4 Simultaneous detection of filling and functionalization. (Top) *Z*-contrast STEM images of amino-functionalized $LuCl_3$@SWCNTs **12** (left) and tag-functionalized $LuCl_3$@SWCNTs **12-I** (right). The brightest rods correspond to the filling material, while the tiny bright dots on the right-side image are generated by the iodine atoms. (Bottom) EDX analysis of compounds **12** (left) and **12-I** (right), and STEM image of the analyzed area in the inset. Images collected by Elzbieta Pach and Dr. B. Ballesteros from ICN 2 (Barcelona).

5.2.1.2 Optimization studies

As explained in Chapter 4, one of the major commitments in the preparation of the final conjugates is the time required for all steps after irradiation. In fact, because of the short half-life of the radionuclide candidates, the synthetic steps leading to the injectable formulation should be as short as possible. To this purpose, we optimized the conditions to reduce the time of the nitrene reaction and the phthalimide deprotection. Besides, we have also worked on the optimization of the treatments to purify the samples after each step.

Optimization of nitrene reaction

In our first trials of nitrene cycloaddition, the reaction time was 18 hours. In the attempt to reduce the time while maintaining good degrees of functionalization, we carried out a screening study on empty SWCNTs by varying the solvent, the temperature, and the time of reaction (Table 5.5). The same work-up procedure (including dialysis against water) was used in each case. Reduction of the reaction time to

12 and 2 hours did not afford any functionalization (according to Kaiser test after phthalimide cleavage), whereas increasing the temperature to 200 and 220 °C resulted in considerable loadings with a reaction time of 12 hours. To draw these conclusions we relied on Kaiser test values, which gives an accurate image of the available functional groups introduced. The outputs of TGA were used to control the consistency of the data between the samples. In the case of sample **14** (160 °C, 12 h), we noticed a relevant incongruence between the low loading calculated by Kaiser test and the high value resulting from TGA. To check whether any side-reaction might occur due to the solvent or its adsorption on the tubes, we performed a blank reaction by sonicating SWCNTs in dry ODCB and heating at 160 °C for 18 h, but without adding the organic azide. The TGA of the resulting compound (after the usual work-up) presented a weight loss of 18% compared to the pristine SWCNTs, which was rather surprising and indicative of a relevant effect due to the sonication or heating of ODCB with the nanotubes. By a literature search, we found that indeed some groups already reported that ODCB (and other chlorinated solvents) can undergo decomposition and polymerization upon ultrasonication, resulting in irreversible chemical interactions with the CNTs, leading to a sort of doping.[33,34] These empirical observations cast a doubtful shadow on some reports on CNT functionalization, where long sonications (up to several hours) in ODCB have been carried out prior to reaction, to achieve good CNT dispersions.[17,19] To avoid these potential doping phenomenon, we decided to use NMP, which was as good as ODCB in dispersing pristine CNTs, and did not show adsorption onto the tubes, according to TGA after a blank reaction. Nitrene reaction performed in NMP at 200 °C for 12 hours afforded the highest degree of functionalization so far (sample **18** in Table 5.5). The degree of functionalization estimated by Kaiser test was 271 μmol/g, while the characterization by TGA showed data consistent with our expectations (Figure 5.5). Repetitions of the nitrene reaction on Sm-filled SWCNTs coming from the same batch of empty nanotubes, afforded an amine loading of 90 μmol/g (at 200 °C) or 146 μmol/g (at 190 °C) after Pht deprotection (compounds **19** and **20**). Although these results are lower than the analog reaction performed on empty SWCNTs (**18**), they are still satisfying, and prove that nitrene cycloaddition occurs rather efficiently on both empty and filled CNTs.

Sample Name	p-CNTs	Solvent	Temperature (°C)	Time (h)	K.T. loading † (μmol/g)	TGA loading † (μmol/g)
13	SWCNTs	ODCB	160	2	25	313
14	SWCNTs	ODCB	160	12	22	785
15	SWCNTs	ODCB	160	18	84	689
16	SWCNTs	ODCB	200	12	231	439
17	SWCNTs	ODCB	220	12	168	636
18	SWCNTs	NMP	200	12	271	930
19	$SmCl_3$@SWCNTs	NMP	200	12	90 (110)	618 (752)
20	$SmCl_3$@SWCNTs	NMP	190	12	146 (178)	731 (890)

Table 5.5 Functionalization loadings determined by K.T. and TGA for nitrene reaction performed on empty SWCNTs-**B2** and $SmCl_3$@SWCNTs-**B2**. †In parenthesis, loading values expressed as μmol/g of carbon, calculated on the basis of the specific filling yield. (Specification on the CNT batch employed for each reactions are reported in Table 5.10)

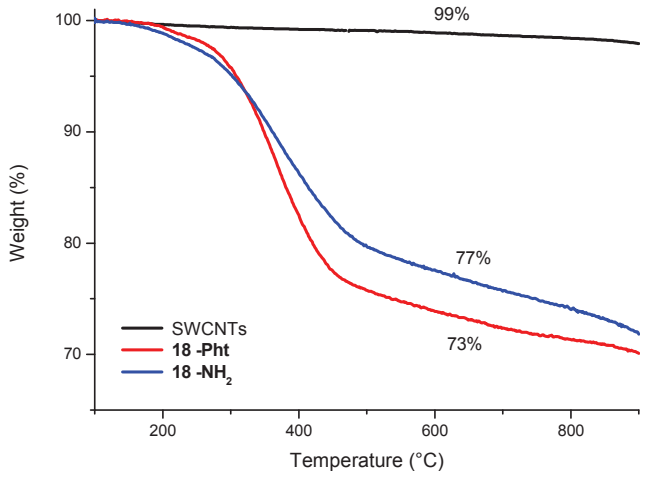

Figure 5.5 TG curves of pristine SWCNTs, phthalimide-functionalized SWCNT (**18-Pht**) and amine-functionalized SWCNTs (**18-NH_2**).

We then explored the nitrene reaction under MW irradiation. Karousis *et al.* have reported the MW-assisted functionalization of carbon nanohorns by nitrene cycloaddition, achieving good yields after 60 minutes of irradiation (100 W) at 220 °C.[28] Such short time of reaction would be very advantageous for our goals. We performed our first attempts of MW-assisted nitrene reaction on $SmCl_3$@SWCNTs trying two different reaction times: 60 and 30 minutes (**21** and **22** in Table 5.6), with NMP as a solvent. In both cases, the reaction occurred successfully, affording a higher loading for the longer time (60 min), although the degree of functionalization obtained with the 30 min reaction was already satisfying (Figure 5.6).

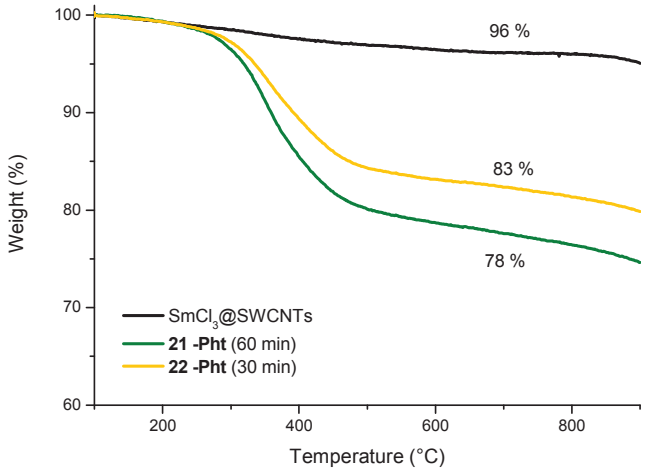

Figure 5.6 TG curves of $SmCl_3$@SWCNT-**B2**, phthalimide-functionalized CNTs **21** and **22** obtained by MW-assisted nitrene reaction with 60 and 30 min reaction time. Weight loss values taken at 650 °C.

For precaution we also performed a blank reaction, by irradiating in the same conditions a dispersion of pristine $SmCl_3$@SWCNTs without the azide, and observed by TGA only a minimal increase of weight loss. This suggests that no side-reaction was occurring, and also that there was no leakage of the filling material. We then carried out a short screening of the reaction conditions by performing the nitrene cycloaddition on empty SWCNTs under MW irradiation (Table 5.6). It is evident that both temperature

and time affect the reaction output, and that a duration of 30 min is sufficient to achieve sufficient degrees of functionalization. Hence, MW irradiation is a valuable option for the functionalization of filled CNTs.

Sample Name	p-CNTs	Temperature (°C)	Time (min)	K.T. loading † (μmol/g)	TGA loading †* (μmol/g)
21	$SmCl_3$@SWCNTs	220	60	135 (164)	654 (796)
22	$SmCl_3$@SWCNTs	220	30	104 (127)	487 (593)
23	SWCNTs	160	60	144	624
24	SWCNTs	180	60	92	604
25	SWCNTs	180	30	107	628
26	SWCNTs	220	60	199	517

Table 5.6 Functionalization loadings determined by K.T. and TGA for MW-assisted nitrene reactions performed on $SmCl_3$@SWCNT-**B2** and SWCNT-**B2**. Reactions were performed in dry NMP with an initial power of 100 W. †In parenthesis, loading values expressed as μmol/g of carbon, calculated on the basis of the filling yield. *Loadings calculated before Pht cleavage.

During the course of these investigations, our partner in Barcelona succeeded in preparing a batch of shorter SWCNTs filled with $LuCl_3$ ($LuCl_3$@SWCNT–**S**, where **S** stays for 'short'), featuring an average length of 530 nm (Table 5.10). It is commonly recognized that shorter nanotubes are more suitable for bioapplications, especially in drug delivery. After having proved the reactivity of this batch toward nitrene reaction, we carried out an optimization screening study on this type of CNTs (Table 5.7). For each time point, the experiment was repeated twice, to study the reproducibility of the reaction. The results show that the variability upon repetition is small, in agreement with what is typically found with CNTs. Upon reduction of the reaction time, the degree of functionalization did not vary linearly. The 2-hour reactions (**31** and **32**) afford a discrete degree of functionalization according to the Kaiser test, however, the 6-hour conditions was the best compromise between time and loadings.

Sample Name	Temperature (°C)	Time (h)	K.T. loading (μmol/g)	TGA loading* (μmol/g)
27	200	12	97	597
28	200	12	126	762
29	200	6	115	624
30	200	6	108	539
31	200	2	71	379
32	200	2	96	538
33	190	6	146	625

Table 5.7 Functionalization loadings determined by K.T. and TGA for nitrene reaction performed on $LuCl_3$@SWCNT-**S**. *Loadings calculated before cleavage.

Taking into account all screening experiments, we remarked that there are significant differences in the average loadings achieved with each batch of pristine CNTs, and that the optimal reaction conditions might be slightly different from one batch to the other. As a general conclusion, we observed that reactions performed at 200 °C for 12 hours usually afforded good degree of functionalization and that the

reaction time can in principle be reduced to 6 hours without decreasing much the final loading. We furthermore proved that microwaves are a valuable option for the functionalization of filled CNTs in very short times, and their employment with irradiated material would be advantageous to reduce the total preparation time.

Optimization of phthalimide cleavage

So far, the cleavage of the phthalimide protecting group has been carried out by stirring an ethanol dispersion of CNTs with 10% v/v hydrazine hydrate overnight. We explored the possibility to reduce the time necessary for an efficient deprotection by running the reaction for 2, 6 and 12 hours. The amine loading determined by Kaiser test was 146 μmol/g, 136 μmol/g and 149 μmol/g, respectively. These results evidenced that 2 hours are sufficient to achieve deprotection.

Optimization of work-up procedure

The work-up after nitrene reaction consists in filtration and washing in different solvents, with sonication steps of 10-15 minutes in a water bath. We investigated the possibility to avoid dialysis that we had so far performed after the nitrene reaction to remove the adsorbed TEG chain. Of two aliquots of Pht-functionalized short $LuCl_3$@SWCNTs, one was submitted to dialysis and the other not. Kaiser test after phthalimide deprotection gave a loading of 108 μmol/g for the dialyzed sample and 96 μmol/g for the non-dialyzed. This result suggests that dialysis is not fundamental, and thorough washing steps are sufficient to remove adsorbed organic compounds.

5.3 CONJUGATION OF A TARGETING ANTIBODY

Our biologist partner at KCL in London have been studying a tumor model that overexpresses epidermal growth factor receptor (EGFR). The EGFR is a plasma membrane receptor that regulates multiple cellular processes and it is overexpressed in many cancer types such as metastatic colorectal cancer and advanced squamous cell carcinoma of the head and neck.[35] Cetuximab (Erbitux®) is a chimeric monoclonal antibody (mAb) able to efficiently target and inhibit the EGFR. It has been approved for clinical use in the treatment of advanced chemo-refractory cancers such as colorectal cancer, non-small-cell lung cancer, head and neck cancer.[36–38] The conjugation of radionuclides to Cetuximab *via* metal chelation has been already investigated with the goal of enhancing its therapeutic efficacy and achieve simultaneous tumor diagnosis and treatment.[39] The anchoring of Cetuximab to CNTs has also been already reported[40–42] to provide targeting properties to CNTs used as carrier. However, to the best of our knowledge, no example of radioactivity delivery by means of Cetuximab-labeled CNTs has been ever reported. It seemed to us very interesting to exploit the high targeting efficiency of this mAb to direct our CNT radioactivity carrier to specific tumor tissues.

5.3.1 FIRST STRATEGY

In our group, small antibodies and proteins had been previously conjugated to CNTs by a maleimide linker (cf. Chapter 3 or ref. [43]). We thus designed a synthetic strategy to covalently tether Cetuximab onto amino-functionalized CNTs *via* a maleimide linker. We performed a scale-up of nitrene reaction on Sm-filled long SWCNTs and finally obtained $SmCl_3$@SWCNT-NH_2 (**34-NH_2**) with an amine loading of 293 μmol/g. A previously synthesized maleimide linker (*N*-succinimidyl 3-maleimidopropionate) was then coupled to the amino groups by amidation, affording conjugate **34-mal** (Scheme 5.10). By Kaiser test the amount of free amines was 65 μmol/g, which, by difference corresponds to a loading of maleimide of 228 μmol/g.

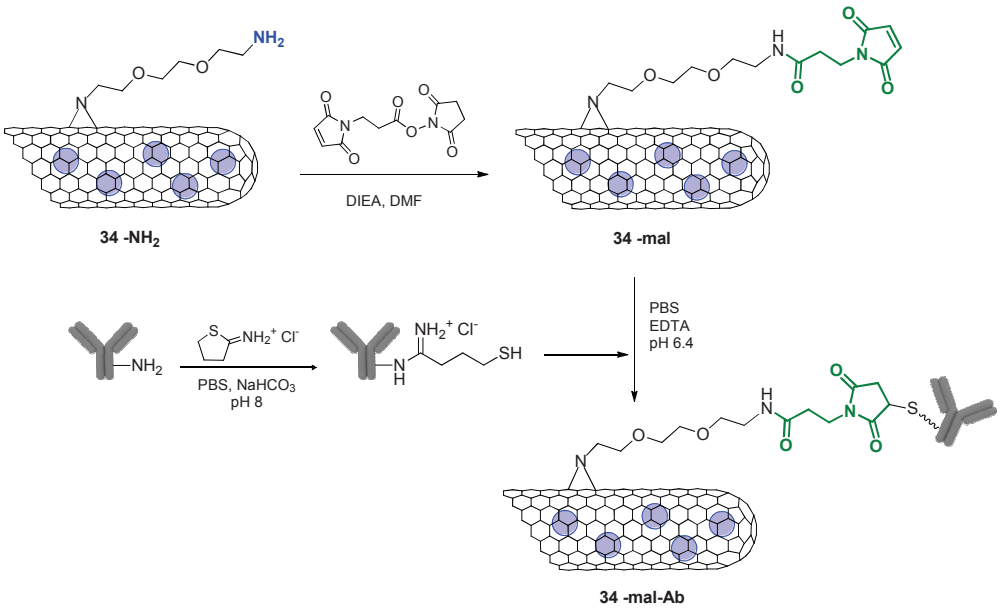

Scheme 5.10 Derivatization of amino-functionalized CNTs with the maleimide linker and subsequent coupling with thiolated Cetuximab.

The double bond of the maleimide is very reactive toward sulfhydryl groups, which are generally present in proteins in the form of cysteine disulfide bonds. However, for an efficient reaction the protein should display a certain number of free thiols, and these should be easily accessible. Because we did not know whether Cetuximab displayed any free and accessible thiol group, we decided to generate thiol moieties by derivatization of the amine residues with the commonly used Traut's reagent (2-iminothiolane) (Scheme 5.10).[44,45] The thiolated Cetuximab was then reacted with conjugate **34-mal** by shaking the two reagents for 1 h at r.t. After centrifugation and removal of the supernatant, the re-dispersed CNTs were thoroughly dialyzed to remove the adsorbed antibody. The final conjugate (**34-mal-Ab**) was characterized by TGA and gel electrophoresis (Figure 5.7). By comparing the thermographs of **34-mal-Ab** with that of the maleimide precursor we estimated the loading of Ab to be 44 mg/g, which is not very high. We performed gel electrophoresis of the compound under non-reducing and reducing conditions. Under reducing conditions, the addition of β-mercaptoethanol to the sample denatures the protein by reducing the disulfide bonds. In this way, the quaternary protein structure is broken and the subunits migrate independently through the gel. In non-reducing conditions the band of Cetuximab can be

visualized at the corresponding size position (ca. 150 kDa), while in reducing conditions bands of the protein fragments appear at ca. 55 and 36 kDa (Figure 5.7). For the CNT conjugate we could not detect the bands relative to the antibody under reducing conditions, although the amount of CNTs loaded in the well was relatively high (50 µg). This could be explained by the fact that the amount of Ab attached to the nanotubes was very low, and gel electrophoresis may not be sufficiently sensitive to allow the detection of the Ab at the employed concentration.

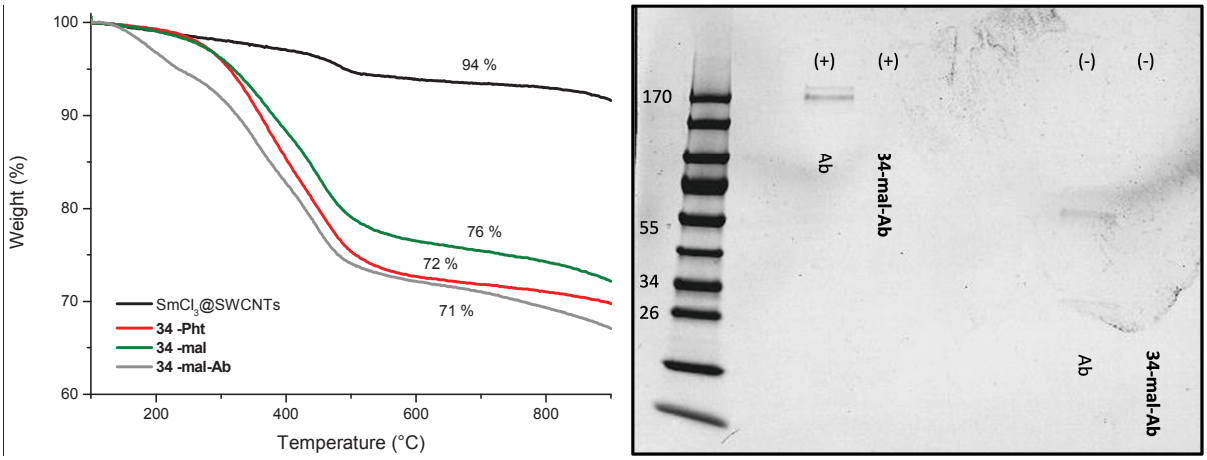

Figure 5.7 (Left) TG curves of pristine $SmCl_3$@SWCNT-**B3** and conjugates **34-Pht**, **34-mal** and **34-mal-Ab**. (Right) Gel electrophoresis of Cetuximab and **34-mal-Ab** run under non-reducing (+) and reducing conditions (-) at 150 kV. Gel stained with Coomassie blue. Protein size marker on lane 1 (size in kDa).

The causes of this low degree of functionalization could be attributed to the fact that the thiolation of Cetuximab was probably not very efficient, and only a low amount of thiol groups might have been introduced on the antibody. We decided to discard this strategy and study a different approach to append Cetuximab onto the CNTs.

5.3.2 SECOND STRATEGY

In a recent report, Bonifazi and co-workers succeeded in conjugating Cetuximab to functionalized MWCNTs by EDC-assisted amidation between carboxylic groups on the antibody and amino groups present on the CNTs.[40] Molecular dynamics simulations of the structure of Cetuximab also revealed that 40% of carboxylic acids are buried in the mAb's tertiary structure, while the remaining 60% is homogenously distributed on the outer surface and therefore potentially reactive toward amidation reactions with amines. As our functionalized CNTs do also display free amino groups on the sidewalls, we decided to adopt their protocol to anchor Cetuximab directly by its carboxylic groups. Besides, this approach would allow to achieve the final conjugate with one step less compared to our first strategy. The previously synthesized amino-functionalized $SmCl_3$@SWCNTs **19-NH_2** (amine loading of 90 µmol/g) were incubated for 24 h with Cetuximab in the presence of EDC and sulfo-NHS (NHSS) in buffer conditions (Scheme 5.11Scheme 5.1). Since proteins can have a strong affinity for CNTs, we carried out a control reaction to check if non-covalent immobilization of the antibody also occurred. Conjugate

19-NH_2 was mixed with Cetuximab in the absence of coupling reagents (Scheme 5.11), under the same conditions of the covalent reaction.

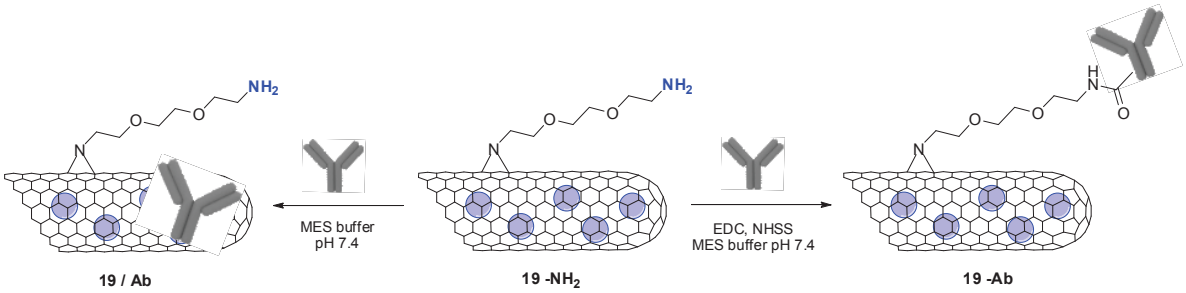

Scheme 5.11 Covalent derivatization of **19-NH_2** with Cetuximab (**19-Ab**) and control reaction in the absence of coupling reagents (**19/Ab**).

By comparing the weight loss of **19-Ab** (obtained by covalent amidation) with that of **19-NH_2**, we estimated that the loading of antibody on CNTs was 250 mg/g, which is sensibly higher than that obtained in the previous approach (Figure 5.8). However, the TG curve of the non-covalent conjugate (**19/Ab**) also displayed a significant weight loss (20% over **19-NH_2**), which corresponds to a loading of mAb of 200 mg/g. This result suggests that a non-negligible amount of antibody was absorbed on the CNTs and was not removed despite the thorough washing and dialysis steps. To further quantify the concentration of Cetuximab in the covalent conjugate, we performed bicinchoninic acid (BCA) protein assay, which is a very sensitive colorimetric assay commonly employed for the quantification of proteins.[46] This test is based on the reduction of copper (II) ions by the amino acid residues and consequent formation of a colored chelate complex with bicinchoninic acid. The amount of Cu^{2+} reduced is proportional to the amount of protein present in the solution. The concentration of Cetuximab on **19-Ab** determined by BCA was124 mg/g of samples. As well as for TGA, in this result the contribution of non-covalently attached Ab cannot be excluded.

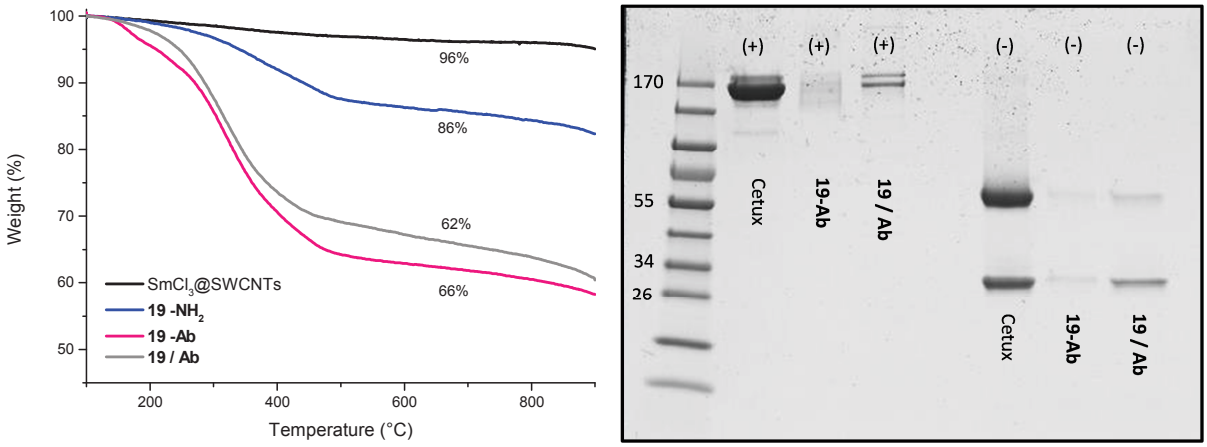

Figure 5.8 (Left) TG curves of pristine $SmCl_3$@SWCNTs-**B2** and conjugates **19-NH_2**, **19-Ab** and **19/Ab**. (Right) Gel electrophoresis of Cetuximab, **19-Ab** and **19/Ab** run under non-reducing (+) and reducing conditions (-) at 150 keV. Gel stained with Coomassie blue. Protein size marker on lane 1 (size in kDa).

The mAb immobilization was then evaluated by gel electrophoresis for both **19-Ab** and **19/Ab** under non-reducing and reducing conditions (Figure 5.8). In non-reducing conditions, for the non-covalent conjugate **19/Ab** the band of the unbound Cetuximab is clearly visible at the corresponding size position (150 kDa). Whereas, for the covalent conjugate (**19-Ab**), we can only see a shadow in correspondence to the mAb position. This suggests that most of Cetuximab is covalently bound to the CNTs, although the presence of a small amount of non-conjugated mAb cannot be excluded. Under reducing conditions, the breakage of the antibody structure into heavy and light chains results in two bands at ca. 25 and 50 kDa. These are visible for the non-covalent conjugate (**19/Ab**), while they are barely detectable for **19-Ab**. Considering TGA and BCA loading values, we would have expected to see more intense bands for compound **19-Ab** under reducing conditions. We can speculate that either the reduction operated by β-mercaptoethanol was not very efficient, or that the part of mAb covalently attached to the CNTs is not released upon reduction and is therefore not migrating.

5.3.2.1 Immunostaining

We further characterized the antibody-CNT conjugates by electron microscopy, performing an immunostaining with a secondary antibody conjugated with gold nanoparticles (AuNPs). This experiment has the double goal of allowing to visualize the Cetuximab attached to the CNTs and to prove its ability to recognize a specific anti-antibody. The antibody-functionalized conjugate **19-Ab** and the control reaction **19/Ab** were stained with an anti-human IgG linked with colloidal AuNP (15 nm diameter), able to recognize Cetuximab (a human IgG). As a further control, the same samples were separately stained with an anti-rabbit IgG/AuNP (15 nm), which instead is not specific toward human IgGs. By TEM imaging of **19-Ab** stained with anti-human IgG/AuNP, a multitude of black dots corresponding to the AuNPs were visible all along the CNTs (Figure 5.9). In the dark-field STEM images it is possible to distinctly recognize both the AuNPs as bright big dots, and the samarium-filling. Almost no AuNP are visible in the images corresponding to **19-Ab** incubated with the anti-rabbit IgG, proving that there is no unspecific binding between this secondary antibody and Cetuximab, neither adsorption of the IgG onto the CNTs. Interestingly, for the non-covalent conjugate (**19/Ab**) we did not observe any specific labeling of the secondary anti-human IgG, as if no adsorbed Cetuximab was present on the CNTs (Figure 5.9). Further characterization of **19-Ab** stained with anti-human IgG was performed by EDX analysis and EDX elemental mapping, confirming the presence of both Au and Sm, and their location in the analyzed area (Figure 5.10). By this immunostaining experiment we could therefore prove that Cetuximab was efficiently immobilized on the Sm-filled CNTs and that its affinity toward an appropriate secondary antibody was preserved upon conjugation.

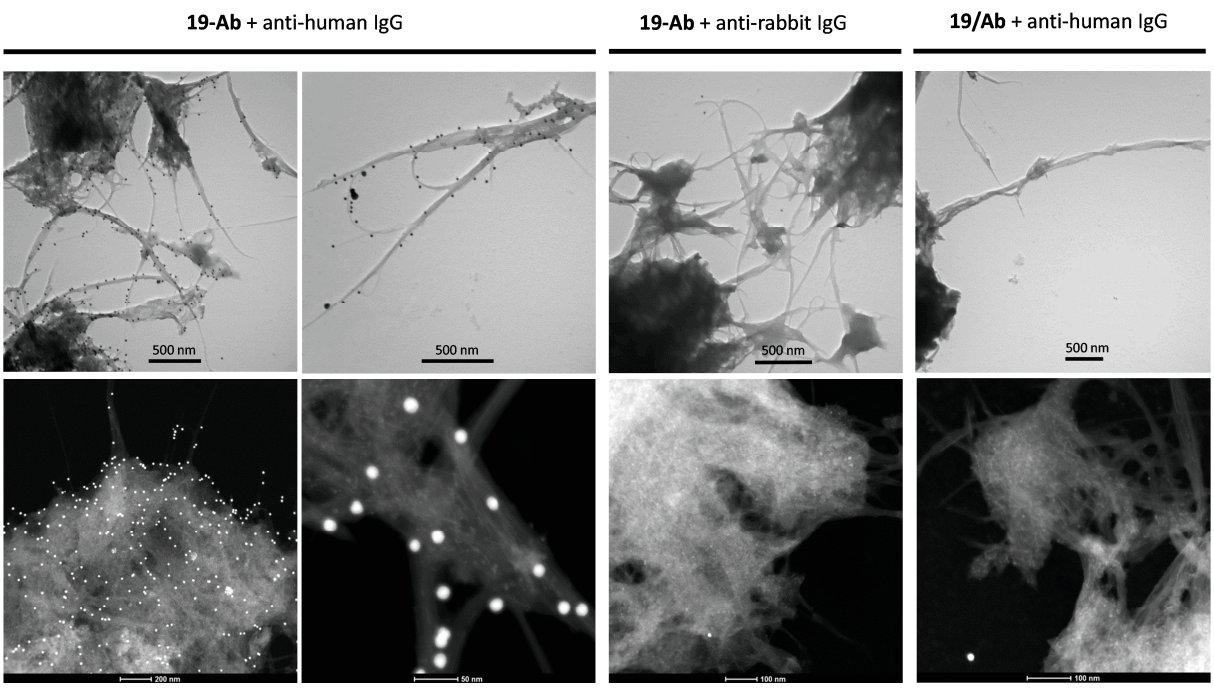

Figure 5.9 TEM images (top raw) and dark-field STEM images (bottom raw) of conjugate **19-Ab** after staining with anti-human and anti-rabbit IgG/AuNP, and of conjugate **19/Ab** after staining with anti-human IgG/AuNP. STEM images were collected by Elzbieta Pach and Dr. B. Ballesteros from ICN 2 (Barcelona).

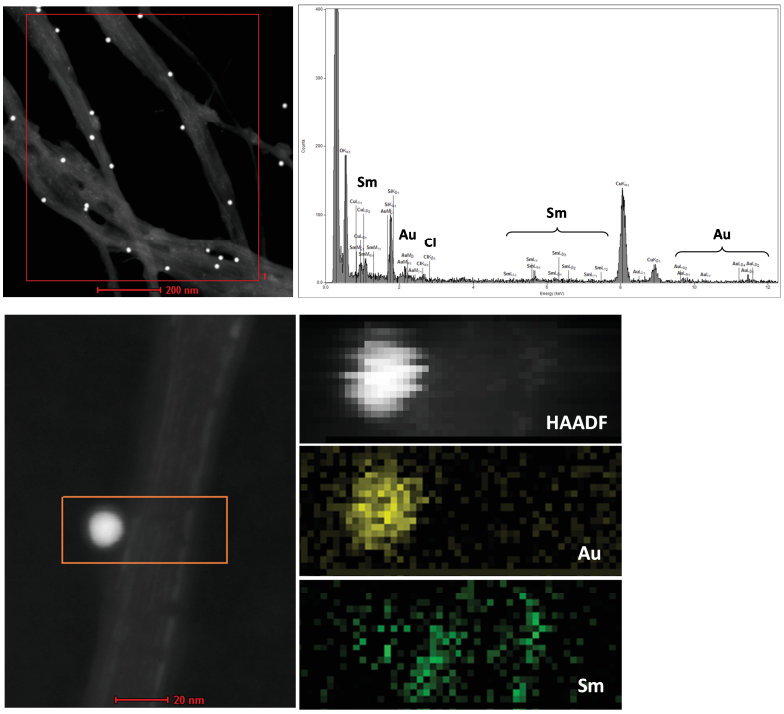

Figure 5.10 Dark-field STEM images of conjugate **19-Ab** after staining with anti-human IgG/AuNP. (Top) EDX analysis of the area in the red rectangle. (Bottom) STEM HAADF image, Au and Sm mapping of the area in the orange rectangle by EDX. Images and analysis collected by Elzbieta Pach and Dr. B. Ballesteros from ICN 2 (Barcelona).

5.3.2.2 Biological evaluation

The synthesized CNT-Ab conjugate was then tested *in vitro* and *in vivo* by Dr. Aritz Pérez from our group. To achieve a comparative view of the biological profile of the conjugate **19-Ab**, we also tested the non-covalent conjugate **19/Ab**, the amino-functionalized precursor **19-NH$_2$**, and a sample of empty amino-functionalized SWCNTs (**9-NH$_2$**) obtained by nitrene reaction. The latter sample was employed in the experiments to verify whether empty and filled SWCNTs displayed a different behavior. A number of experiments have been carried out to assess the toxicological profile, biocompatibility, uptake and targeting ability of the CNT conjugates. However, herein we will only describe the most relevant experiments and discuss the obtained results.

Cell viability and pro-inflammatory response

We first investigated the cytotoxicity of the synthesized compounds on RAW264.7 cells, which correspond to a cell line of murine macrophages. Macrophages are involved in the immune response and thus the employment of this type of cells allows to study both the cytotoxic effects and the inflammatory response that could be caused by CNTs. RAW264.7 cells were treated with the CNT conjugates at different concentrations and after 24 hours of incubation, the number of viable cells was calculated by flow cytometry. From Figure 5.11 we can see a significant decrease of cell viability only for **19/Ab** at high concentrations. Nevertheless, the percentage of viable cells remains around 70%.

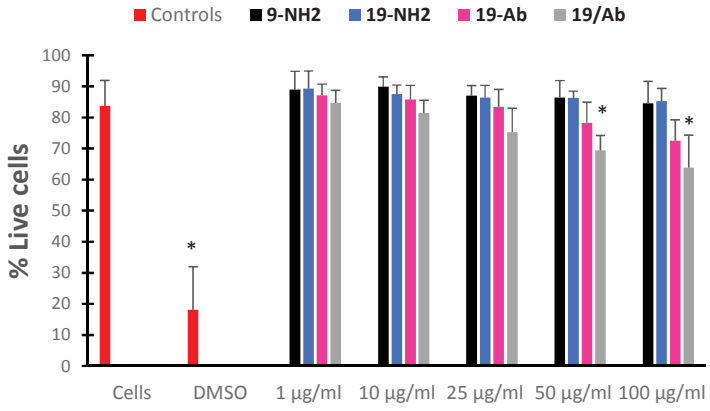

Figure 5.11 Cell viability after 24 hour incubation with **9-NH$_2$**, **19-NH$_2$**, **19-Ab** and **19/Ab** at different concentrations (1, 10, 25, 50 and 100 µg/ml). Red bars represent the positive (non-treated cells) and negative (DMSO 20%) controls. Error bars for standard deviation (n=4). *p < 0.05 with respect to non-treated cells.

Furthermore, the levels of interleukin-6 (IL6) and TNFα present in the cell supernatant were determined to evaluate the inflammatory response. IL6 and TNFα are two cytokines whose secretion is enhanced during cell activation for an immune response. In Figure 5.12 we can observe relevant levels of cytokines for cell treated with high concentration of the CNT-Ab conjugates (covalent and non-covalent), compared to untreated cells and amino-functionalized CNTs. This suggests that the two compounds probably trigger an acute immune response. Nevertheless, the amount of cytokines for **19-Ab** and **19/Ab** is considerably lower than that in the positive control.

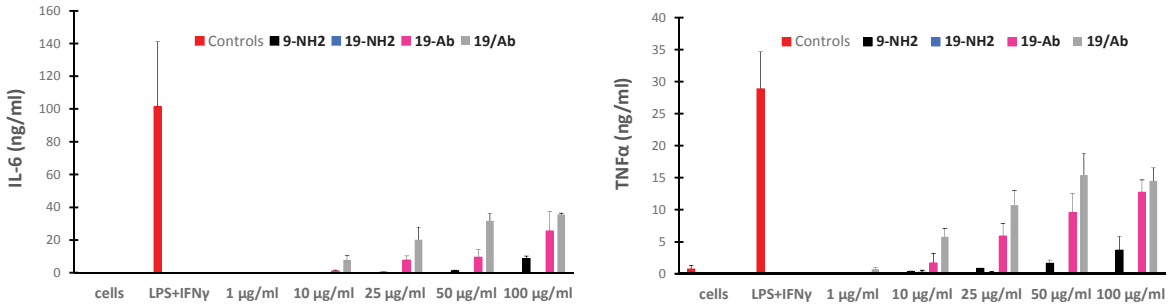

Figure 5.12 Graphs representing the amount of IL6 (left) and TNFα (right) produced by RAW264.7 cells after 24 hour incubation with **9-NH$_2$**, **19-NH$_2$**, **19-Ab** and **19/Ab** at different concentrations (1, 10, 25, 50 and 100 μg/ml). Red bars represent the positive (non-treated cells) and negative (LPS+IFNγ) controls. Error bars for standard deviation (n=4). *p < 0.05 with respect to non-treated cells.

Both cell viability and cytokine measurements demonstrate the absence of remarkable toxic effects caused by the CNT samples toward RAW264.7 macrophages. A slight increase of the cytotoxicity could be observed at high concentrations only for the conjugates presenting the antibody. However, the behavior of the Ab-conjugates (**19-Ab**, **19/Ab**) does not differ much from that of the amino-functionalized CNTs (empty or filled).

These compounds were also tested in human peripheral blood mononuclear cells (PBMC), affording similar outcomes (data not shown). Furthermore, a group of mice was injected with 150 μg of either **19-NH$_2$**, **19-Ab** or **19/Ab**. In every case, no acute immune response (1, 7 or 13 days after injection) was observed, demonstrating the biocompatibility of our functionalized CNTs also *in vivo* (data not shown).

Uptake and binding: evaluation by flow cytometry

As previously mentioned, Cetuximab can target the EGFR which is overexpressed by many cancer cells. In order to verify the ability of **19-Ab** to effectively target the EGFR and be taken up by the cells, we tested it on two different cell lines: U87 glioblastoma cells overexpressing the EGFR (U87-EGFR+) and CHO (Chinese hamster ovary) cells, which do not express EGFR. As the CHO cells do not exhibit the EGFR, they are intended to work as a negative control for the targeting, and they should therefore not internalize the Ab-CNTs. Both type of cells were separately incubated with **19-Ab**, **19/Ab** and **19-NH$_2$** for 1, 3 and 24 hours. Afterwards, the cells were incubated with a secondary anti-human IgG labeled with Cy3 and specific toward Cetuximab. This allowed the assessment of the uptake by flow cytometry. From the obtained results (Figure 5.13), it is clear that no uptake occurred in CHO cells, whereas the U87 cells were able to internalize Cetuximab alone and both Ab-CNT conjugates (covalent and non-covalent), even after 1 h incubation. Looking at the percentages for the U87 cells, we can see that almost the totality of the cells have taken up nanotubes. For the CHO cells instead, the amount of cells that internalized the different tested CNTs is below 10%. Furthermore, no internalization of the amino-functionalized CNTs (**19-NH$_2$**) was observed, highlighting the targeting efficiency provided by the presence of Cetuximab onto CNTs. Both the absence of internalization of **19-NH$_2$** and the low uptake levels in CHO cells demonstrate the ability of the Cetuximab-functionalized CNTs to specifically bind and target cells that overexpress the EGFR.

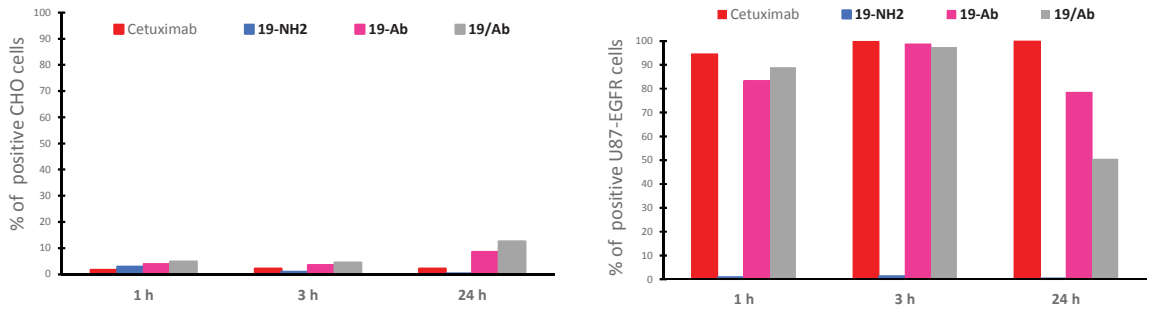

Figure 5.13 Bars represent the % of Cy3 positive cells in CHO cell line (left) or U87 cells (right) after the treatment for 1, 3 or 24 hours with each of the CNTs tested (**19-NH_2**, **19-Ab** and **19/Ab)** at 10 µg/ml.

From the same experiment, it was also possible to assess the mean fluorescence intensity in U87 cells, which is representative of the number of CNTs that were internalized by each cell (Figure 5.14). This quantification is an indirect estimation of the amount of compound inside one cell. While the graphs in Figure 5.13 shows the number of cells that internalized nanotubes, Figure 5.14 indicates how many CNTs have been internalized by one cell. The more the band is shifted to the right, the higher the mean fluorescence within the cell, and thus the internalized compound.

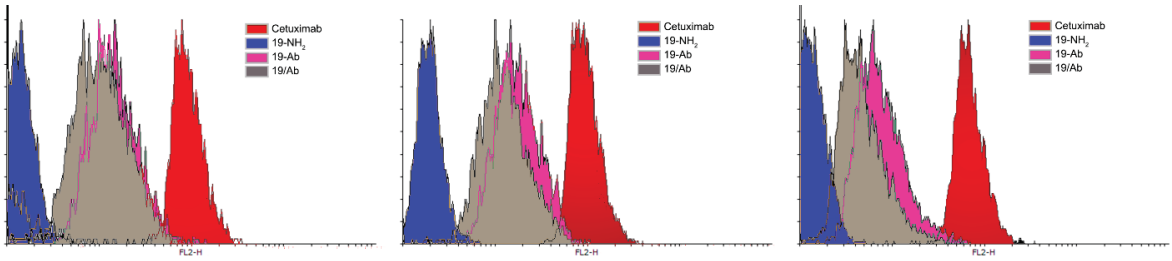

Figure 5.14 Histograms representing the mean fluorescence intensity in U87 cells after incubation with 10 µg/ml CNTs (**19-NH_2**, **19-Ab** and **19/Ab**) or 2.5 µg/ml of Cetuximab for 1 (left), 3 (middle) and 24 hours (right).

Also in this case, we can remark a strong difference between **19-NH_2** and the Ab-conjugates, **19-Ab** and **19/Ab**. Only a small difference can be observed between the covalent and non-covalent conjugates for longer incubation time. After 24 hour incubation, the band of **19-Ab** appears shifted to the right, signifying that its internalization is slightly enhanced compared to **19/Ab**. These results are in agreement with the previous ones, showing a good level of internalization of both **19-Ab** and **19/Ab**. The level of uptake is almost equal for the two conjugates, suggesting that the amount of antibody attached to the CNTs (either covalently or not) is similar, which is in agreement with the TGA results. The precursor conjugate devoid of Cetuximab (**19-NH_2**) is instead not internalized, as expected.

Uptake and binding: evaluation by elemental analysis

Considering that the synthesized conjugates are filled with metal ions (samarium), we exploited inductively coupled plasma atomic emission spectrometry (ICP-AES) to get a further proof of the CNT uptake by the cells. By this technique it is in fact possible to determine the samarium content in a given sample, which is an indirect measurement of the extent of CNTs that have been internalized. By

comparison of the samarium content found in CHO and U87 cells after 24 hour incubation with **19-Ab**, we can affirm that the uptake of nanotubes was higher in the case of U87 cells (Table 5.8). A certain amount of Sm was found also in the CHO cells, suggesting that a small degree of non-specific uptake occurred. However, the values of Sm content per cell clearly highlight that U87 cells were more efficient in internalizing the CNTs, proving the targeting ability conferred by Cetuximab. These outputs confirm once more the results obtained by flow cytometry and show the targeting efficiency of the synthesized conjugates.

Cell line	**Entry**	**Sm** (pg/cell)
CHO	Ø	< 0.10
CHO	**19-Ab**	1.59 ± 0.04
U87	Ø	< 0.10
U87	**19-Ab**	5.60 ± 0.08

Table 5.8 ICP-AES results indicating the Sm content in CHO and U87 cells after incubation for 24 hours with **19-Ab** (25 µg/ml) or without (Ø for untreated cells).

5.3.3 FLUORESCENCE LABELING

To further investigate the interactions of CNTs with cells and assess the internalization mechanism, we decided to derivatize the amino-functionalized CNTs with a fluorescent tag, such as cyanine 5 (Cy5) and fluorescein isothiocyanate (FITC). By amidation reaction of CNTs **20-NH$_2$** we prepared two different fluorescently-labeled conjugates: **20-Cy5** and **20-FITC** (Scheme 5.1).

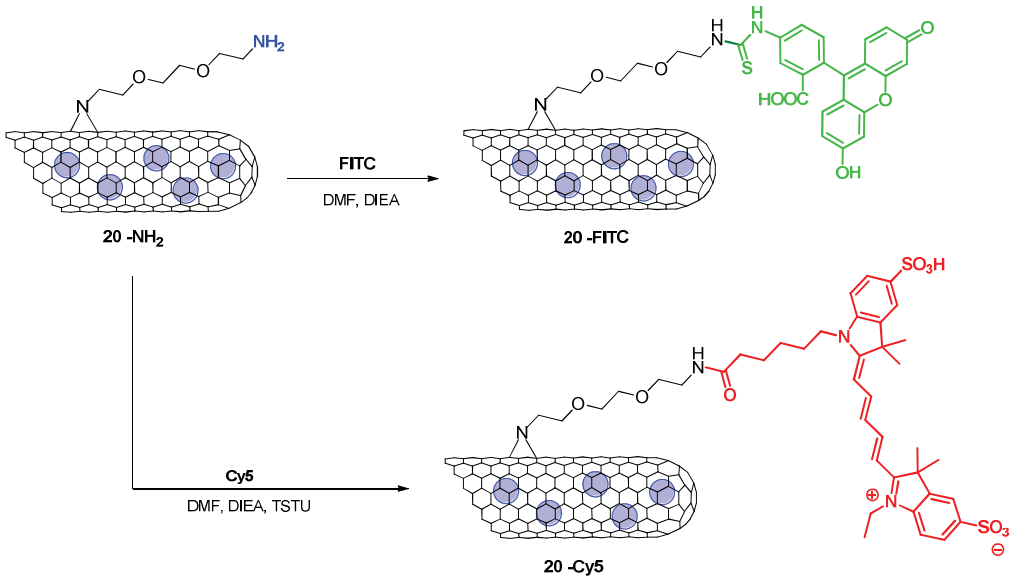

Scheme 5.12 Labeling of **20-NH$_2$** with Cy5 (left) and with FITC (right).

The carboxylic group of Cy5 was preliminarily activated with *N,N,N′,N′*-tetramethyl(succinimido) uronium tetrafluoroborate (TSTU), in the presence of DIEA to form the corresponding NHS.[47] The coupling of Cy5-NHS with the amino group onto CNTs was then performed *in situ*. The reaction between the isothiocyanate of FITC and the amino groups of **20-NH$_2$** occurred instead without addition of coupling reagents. By comparison with the precursor, the loading of dye determined by Kaiser test was 109 μmol/g for **20-Cy5** and 102 μmol/g for **20-FITC**, while the weight increase estimated by TGA corresponded to a dye loading of 71 μmol/g and 87 μmol/g, respectively (Figure 5.15). The results obtained by Kaiser test and TGA were in good agreement. It is worth to note that both reactions afforded a similar loading of fluorescent dye.

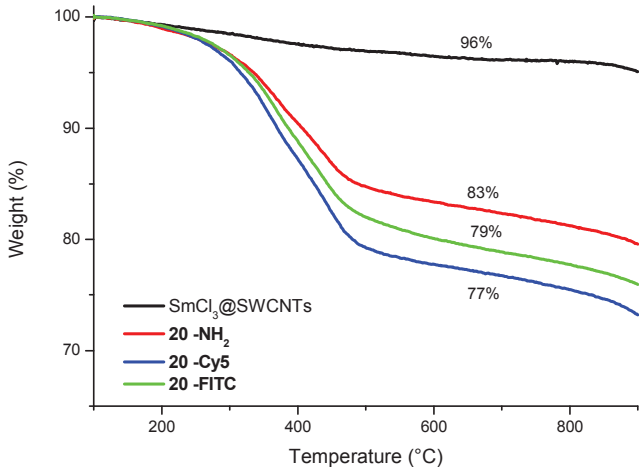

Figure 5.15 TG curves of pristine $SmCl_3$@SWCNTs and conjugates **20-NH$_2$**, **20-Cy5** and **20-FITC**.

After excitation at the specific wavelengths (620 nm for Cy5, 470 nm for FITC), the conjugates showed an intense fluorescence emission (data not shown). Nevertheless, upon incubation of the two conjugates with cells, it was not possible to clearly detect fluorescence in the cells, even using high concentrations of CNTs. We hypothesized that, despite being the CNTs fluorescently labeled, the total amount of dye was not sufficient to detect their fluorescence *in vitro*. Another hypothesis is that fluorescence quenching may occur due to aggregation of the CNTs in the cellular media, or due to charge transfer between the dye and the CNTs.

To increase the loading of dye on the CNTs and prevent the quenching, we designed a different strategy based on the conjugation of a labeled antibody onto the CNTs. Antibodies are in fact commonly labeled with fluorescent molecules to study their behavior *in vitro* and *in vivo*. Usually, proteins are labeled with fluorophores by amidation between the primary amino groups of the amino acid residues and the NHS-ester of the fluorophore.[48] By attaching the dye to the amine groups of Cetuximab and then tethering the labeled Cetuximab to the CNTs *via* the carboxylic groups, we can exploit non-competing binding sites of the antibody and in principle multiply the amount of fluorescent probes on the CNTs. With this strategy, we could moreover mimic the previously synthesized Ab-conjugate and further assess its biological profile. After pre-activation of Cy5 to introduce the reactive NHS-ester, we accomplished the labeling of Cetuximab with Cy5 by coupling reaction (Scheme 5.13). The labeled antibody (**Ab-Cy5**) was thoroughly purified by size-exclusion chromatography and dialysis, to remove unreacted mAb and Cy5.

The degree of labeling (DL) estimated by UV-Vis spectroscopy was 4.4, meaning that an average of 4.4 molecules of Cy5 was bound to one molecule of Cetuximab.

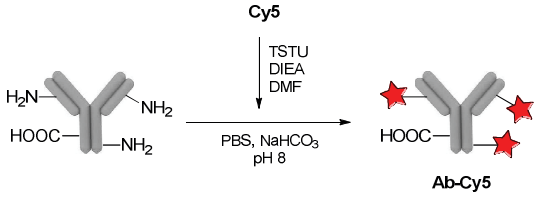

Scheme 5.13 Multi-labeling of Cetuximab with Cy5.

The **Ab-Cy5** was then coupled to short $LuCl_3$@SWCNTs previously functionalized by the nitrene reaction (**33-NH_2**). We concomitantly investigated the possibility to optimize the reaction conditions with the aim to shorten the reaction time and work-up steps. CNTs **33-NH_2** were incubated with **Ab-Cy5** for 2, 6 and 24 h, following the same protocol used for the preparation of **19-Ab** (Scheme 5.14). For all time points, the corresponding control reaction (without coupling reagents) was performed simultaneously, and all conjugates were treated and purified in the same conditions. During the washing steps (centrifugation, supernatant removal and CNT re-dispersion), it was possible to verify the thorough removal of non-reacted mAb by UV-Vis spectroscopy, thanks to the intense UV absorption of Cy5 on the Ab. Furthermore, to assess if dialysis was necessary, one aliquot of the 24 h reaction was submitted to dialysis against PBS, while another aliquot was not dialyzed.

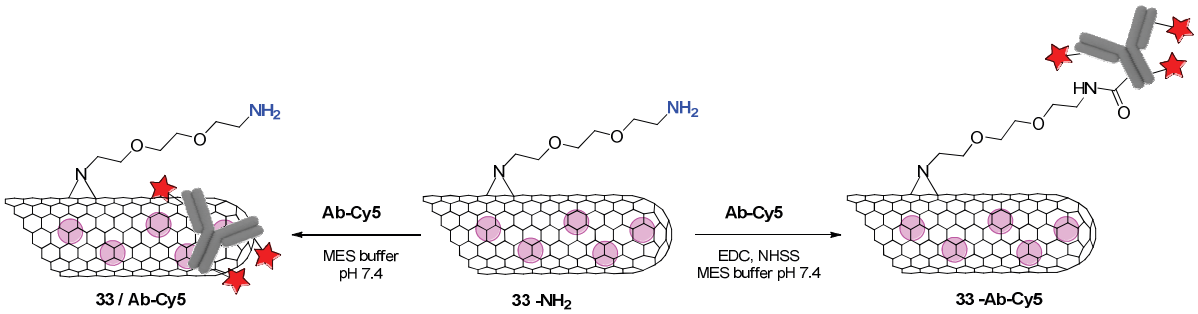

Scheme 5.14 Covalent derivatization of **33-NH_2** with labeled Cetuximab (**Ab-Cy5**) and control reaction in the absence of coupling reagents (**33**/**Ab-Cy5**).

By TGA, we did not observe significant differences between the covalent reaction and the control sample for all time points, meaning that there is a strong adsorption of the antibody on the CNTs (Figure 5.16 and Table 5.9). In addition, the loadings calculated for all time points were very similar between each other, highlighting no difference between short and long incubation times. The effect of dialysis was also not significant. It is however worth to remark, that prior to TGA, all samples were dialyzed against water for 2 days. This step is fundamental to remove the salts present in the buffer, which would otherwise substantially affect the TGA outputs. As a consequence, part of the non-covalently bound Ab could have been removed from all samples.

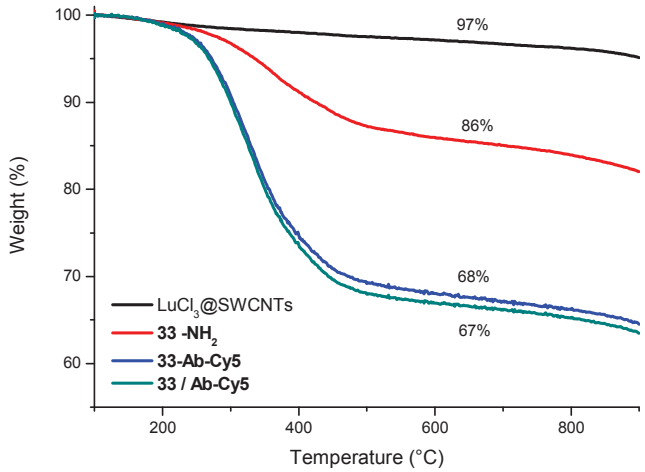

Figure 5.16 Example of TGA graph showing the curves of pristine $LuCl_3$@SWCNTs, conjugates **33-NH_2**, and conjugates **33-Ab-Cy5** and **33/Ab-Cy5** obtained after 24 h incubation and dialyzed against PBS.

The BCA assay used to determine the protein concentration gave similar outputs as TGA. There is indeed no specific trend in the loadings of the different incubation time points, neither differences between covalent and non-covalent reactions (Table 5.9).

	2 h		**6 h**		**24 h dialyzed**		**24 h non-dialyzed**	
	TGA	*BCA*	*TGA*	*BCA*	*TGA*	*BCA*	*TGA*	*BCA*
33-Ab-Cy5	175	408	189	557	179	379	194	673
33/Ab-Cy5	193	408	177	672	189	462	189	693

Table 5.9 Functionalization loadings determined by TGA (mg/g) and BCA (mg/g) for compounds **33-Ab-Cy5** and **33/Ab-Cy5** after different incubation times, with and without coupling reagents, respectively.

Finally, all conjugates were analyzed by gel electrophoresis under non-reducing and reducing conditions (Figure 5.17). For the non-reducing conditions, we can observe a difference at the 24 h time point between the covalent conjugate and the corresponding control. In fact, for the covalent conjugate, the band of the antibody is not really intense, while it appears clearly under reducing conditions. This results confirms that the mAb is covalently attached to the CNTs.

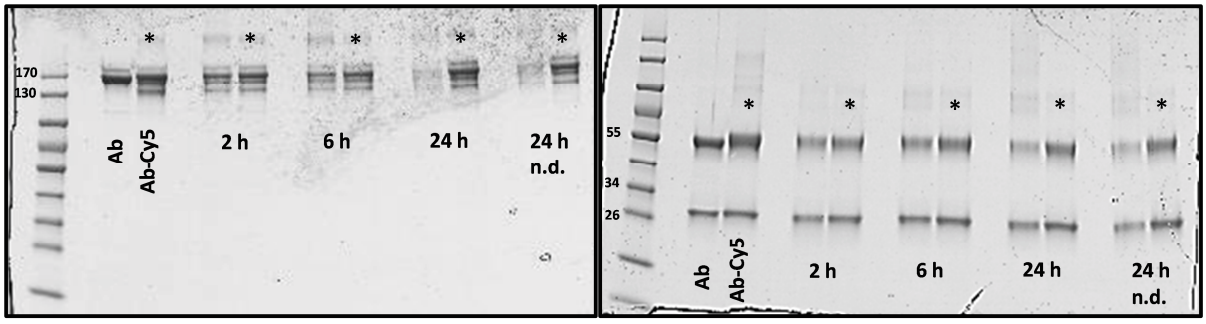

Figure 5.17 Gel electrophoresis under non-reducing (left) and reducing conditions (right) at 200 kV showing Cetuximab (**Ab**), labeled Cetuximab (**Ab-Cy5**) and conjugates **33-Ab-Cy5** and **33/Ab-Cy5** at the different time points and at 24 h non-dialyzed (n.d.). Starred lanes correspond to the control conjugates **33/Ab-Cy5** at the same time point. Gel stained with Coomassie blue. Protein size marker on the first lane (size in kDa).

The same behavior can be seen for the non-dialyzed conjugates (covalent and control), suggesting that dialysis is unnecessary. From gel electrophoresis we can also conclude that incubation times longer than 6 h are necessary to achieve a certain extent of covalently attached antibody. Indeed, only non-covalent interaction is observed for shorter time points (2 and 6 h), for both covalent and non-covalent reactions. However, the employed purification protocols (multiple centrifugation and dialysis) are not sufficient to totally remove the adsorbed mAb.

5.3.3.1 Biological evaluations

Assessment of the uptake mechanism

These newly synthesized fluorescent compounds represented a useful tool to analyze the internalization mechanism of the CNTs. In fact, the presence of the fluorescent tag on the CNTs allows both to visualize their intracellular distribution by confocal microscopy, and to quantify the extent of internalization by flow cytometry. The cellular internalization of CNTs can occur by two different mechanisms.[49] Nanotubes can reach the cytoplasm by active endocytosis or through a passive way, also known as "nanoneedle" mechanism.[49] To elucidate the internalization mechanism, cells were incubated with fluorescent CNTs (**33-Ab-Cy5** and **33/Ab-Cy5** from the 24 h time point) at two different temperatures: 4 °C and 37 °C. At low temperatures (*i.e.* 4 °C), the active cellular mechanisms are blocked, therefore only passive diffusion can occur. This experiment was performed on both CHO and U87 cells, to assess also the targeting properties of the conjugates. From the results obtained by flow cytometry (Figure 5.18), it is evident that the uptake of CNTs was significantly lower in CHO cells compared to U87 cells for both conjugates. Moreover, for the U87 cells, the uptake reaches 100% of cells already at 10 µg/mL. Therefore, both **33-Ab-Cy5** and **33/Ab-Cy5** display good targeting properties toward EGFR and the targeting efficiency of Cetuximab has not been compromised by the conjugation on the CNTs and the labeling. In the case of U87 cells, no significant difference can be observed between the incubation at 4 °C or 37 °C.

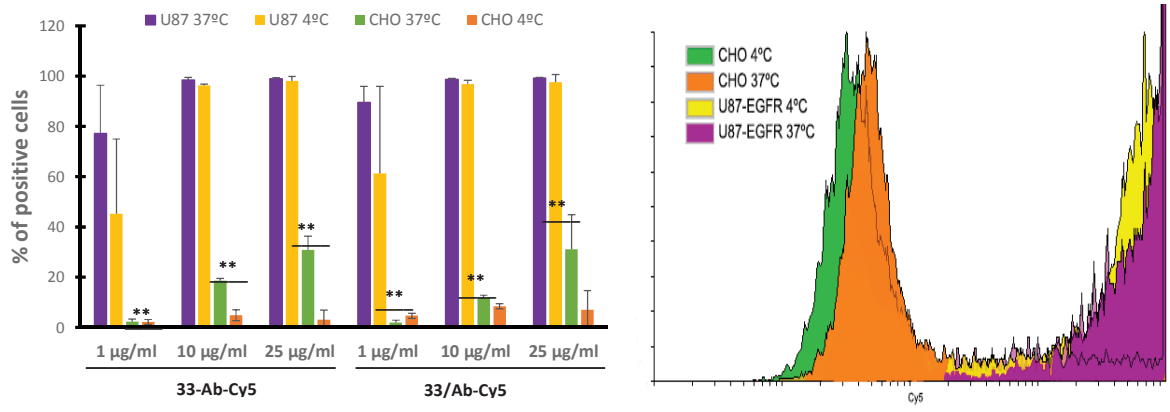

Figure 5.18 (Left) Bars represent the % of Cy5 positive cells in CHO or U87 cells after 2 hour incubation with **33-Ab-Cy5** and **33/Ab-Cy5** (obtained after 24 h incubation) at 1, 10 and 25 µg/ml either at 4 °C or at 37 °C. Error bars represent standard deviation (n=3). **p <0.01 with respect to U87 cells. (Right) Example of histogram representing the mean fluorescence intensity of CHO and U87 cells after 2 hour incubation with **33-Ab-Cy5** at 25 µg/ml at 4 °C and at 37 °C.

Since endocytosis is blocked at 4 °C, these results suggest that CNTs enter the cells by a passive mechanism. On the contrary, in CHO cells, CNTs seem to enter *via* an active mechanism, as representative levels of cellular internalization are detected only at 37 °C. Interestingly, this indicates that different types of cells adopt different mechanisms toward the internalization of CNTs. Looking at the quantity of CNTs internalized by the cells (Figure 5.18 -rightside), the difference between CHO and U87 clearly stands out, meaning that only a small amount of CNTs have been taken up by CHO cells, with a slightly increase at 37 °C. Finally, no differences can be detected between the covalent and the non-covalent conjugates (**33-Ab-Cy5** and **33/Ab-Cy5**), and the percentage of cells that took up the CNTs (Figure 5.18) as well as the mean fluorescence intensity (data not shown) are similar for both conjugates. These results are in agreement with the data obtained by TGA and BCA (Table 5.9), suggesting that a similar amount of antibody is present on the CNTs, either covalently bound or simply adsorbed.

Intracellular distribution

The functionalization of CNTs with a fluorescently-labeled antibody allowed to study the localization of CNTs within the cells by means of confocal microscopy. Conjugates **33-Ab-Cy5** and **33/Ab-Cy5** were incubated with CHO and U87 cells for 2 hours. From the microscopy images in Figure 5.20, a higher amount of CNTs can be seen inside U87 cells in comparison to CHO cells, although there is no significant difference between the two conjugates. By this experiment it was possible to have a visual proof of the targeting ability of the synthesized compounds, whose uptake is sensibly higher in U87 cells. However, we could not exactly determine whether the nanotubes were inside the cells or only localized on the membrane (where the EGFR is). For a better comprehension, a colocalization experiments is planned, where the plasma membrane is as well stained.

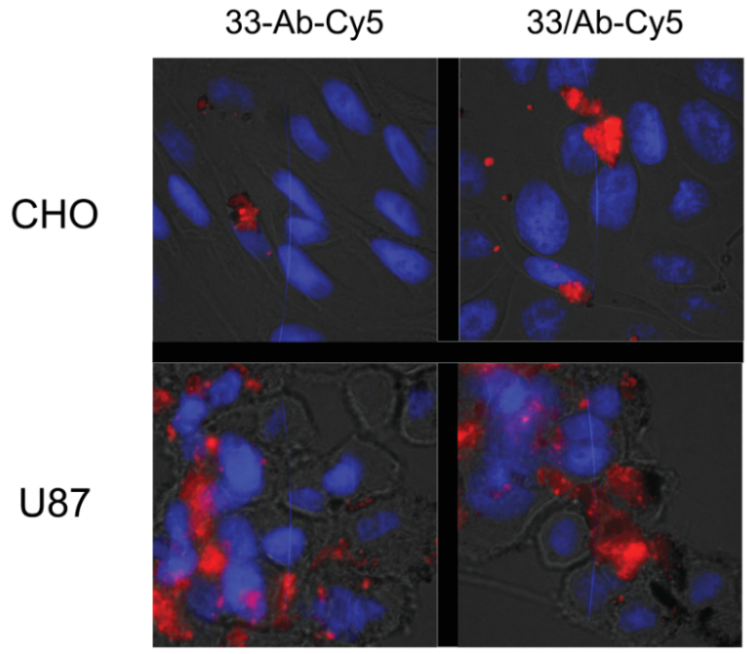

Figure 5.19 Fluorescence images of CHO and U87 cells treated for 2 hours with **33-Ab-Cy5** and **33/Ab-Cy5** (25 μg/ml) at 37 °C. Red color corresponds to the Cy5 on CNTs, while blue represents the stained nuclei.

5.3.4 FUNCTIONALIZATION OF RADIOACTIVE FILLED CNTS

Along our investigations we have been mainly working with SWCNTs, and the tested filled tubes were only SWCNTs. In fact, for MWCNTs, while the large internal diameter facilitates the filling process, it hampers the tip closure. Very recently, the ICMAB partner succeeded in preparing a batch of short sealed and filled MWCNTs ($SmCl_3$@MWCNTs). They then filled both SWCNTs and MWCNTs with 152-enriched samarium, which is the suitable isotope leading to ^{153}Sm after irradiation. Due to short-timing with the planned irradiation dates, we could not perform thorough preliminary investigations on these batches. The sample of $^{152}SmCl_3$@MWCNTs was irradiated in IBA facilities (Saclay), and an aliquot was sent to KCL (London) for functionalization and animal studies. The hot material (950 MBq) was diluted with cold $SmCl_3$@MWCNTs of the same batch (to reach an injectable amount) and submitted to functionalization by nitrene reaction followed by antibody conjugation, using the best reaction protocols (nitrene reaction: 200 °C, 6 h; deprotection: 2h; mAb coupling: 24 h). Aliquots of CNTs were taken apart after each step to allow characterization after decay. The final conjugates were then injected in mice inoculated with lung tumor, to assess the therapeutic effect. To evaluate the biodistribution of the compounds and its targeting ability, another aliquot of the radioactive functionalized CNTs were injected in mice bearing lung tumor, glioma tumor or subcutaneous melanoma, and in tumor-free mice. The interpretation of the data obtained by these studies is still in progress. The irradiation of $^{152}SmCl_3$@SWCNTs and subsequent functionalization will be planned in the future weeks, according to the reactor availability at IBA.

5.4 CONCLUSIONS

Within the RADDEL project we have investigated the reactivity of different types of empty and filled carbon nanotubes toward two [2+1] cycloaddition reactions, *i.e.* Bingel reaction and nitrene reaction. Bingel reaction was carried out using a phthalimide protected malonate and the corresponding bromomalonate as precursors, but did not afford functionalization for any of the employed pristine CNTs. The reaction was explored also at higher temperatures, by MW-irradiation and with a Boc-protected malonate, but all attempts were unsuccessful according to Kaiser test after amine deprotection, Raman spectroscopy and TGA. It was instead possible to achieve good degrees of CNT functionalization by nitrene cycloaddition, starting from an organic azide precursor bearing a Pht-protected amino group. The presence and availability of the amine functionalities onto CNTs toward further derivatization was confirmed by microscopy imaging after coupling with a triiodophenyl motif. An optimization survey was carried out to reduce the time of the synthetic steps leading to the amino-functionalized conjugates. This investigation evidenced that the best compromise between time and loading was to perform nitrene reaction at 200 °C for 6 h in NMP, while the phthalimide deprotection can be efficiently achieved after 2 h hydrazine-treatment. Besides, MW-assisted nitrene reaction can be a valuable option to afford good loading in very short time (30-60 min). The dialysis of the conjugates after cycloaddition can also be avoided, provided that thorough washing steps are carried out. We then explored different strategies to achieve the derivatization of amino-functionalized CNTs with Cetuximab, an antibody that targets the

EGFR. The first approach using the maleimide linker did not lead to high loading of mAb as we could not detect the band of the antibody by gel electrophoresis. We therefore investigated a different and shorter conjugation strategy, which involved the coupling of the amino groups on CNTs to the carboxylic groups of the antibody. The reaction afforded Sm_3Cl@SWCNT-Ab (**19-Ab**) with higher loading of mAb. In the control compound (**19/Ab**), obtained by performing the reaction without coupling reagents, we could detect a consistent amount of adsorbed mAb both by TGA and gel electrophoresis. However, by immunostaining the mAb-conjugates with a secondary anti-human antibody labeled with AuNP, we could visualize the mAb only on the covalent conjugate (**19-Ab**). The microscopic imaging of the immunostained CNTs proved that Cetuximab was efficiently immobilized onto the CNTs and that it still preserved its affinity toward a counter antibody. Cytotoxicity assays performed on RAW264.7 macrophages and PBMC cells highlighted that all CNT conjugates (covalent, non-covalent and precursor) are not substantially provoking cell death nor inflammatory response, except for high CNT concentrations. Both *in vitro* and *in vivo* results suggest that the compounds have a good biocompatibility and are not toxic in the tested cell lines. Evaluation of the targeting ability by flow cytometry and ICP-AES proved that both the mAb-CNT conjugates (**19-Ab** and **19/Ab**) can efficiently target and bind with cells that do overexpress the EGFR (U87), while no uptake was observed in a control cell line (CHO). However, no significant difference was found between the covalent conjugate and the control. Finally, the fluorescent labeling of CNTs has been explored with the aim of further investigating the internalization mechanisms. Two conjugates featuring FITC and Cy5 directly attached to the amino groups of CNTs were first prepared, but did not show sufficient levels of fluorescence upon incubation with the cells. A different strategy was then investigated, which involved the coupling of CNTs with fluorescently-labeled Cetuximab. The conjugation was performed with different reaction times, but it proved to afford the covalent conjugate with times above 6 h. The evaluation of the cellular uptake by flow cytometry and confocal microscopy proved once more that the mAb-CNT conjugates are able to target and be uptaken by EGFR-overexpressing cells (U87), without substantial difference between **33-Ab-Cy5** or **33/Ab-Cy5**. Furthermore, the internalization mechanism in this cell lines appears to be a passive one, while in the CHO an active entry seems to occur.

Overall, we have developed an optimized synthetic approach for the covalent functionalization of filled CNTs by nitrene reaction and their further conjugation with antibodies targeting specific cancer cells. We have succeeded to prepare a novel antibody-CNT conjugate which displays elevated targeting affinity toward the EGFR and low cytotoxicity. We have then employed our optimized protocol to perform the functionalization of radioactive filled CNTs and we are currently assessing their therapeutic efficacy and their *in vivo* biodistribution. We believe that our synthetic strategy is a valuable approach for the preparation of targeted CNT carriers and that our conjugates are promising tool to achieve the targeted delivery of radioactivity.

5.5 EXPERIMENTAL PART

5.5.1 COMPOUNDS SYNTHESIS AND CHARACTERIZATION

Materials and Methods

The chemicals and solvents were obtained from commercial suppliers and used without further purification. All CNT batches were provided by our partner Dr. Gerard Tobias from ICMAB – CSIC (Bellaterra, Barcelona) and detailed information are provided in the Annex. Cetuximab was provided by our partner Dr. Al-Jamal from KCL (London) as pharmaceutical formulation Erbitux® (C = 5 mg/mL). The solvents used for synthesis were analytical grade. When anhydrous conditions were required, high quality commercial dry solvents were used. For the fluorescent tagging, fluorescein isothiocyanate (FITC) isomer 1 (95%) and cyanine 5 (Cy5) were employed, and they were purchased from Alfa Aesar and provided by the group of Anthony Romieu (Université de Bourgogne in Dijon), respectively. *N*-succinimidyl 3-meleimidopropionate was synthesized as described in Chapter 3. Water was purified using a Millipore filter system MilliQ®. When stated, suspensions were sonicated in a water bath (20 W, 40 kHz). Thin layer chromatography (TLC) was conducted on pre-coated aluminum plates with 0.25 mm Macherey-Nagel silica gel with fluorescent indicator UV254. Chromatographic purifications were carried out with silica gel (Merck Kieselgel 60, 40-60 μm, 230-400 mesh ASTM). For the labeled antibody purification, the column was assembled by packing Sephadex G-25 Fine (GE Healthcare) with PBS buffer. ^{1}H-NMR and ^{13}C-NMR spectra were recorded in deuterated solvents using Bruker spectrometers (Avance III - 400 MHz and Avance I - 500 MHz). Chemical shifts are reported in ppm using the residual signal of deuterated solvent as reference. The resonance multiplicity is described as *s* (singlet), *t* (triplet), *qt* (quintuplet), *m* (multiplet), *bs* (broad singlet), and *bt* (broad triplet). Coupling constants (*J*) are given in Hz. For CNTs filtration, PTFE membrane from Millipore were employed. If not differently specified, dialysis of CNT compounds was carried out employing membrane with MWCO 12000-14000 Da, purchased from Spectrum Laboratories, Inc. Mini-dialysis and buffer exchange were performed in Slide-A-Lyzer dialysis tubes (10000 MWCO) from Thermo Scientific. Protein concentration was carried out with Amicon Ultra-15 centrifugal filters (10000 MWCO) from Millipore. Centrifugation was performed either on a Eppendorf 5804 R apparatus, or on a Beckman Avanti J-25 centrifuge equipped with JS-7.5 rotor. The UV–vis analysis were performed on a Varian Cary 5000 spectrophotometer and the Kaiser test was performed according to reported procedures.[50,51] The BCA protein assay kit was purchased by Thermo Fischer Scientific and the assay was performed according to the provider protocol. FT-IR spectra were measured on a Perkin Elmer Spectrum One ATR-FT-IR spectrometer with direct deposition of the compound. Raman spectroscopy was performed on a Renishaw inVia microRaman equipped with a Leica microscope. Spectra were recorded using 514 nm laser (5% laser power) using X 50 objective lens. TGA was performed on a TGA1 (Mettler Toledo) apparatus from 30 °C to 900 °C with a ramp of 10 °C min^{-1} under N_2 using a flow rate of 50 mL/min and platinum pans. For TGA of the CNT-antibody conjugates, an aliquot of the conjugate in PBS was previously dialyzed against deionized water to remove the buffer salts and lyophilized. For the loading estimation, values of weight loss were picked at 650 °C. LC/MS analyses were performed on ThermoFisher Finnigan LCQ Advantage Max instrument. MS experiments were performed on a Bruker

Daltonics microTOF spectrometer (Bruker Daltonik GmgH, Bremen, Germany) equipped with an orthogonal electrospray (ESI) interface. Calibration was performed using Tunning mix (Agilent Technologies). Sample solutions were introduced into the spectrometer source with a syringe pump (Harvard type 55 1111: Harvard Apparatus Inc., South Natick, MA, USA) with a flow rate of 5 μL/min. TEM analysis were performed on a Hitachi H7500 microscope (Tokyo, Japan) with an accelerating voltage of 80 kV, equipped with a AMT Hamamatsu camera (Tokyo, Japan).

HRTEM, STEM and EDX analysis were performed by Elzbieta Pach and Dr. Belén Ballesteros in ICN 2 (Barcelona). MW-assisted reactions were performed in the laboratory of Prof. M. Prato and T. Da Ros, in University of Trieste.

Synthesis of organic precursors

Synthesis of N-*[2-(2-hydroxyethoxy)ethoxy]ethylphthalimide* **1**

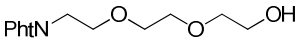

2-[2-(2-Chloroethoxy)ethoxyethanol (10 g, 59 mmol) was added to a solution of potassium phthalimide (12.08 g, 65 mmol) in DMF (100 mL) and stirred at 100°c for 17 h. The precipitated phthalimide salts were then removed by filtrating the solution over a celite pad. The filtrate was concentrated, diluted with H_2O (50 mL) and extracted with DCM (3x50 mL). The combined organic phases were dried over $MgSO_4$ and concentrated, affording a white viscous solid (15.7 g, 95% yield).

^{1}H NMR ($CDCl_3$, 400 MHz) δ (ppm): 7.86-7.83 (2H, m), 7.71-7.69 (2H, m), 3.90 (2H, t, *J* = 5.7 Hz), 3.75 (2H, t, *J* = 5.7 Hz), 3.66-3.59 (6H, m), 3.52 (2H, t, *J* = 4.3 Hz), 2.26 (1H, br s). All structural assignments were in agreement with previously reported data.[6]

Synthesis of compound **2**

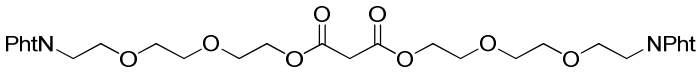

Malonyl chloride (0.36 mL, 3.71 mmol) was slowly dropped on a solution of compound **1** (2.07 g, 7.42 mmol) and pyridine (0.60 mL, 7.42 mmol) in dry DCM (150 mL) at 0 °C, under argon, and the solution was stirred at r.t. for 1.30 h. Afterwards, the resulting blue solution was concentrated by rotary evaporation and the residue was extracted with DCM, dried over $MgSO_4$ and purified by FC (eluant AcOEt/Cy in gradient from 7:3 to 8:2), obtaining **2** as a yellowish oil (1.23 g, 53% yield).

^{1}H NMR ($CDCl_3$, 500 MHz) δ (ppm): 7.84-7.80 (4H, m), 7.71-7.68 (4H, m), 4.19 (4H, t, *J* = 4.8 Hz), 3.88 (4H,t, *J* = 5.8 Hz), 3.72 (4H, t, *J* =5.8 Hz), 3.63-3.61 (8H, m), 3.58-3.56 (4H, m), 3.40 (2H, s). ^{13}C NMR ($CDCl_3$, 125 MHz) δ (ppm): 168.17, 166.41, 133.90, 132.01, 123.16, 70.46, 69.95, 68.77, 67.87, 64.47, 41.13, 37.13. MS (ESI, *m/z*): 649.20 $[M+Na]^+$. HR-MS (ESI): *m/z* = 649.2017 $[M+Na]^+$ (calcd for $C_{31}H_{34}N_2O_{12}Na$ *m/z* = 649.2004). FT-IR (neat, ν /cm^{-1}): 2952, 2871, 1706, 1388, 1320, 1110, 1022, 718.

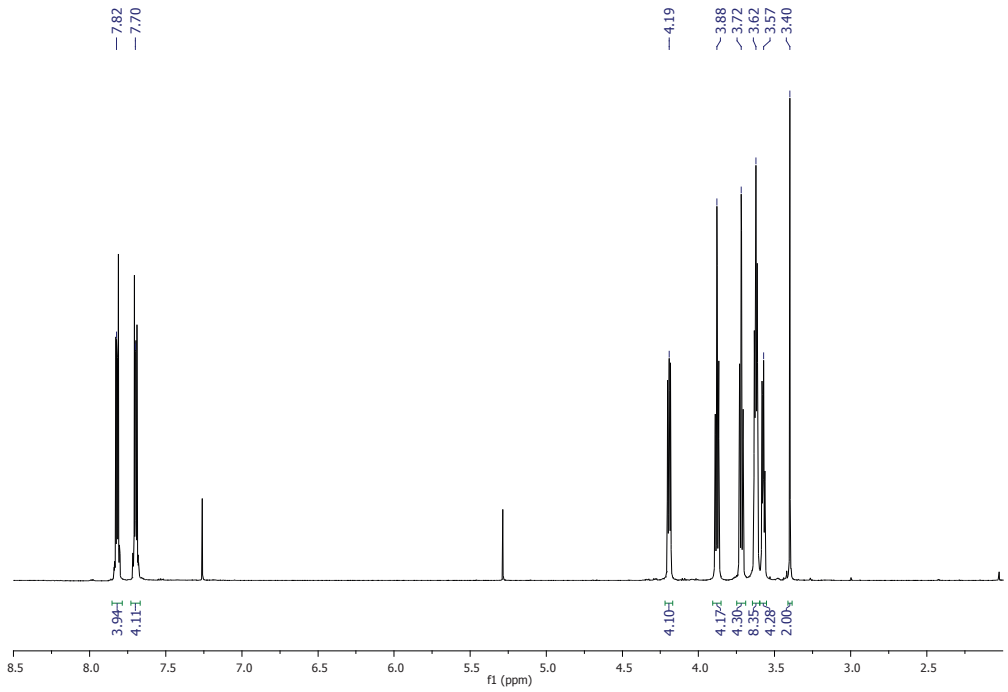

Synthesis of compound **3**

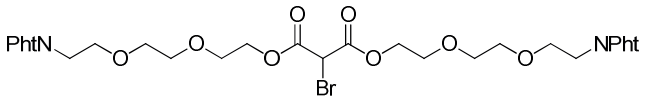

DBU (100 µL, 0.7 mmol) was added to a solution of malonate **2** (0.44 g, 0.7 mmol) in dry THF (180 mL) at 0 °C under argon, and the solution was stirred at the same temperature for 30 min and at r.t. for other 30 min. After cooling down to -78 °C, CBr_4 (232 mg, 0.7 mmol) was added, and the mixture was stirred at -78 °C for 1.30 h and at r.t. for 1 h. The reaction was then quenched with NH_4Cl, the organic phase was separated, diluted with hexane (50 mL), washed twice with brine, dried over $MgSO_4$ and concentrated at reduced pressure. The resulting oil was purified by FC (eluant AcOEt/Cy in gradient from 1:1 to 7:3) affording bromomalonate **3** as yellow oil (270 mg, 54% yield).

^{1}H NMR ($CDCl_3$, 300 MHz) δ (ppm): 7.82-7.78 (4H, m), 7.71-7.67 (4H, m), 4.88 (1H, s), 4.25 (4H, q, *J* = 4.8 and 3.5 Hz), 3.86 (4H,t, *J* = 5.7 Hz), 3.70 (4H, t, *J* =5.7 Hz), 3.64-3.57 (12H, m). ^{13}C NMR ($CDCl_3$, 75 MHz) δ (ppm): 168.17, 164.43, 133.91, 132.02, 123.17, 70.56, 70.00, 68.47, 67.89, 66.06, 41.87, 37.19. MS: *m/z* 704.5 (M^+,100), 706.5 (94). The compound was used immediately after preparation, without any further characterization.

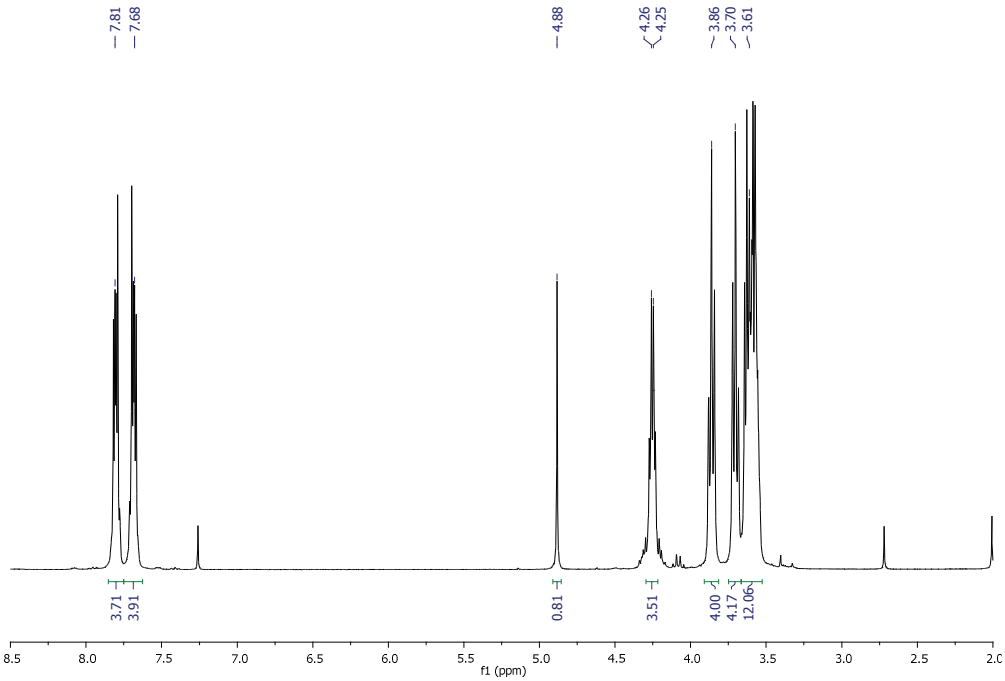

*Synthesis of 2-[2-(2-azidoethoxy)ethoxy]ethanol (**4**)*

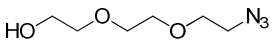

Sodium azide (19 g, 0.3 mol) and sodium iodide (0.90 g, 6 mmol) were added to a solution of 2-[2-(chloroethoxy)ethoxy]ethanol (5 g, 30 mmol) in H_2O (30 mL) and the mixture was stirred at 60 °C for 12 h. After filtration of the crude, the aqueous layer was extracted with EtOAc (3 x 30 mL). Combined organic phases were dried over Na_2SO_4, filtered and concentrated under reduced pressure, affording **4** as transparent oil (4.20 g, 81% yield).

^{1}H NMR ($CDCl_3$, 500 MHz) δ (ppm): 3.73 (2H, t, J = 4.5 Hz), 3.68 (6H, s), 3.62-3.60 (2H, m), 3.39 (2H, t, J = 5.0 Hz). MS (ESI, *m/z*): 198.08 $[M+Na]^+$. HR-MS (ESI): *m/z* =198.0836 $[M+Na]^+$ (calcd for $C_6H_{13}N_3O_3Na$ *m/z* = 198.0849). All structural assignments were in agreement with previously reported data.[13,52]

Synthesis of Boc-propargyl amine

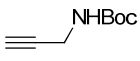

A solution of Boc_2O (3.96 g, 18 mmol) in DCM (25 mL) was dropped over 30 min on a solution of propargyl amine in DCM (20 mL) at 0 °C, and the resulting solution was then stirred at r.t. for 1 h. The solvent was removed under reduced pressure and the remaining yellow oil was purified by FC (eluant EtOAc/Cy 1:9) affording the product as white crystals (2.50 g, 90% yield).

^{1}H NMR ($CDCl_3$, 400 MHz) δ (ppm): 4.67 (2H, br s), 3.92 (2H, d, *J* = 2.7 Hz), 2.22 (1H, t, *J* = 2.5 Hz), 1.45 (9H, s). All structural assignments were in agreement with previously reported data.[53]

Synthesis of compound **5**

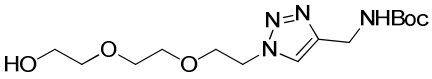

2-[2-(azidoethoxy)ethoxy]ethanol **4** (2.0 g, 11.4 mmol), Boc-propargyl amine (1.78 g, 11.4 mmol) and sodium ascorbate (113 mg, 0.57 mmol, 5%) were dissolved in a mixture of *t*-BuOH/H_2O 1:2 (10 mL). After the addition of $CuSO_4 \cdot 5H_2O$ (285 mg, 1.14 mmol, 10%), the solution was stirred at r.t. for 48 h, under argon. The reaction mixture was then diluted with water (20 mL), extracted with chloroform (3 x 15 mL), and the organic phases were dried over $MgSO_4$ and concentrated. After FC purification (eluant EtOAc/Cy in gradient from 1:9 to 7:3), the product was obtained as transparent oil (1.55 g, 41% yield).

^{1}H NMR ($CDCl_3$, 500 MHz) δ (ppm): 7.90 (1H, s), 5.38 (1H, br s), 4.54 (2H, t, *J* = 4.9 Hz), 4.41 (2H, d, *J* = 5.3 Hz), 3.87 (2H, t, *J* = 4.9 Hz), 3.76 (2H, t, *J* = 4.5 Hz), 3.62 (4H, s), 3.58 (2H, t, *J* = 4.5 Hz), 2.88 (1H, br s), 1.42 (9H, s). ^{13}C NMR ($CDCl_3$, 125 MHz) δ (ppm): 155.94, 144.95, 123.76, 79.81, 72.41, 70.37, 70.12, 69.13, 61.60, 50.33, 35.70, 28.34. MS (ESI, *m/z*): 353.18 $[M+Na]^+$. HR-MS (ESI): *m/z* = 353.1770 $[M+Na]^+$ (calcd for $C_{14}H_{26}N_4O_5Na$ *m/z* = 353.1795). FT-IR (neat, *v* /cm^{-1}): 3347, 2876, 1694, 1520, 1458, 1367, 1249, 1166, 1120, 1059, 928.

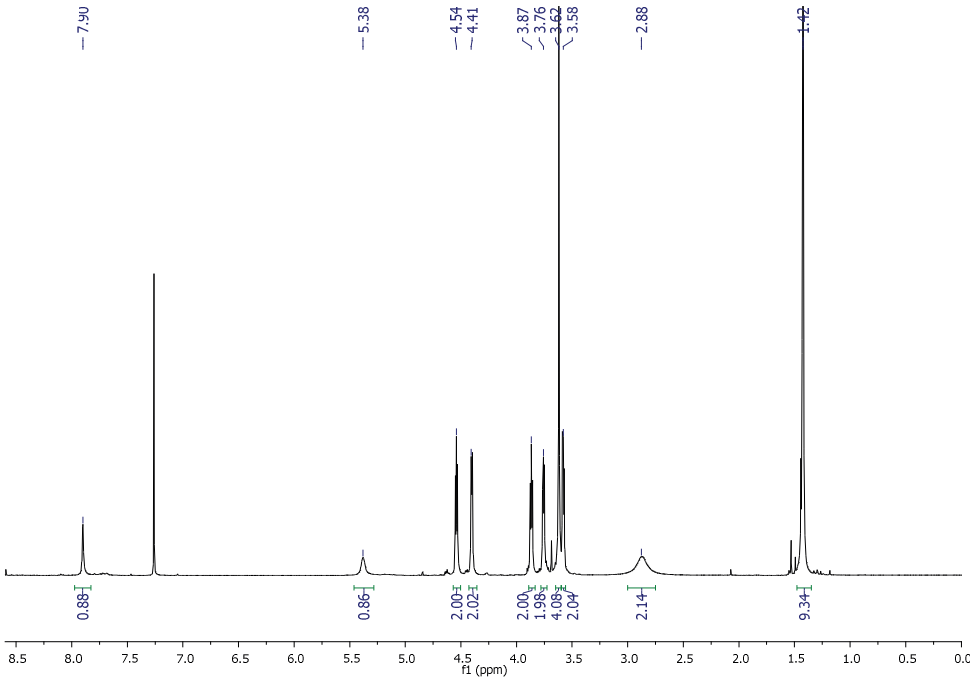

Synthesis of compound **6**

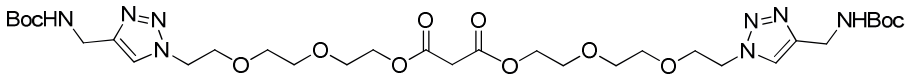

Malonyl chloride (0.23 mL, 2.34 mmol) was slowly dropped on a solution of **5** (1.55 g, 4.69 mmol) and pyridine (0.38 mL, 4.69 mmol) in dry DCM (30 mL), at 0° C under Ar, and the resulting solution was stirred at 0 °C for 2 h. The crude was concentrated, washed with H_2O (2 x 20 mL) and further purified by FC (eluant DCM/MeOH in gradient from 99:1 to 85:15), affording compound **6** as transparent oil (1.01 g, 59% yield).

^{1}H NMR ($CDCl_3$, 500 MHz) δ (ppm): 7.70 (2H, s), 5.28 (2H, br s), 4.53 (4H, t, J = 5.0 Hz), 4.39 (4H, d, J = 3.4 Hz), 4.28 (4H, t, J = 4.7 Hz), 3.86 (4H, t, J = 5.0 Hz), 3.66 (4H, t, J = 4.7 Hz), 3.59 (8H, s), 3.44 (2H, s), 1.42 (18H, s). ^{13}C NMR (125 MHz, $CDCl_3$) δ (ppm) 166.44, 155.79, 123.20, 79.58, 70.49, 70.41, 69.38, 68.82, 64.42, 50.38, 41.21, 35.91, 28.34. MS (ESI, *m/z*): 729.36 $[M+H]^+$. HR-MS (ESI): *m/z* = 729.3764 $[M+H]^+$ (calcd for $C_{31}H_{53}N_8O_{12}$ *m/z* = 729.3777). FT-IR (neat, ν /cm^{-1}): 3352, 2987, 2875, 1699, 1512, 1453, 1365, 1277, 1249, 1163, 1125, 1044, 935, 912, 861, 779.

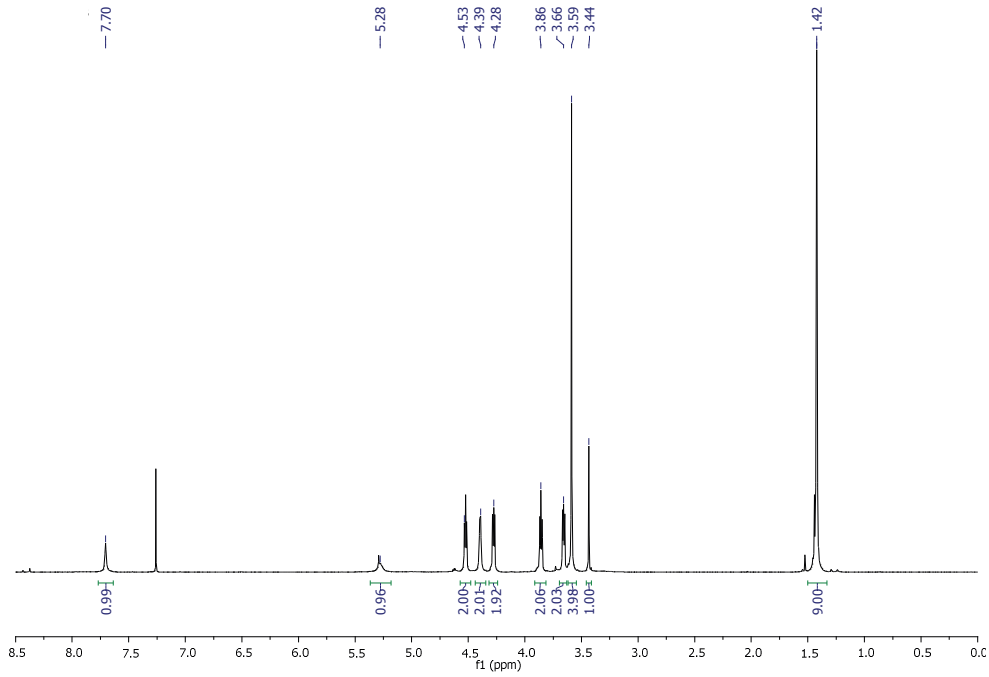

Synthesis of compound **7**

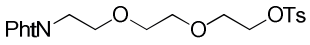

p-Toluensulfonyl chloride (6.63 g, 34.8 mmol) was slowly added to a solution of compound **1** (6.48 g, 23.20 mmol) and Et_3N (6.4 mL, 46.4 mmol) in MeCN (50 mL), at 0 °C and under argon. The mixture was stirred at 0 °C for 20 min and at r.t. for 1h, and the crude was then poured into water (40 mL),

extracted with EtOAc (3 x 30 mL) and dried over $MgSO_4$. The concentrated crude was further purified by FC (eluant EtOAc/Cy in gradient form 1:3 to 1:1), affording **7** as yellow oil (6.90 g, 69% yield).

^{1}H NMR ($CDCl_3$, 500 MHz) δ(ppm): 7.83-7.81 (2H, m), 7.76 (2H, d, *J* = 8.3 Hz), 7.70-7.69 (2H, m), 7.32 (2H, d, *J* = 8.3 Hz), 4.08 (2H, t, *J* = 4.8 Hz), 3.86 (2H, t, *J* = 5.8 Hz), 3.68 (2H, t, *J* = 5.8 Hz), 3.61 (2H, t, *J* = 4.8 Hz), 3.55 (2H, dd, *J* = 6.2 and 5.6 Hz), 3.51 (2H, dd, *J* = 6.1 and 5.6 Hz), 2.43 (3H, s). All structural assignments were in agreement with previously reported data.[29]

Synthesis of compound **8**

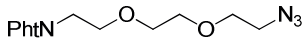

A solution of tosylate **7** (6.9 g, 15.91 mmol) in MeCN (50 mL) was treated with NaN_3 (3.10 g, 47.75 mmol) and a catalytic amount of NaI, and refluxed (90 °C) for 48 h under argon. Because of the inherent risk related with the manipulation of azides, especially at high reaction temperatures, all manipulations were carried out with extra care using a protection screen during reaction. The cooled mixture was diluted with water (30 mL) and extracted with DCM (4 x 20 mL). The combined organic phases were dried over $MgSO_4$, concentrated and purified by FC (eluant EtOAc/Cy in gradient form 1:3 to 1:2), affording the product as an orange oil (3.9 g, 80% yield).

^{1}H NMR ($CDCl_3$, 400 MHz) δ(ppm): 7.85-7.83 (2H, m), 7.72-7.70 (2H, m), 3.90 (2H, t, *J* = 5.8 Hz), 3.75 (2H, t, *J* = 5.7 Hz), 3.66-3.64 (2H, m), 3.62-3.59 (4H, m), 3.30 (2H, t, *J* = 5.1 Hz). All structural assignments were in agreement with previously reported data.[29]

Antibody derivatization

Thiolation of Cetuximab

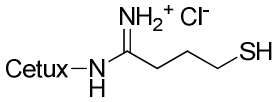

The Ab formulation Erbitux® was dialyzed overnight against 5 mM EDTA/PBS buffer (pH 7.8, adjusted with $NaHCO_3$), to remove the additive present in the pharmaceutical formulation. A freshly prepared solution of 2-iminothiolane (60 µL, 11 mM) in 5 mM EDTA/PBS buffer was added to an aliquot of Ab (1.1 mL, C = 5 mg/mL) in the same buffer. The solution was shaken at r.t. for 1 h, and then dialyzed against 5 mM EDTA/PBS buffer (pH 6.5) at 4 °C for 24 h, to remove the excess of Traut's reagent. The so-obtained Ab (C = 0.5 mg/mL) was immediately used for the coupling with maleimide functionalized CNTs.

*Fluorescent labeling of Cetuximab (**Ab-Cy5**)*

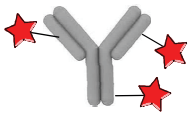

Pre-activation of Cy5: a 10 mg/mL solution of Cy5 was prepared by dissolving Cy5 (5.99 mg, 7.04 μmol) in dry DMF (500 μL), under argon. DIEA (12 μL) and 40 μL of a 0.15 M solution of TSTU in dry DMF (corresponding to 7 μmol of TSTU) were then added to the Cy5 and the reaction mixture was stirred at r.t. for 4 h, in the dark. The activated Cy5 (300 μL, ca. 3 mg) was added to a 5 mg/mL solution of Cetuximab in PBS (6 mL) at pH 8 (adjusted with 1 M $NaHCO_3$) and gently stirred for 2 h, in the dark. The reaction mixture was then filtered through a Sephadex G-25 column with PBS (pH 7.4) as elution buffer and the fractions corresponding to the Ab-Cy5 were joined together and concentrated in a Amicon centrifugal filter (MWCO 10000). By measuring the UV-Vis absorbance of the conjugate, the degree of loading was calculated according to:

$$DL = \frac{A_{650} \times \varepsilon_{280}}{(A_{280} - A_{650} \times CF) \times \varepsilon_{650}}$$

where: A_{280} and A_{650} = absorbance of the conjugate solution at 280 nm and 650 nm
CF = correction factor due to the contribution of the dye at 280 nm (0.05)
ε_{280} = molar extinction coefficient of the antibody (203000 $cm^{-1}M^{-1}$)
ε_{650} = molar extinction coefficient of the dye (250000 $cm^{-1}M^{-1}$)

Labeled Cetuximab (**Ab-Cy5**) was obtained with a DL = 4.4 and with 83% yield.

Synthesis of f-CNTs

General procedure for Bingel reaction

Malonate derivative **2** (200 mg, 1 eq.) and I_2 (89 mg, 1 eq.) were added to a dispersion of CNTs (10 mg) in dry ODCB (15 mL), obtained by bath-sonicating the nanotubes in the solvent for 30 min, under argon. DBU (0.20 mL, 2 eq.) was added drop-wise and the mixture was stirred at the selected temperature for 24 h, and afterward diluted with EtOH (15 mL) and filtered over a PTFE membrane (0.1 μm). The black solid was re-dispersed in ODCB (10 mL) by sonication (10 min) and precipitated from acetone (20 mL) by centrifugation (4500 rpm, 10 min). This re-dispersion/centrifugation cycle was repeated twice. The CNTs were then dispersed in a small volume of ddH_2O by sonicating for 15 min (a small aliquots of MeOH was added when good dispersions were not achievable) and dialyzed against ddH_2O for 2 days. To recover the CNTs, the dialyzed dispersion was filtered (0.1 μm) and the black solid was re-dispersed in MeOH (20 mL) by sonication (10 min) and re-filtrated. This cycle was repeated with acetone (20 mL) and the obtained CNTs were finally dried under vacuum. The so-obtained sample was analyzed by TGA for the assessment of the loading.

General procedure for MW-assisted Bingel reaction

In a capped MW glass tube, SWCNTs (5 mg) were dispersed in dry NMP (1 mL) by sonicating for 15 min, under argon. I_2 (33 mg, 0.13 mmol), DBU (400 μL, 0.26 mmol) and a solution of the selected malonate precursor (100 mg) in dry NMP (1 mL), were then added to the suspension, and this was stirred in the microwave apparatus at 120 °C (fixed temperature) for 30 min with an average power of 40, 50 or 60 WTable 5.7. The mixture was then diluted with EtOH (5 mL), filtered through a PTFE membrane (0.1 μm), and the CNTs recovered on the membrane were washed by dispersing them in DMF (15 mL), sonicating for 10 min and filtrating. This washing sequence was further repeated with MeOH (x 2) and acetone (x 1). The CNTs were then dialyzed and dried as above described and TGA of sample was performed.

General procedure for phthalimide deprotection

Hydrazine hydrate (10% v/v) was added to a 1 mg/mL dispersion of Pht-protected CNTs in EtOH, obtained by sonicating them for 10 min. The dispersion was stirred overnight (or other specified time) at r.t., and then diluted with EtOH (twice the reaction volume) and filtered (0.1 μm). The recovered CNTs were re-dispersed in MeOH by sonication (10 min) and filtrated. This washing cycle was repeated again with MeOH and with acetone (x 2), and the black solid on the membrane was finally dried in *vacuum*. Kaiser test and TGA were performed to assess the functionalization degree.

General procedure for Boc deprotection

Boc-protected CNTs (5 mg) were sonicated for 10 min in a 2M solution of HCl in 1,4-dioxane (5 mL), and the mixture was stirred overnight at r.t. Following filtration of the reaction mixture (0.1 μm), the CNTs were washed with DMF, MeOH (x 2) and acetone (x 2) and dried *in vacuo*. Kaiser test and TGA were performed to assess the functionalization degree.

General procedure for nitrene reaction –small scale

In a flame-dried Schlenk tube, pristine CNTs (5 mg) were dispersed in dry ODCB (or NMP) (4 mL) by sonicating for 15 min under argon. A solution of azide **8** (100 mg) in dry ODCB (or NMP) (1 mL), was then added to the CNT dispersion by syringe, and the mixture reacted in an oil bath for the selected time at the selected temperature, under vigorous stirring and under argon (see Table 5.3, Table 5.5 and Table 5.7). The cooled mixture was then diluted with EtOH (10 mL) and filtered (0.1 μm). The CNTs recovered on the filter were washed by dispersing them in DMF (10 mL), sonicating for 10 min and filtrating. This washing sequence was further repeated with MeOH (x 2) and with acetone (x 2). The CNTs were then dialyzed and dried as above described and TGA of the sample was performed.

General procedure for tagging of compounds **9**, **10**, **11** *and* **12**

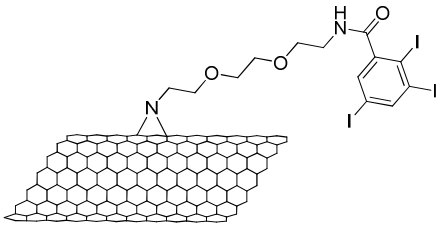

Amino-functionalized CNTs (5 mg) were dispersed in dry DMF (5 mL) by sonicating for 30 min. 2,3,4-Triiodobenzoic acid (100 mg, 20 eq. w/w, 0.2 mmol), HOBt (54 mg, 0.4 mmol) and DIEA (0.25 mL, 5% v/v) were then added to the dispersion at r.t., and finally EDC·HCl (154 mg, 0.8 mmol) was added at 0 °C. The mixture was briefly sonicated and then stirred at r.t. for 48 h. After filtration, the recovered CNTs were washed with DMF (x 2), MeOH (x 2) and acetone (x 1), and finally dried *in vacuo*. The obtained tag-functionalized CNTs (**9 -I**, **10 -I**, **11 -I** and **12 -I**) were then characterized by Kaiser test, TGA, Z-contrast STEM and EDX.

General procedure for MW-assisted nitrene reaction

Pristine SWCNTs (5 mg) were dispersed in dry NMP (4 mL) by sonicating 15 min in a capped MW glass vial, under argon. A solution of azide **8** (100 mg) in dry NMP (1 mL) was added to the CNT dispersion, this was flushed with argon for few minutes and finally stirred in the microwave apparatus at the selected temperature (see Table 5.6) for 60 min (or 30 min) with an average power of 100 W. The mixture was then diluted with DMF (5 mL), filtered through a PTFE membrane (0.1 μm), and the CNTs recovered on the membrane were washed with DMF (x 1), MeOH (x 2) and acetone (x 1). After dialysis against ddH_2O and vacuum-drying, the CNT samples were characterized by TGA.

Synthesis of $SmCl_3$@SWCNT-NH_2 (**34-NH_2**)

In a flame-dried Schlenk tube, $SmCl_3$@SWCNTs (15 mg) were dispersed in dry ODCB (12 mL) by sonicating for 15 min under argon. A solution of azide **8** (300 mg) in dry ODCB (3 mL), was then added to the CNT dispersion by syringe, and the mixture was stirred at 200 °C for 12 h. After cooling, the mixture was diluted with EtOH (15 mL) and filtered (0.1 μm). The CNTs recovered on the filter were washed with DMF (x 1), MeOH (x 2) and acetone (x 2), dialyzed for 48 h against ddH_2O. The dialyzed nanotubes (**34-Pht**) were recuperated by filtration, washed with MeOH (x 1) and acetone (x 1) and finally dried under vacuum. The degree of functionalization estimated from the weight loss comparison with pristine $SmCl_3$@SWCNTs is 22.8 %, corresponding to a loading of 789 μmol/g.

For the deprotection, CNTs (13 mg) were dispersed in EtOH (10 mL) by sonicating for 10 min, and afterwards treated with hydrazine hydrate (1.3 mL). The dispersion was stirred overnight at r.t., and then diluted with EtOH (15 mL) and filtered (0.1 μm). The CNTs were washed with MeOH (x 2) and acetone (x 2) and finally dried in *vacuo*. The free amine loading calculated by Kaiser test is 293 μmol/g.

Synthesis of $SmCl_3$@SWCNT-mal (**34-mal**)

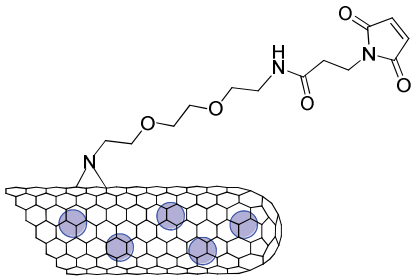

Conjugate **34-NH_2** (15 mg) was dispersed in dry DMF (7 mL) by sonicating for 20 min under argon. A solution of *N*-succinimidyl 3-meleimidopropionate (104 mg) in dry DMF (2 mL), and DIEA (0.7 mL) were then added to the CNT dispersion, and this was stirred at r.t. for 48 h. After filtration over a PTFE membrane (0.1 μm), the recovered CNTs were washed with DMF (x 2), MeOH (x 2) and acetone (x 1), and finally dried *in vacuo*. The free amine loading of meleimido-functionalized CNTs calculated by Kaiser test is 65 μmol/g, which corresponds to a degree of functionalization of 228 μmol/g. The estimation of the degree of functionalization obtained from TG analysis corresponds to 607 μmol/g.

Synthesis of $SmCl_3$@SWCNT-mal-Ab (**34-mal-Ab**)

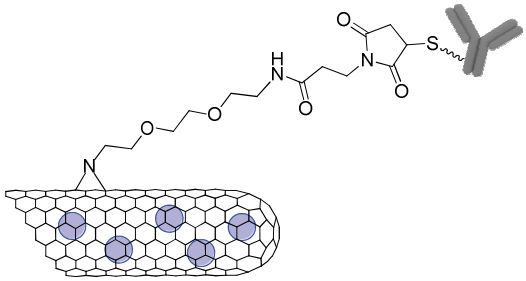

Conjugate **34-mal** (8.5 mg) was dispersed in a solution of thiolated Cetuximab (8.5 mL, 0.5 mg/mL) in 5 mM EDTA/PBS (pH 6.4) by sonicating for 1 min in cold water. The mixture was shaken at r.t. for 24 h and then centrifuged (4500 rpm, 4 °C, 5 min). The supernatant was removed and the CNTs were re-dispersed in PBS buffer pH 7.4 by sonicating 30 sec in cold water. Centrifugation and re-dispersion in fresh PBS were repeated until no Ab could be detected in the supernatant by UV-Vis. The CNT dispersion was then dialyzed (MWCO 300000 Da) against PBS buffer pH 7.4 for 48 h at 4 °C. Conjugate **34-mal-Ab** was characterized by TGA and GE and stored at 4 °C in a PBS solution (1.3 mg/mL). The loading of antibody estimated from TG analysis is 44 mg/g.

Scale-up for the synthesis of $SmCl_3$@SWCNT-NH_2 (**19-NH_2** *and* **20-NH_2**)

In a flame-dried Schlenk tube, $SmCl_3$@SWCNTs (30 mg) were dispersed in dry NMP (25 mL) by sonicating for 15 min under argon. A solution of azide **8** (560 mg) in dry NMP (5 mL), was then added to the CNT dispersion by syringe and the mixture was stirred at 200 °C for 12 h. The cooled mixture was

then diluted with EtOH (15 mL) and filtered (0.1 μm). The CNTs recovered on the filter were washed with EtOH (x 1), MeOH (x 2) and acetone (x 2) and dialyzed for 48 h against ddH_2O. The dialyzed nanotubes were recuperated by filtration, washed with MeOH (x 1) and acetone (x 1) and finally dried under *vacuum*. The degree of functionalization estimated from the weight loss comparison with pristine $SmCl_3$@SWCNTs is 17.1% for **19-Pht** (corresponding to a loading of 618 μmol/g), and 20% for **20-Pht** (corresponding to a loading of 731 μmol/g).

For the deprotection, CNTs (28 mg) were dispersed in EtOH (25 mL) by sonicating for 10 min, and afterwards treated with hydrazine hydrate (3 mL). The dispersion was stirred at r.t. for 2 h, and then diluted with EtOH (15 mL) and filtered (0.1 μm). The recovered CNTs were washed with MeOH (x 2) and acetone (x 2), and finally dried under vacuum. For conjugate **19-NH_2**, the free amine loading calculated by Kaiser test is 90 μmol/g, while the degree of functionalization estimated by TGA is 711 μmol/g, which corresponds to a phthalimide loss of 513 μmol/g (by comparison of the weight loss with the precursor). For conjugate **20-NH_2**, the free amine loading calculated by Kaiser test is 146 μmol/g, while the degree of functionalization estimated by TGA is 918 μmol/g, which corresponds to a phthalimide loss of 519 μmol/g.

*Synthesis of $SmCl_3$@SWCNT-Ab (**19-Ab**) and control (**19/Ab**)*

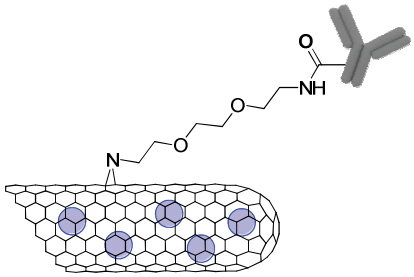

An aliquot of Erbitux® (2 mL) was submitted to buffer exchange in a Slide-a-Lyzer Mini Device (MWCO 10000) against MES buffer pH 7, in order to bring Cetuximab in the required buffer medium. MES buffer 50 mM was prepared by dissolving MES (9.76 g) in ddH_2O (800 mL) and pH was adjusted to 7 with 10 N NaOH before bringing the solution to 1 L volume.

Conjugate **19-NH_2** (16 mg) was dispersed in DMF (1.3 mL) by sonicating for 15 min in a centrifuge plastic tube. A solution of EDC·HCl (6 mM) and sulfo-NHS (4.4 mM) in MES (2.5 mL) was then added to the dispersion under sonication. After 5 min, Cetuximab (1 mg/mL in MES, 11 mL) was added and the mixture was gently stirred at r.t. for 24 h. The reaction mixture was homogenized by sonicating for 30 sec and the CNTs were precipitated by centrifugation (4500 rpm, 10 min, 15 °C). The supernatant was removed, the CNTs were re-dispersed in PBS (20 mL) by sonicating for 10 min. Centrifugation, buffer removal and re-dispersion were repeated at least 3 times in order to remove non-reacted antibody. The CNT dispersion was then dialyzed (MWCO 300000 Da) against PBS for 24 h. The obtained **19-Ab** was finally stored at 4 °C in PBS solution (3.5 mg/mL). The loading of antibody estimated by TGA is 250 mg/g, whereas by BCA assay is 124 mg/g.

For the control reaction, the same procedure was carried out proportionally on a smaller amount of **19-NH_2** (3.1 mg) and without addition of EDC·HCl and sulfo-NHS. The obtained conjugate **19/Ab** was stored at 4 °C in PBS solution (1.57 mg/mL). The loading of antibody determined by TGA is 200 mg/g.

*Synthesis of $SmCl_3$@SWCNT-Cy5 (**20-Cy5**)*

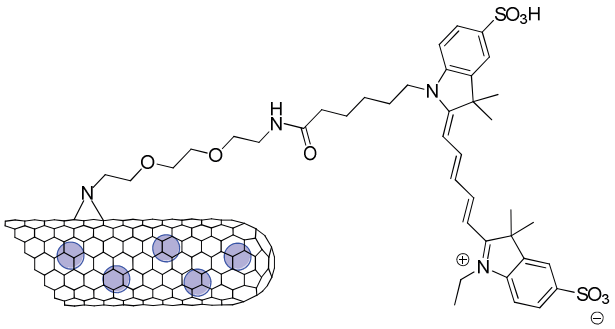

Pre-activation of Cy5: DIEA (17 µL) and a solution of TSTU (2.6 mg) in dry DMF (1.5 mL) were added to a solution of Cy5 (2.5 mg) in dry DMF (1.5 mL), under argon. The reaction mixture was stirred at r.t. for 7 h, in the dark.

A dispersion of CNTs **20-NH_2** (6 mg) and DIEA (17 µL) in dry DMF (2 mL) was then added to the cyanine solution, sonicated for 5 min and stirred at r.t. for 2 days, in the darkness. The suspension was filtered (0.1 µm) and the CNTs were washed with DMF (x 2), MeOH (x 2) and acetone (x 1) and finally dried under vacuum. The residual amine loading determined by Kaiser test is 35 µmol/g which, by difference with the loading of the precursor, corresponds to a degree of functionalization of 109 µmol/g. The loading of Cy5 estimated by TGA is 71 µmol/g, corresponding to 56 mg/g.

*Synthesis of $SmCl_3$@SWCNT-FITC (**20-FITC**)*

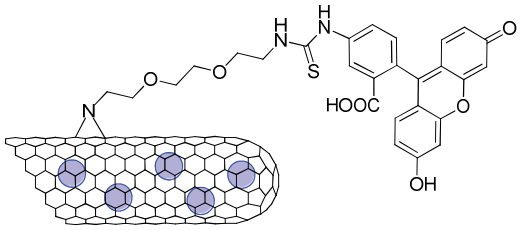

CNTs **20-NH_2** (6 mg) were sonicated in dry DMF (3 mL) for 10 min under argon. DIEA (25 µL) and a solution of FITC (6 mg) in dry DMF (1.5 mL) were added, the dispersion was sonicated for 2 min and then stirred for 2 days in the darkness. The CNTs were recovered by filtration (0.1 µm) and washed with DMF (x 2), 0.1 M HCl (x 1), MeOH (x 2) and acetone, and finally dried under vacuum. The residual amine loading determined by Kaiser test is 42 µmol/g which, by difference with the loading of the precursor, corresponds to a degree of functionalization of 102 µmol/g. The loading of FITC calculated from the TG analysis is 87 µmol/g, which corresponds to 34 mg/g.

*Synthesis of $LuCl_3$@SWCNT-Ab-Cy5 (**33-Ab-Cy5**) and control (**33-Ab-Cy**)*

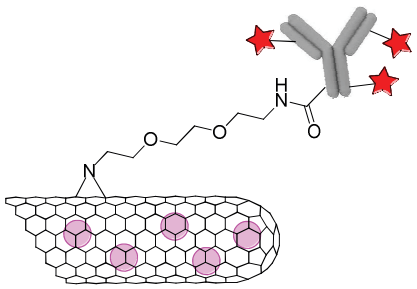

Ab-Cy5 (8 mL, 3.8 mg/mL) was submitted to buffer exchange in a Slide-a-Lyzer Mini Device (MWCO 10000) against 50 mM MES buffer pH 7. Conjugate **33-NH_2** (4 mg) was dispersed in DMF (400 µL) by sonicating for 15 min in a centrifuge plastic tube. A solution of EDC·HCl (6 mM) and sulfo-NHS (4.4 mM) in MES (800 µL) was then added to the dispersion under sonication. For the control reactions, MES buffer (800 µL) without EDC·HCl and sulfo-NHS was added instead. After 5 min, **Ab-Cy5** (0.96 mg/mL in MES, 2.8 mL) was added to the CNT dispersion and the mixture was gently stirred at r.t. for 2, 6 or 24 h. The reaction mixture was homogenized by sonicating for 30 sec and the CNTs were precipitated by centrifugation (4500 rpm, 10 min, 12 °C). The supernatant was removed, the CNTs were re-dispersed in PBS (3 mL) by sonicating for 10 min. Centrifugation, buffer removal and re-dispersion were repeated 4 times and the decanted fraction were analyzed by UV-Vis to check the absences of non-reacted **Ab-Cy5**. The CNT dispersion was then dialyzed (MWCO 300000 Da) against PBS for 24 h (except for the specified non-dialyzed conjugates at 24 h time point). The obtained conjugates were stored at 4 °C in PBS solution. The loading of antibody was determined by TGA and BCA protein assay and values are reported in Table 5.9. Gel electrophoresis of all samples was run under non-reducing and reducing conditions.

5.5.2 BIOLOGICAL INVESTIGATIONS

Gel Electrophoresis

Gel electrophoresis were performed on Mini-PROTEAN® TGX™ 4-20% Tris-glycine gels purchased by Bio-Rad Laboratories (Hercules, California). Tris-glycine buffer was used to fill the tank. Prior to loading, the samples were added with Laemmli buffer for non-reducing conditions or reducing conditions (Laemmli buffer supplemented with 5% β-mercaptoehtanol). The first well was always loaded with the protein ladder. The gel was run at a voltage of 150 V or 200 V for ca. 60 min and then stained overnight with Coomassie blue. Finally, the staining solution was removed and the gel extensively washed with distilled water to allow the visualization of the proteins bands.

Immunostaining

For the colloidal gold immunostaining, 20 µL of CNT dispersion (20 µg/mL) in PBS were drop-casted on the TEM grids and allowed to dry in the air. The TEM grids were first incubated with acetylated BSA in UPS water (1% w/w) for 45 min and then incubated for 2 h with 20 µL of staining solution (anti-Human IgG/AuNP or anti-Rabbit IgG/AuNP). The staining solutions were prepared as following: the secondary IgG/AuNP was dissolved in BSA (0.1% w/w in PBS) in a 1:50 volume ratio. After incubation, the excess of immunoglobulin was rinsed away by incubating the grids with 300 µL of PBS for 5 min (3 times), and finally with 300 µL of ddH_2O. After drying in the air the grid were observed by TEM (in Strasbourg) and STEM (in ICN 2 – Barcelona).

Cell culture: RAW macrophages

Phagocytic RAW 264.7 murine macrophage cell line was the model selected to evaluate the cytotoxicity. Briefly, RAW 264.7 cells were cultured in RPMI 1640 supplemented with 10% heat inactivated Fetal Bovine Serum (FBS), 100 U/ml gentamycin, β-mercaptoethanol (50 µM) and HEPES (20 mM) under controlled atmosphere (37°C, 5% CO_2). When confluence reached 70-80%, RAW 264.7 cells were detached with SE buffer (PBS containing 2 mM EDTA and 2% FBS), reseeded in 96 well plates at a density of 10^5 cells/well and allowed to adhere overnight (37 °C, 5% CO_2) prior to CNTs addition.

Cell viability in RAW macrophages

Cells were then treated with 1, 10, 25, 50 and 100 µg/ml of the different CNTs. DMSO (20%) was used as death positive control and LPS+IFNγ as a cytokine inducer control. After 24 h incubation, supernatants were collected for cytokine determination and cells were harvested with SE buffer and stained with both APC-Annexin V (AnnV; BD Pharmingen 550475) and propidium iodide (PI, 0.2 µg/ml; Sigma-Aldrich) in a calcium containing buffer. Early apoptosis is shown by AnnV positive staining; double AnnV and PI stained cells will be considered necrotic or late apoptotic while the absence of staining shows viable cells. (Figure 5.12). The percentage of live (AnnV-/PI-), early apoptotic (AnnV+/PI-) and late apoptotic/necrotic (AnnV+/PI+ and AnnV-/PI+) cells was determined by acquiring at least 25,000 events using a Gallios flow cytometer (Beckman Coulter, Villepinte-France) and analyzing the data with Flowing Software 2.5.1.

Cytokine determination by ELISA

Polyvinyl microtiter plates were coated with 50 µl/well of Specific Purified Rat Anti-Mouse IL6 (BD Pharmingen 554400) or Specific Purified Rat Anti-Mouse TNFα (BD Pharmingen 557516) diluted in 0.05 M carbonate pH 9.6 buffer and incubated overnight at 4 °C. After washings with PBS containing 0.05% Tween (PBS-T), a saturation step was performed by adding 100 µl/well of PBS containing 10% FBS for 1 h at 37 °C. After washings with PBS-T, 50 µl of culture supernatants (from the viability experiment) were added and incubated at 37 °C for 2 h. Plates were then washed with PBS-T and 50

µl/well of secondary Biotin Rat Anti-Mouse IL6 (BD Pharmingen 554402) or secondary Biotin Rat Anti-Mouse TNFα (BD Pharmingen 557432) were added and incubated for 1 h at room temperature. Then, plates were washed with PBS-T, and 50 µl/well of streptavidin conjugated to horse radish peroxidase (diluted 1/500) were added. The plates were incubated for 30 min at r.t., and then washed extensively with PBS-T and ddH_2O . The enzymatic reaction, revealing the presence of cytokines in the tested supernatants, was visualized by adding 3,3',5,5'-tetramethylbenzidine in the presence of H_2O_2. The resulting absorbance was measured at 450 nm after the reaction was stopped with 1 N HCl. Recombinant IL6 (BD Pharmingen 554582) or recombinant TNFα (BD Pharmingen 554589) were used as standards.

Cell culture: U87 and CHO cells

U87 glioblastoma cells were modified to overexpress EGFR receptor by the group of Prof. Al-Jamal in KCL. Both U87-EGFR+ and CHO cell lines were provided by the KCL partner. U87-EGFR+ were cultured under controlled atmosphere (37°C, 5% CO_2) in Dulbecco's Modified Eagle Medium (DMEM) supplemented with 10% FBS, 100 U/ml gentamycin and 1% Penicillin-Streptomycin, whereas for CHO cell line RPMI 1640 supplemented with 10% FBS and 1% Penicillin-Streptomycin was used. When confluency reached 70-80%, cells were tripsinized, and reseeded in 24 well plates at a density of 10^5 cells/well and allowed to adhere overnight (37 °C, 5% CO_2) prior to CNTs addition.

Cellular uptake experiment

Cells were treated with 10 µg/ml of CNT **19-NH_2**, **19-Ab** and **19/Ab**. As a positive control 2.5 µg/ml of Cetuximab (Erbitux®, Merck KGaA) were added. 1, 3 and 24 hours after the addition of the CNTs, cells were washed twice with PBS, fixed with 4% paraformaldehyde (PFA) for 15 min, permeabilized with Triton X-100 (0.1% in PBS) for 10 min, blocked with 1% BSA for 30 min and finally, incubated for 2 h with a fluorescent Cy3-Goat Anti-Human IgG (H+L) (109-165-088-JIR, Stratech Scientific Ltd) secondary antibody that binds Cetuximab, before being subjected to flow cytometry analysis. The percentage of Cy3 positive cells and the mean fluorescent intensity were determined by acquiring at least 10,000 events using a FACSCalibur flow cytometer (BD, Franklin Lakes, NJ) and analyzing the data with Flowing Software 2.5.1

ICP-AES

U87-EGFR+ and CHO cells were seeded in quadruplicate onto 24-well plates at a density of 10^5 cells/well and allowed to adhere overnight prior to exposure to **19-Ab** (25 µg/ml). 24 h later cells were extensively washed with cold PBS, tripsinized, collected and stored in a glass vial until analysis. ICP-AES analyses were performed on an Agilent 7500ce apparatus.

Cellular uptake with fluorescent CNTs

U87-EGFR+ and CHO cells were seeded onto 24 well/plates (10^5 cells/well) and allowed to adhere overnight. Afterwards, cells were treated with 1, 10 or 25 μg/ml of **33-Ab-Cy5** and **33/Ab-Cy5** and incubated either at 4 °C or at 37 °C for 2 h to compare the non-active and active uptake mechanisms, respectively. Cells were then extensively washed with cold PBS, tripsinized, collected and analyzed with Gallios flow cytometer (Beckman Coulter, Villepinte-France). The percentage of fluorescent cells and their mean fluorescent intensity was determined by acquiring at least 10,000 events and analyzing the data with Flowing Software 2.5.1.

Confocal Microscopy experiment

Cells were seeded onto polystyrene culture chambers (Falcon 354108) and allowed to adhere overnight (10^5 cells/well). Fluorescent CNTs **33-Ab-Cy5** and **33/Ab-Cy5** (25 μg/ml) were then added and incubated for 2 h at 37 °C. Cells were then extensively washed with cold PBS, fixed with 4% PFA and treated with DAPI (0.1% in PBS) in order to stain the nuclei of the cells. Images were obtained with an Axio Observer Z1 microscope (Zeiss) connected to a Spinning Disk Confocal head (Yokogawa) and ImageJ software was used for further analyses.

5.6 ANNEX: CNTS PURIFICATION AND FILLING

Our partner in Barcelona (ICMAB – CSIC), focused on the optimization of methods for purification, shortening and filling of both SWCNTs and MWCNTs. We here report a brief explanation and description of how these steps are generally carried out, and of the methodologies employed by our partner. During a short stay at ICMAB, I was myself involved in the purification and filling of one batch of pristine CNTs that I later employed for functionalization.

5.6.1 INTRODUCTION

Purification

All along the project, commercially available pristine CNTs produced by CVD were employed. As-produced pristine CNTs (both SWCNTs and MWCNTs) contain impurities such as metal nanoparticles (from the catalyst used for the growth of CNTs), graphitic particles and amorphous carbon, therefore their purification is fundamental for the desired biomedical applications. Most metal particles present in as-produced CNTs are surrounded by concentric graphitic shells, which prevent their simple dissolution by aqueous acids.[54] The graphite layer can be removed by different methods such as nitric acid, hydrogen peroxide, air treatment; however these methods lead to an extensive disruption of the CNT tubular structure.[54] Steam treatment at high temperatures is instead less aggressive as steam is a mild oxidizing agent that can remove the amorphous carbon without introducing major defects and functional groups.[54,55] The longer the steam treatment, the more carbon (in its different forms, *i.e.* amorphous, graphitic or nanotube) is removed, therefore longer treatments result in consistent consumption of CNTs. According to our partner's studies, 4-hour treatment with steam at 900 °C is a good compromise between quality of the sample and weight loss. The process of steam purification also causes the opening of the tube ends (for both SWCNTs and MWCNTs) and a slight reduction of the nanotube length.[54,55] This treatment is then followed by reflux of the CNTs with concentrated HCl to remove the nude metal particles which can now be readily dissolved by acids. The quality of the purified samples and the absence of particles can be verified by HRTEM, while TGA in air allows to determine the amount of residual metal particles.

Filling and sealing

The filling of carbon nanotubes with inorganic compounds, in the specific case metal halides, can be achieved by molten-phase capillary wetting.[56,57] In this process the salt is heated above its melting point inside a sealed ampoule under vacuum and in the presence of CNTs. The molten material percolates into the opened nanotubes by capillary action. Once filled, cooling the system back to room temperature causes the dangling bonds at the ends of the nanotubes to seal by radical recombination.[58] While this evidence has been variously reported for SWCNTs, the complete sealing of filled MWCNTs under similar conditions is more difficult to achieve because of their larger diameter. Therefore, more

investigations need to be carried out on this topic. The excess of material external to the CNTs can be dissolved away by extensive washings with an appropriate solvent. The filling yield (*i.e.* the mass ratio between the encapsulated material and carbon) can be exactly determined by thermogravimetric analysis of the sample in flowing air.[59] Another very useful technique to characterize endohedral nanotubes is HRTEM, which is the only microscopic technique that allows to see through the sidewalls of nanotubes and visualize their content with atomic resolution. By HRTEM it is possible to prove that molecules are genuinely located inside nanotubes and reveal structural information about their packing. In fact, metal halides encapsulated within nanotubes can be found in an amorphous phase or arranged in a crystal form.[32,60]

5.6.2 EXPERIMENTAL PART

In the following table are listed the various type of pristine CNTs we have employed in our investigations, along with their main characteristics. A brief description of the experimental protocol for their preparation is reported just below, to highlight the main differences between one batch and the other.

Sample Name	CNT type	Median Length (nm)	Mean Length (nm)	Filling	Filling Yield [wt %]	Reactions
SWCNT –**B1**	SW	420	690	/	/	**9**
SWCNT –**B2**	SW	420	690	/	/	**13-18 23-26**
$SmCl_3$@SWCNT –**B1**	SW	420	690	$SmCl_3$	16.02	**11**
$SmCl_3$@SWCNT –**B2**	SW	420	690	$SmCl_3$	17.86	**19-22**
$SmCl_3$@SWCNT –**B3**	SW	420	690	$SmCl_3$	18.36	**34**
$LuCl_3$@SWCNT	SW	420	690	$LuCl_3$	15.82	**12**
$LuCl_3$@SWCNT **-S**	SW	266	530	$LuCl_3$	29.94	**27-33**
MWCNT	MW	1630	2093	/	/	**10**
$SmCl_3$@MWCNT	MW	225	308	$SmCl_3$	16.71	

Table 5.10 Specifications on the batches of pristine CNTs used for our reactions (corresponding number in the last column). Samples and data provided by ICMAB partner.

General procedure for the purification of SW and MWCNTs

CNTs were ground with a mortar and then heated for 4 h at 900 °C inside a quartz tube, in the presence of steam and under argon. Steam-treated CNTs were then dispersed in HCl (37% with H_2O, 1:1) and heated at 110 °C overnight. The dispersion was then filtered, the CNTs on the membrane were washed with H_2O until neutral pH of the filtrate, and finally dried at 100 °C.

Preparation of short SWCNTs

CNTs were treated with freshly prepared piranha solution (H_2SO_4/H_2O_2, 4:1) for 2 h. After quenching of the reaction with H_2O, the mixture was filtered and the CNTs on the membrane were washed with water and dried at 100 °C. The CNTs were then steam-treated at 900 °C for 1 h, and purified with HCl as above-described.

Filling of SWCNTs

CNTs were ground with the chosen filling material in a 1:10 weight ratio, under inert atmosphere (glove box). The mixture was then sealed in a quartz tube under vacuum, and the sample was annealed in a furnace at 900 °C (for $SmCl_3$), or 960 °C (for $LuCl_3$) for 12 h. The sample was then dispersed in H_2O by sonicating for 15 min, heated at 65 °C for 3-4 h, filtered and rinsed with ddH_2O. This washing protocol was repeated three times (or more) in case TEM characterization evidenced the presence of residual external material.

5.7 BIBLIOGRAPHY

[1] C. Bingel, *Chem. Ber.* **1993**, *126*, 1957.

[2] X. Camps, A. Hirsch, *J. Chem. Soc. Perkin Trans. 1* **1997**, 1595.

[3] J. M. Ashcroft, K. B. Hartman, Y. Mackeyev, C. Hofmann, S. Pheasant, L. B. Alemany, L. J. Wilson, *Nanotechnology* **2006**, *17*, 5033.

[4] C. Thilgen, S. Sergeyev, F. Diederich, *Templates in Chemistry I*, Springer Berlin Heidelberg, Berlin, Heidelberg, **2004**.

[5] I. Nierengarten, J.-F. Nierengarten, *Chem. Asian J.* **2014**, *9*, 1436.

[6] H. Sato, E. Hayashi, N. Yamada, M. Yatagai, Y. Takahara, *Bioconjugate Chem.* **2001**, *12*, 701.

[7] C. F. Richardson, D. I. Schuster, S. R. Wilson, *Org. Lett.* **2000**, *2*, 1011.

[8] T. Umeyama, N. Tezuka, M. Fujita, Y. Matano, N. Takeda, K. Murakoshi, K. Yoshida, S. Isoda, H. Imahori, *J. Phys. Chem. C* **2007**, *111*, 9734.

[9] K. S. Coleman, S. R. Bailey, S. Fogden, M. L. H. Green, *J. Am. Chem. Soc.* **2003**, *125*, 8722.

[10] S. Perreault, C. Spino, *Org. Lett.* **2006**, *8*, 4385.

[11] A. de la Hoz, A. Díaz-Ortiz, A. Moreno, *Chem. Soc. Rev.* **2005**, *34*, 164.

[12] P. Appukkuttan, V. P. Mehta, E. V Van der Eycken, *Chem. Soc. Rev.* **2010**, *39*, 1467.

[13] H. Takayama, S. Takahashi, T. Moriya, H. Osada, Y. Iwabuchi, N. Kanoh, *Chembiochem* **2011**, *12*, 2748.

[14] I. E. Głowacka, J. Balzarini, A. E. Wróblewski, *Arch. Pharm. (Weinheim).* **2013**, *346*, 677.

[15] F. A. Carey, R. J. Sundberg, in *Advanced Organic Chemistry Part B Reaction Synthesis*, Springer US, Boston, MA, **1995**, pp. 301–350.

[16] C. J. Moody, G. H. Whitham, *Reactive Intermediates*, Oxford University Press, Oxford, **1992**.

[17] M. Holzinger, J. Steinmetz, D. Samaille, M. Glerup, M. Paillet, P. Bernier, L. Ley, R. Graupner, *Carbon* **2004**, *42*, 941.

[18] M. Holzinger, O. Vostrowsky, A. Hirsch, F. Hennrich, M. Kappes, R. Weiss, F. Jellen, *Angew. Chem. Int. Ed.* **2001**, *40*, 4002.

[19] M. Holzinger, J. Abraham, P. Whelan, R. Graupner, L. Ley, F. Hennrich, M. Kappes, A. Hirsch, *J. Am. Chem. Soc.* **2003**, *125*, 8566.

[20] C. Gao, H. He, L. Zhou, X. Zheng, Y. Zhang, *Chem. Mater.* **2009**, *21*, 360.

[21] H. Leinonen, J. Rintala, A. Siitonen, M. Lajunen, M. Pettersson, *Carbon* **2010**, *48*, 2425.

[22] A. B. Smith, H. Tokuyama, *Tetrahedron* **1996**, *52*, 5257.

[23] J. Averdung, J. Mattay, D. Jacobi, W. Abraham, *Tetrahedron* **1995**, *51*, 2543.

[24] M. Cases, M. Duran, J. Mestres, N. Martín, M. Solà, *J. Org. Chem.* **2001**, *66*, 433.

[25] A. Yashiro, Y. Nishida, M. Ohno, S. Eguchi, K. Kobayashi, *Tetrahedron Lett.* **1998**, *39*, 9031.

[26] J. A. Deyrup, R. B. Greenwald, *Tetrahedron Lett.* **1966**, *7*, 5091.

[27] C. Wentrup, in *Synthetic and Mechanistic Organic Chemistry* (Eds: F. Minisci, J.B. Hendrickson, C. Wentrup), Springer-Verlag, Berlin/Heidelberg, **1976**, pp. 173–251.

[28] N. Karousis, T. Ichihashi, M. Yudasaka, S. Iijima, N. Tagmatarchis, *Chem. Commun.* **2011**, *47*, 1604.

[29] G. Lu, S. Lam, K. Burgess, *Chem. Commun.* **2006**, 1652.

[30] J. Liu, C. M. Hadad, M. S. Platz, *Org. Lett.* **2005**, *7*, 549.

[31] S. Y. Hong, G. Tobias, B. Ballesteros, F. El Oualid, J. C. Errey, K. J. Doores, A. I. Kirkland, P. D. Nellist, M. L. H. Green, B. G. Davis, *J. Am. Chem. Soc.* **2007**, *129*, 10966.

[32] S. Y. Hong, G. Tobias, K. T. Al-Jamal, B. Ballesteros, H. Ali-Boucetta, S. Lozano-Perez, P. D. Nellist, R. B. Sim, C. Finucane, S. J. Mather, M. L. H. Green, K. Kostarelos, B. G. Davis, *Nat. Mater.* **2010**, *9*, 485.

[33] S. Niyogi, M. A. Hamon, D. E. Perea, C. B. Kang, B. Zhao, S. K. Pal, A. E. Wyant, M. E. Itkis, R. C. Haddon, *J. Phys. Chem. B* **2003**, *107*, 8799.

[34] K. R. Moonoosawmy, P. Kruse, *J. Am. Chem. Soc.* **2008**, *130*, 13417.

[35] J. Rubin Grandis, M. F. Melhem, W. E. Gooding, R. Day, V. A. Holst, M. M. Wagener, S. D. Drenning, D. J. Tweardy, *J. Natl. Cancer Inst.* **1998**, *90*, 824.

[36] T. K. Owonikoko, S.-Y. Sun, S. S. Ramalingam, *Clin. Lung Cancer* **2009**, *10*, 230.

[37] A. M. Egloff, J. R. Grandis, *Semin. Oncol.* **2008**, *35*, 286.

[38] F. Ciardiello, G. Tortora, *Clin. Cancer Res.* **2001**, *7*, 2958.

[39] W. Sihver, J. Pietzsch, M. Krause, M. Baumann, J. Steinbach, H.-J. Pietzsch, *Pharmaceuticals (Basel).* **2014**, *7*, 311.

[40] R. Marega, F. De Leo, F. Pineux, J. Sgrignani, A. Magistrato, A. D. Naik, Y. Garcia, L. Flamant, C. Michiels, D. Bonifazi, *Adv. Funct. Mater.* **2013**, *23*, 3173.

[41] P.-C. Lee, Y.-C. Chiou, J.-M. Wong, C.-L. Peng, M.-J. Shieh, *Biomaterials* **2013**, *34*, 8756.

[42] Z. Liu, X. Li, S. M. Tabakman, K. Jiang, S. Fan, H. Dai, *J. Am. Chem. Soc.* **2008**, *130*, 13540.

[43] E. Venturelli, C. Fabbro, O. Chaloin, C. Ménard-Moyon, C. R. Smulski, T. Da Ros, K. Kostarelos, M. Prato, A. Bianco, *Small* **2011**, *7*, 2179.

[44] R. R. Traut, A. Bollen, T.-T. Sun, J. W. B. Hershey, J. Sundberg, L. R. Pierce, *Biochemistry* **1973**, *12*, 3266.

[45] R. Jue, J. M. Lambert, L. R. Pierce, R. R. Traut, *Biochemistry* **1978**, *17*, 5399.

[46] P. K. Smith, R. I. Krohn, G. T. Hermanson, A. K. Mallia, F. H. Gartner, M. D. Provenzano, E. K. Fujimoto, N. M. Goeke, B. J. Olson, D. C. Klenk, *Anal. Biochem.* **1985**, *150*, 76.

[47] W. Bannwarth, R. Knorr, *Tetrahedron Lett.* **1991**, *32*, 1157.

[48] H. Sahoo, *RSC Adv.* **2012**, *2*, 7017.

[49] L. Lacerda, J. Russier, G. Pastorin, M. A. Herrero, E. Venturelli, H. Dumortier, K. T. Al-Jamal, M. Prato, K. Kostarelos, A. Bianco, *Biomaterials* **2012**, *33*, 3334.

[50] E. Kaiser, R. L. Colescott, C. D. Bossinger, P. I. Cook, *Anal. Biochem.* **1970**, *34*, 595.

[51] C. Samorì, R. Sainz, C. Ménard-Moyon, F. M. Toma, E. Venturelli, P. Singh, M. Ballestri, M. Prato, A. Bianco, *Carbon* **2010**, *48*, 2447.

[52] M. A. Brun, K.-T. Tan, R. Griss, A. Kielkowska, L. Reymond, K. Johnsson, *J. Am. Chem. Soc.* **2012**, *134*, 7676.

[53] T. T. Denton, X. Zhang, J. R. Cashman, *J. Med. Chem.* **2005**, *48*, 224.

[54] B. Ballesteros, G. Tobias, L. Shao, E. Pellicer, J. Nogués, E. Mendoza, M. L. H. Green, *Small* **2008**, *4*, 1501.

[55] G. Tobias, L. Shao, C. G. Salzmann, Y. Huh, M. L. H. Green, *J. Phys. Chem. B* **2006**, *110*, 22318.

[56] P. M. Ajayan, S. Iijima, *Nature* **1993**, *361*, 333.

[57] D. Ugarte, T. Stöckli, J. M. Bonard, A. Châtelain, W. A. de Heer, *Appl. Phys. A Mater. Sci. Process.* **1998**, *67*, 101.

[58] L. Shao, G. Tobias, Y. Huh, M. L. H. Green, *Carbon* **2006**, *44*, 2855.

[59] B. Ballesteros, G. Tobias, M. A. H. Ward, M. L. H. Green, *J. Phys. Chem. C* **2009**, *113*, 2653.

[60] R. R. Meyer, *Science* **2000**, *289*, 1324.

CHAPTER 6

CONCLUSIONS AND PERSPECTIVES

Carbon nanotubes are a unique material that proved to have many promising applications, especially in the fields of nanoelectronics, composite materials and nanotechnology. In the last decade the potential exploitation of this material in the biomedical field has attracted great interest due to the ability of CNTs to be internalized into cells, paving the way for the possible use of CNTs as drug or gene delivery system. In this context, we focused our interest in developing new carbon nanotube bio-conjugates with the ultimate aim of achieving anticancer therapy. Specifically, the researches described in this Thesis have been addressed toward the investigation of new chemical strategies for the preparation of CNT carriers of genes (siRNA), therapeutic nanobodies or radioactivity.

In the first experimental section (Chapter 2), we have described the preparation of amino-functionalized MWCNTs as carriers of siRNA. Several studies have employed CNTs functionalized with positively-charged groups for the delivery of genomic material *in vitro* and *in vivo*, showing promising results. Our group had also previously remarked that the type of chemical functionalization used to surface-modify oxMWCNTs can lead to significant differences in nanotube cellular uptake and delivery ability. In this study, we designed and explored six synthetic strategies to achieve the direct conversion of the carboxylic groups of oxMWCNTs into amino groups, without extending the lateral chain. The aim was to further clarify the relationship between the CNT surface functionalization and the siRNA complexation ability. We succeeded to introduce nitrogen-containing fucntional groups (most probably amines) onto the CNTs. However, the degree of conversion of –COOH into $–NH_2$ was not very high, suggesting that a consistent amount of carboxylic groups was still present. We then evaluated the ability of the amino-functionalized MWCNTs to complex siRNA and to achieve gene transfection inside a tumor cell line. Two of the synthesized conjugates showed good complexation efficacy and were able to be uptaken by the cells without triggering any short-term toxic effect. By this study, it was evident that the synthetic strategy employed to modify the CNT surface can have a strong impact on the behavior of the final conjugate in a biological environment. Though, characterization and understanding of the surface chemistry are indeed crucial to gain a better comprehension of this behavior.

The second research project (Chapter 3) concerned the preparation of a novel CNT construct for the delivery of VHH, a therapeutic nanobody. VHHs are nowadays largely investigated as a valid alternative to full antibodies, thanks to their smaller size and high affinity for the target. The VHH we employed is able to target β-catenin, whose overexpression is associated with many cancers. We have conjugated VHH to oxMWCNTs through a designed linker featuring a cleavable disulfide bond, to access the controlled intracellular release of the therapeutic. In one of the constructs, VHH was directly linked to the disulfide bond of the linker (PEG_4-SPDP), while in another, VHH was distanced from the cleavage site by a maleimide spacer. For comparison, a third VHH-CNT conjugate devoid of cleavable linker was synthesized. SPR analysis of the three conjugates proved that the nanobody affinity toward β-catenin was still preserved after conjugation. *In vitro* and *in vivo* assessment of the efficacy of the conjugates showed their toxicity toward a carcinoma cell line overexpressing β-catenin and their ability to afford tumor reduction and prolonged survival of tumor-bearing mice. Despite no clear evidence proved the better efficacy of the two conjugates presenting the disulfide linker over the un-cleavable conjugate, all biological results evidenced that these novel CNT-VHH constructs are efficient against the tested tumor and could therefore be further optimized to achieve a powerful tool for the delivery of therapeutic nanobodies.

The last research work described in this Thesis (Chapter 5) was accomplished within the Marie Curie ITN project named RADDEL, which is aimed at the development of CNT-based carriers for targeted delivery of radiotherapy. The fact that the hollow interior of CNTs can be exploited to confine the radionuclide, while the sidewalls can be externally decorated with biologically active molecules,

renders CNT a highly suitable carrier of radioactivity. In fact, upon sealing of the filled CNTs, the radionuclide is confined inside the nanotubes and the targeting ability provided by the external biomolecule can direct its delivery toward a specific site. Within this framework, we have focused our researches on the functionalization of different types of pristine empty and filled CNTs by [2+1] cycloaddition (Bingel and nitrene reactions) and on the subsequent conjugation of a targeting antibody. Our attempts to functionalize CNTs by Bingel reaction, using different malonate precursors or reaction conditions, did not lead to satisfying degrees of loading. On the other hand, nitrene cycloaddition of an organic azide onto CNTs proved to be an efficient strategy to achieve the functionalization of many types of pristine CNTs with good loadings. Functionalized CNTs were further derivatized with a tagging molecule (for microscopic characterization), fluorescent probes (for assessment of cellular internalization pathways) or a targeting monoclonal antibody (for targeted delivery). Through a number of reaction screenings we succeeded to set up an optimized protocol to achieve the complete preparation of mAb-functionalized filled CNTs in a relatively short time, in view of the translation of this protocol on radioactive material. The characterization of the mAb-CNT conjugates by different techniques proved that the mAb (Cetuximab) was successfully immobilized onto nitrene-functionalized CNTs, and that its affinity toward a counter antibody was still preserved. *In vitro* and *in vivo* assays suggested that the mAb-CNT conjugates have a good biocompatibility and are not toxic in the tested cell lines. Furthermore, we demonstrated that these compounds showed good ability to target and bind their receptor, the EGFR, which is overexpressed by many cancer cells. However, no substantial difference could be found between the covalent mAb-CNT conjugate and its non-covalent control. Finally, the mechanism adopted by the cells to internalize these compounds seems to depend on the specific type of cells, although further investigations on this subject are needed to clarify the CNT entry pathway and their intracellular localization. We have very recently employed our optimized protocol to perform the functionalization of radioactive filled CNTs and we are currently assessing their therapeutic efficacy and their *in vivo* biodistribution in collaboration with our partners in KCL (London). Overall, the synthetic strategy that we designed looks like a promising approach for the functionalization of filled CNTs with a targeting mAb to achieve the delivery of radiotherapy. Further investigations envisaging different targeting molecules, functional chains and/or radionuclides may be performed to prepare new conjugates with different therapeutic properties. Indeed, the possibility to select different radionuclide/targeting molecule pairs widens the applicative range of our strategy and offers the option to tune the properties of the radiopharmaceutical according to the specific targeted tumor. This is a very valuable aspect of our strategy that could have a very high and wide potential in the field of radiotherapy.

To conclude, we have explored new methodologies and chemical approaches for the covalent functionalization of CNTs for applications in the biomedical field. Our studies constitute a proof-of-principle that CNTs are a promising tool to achieve the delivery of anticancer therapeutics. We therefore believe that the investigations on the potential of CNTs as a carrier are still of valuable interest, in association with researches to improve their characterization and studies of their toxicological profile. For any clinical translation of CNT conjugates it is indeed crucial to have a full understanding of their behavior under all perspectives (chemical, physical, toxicological, therapeutic).

LIST OF PUBLICATIONS AND COMMUNICATIONS

PUBLICATIONS

1. C. Spinato, D. Giust, I. A. Vacchi, C. Ménard-Moyon, K. Kostarelos, A. Bianco *"Different Chemical Strategies to Aminate Oxidized Multi-Walled Carbon Nanotubes for siRNA Complexation and Delivery"*, to be submitted

2. I. A. Vacchi, C. Spinato, J. Raya, D. Bégin, A. Bianco, C. Ménard-Moyon "*Assessment of Graphene Oxide Reactivity: Controlled Derivatization by Chemoselective Reactions"*, submitted.

3. C. Spinato, C. Ménard-Moyon, A. Bianco (2014) *"Chemical Functionalization of Graphene for Biomedical Applications"*, (ed. V. Gerogakilas) Wiley-VCH Verlag GmbH & Co., Chapter 4, pag. 95-137.

COMMUNICATIONS

1. NANOBIOAPP 2015 "Latest Advances on Nanomaterials for Biomedical Applications", Barcelona (Spain), 21-23 Sept. 2015, oral presentation.

2. Journée des Doctorants en Chimie, EDC Strasbourg, 7 Nov. 2014
   C. Spinato, A. Perez Ruiz de Garibay, C. Ménard-Moyon, B. Ballesteros, G. Tobias, K. Al-Jamal, A. Bianco "*Functionalization of filled CNTs by [2+1] cycloaddition for the targeted delivery of radioactivity*", oral presentation.

3. Colloque du Groupe Français d'Etude des Carbones (GFEC), Nouan-le-Fouzelier (France), 12-15 May 2014
   C. Spinato, C. Ménard-Moyon, B. Ballesteros, G. Tobias, K. Al-Jamal, A. Bianco "*Functionalization of filled CNTs by [2+1] cycloaddition for the targeted delivery of radioactivity"*, oral presentation.

4. ChemOnTubes 2014, Riva del Garda (Italy), 30 March - 3 April 2014
   C. Spinato, C. Ménard-Moyon, B. Ballesteros, G.Tobias, J. Raya, K. Kostarelos, A. Bianco "*Chemical modification of carbon nanomaterials for targeted therapies"*, poster presentation

5. School of Nanomedicine, Trieste (Italy), 10-11 September 2013
   C. Spinato, C. Ménard-Moyon, A. Bianco "*Functionalization of filled CNTs by [2+1] cycloaddition for the targeted delivery of radioactivity*", poster presentation.

6. ERC Grantees Conference 2012 "Frontiers Research Chemistry", Strasbourg (France), 22-24 November 2012
   A. Battigelli, V. Kanala, C. Spinato, C. Ménard-Moyon, A. Bianco "*Carbon Nanotubes in Biomedicine*", poster presentation.

Cinzia SPINATO

Development of chemical strategies to prepare multifunctional carbon nanotubes for anticancer therapy

Résumé

L'application de nanotubes de carbone (CNTs) dans le domaine biomédical a été largement explorée grâce à leur propriétés physico-chimiques et à leur biocompatibilité. Par la fonctionnalisation extérieur et/ou intérieur des CNTs c'est possible de préparer des nouveaux conjugués avec diffèrent propriétés et applications. On a exploré la modification des nanotubes par voie covalente pour leur utilisation comme vecteurs de biomolécules pour achever la thérapie anticancéreuse. Pendant ma Thèse, j'ai travaillé sur trois projets: l'application de différentes approches pour la conversion des groupes acides carboxyliques de MWCNTs oxydés en amines, dans le but de préparer des conjugués capables de complexer du siRNA (petits ARN interférents). Dans un second projet, j'ai développé des conjugués à base de nanotubes de carbone couplés avec un fragment d'anticorps thérapeutique via une liaison clivable afin d'en étudier le potentiel antitumoral. Dans le dernier projet, on a achevé la fonctionnalisation de CNTs remplis avec des molécules radioactivables par cycloaddition de nitrene et ensuite conjugué un anticorps de ciblage tumoral. Le but été d'utiliser les nanotubes comme vecteurs pour la délivrance de radioactivité à l'intérieur des cellules tumorales ciblées par l'anticorps. On a aussi conduit des investigations biologique, afin d'évaluer la toxicité et l'efficace de ce conjugué.

Mots-clés : nanotubes de carbone, réaction nitrene, délivrance de molécules thérapeutiques, radiothérapie.

Abstract

The application of carbon nanotubes (CNTs) in the biomedical field has been widely explored thanks to their physico-chemical properties and their biocompatibility. By the external and/or internal functionalization of CNTs it is possible to prepare novel conjugates tailoring different properties and applications. We have investigated the covalent derivatization of CNTs by different chemical strategies to achieve suitable carriers for anticancer therapy. In one project, we have explored the conversion of the carboxylic groups of oxidized CNTs into amino groups, and the ability of these conjugates to complex genetic material, for gene delivery. In another project, CNTs have been functionalized with linkers bearing a cleavable disulfide bond, and further conjugated to a therapeutic nanobody for controlled intracellular drug release. Finally, we have investigated the reactivity of close-ended CNTs filled with radioactivable material toward Bingel and nitrene cycloadditions and the conjugation of a targeting antibody, for the target delivery of radioactivity. By several characterization techniques we have proved that the antibody is covalently grafted to the CNT-carrier and it still possesses its targeting ability. Investigations on the biological profile of these conjugates (cytotoxicity, targeting, uptake, biodistribution) have been also carried out.

Keywords: carbon nanotubes, nitrene reaction, drug delivery, gene silencing, radiotherapy.